

# Fourth Case Study: Reference Data and Codes

**NWMO TR-2012-08**

**November 2012**

**F. Garisto, M. Gobien, E. Kremer and C. Medri**

Nuclear Waste Management Organization

**nwmo**

NUCLEAR WASTE  
MANAGEMENT  
ORGANIZATION

SOCIÉTÉ DE GESTION  
DES DÉCHETS  
NUCLÉAIRES



**Nuclear Waste Management Organization**  
22 St. Clair Avenue East, 6<sup>th</sup> Floor  
Toronto, Ontario  
M4T 2S3  
Canada

Tel: 416-934-9814  
Web: [www.nwmo.ca](http://www.nwmo.ca)

**Fourth Case Study: Reference Data and Codes**

**NWMO TR-2012-08**

November 2012

F. Garisto, M. Gobien, E. Kremer and C. Medri

Nuclear Waste Management Organization





## ABSTRACT

**Title:** Fourth Case Study: Reference Data and Codes  
**Report No.:** NWMO TR-2012-08  
**Author(s):** F. Garisto, M. Gobien, E. Kremer and C. Medri  
**Company:** Nuclear Waste Management Organization  
**Date:** November 2012

### Abstract

The Fourth Case Study is an illustrative postclosure safety assessment of a conceptual repository for nuclear used fuel located at 500 m depth at a hypothetical site on the Canadian Shield.

The conceptual design differs from the Third Case Study in that it considers vertical in-floor borehole placement of used fuel containers (UFCs) rather than the horizontal or in-room placements investigated previously. The reference UFC design has also been updated: it retains the outer copper shell for corrosion protection and inner steel vessel for structural support; however, the capacity of the UFC has increased from 324 to 360 fuel bundles.

While the hypothetical site where the repository is excavated is the same as in the Third Case Study, the exact location has shifted approximately 1500m to the north east and the depth has changed from 670 m below ground surface (mBGS) to 500 mBGS. Furthermore, the geosphere has been assigned different properties.

The main safety assessment codes used in the Fourth Case Study are:

- FRAC3DVS-OPG – for 3D groundwater flow and radionuclide transport;
- RSM – a simple screening model used to identify the key radionuclides;
- SYVAC3-CC4 – the primary safety assessment system model (container, repository, geosphere, biosphere);
- HIMv2.0 – for calculating dose consequences for the human intrusion scenario.

These codes and their datasets are maintained under a software quality assurance system at NWMO. The codes are described briefly in this report.

The reference datasets are based on a combination of the site conceptual model information and the repository design description, with most of the general material properties and other input parameters adopted from the previous work, updated where available by more recent studies. This report provides a summary of all the data selected, and indicates the references where more details about the derivation of the data may be found.



**TABLE OF CONTENTS**

	<b><u>Page</u></b>
<b>ABSTRACT .....</b>	<b>v</b>
<b>1. INTRODUCTION .....</b>	<b>1</b>
<b>1.1 BACKGROUND .....</b>	<b>1</b>
<b>1.2 REPORT OUTLINE.....</b>	<b>1</b>
<b>2. OVERVIEW .....</b>	<b>3</b>
<b>2.1 REPOSITORY CONCEPT .....</b>	<b>3</b>
<b>2.2 CONCEPTUAL MODELS .....</b>	<b>3</b>
<b>2.3 DATA .....</b>	<b>4</b>
<b>3. COMPUTER MODELS .....</b>	<b>8</b>
<b>3.1 MODELS, DATA AND TOOLS .....</b>	<b>8</b>
<b>3.2 COMPUTER MODEL DESCRIPTIONS .....</b>	<b>11</b>
<b>3.3 SOFTWARE QUALITY ASSURANCE .....</b>	<b>16</b>
<b>4. USED FUEL DATA .....</b>	<b>19</b>
<b>4.1 USED FUEL WASTEFORM.....</b>	<b>19</b>
<b>4.2 USED FUEL COMPOSITION.....</b>	<b>20</b>
<b>4.3 NUCLIDE AND ELEMENT INVENTORIES OF UO<sub>2</sub> FUEL .....</b>	<b>22</b>
<b>4.4 INSTANT RELEASE FRACTION .....</b>	<b>29</b>
<b>4.5 FUEL DISSOLUTION RATE.....</b>	<b>38</b>
<b>5. CONTAINER .....</b>	<b>41</b>
<b>5.1 CONTAINER DIMENSIONS .....</b>	<b>41</b>
<b>5.2 DEFECTIVE CONTAINER.....</b>	<b>43</b>
<b>5.3 WATER COMPOSITION.....</b>	<b>45</b>
<b>5.4 SOLUBILITY LIMITS .....</b>	<b>46</b>
<b>6. REPOSITORY DATA .....</b>	<b>49</b>
<b>6.1 PHYSICAL LAYOUT .....</b>	<b>49</b>
<b>6.2 BUFFER.....</b>	<b>56</b>
<b>6.3 BACKFILL .....</b>	<b>61</b>
<b>6.4 CONCRETE .....</b>	<b>64</b>
<b>6.5 ASPHALT .....</b>	<b>65</b>
<b>7. GEOSPHERE DATA.....</b>	<b>67</b>
<b>7.1 GENERAL SITE DESCRIPTION .....</b>	<b>67</b>
<b>7.2 HYDRAULIC CONDUCTIVITY .....</b>	<b>68</b>
<b>7.3 PHYSICAL AND CHEMICAL CHARACTERISTICS .....</b>	<b>71</b>
<b>7.4 GEOSPHERE TRANSPORT PARAMETERS .....</b>	<b>73</b>
<b>7.5 EDZ TRANSPORT PARAMETERS.....</b>	<b>76</b>
<b>7.6 GEOSPHERE SORPTION PARAMETERS.....</b>	<b>82</b>
<b>7.7 WELL LOCATION AND DEPTH.....</b>	<b>86</b>
<b>7.8 OTHER GEOSPHERE PARAMETERS .....</b>	<b>88</b>
<b>7.9 GEOSPHERE NODE DATA .....</b>	<b>88</b>

<b>8.</b>	<b>BIOSPHERE DATA .....</b>	<b>89</b>
8.1	SITE AND SURFACE WATER .....	89
8.2	DISCHARGE ZONES .....	89
8.3	CLIMATE AND ATMOSPHERE .....	94
8.4	SOILS AND SEDIMENT .....	94
8.5	FARMING YIELDS.....	100
<b>9.</b>	<b>DOSE PATHWAYS DATA.....</b>	<b>101</b>
9.1	HUMAN LIFESTYLE CHARACTERISTICS .....	101
9.2	HUMAN PHYSICAL CHARACTERISTICS.....	106
9.3	AIR CONCENTRATION PARAMETERS.....	106
9.4	MISCELLANEOUS PHYSICAL PARAMETERS .....	109
9.5	ANIMAL CHARACTERISTICS .....	110
9.6	DOSE COEFFICIENTS .....	113
<b>10.</b>	<b>SUMMARY .....</b>	<b>119</b>
	<b>REFERENCES .....</b>	<b>120</b>
	<b>APPENDIX A: COMPUTER PROGRAM ABSTRACT FOR SYVAC3-CC4 .....</b>	<b>133</b>
	<b>APPENDIX B: COMPUTER PROGRAM ABSTRACT FOR RSM .....</b>	<b>141</b>
	<b>APPENDIX C: COMPUTER PROGRAM ABSTRACT FOR HIMv2.0.....</b>	<b>147</b>
	<b>APPENDIX D: USED FUEL INVENTORY UNCERTAINTY.....</b>	<b>151</b>
	<b>APPENDIX E: USED FUEL DISSOLUTION MODEL .....</b>	<b>155</b>
	<b>APPENDIX F: SYVAC3-CC4 GEOSPHERE MODEL DATA.....</b>	<b>165</b>
	<b>APPENDIX G: HUMAN INTRUSION MODEL DATA.....</b>	<b>187</b>

**LIST OF TABLES**

	<b><u>Page</u></b>
Table 2.1: Parameter PDF types and attributes.....	7
Table 3.1: Description of software tools.....	11
Table 3.2: SYVAC3-CC4, version SCC409.....	13
Table 3.3: FRAC3DVS-OPG, version 1.3.....	14
Table 3.4: RSM, version RSM110.....	15
Table 3.5: HIMv2.0.....	16
Table 4.1: Used fuel parameters (Tait et al. 2000).....	19
Table 4.2: Radionuclides included in the detailed CC4 radiological assessment.....	20
Table 4.3: Potentially chemically hazardous elements and radionuclide decay chains included in the CC4 chemical hazard assessment*.....	21
Table 4.4: Inventories of radionuclides of interest in UO <sub>2</sub> fuel for 220 MWh/kgU burnup and 30 years cooling (Tait et al. 2000).....	27
Table 4.5: Inventories of chemical elements of interest in UO <sub>2</sub> fuel for 220 MWh/kgU burnup and 30 years cooling (Tait et al. 2000).....	28
Table 4.6: Instant release fractions for CANDU fuel.....	30
Table 4.7: Rationale for selection of instant release fractions for elements with no measured data.....	36
Table 4.8: Radiation doses at fuel surface (220 MWh/kgU) <sup>#</sup> .....	39
Table 4.9: Used fuel dissolution rate parameters (see Appendix E).....	40
Table 5.1: Container internal parameters.....	41
Table 5.2: Container external parameters.....	41
Table 5.3: Defective container scenario parameters.....	43
Table 5.4: Free water diffusivity (at 25°C).....	44
Table 5.5: Contact water composition (Duro et al 2010).....	45
Table 5.6: Element solubilities used in the Fourth Case Study <sup>1</sup> .....	48
Table 6.1: Placement room parameters.....	50
Table 6.2: Properties of as placed materials in the repository.....	54
Table 6.3: Shaft seal design.....	56
Table 6.4: Compacted bentonite properties at saturation.....	57
Table 6.5: Effective diffusivities for bentonite and dense backfill at 25°C.....	59
Table 6.6: Sorption coefficients for bentonite, dense backfill and concrete.....	60
Table 6.7: Capacity factors for bentonite and dense backfill.....	62
Table 6.8: Properties of light backfill pellets at saturation.....	63
Table 6.9: Properties of dense backfill blocks at saturation.....	64
Table 6.10: Properties of backfill at saturation assuming homogenization of light backfill pellets and dense backfill blocks.....	64
Table 6.11: Properties of 70% bentonite / 30% sand at saturation.....	64
Table 6.12: Properties of concrete at saturation.....	65
Table 6.13: Properties of asphalt at saturation.....	66
Table 7.1: Geosphere conductivity profile.....	70
Table 7.2: Physical characteristics of geosphere zones.....	72
Table 7.3: Chemical characteristics of geosphere zones.....	72
Table 7.4: Geochemistry parameters.....	74
Table 7.5: Effective diffusivities in geosphere zones [m <sup>2</sup> /a].....	75
Table 7.6: Properties of the different excavation damage zones.....	81
Table 7.7: Transverse, radial, and axial EDZ properties <sup>1</sup> .....	81
Table 7.8: Values of $[\rho_s(1-\epsilon_{\text{expt}})/\epsilon_{\text{expt}}]$ for several geological materials.....	83

Table 7.9: Reference values of $K_d$ for fractures and crushed rock <sup>1,2</sup> .....	84
Table 7.10: Well model geosphere parameters .....	87
Table 7.11: Other properties .....	88
Table 8.1: Lake properties .....	92
Table 8.2: Discharge zone areas .....	93
Table 8.3: Climate and atmosphere parameters .....	95
Table 8.4: Soil properties .....	96
Table 8.5: Plant/soil concentration ratios .....	98
Table 8.6: Soil $K_d$ values <sup>1</sup> [L/kg] and lake sedimentation rates [1/a] .....	99
Table 8.7: Farming yield data .....	100
Table 9.1: Human lifestyle characteristics for farm household .....	102
Table 9.2: Irrigation rate parameters <sup>1</sup> .....	104
Table 9.3: Timing parameters .....	105
Table 9.4: Human physical characteristics .....	106
Table 9.5: Volatilization parameters .....	108
Table 9.6: Physical parameters .....	109
Table 9.7: Food energy and water content .....	109
Table 9.8: Nutrient content of foods <sup>1</sup> .....	110
Table 9.9: Domestic animal data <sup>1</sup> .....	110
Table 9.10: Animal ingestion transfer coefficients .....	111
Table 9.11: Animal inhalation transfer coefficients .....	112
Table 9.12: Adult human dose coefficients .....	114
Table 9.13: Parameters for human specific activity models .....	116
Table 9.14: No-effect concentrations for non-human biota .....	117
Table 9.15: Proposed acceptance criteria for protection of humans and non-human biota from non-radiological impacts .....	118

**LIST OF FIGURES**

	<b><u>Page</u></b>
Figure 1.1: Illustration of the multi-barrier deep geologic repository concept considered in the Fourth Case Study. ....	2
Figure 2.1: General conceptual model(s) describing defective containers in the Reference Case of the Normal Evolution scenario. There are no contaminant releases from non-defective containers. ....	5
Figure 2.2: General conceptual model for the Human Intrusion Scenario. Two critical groups are considered - the drill crew and a site resident. Only radiological impacts are evaluated.....	6
Figure 3.1: Illustration of relationship between the computer models used in the Fourth Case Study and supporting data. ....	9
Figure 3.2: Software change control process followed for the NWMO postclosure safety assessment software and data. ....	18
Figure 4.1: Distribution of burnups and cumulative distribution for all fuel bundles (discharged up to September 2006) for all OPG owned reactors. ....	23
Figure 4.2: Radioactivity of used fuel (220 MWh/kgU burnup) as a function of time after discharge from reactor. The fission products dominate at short times, but have decayed to low levels after 1000 years. After about 1 million years, the remaining activity is largely that due to the natural uranium content of the fuel.....	26
Figure 4.3: Distribution of maximum linear power ratings and cumulative distribution for all fuel bundles (discharged up to September 2006) from all OPG owned reactors. The standard deviation of the distribution is approximately 7.7 kW/m or, for a Bruce bundle, approximately 140 kW/bundle.....	31
Figure 4.4: Fission gas (gap) release as a function of peak linear power rating for CANDU fuels with burnups less than 400 MWh/kgU .....	33
Figure 4.5: Total instant release fractions (=gap + grain boundary inventories) for iodine and cesium (data from Stroes-Gascoyne 1996) .....	33
Figure 4.6: Cl-36 releases from CANDU fuel (data from Tait et al. 1997).....	34
Figure 5.1: Container design showing copper outer shell, inner steel vessel, and fuel assemblies inside support tubes. ....	42
Figure 6.1: Plan view of underground repository .....	51
Figure 6.2: Longitudinal view of placement room .....	52
Figure 6.3: Cross-sectional view of placement room .....	53
Figure 6.4: Longitudinal view of the placement room seal.....	55
Figure 7.1: The hypothetical subregional surface topography, indicating major lakes and rivers and repository location. The topography is relatively flat. ....	67
Figure 7.2: Perspective view of 200 km <sup>2</sup> subregional area. Top figure shows surface lineaments and surface water features. Bottom figure shows fracture network at repository level (500 m depth) and location of the repository. ....	69
Figure 7.3: The conductivity versus depth profiles of the rock mass and fracture used for Fourth Case Study geosphere. Data from the Whiteshell (Manitoba) and Atikokan (Ontario) Research Areas on the Canadian Shield are shown, illustrating both the typical scatter in data and the trend for lower permeability with depth.....	70
Figure 7.4: Illustration (not to scale) of distinct regions of the EDZ in: (top) the placement rooms and (bottom) access drifts or tunnels. ....	78
Figure 8.1: Close-up of the area around the repository site, showing the major water bodies (lakes, rivers and streams) and wetlands. The projected location of the repository at surface is also shown.....	90

Figure 8.2: Discharge points of particle track released from repository (plan view). Surface water features, including wetlands, are outlined in blue. These tracks are based on the no-well case. .... 90



## 1. INTRODUCTION

### 1.1 BACKGROUND

Three major Canadian case studies have been completed on the postclosure safety assessment of the deep geologic repository concept for disposal of used CANDU fuel in the Canadian Shield - the Environmental Impact Statement (EIS) case study (AECL 1994; Goodwin et al. 1994), the Second Case Study (SCS) (Goodwin et al. 1996), and the Third Case Study (TCS) (Gierszewski et al. 2004a, Garisto et al. 2004a).

The EIS study considered titanium alloy containers with 72-fuel-bundle capacity placed vertically into boreholes along the repository rooms, and assumed the repository was located in sparsely-fractured granitic rock, similar to that at the Whiteshell Research Area, with very low permeability. The SCS considered 72-bundle copper containers placed horizontally within the repository rooms, and assumed the repository was located in granitic rock with substantially higher permeability than in the EIS study. The Third Case Study used an updated copper container with a 324-bundle capacity, placed horizontally within the repository rooms (Gierszewski et al. 2004a). A variant case in which the containers were placed in horizontal boreholes was also investigated (Garisto et al. 2005a, 2005b). In the Third Case Study, the repository was located in granitic rock that is characterized by an intermediate permeability and a geostatistically-generated discrete fracture network.

The Fourth Case Study (FCS) considers a fourth variation of the deep geologic repository concept and site, as shown in Figure 1.1 (NWMO 2012a). The main objective of the Fourth Case Study is to assess key aspects of the postclosure safety of a deep geologic repository based on a more recent Canadian design concept. The present report documents the data and computer codes used for this study. This information should be considered within the following context.

- The Fourth Case Study focuses on key scenarios, including the expected or Normal Evolution scenario, but is not a complete postclosure safety assessment.
- The Fourth Case Study is based on a specific repository design (in-floor borehole container emplacement) and reference container design.
- The site is hypothetical. It is assumed that a sufficient volume of competent rock is available for the repository. The depth of 500 m was assumed for this illustrative assessment, and would be optimized for a real site. There is no site-specific data and, hence, no Geosynthesis, i.e., a geoscientific explanation of the overall understanding of site characteristics and evolution (past and future) as they relate to demonstrating long-term repository performance and safety.

### 1.2 REPORT OUTLINE

This report describes the main computer codes and data used in the postclosure safety assessment calculations for the Fourth Case Study. It is organized as follows:

- **Section 2** provides an overview of the repository design, models and general data selection principles;

- **Section 3** summarizes the computer codes used and their main features, and the software quality assurance approach;
- **Section 4** provides the used fuel wastefrom data;
- **Section 5** provides the container data;
- **Section 6** provides the emplacement room and repository data;
- **Section 7** provides the geosphere data;
- **Section 8** provides the local surface biosphere data; and
- **Section 9** provides the biosphere data, specifically the data used for calculating dose rates to a critical human group assumed to be living at the site in the future.

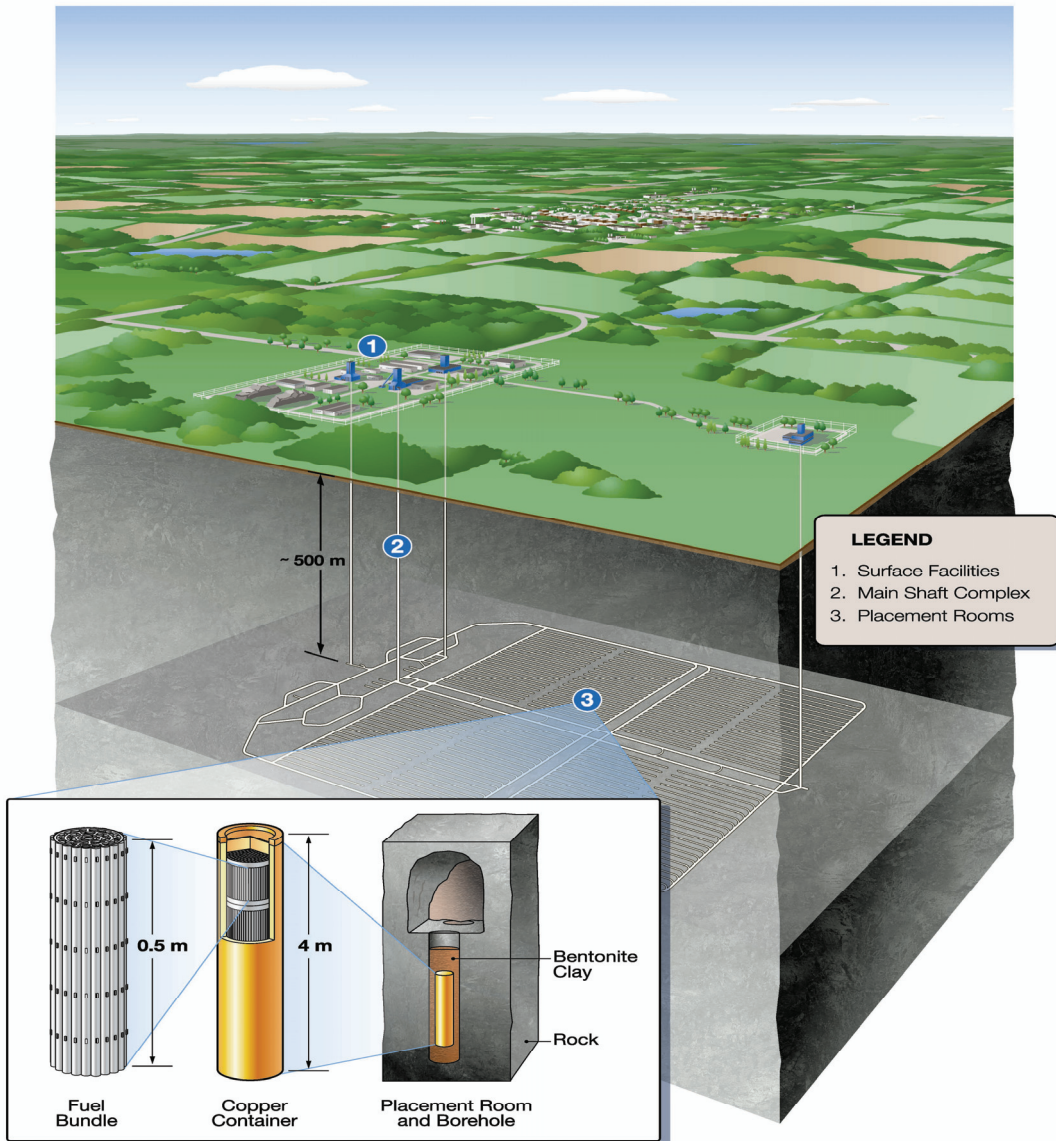


**Figure 1.1: Illustration of the multi-barrier deep geologic repository concept considered in the Fourth Case Study.**

## 2. OVERVIEW

### 2.1 REPOSITORY CONCEPT

The main features of the hypothetical Fourth Case Study repository are as follows (see also Figure 1.1):

- The repository is located at a depth of 500 m below the surface in granitic rock on the Canadian Shield.
- The repository is located in a region in which there are no known mineral deposits or other economically exploitable geological resources.
- The repository is constructed by the room-and-pillar method, with the repository excavated at a single level.
- The repository contains approximately 4.6 million bundles of used CANDU fuel.
- At the time of emplacement, the used-fuel bundles have been discharged from the reactor for a minimum of 30 years.
- Prior to emplacement, used-fuel bundles are sealed inside durable copper and steel containers.
- The used fuel containers are placed in boreholes drilled into the floor of the rooms.
- The outer surface temperature of the container after emplacement is constrained (by design) to a maximum value of 100°C.
- Each container is surrounded by a 100% bentonite clay buffer material.
- As emplacement proceeds, the open space in each room is filled with backfill, and the filled rooms are closed off by composite seals made of clay-based and cement-based materials.
- At the end of a postclosure monitoring period, all tunnels, shafts, and exploration boreholes in the vicinity of the repository are sealed using backfill and a combination of clay-based and cement-based materials.

### 2.2 CONCEPTUAL MODELS

Five scenarios are considered in the Fourth Case Study:

1. An expected or **Normal Evolution Scenario**, in which the repository is built according to design, and the overall system behaves as expected. However, it is assumed that three of the containers placed in the repository have undetected manufacturing defects and that groundwater fills the container as soon as the repository becomes saturated, creating an early pathway for contaminant releases out of the container.

The Normal Evolution Scenario includes a discrete fracture network in the geosphere (see Section 7) and considers the impact of glaciation (NWMO 2012a).

2. A **Human Intrusion Scenario**, in which the engineered and natural repository barriers are bypassed by a borehole that is inadvertently drilled through a container, bringing used fuel material directly to the surface.
3. An **All Containers Fail Scenario**, in which all containers are assumed to fail at 60,000 years, the time of the first major ice-sheet advance over the repository site in the glacial cycle defined by Garisto et al. (2010).

4. A **Shaft Seal Failure Scenario**, in which there is rapid and extensive degradation of the shaft seals.
5. A **Fracture Seal Failure Scenario**, in which there is rapid and extensive degradation of the seals around the fracture passing through the repository footprint (see Figure 6.1).

The conceptual models for analysing the Normal Evolution and Human Intrusion scenarios are described in more detail in NWMO (2012a). However, in order to provide an outline of the code features and data required to support these analyses, a general conceptual model for these scenarios is provided in Figures 2.1 and 2.2.

The conceptual models for the other three scenarios are identical to that for the Normal Evolution scenario since differences between the scenarios can be represented by modifying parameter values.

For quantitative analysis, these conceptual models are implemented as computer models or "codes". The main codes used are listed below, and described in Section 3:

#### Normal Evolution Scenario

- FRAC3DVS-OPG v1.3.0- Groundwater flow and transport in the repository and geosphere
- RSM v1.1 - Screening system model
- SYVAC3-CC4 Version SCC409- Integrated system model

#### Human Intrusion Scenario

- HIMv2.0 - Human intrusion model

#### Severe Shaft Seal Failure Scenario

- FRAC3DVS-OPG v1.3.0 - Groundwater flow and transport in the repository and geosphere

## **2.3 DATA**

### **2.3.1 Data Sources**

For analyses of the Normal Evolution scenario, the starting point for the data used in the Fourth Case Study was that used in the Third Case Study (Garisto et al. 2004b). The parameters needed for the Fourth Case Study were compared with those from the Third Case Study, and many of the latter values were judged to be reasonable for this study and kept without changes. Several parameters were revised, however, for the specific Fourth Case Study repository and geosphere setting (e.g., parameters describing the repository design).

Notable data updates (besides the repository and geosphere specifics) are the radionuclide sorption coefficients for the buffer material and geosphere host rock, and the radionuclide solubilities, which are based on more recent reviews and evaluations. Finally, the used fuel dissolution model was revised (essentially the same processes are modelled but the detailed representation is different), and its input parameters were revised accordingly.

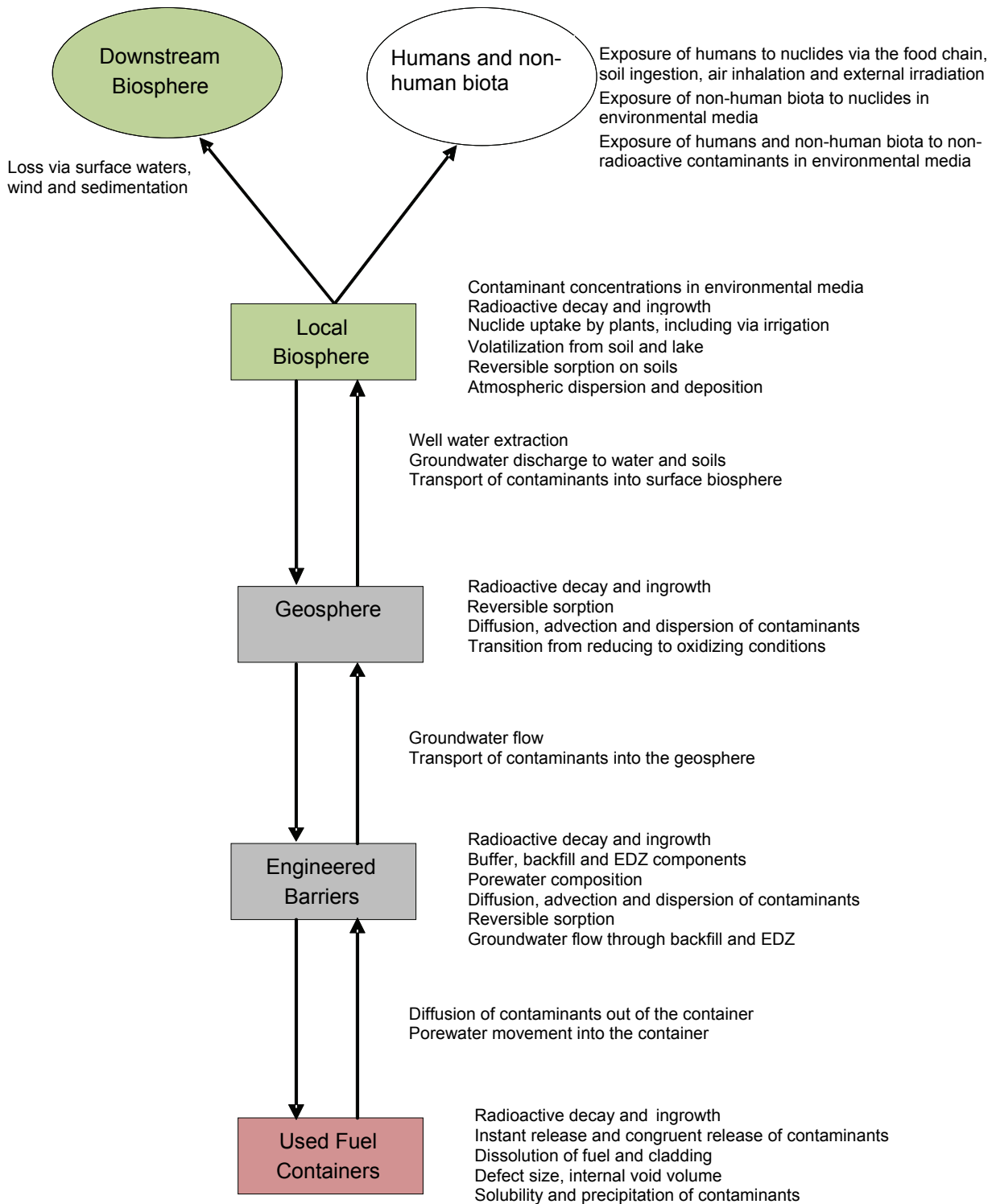


**Figure 2.1: General conceptual model(s) describing defective containers in the Reference Case of the Normal Evolution scenario. There are no contaminant releases from non-defective containers.**

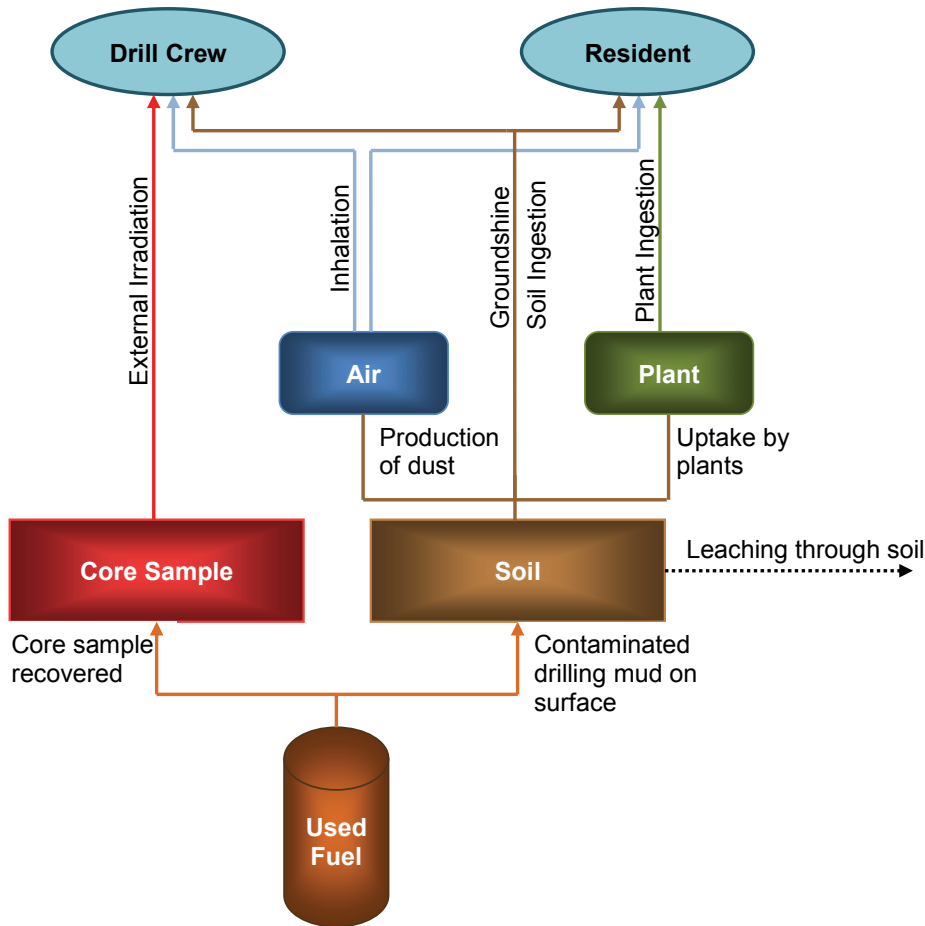


**Figure 2.2: General conceptual model for the Human Intrusion Scenario. Two critical groups are considered - the drill crew and a site resident. Only radiological impacts are evaluated.**

Most parameter values used in the Fourth Case Study are defined in Sections 4 to 9 of this report. This includes all design, inventory, material, geosphere, biosphere, and dose conversion data. Exposure-specific parameters for the Human Intrusion scenario are described in Appendix G.

### 2.3.2 Parameter Variability

For some model input parameters, there is a clearly appropriate value. However, for many parameters, a range of values may be possible because of natural variability or measurement uncertainties or uncertainties arising from the modelling basis. An example of natural variability is human diet - the amount that people eat is naturally variable from person to person, and from time to time. An example of model-based uncertainty is the sorption  $K_d$  parameter, since this is an effective parameter that represents the net effect of possibly several processes that may be occurring at the microscopic scale.

The format of the input data described here allows the specification of data using probability density functions (PDF) to indicate both the likely values as well as their range. In particular, Table 2.1 lists the PDF types supported within the Fourth Case Study data. Correlations between two parameters are supported if the two correlated parameters are described by either a normal distribution or a lognormal distribution. Presently, the SYVAC3-based computer models (RSM and CC4) can use this information directly; however other models (such as FRAC3DVS-OPG) must be supplied with specific input values.

Generally, even though a parameter may be described by a range, it is not so clear how to characterize that range in a PDF. Mishra (2002) discusses general factors that can be considered in selecting a PDF type, including the following suggestions in the absence of a mechanistic basis for selection:

- Uniform (log-uniform) - low state of knowledge (e.g., bounds only),
- Triangular (log-triangular) - low state of knowledge (e.g., bounds and best estimate),
- Normal - additive processes, and
- Lognormal - multiplicative processes.

The intent, in general, is to define best-estimate values for the dataset. For example, the reference radionuclide inventories are based on the average fuel burnup of 220 MWh/kgU. Uncertainties in the best-estimate values can be characterized through the probability density functions. Conservative analyses can then use values selected from the appropriate part (e.g., tails) of the distribution. For example, the 5<sup>th</sup> percentile sorption ( $K_d$ ) parameters could be used for screening analysis.

Conditions corresponding to extreme values should be considered for separate and explicit treatment as specific "what if" analyses, rather than by inclusion in the main dataset. For example, the buffer sorption parameters are based on reducing conditions. The PDF reflects the variability or uncertainty in sorption for given conditions, as well as the range of reducing conditions expected in the buffer. The effects of oxidizing conditions, if considered, would be treated as a separate case and not part of the best-estimate buffer sorption PDF.

**Table 2.1: Parameter PDF types and attributes**

<b>Distribution Type</b>	<b>Attributes</b>
Constant	Value
Uniform	Lower bound, upper bound
Loguniform	Lower bound, upper bound
Piecewise uniform	Lower and upper bound, probability for each piece
Triangular	Lower bound, peak value, upper bound
Normal	Mean, standard deviation, optional lower and upper bounds
Lognormal	Geometric mean, geometric standard deviation, optional lower and upper bounds

### **3. COMPUTER MODELS**

The Fourth Case Study analyses use computer models (or "codes") to numerically represent the conceptual models considered. In this section, the computer models used in this study are briefly described, as well as the general software quality assurance system supporting these codes.

#### **3.1 MODELS, DATA AND TOOLS**

##### **3.1.1 Reference Models**

There are two categories of computer models used in the Fourth Case Study postclosure safety assessment - detailed (or "process") models and integrated system models. In general, the detailed models address specific topics, usually with the inclusion of mechanistic effects or with greater resolution in space or time. These detailed models either provide supporting data or validation tests, or else identify the important parameters and processes for use in the integrated system models. The latter system models incorporate the most important features, events and processes describing the behaviour of the repository, from waste form to dose consequences.

Figure 3.1 identifies the codes used in the Fourth Case Study assessment, and their interrelationship. Initially, information from used fuel characteristics, engineering design, and site characterization are used in conjunction with specialized codes to develop a site-specific system description. For example, the initial inventory is determined using ORIGEN-S, while the site characterization information is collected into a detailed groundwater flow model under FRAC3DVS-OPG.

The results from the RSM model are used to screen the initial inventories of radionuclides and chemical elements in the fuel in order to identify a short list of most concern. Detailed transport calculations for scenarios involving groundwater transport of contaminants are then undertaken with the FRAC3DVS-OPG transport model and the SYVAC3-CC4 system model. FRAC3DVS-OPG calculates advective-dispersive transport through the repository and geosphere using a detailed 3-D model, and interfaces with SYVAC3-CC4 for source terms and biosphere consequence calculations. SYVAC3-CC4 contains a set of submodels that represent the whole repository, including the repository (used fuel, defective containers, etc.), the geosphere (advective and diffusive transport, well, etc.) and the biosphere (food chain model, surface waters, etc.). The FRAC3DVS-OPG and SYVAC3-CC4 models are complementary since they use very different numerical approaches and have different strengths.

The Human Intrusion scenario is separately analyzed using the Human Intrusion Model for the Fourth and Fifth Case Studies (HIMv2.0) (Medri 2012), which is built on the AMBER software platform (Quintessa 2009a, 2009b). AMBER is a graphical-user interface based software tool that allows users to build dynamic compartment models to represent, for example, the migration and fate of radioactive and non-radioactive contaminants in environmental systems.



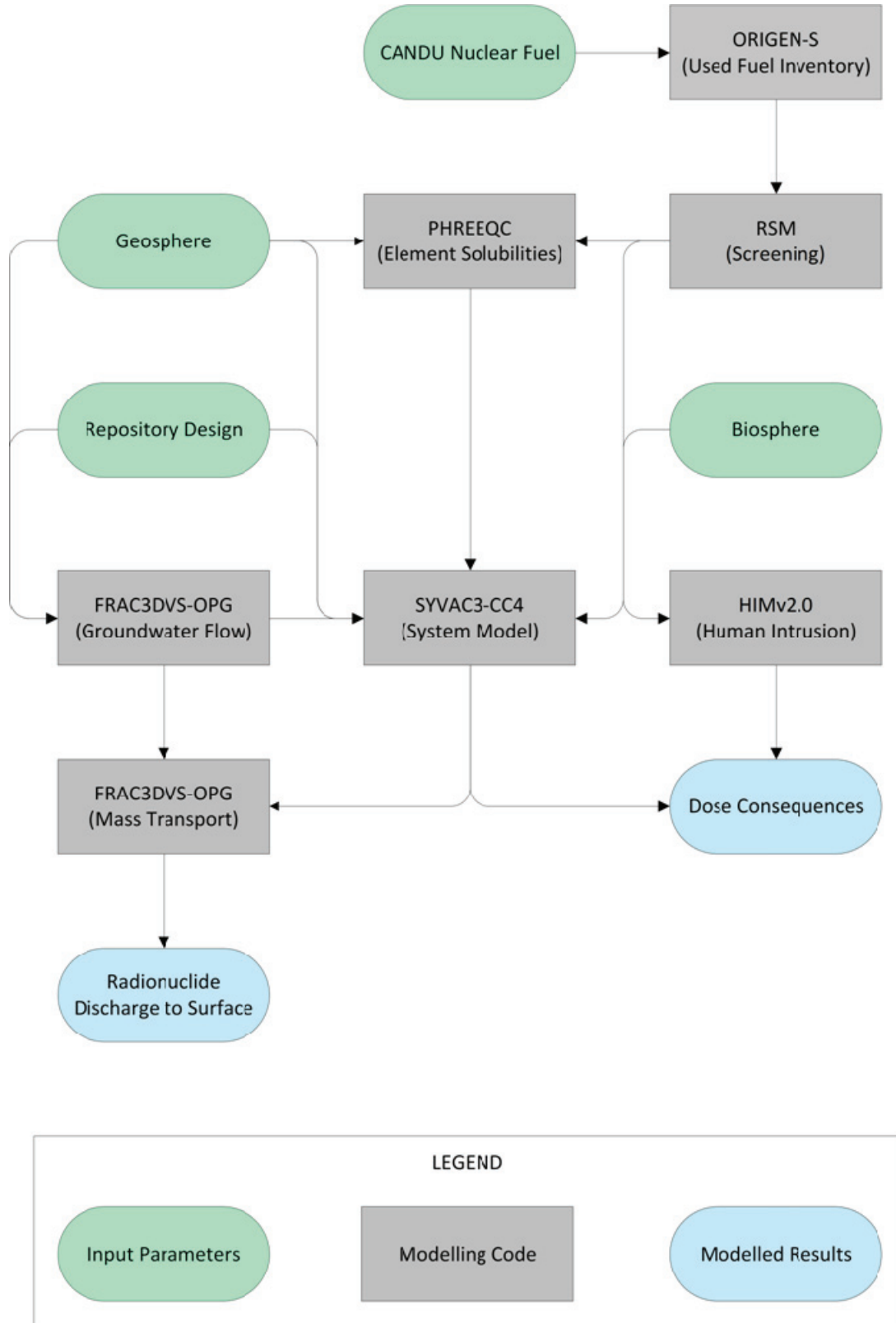


Figure 3.1: Illustration of relationship between the computer models used in the Fourth Case Study and supporting data.

In addition, the assessment is supported by detailed models, notably CCM for near-field chemistry (container corrosion, oxygen consumption, microbial activity) and PHREEQC for solubilities. Analysis of coupled thermal-hydro-mechanical (THM) phenomena in geological media, including moisture transfer in unsaturated soils, was performed using three different codes for comparison and verification (Guo 2009; SNC-Lavalin 2011): the finite-element codes CODE\_BRIGHT and the finite-difference code FLAC3D v.3.1

### **3.1.2 Reference Data**

The main system model – SYVAC3-CC4 – has reference datasets associated with it. These are also maintained under a software configuration management system. Specific reference datasets are prepared as required; for example, for major safety assessments or major database updates. These reference datasets and their documentation are maintained under control of the NWMO.

All data are stored as text files, one for each parameter, in a XML format that is readable by the input file generation software. The data file format allows the description and storage of parameters as probability density functions and stores other information such as: parameter definition, data contributor, date data was entered, distribution bounds, any correlation, justification and references for the data, and information on when the data was checked and who checked it. This latter information is important for quality assurance.

The reference datasets are placed in controlled access directories, and their version is indicated by a date label, corresponding to when the dataset was released for use. For example, the SYVAC3-CC4 dataset used in Fourth Case Study is SCC409\2012\_07. The main purpose of this report is to describe the source of data in this SYVAC3-CC4 dataset.

The RSM dataset used in the Fourth Case Study is RSM110\2012\_05. The RSM dataset is described by Gobien and Garisto (2012). It contains data on many more radionuclides and chemical elements than does the SYVAC3-CC4 dataset.

Only part of the repository, geosphere and biosphere data required by the FRAC3DVS-OPG model are described in detail in this report. For example, the hydraulic conductivities of the buffer material and geosphere are described, but the detailed data describing the fracture locations and the surface topography are not provided here. These are however available in electronic format in the archives of the contractor Geofirma Engineering Ltd.

Finally, the data used by the Human Intrusion model HIMv2.0 is embedded directly within the AMBER code describing the model. These data are provided in Appendix G.

### **3.1.3 Software Tools**

The safety assessment codes and system models are supported by software tools as listed in Table 3.1. They support the codes in various capacities such as post-processing the raw output, pre-processing input data, and improving software quality.

Continuing effort on improving coding, data and documentation of the safety assessment models has led to the development of several software quality assurance support tools. The coding tools, for example, ensure consistency between source code and coding standards, automate certain coding tasks, provide checking that units are balanced in coded equations, and help with the code documentation.

**Table 3.1: Description of software tools**

<b>Output Analysis</b>	
SyView, Version 1.2	A post-processor for SYVAC3-based codes, based on the mView graphical framework
mView, Version 4.10	Geofirma Engineering Ltd.'s pre- and post-processor for FRAC3DVS-OPG
R, Version 2.13.0	A programming environment for data analysis and graphics that is used as a post-processor for SYVAC3-CC4 output
<b>Prepare Reference Datasets and Input Files for SYVAC3-based Codes</b>	
SINGEN, Version 3.2	An application for generating input files for SYVAC3-based codes
<b>Software Quality Assurance</b>	
UNITCK, Version 9	Checks that units balance in Fortran source code

## 3.2 COMPUTER MODEL DESCRIPTIONS

The main documentation associated with each computer model is a theory manual, user manual and testing reports. Documentation for the individual codes is specified in Tables 3.2 – 3.5.

### 3.2.1 SYVAC3-CC4

The main safety assessment code for the Fourth Case Study is referred to as SYVAC3-CC4, Version SCC409 (Table 3.2). It is a system model for assessment of groundwater transport of contaminants from the repository to the biosphere, as in the Normal Evolution scenario. It was designed for the postclosure safety assessment of a deep geologic repository for used CANDU fuel placed in durable containers. It calculates the rate of contaminant releases from used fuel in contact with water, their transport out of defective containers, through the engineered barriers and host rock, and into the biosphere. Dose consequences are calculated for a critical group – a farming household, living in the vicinity of the repository and exposed to contaminants released from the repository. Earlier versions of this code were used for the EIS (Goodwin et al. 1994), Second Case Study (Goodwin et al. 1996) and the Third Case Study (Gierszewski et al. 2004a; Garisto et al. 2004a, 2005a).

The CC4 repository model was developed for emplacement of containers in long horizontal tunnels or boreholes.

### 3.2.2 FRAC3DVS-OPG

The reference groundwater flow and groundwater transport code used in the Fourth Case Study is FRAC3DVS-OPG (Therrien et al. 2010), a 3-D finite-element/finite-difference code (Table 3.3). FRAC3DVS-OPG is the Ontario Power Generation's version of a commercially available code. It is the reference code used in NWMO's geoscience program - thus, providing direct continuity between the site characterization and safety assessment site conceptual models. FRAC3DVS-OPG supports both equivalent-porous-medium and dual-porosity representations of the geologic media. The FRAC3DVS-OPG groundwater flow results are used to derive the

parameters for the CC4 geosphere groundwater transport model. Furthermore, the results of the FRAC3DVS-OPG radionuclide transport calculations can be compared to the corresponding CC4 calculations, allowing verification of the CC4 geosphere transport model.

### **3.2.3 RSM**

One of the simpler models used in the Fourth Case Study analysis is called RSM (Radionuclide Screening Model) (Table 3.4). It models groundwater transport of radionuclides via a simple contaminant transport pathway from the defective containers to humans via a well. By conservative choice of input parameters, it can be used to screen radionuclides so as to objectively identify which are worth analyzing using more detailed models.

### **3.2.4 HIMv2.0**

The Human Intrusion Model for the Fourth and Fifth Case Studies (HIMv2.0) assesses an inadvertent human intrusion scenario. The model considers an exposure scenario where a nuclear waste container is unknowingly intersected by a drilled borehole, and used fuel is brought directly to surface, bypassing all the repository barriers. The dose consequences are estimated for the drill crew and a resident of a home built on the contaminated area. HIMv2.0 is an AMBER based code (see Table 3.5).

### **3.2.5 Specialized Supporting Codes**

Various specialized codes are used to address specific topics or processes.

ORIGEN-S is a CANDU-industry standard code that was used to calculate the radionuclide inventories in the used fuel and Zircaloy cladding at time of emplacement, based on a defined reactor exposure scenario (Tait et al. 2000, Tait and Hanna 2001). The ORIGEN-S code is not part of the Fourth Case Study safety assessment codes, but the results from ORIGEN-S were used to derive a reference used fuel inventory, as described in Section 4.

PHREEQC is a widely used computer code that performs aqueous geochemical calculations (Parkhurst and Appelo 1999). The program is based on equilibrium chemistry (i.e., chemical thermodynamics) of aqueous solutions interacting with minerals, gases, solid solutions and sorption surfaces. PHREEQC was used in the Fourth Case Study to calculate the solubilities of various elements within the defective containers (Duro et al. 2010).

**Table 3.2: SYVAC3-CC4, version SCC409**

Parameter	Comments
Components:	
SYVAC3	Executive module, Version SV3.12
CC4	System model, Version CC4.09
ML3	SYVAC3 math library, Version ML3.03
SLATEC	SLATEC Common Mathematical Library, Version 4.1
Development standard:	Software quality assurance standard is CSA N286.7-99. Source code is compliant with FORTRAN 90 (SLATEC 4.1 is FORTRAN 77).
Main Documentation:	See Appendix A <i>CC4 Theory Manual</i> (NWMO 2012b) <i>CC4 User Manual</i> (Kitson et al. 2012) <i>Summary of Verification and Validation Studies for SYVAC3-PR4 and its Submodels</i> (Garisto and Gierszewski 2001)
Main Features:	<ul style="list-style-type: none"> <li>- Linear decay chains</li> <li>- Nuclide release by instant release and by congruent dissolution</li> <li>- UO<sub>2</sub> dissolution rate calculated using a radiation dose-rate based model</li> <li>- Precipitation in container when solubility limits are exceeded</li> <li>- Durable containers, but some fail due to small pre-existing defects</li> <li>- Cylindrical buffer and backfill layer that surrounds the container and inhibits groundwater flow and radionuclide transport</li> <li>- Multiple sector repository connected to the geosphere at sector-specific nodes chosen considering the local groundwater flow</li> <li>- Geosphere network of 1-D transport tubes that connect the repository to various surface discharge locations, including a well.</li> <li>- Transport is solved considering diffusion, advection/dispersion and sorption, using fast semi-analytic models.</li> <li>- Biosphere model that calculates soil concentrations, well concentrations, and uses a surface water body (e.g., lake) as a final collection point</li> <li>- Dose impacts to a farming family near the repository that uses lake or well water, locally grown crops and food animals, and local building materials and heating fuel materials</li> <li>- Dose impacts to generic biota</li> <li>- Generally time-independent material properties and characteristics for the biosphere and geosphere. However, transitions from one geosphere (or biosphere) state to a different state at specific times can be accommodated.</li> <li>- Ability to represent all input parameters with a probability density function and to run Monte-Carlo type simulations.</li> </ul>

**Table 3.3: FRAC3DVS-OPG, version 1.3**

<b>Parameter</b>	<b>Comments</b>
Components: FRAC3DVS- OPG	Main code, Version 1.3
Development standard:	FORTRAN 95
Key Documentation:	<i>FRAC3DVS-OPG: A Three-dimensional Numerical Model Describing Subsurface Flow and Solute Transport</i> (Therrien et al. 2010)
Main Features:	<ul style="list-style-type: none"> <li>- Linear decay chains</li> <li>- 3-D groundwater flow and solute transport in saturated media</li> <li>- Finite-element and finite-difference numerical solutions</li> <li>- Equivalent porous medium or dual-continuum model; fractures may be represented as discrete 2-D elements</li> <li>- Mixed element types suitable for simulating flow and transport in fractures (2-D rectangular or triangular elements) and pumping/ injection wells, streams or tile drains (1-D line elements)</li> <li>- External flow boundary conditions can include specified rainfall, hydraulic head and flux, infiltration and evapotranspiration, drains, wells, streams and seepage faces</li> <li>- External transport boundary conditions can include specified concentration and mass flux and the dissolution of immiscible substances</li> <li>- 1D hydro-mechanical coupling</li> <li>- Options for adaptive time-stepping and output control procedures and an ILU-preconditioned ORTHOMIN solution package</li> <li>- Newton-Raphson linearization package provides robustness</li> </ul>

**Table 3.4: RSM, version RSM110**

<b>Parameter</b>	<b>Comments</b>
Components:	
SYVAC3	Executive module, Version SV3.10.1
RSM	System model, Version RSM 1.1
Development standard:	Software quality assurance standard is CSA N286.7-99 Source code is compliant with FORTRAN 90
Key Documentation:	See Appendix B <i>RSM Version 1.1 - Theory</i> (Goodwin et al. 2001) <i>RSM Version 1.1 User Manual</i> (D'Andrea 2001) <i>RSM Version 1.1 Verification and Validation</i> (Garisto 2001)
Main Features:	<ul style="list-style-type: none"> <li>- Linear decay chains</li> <li>- Nuclide release by instant release and by congruent dissolution</li> <li>- UO<sub>2</sub> dissolution calculated from user-supplied time-dependent data</li> <li>- Precipitation in container when user-supplied solubility limits exceeded</li> <li>- Durable containers, but some fail due to small pre-existing defects</li> <li>- 1-D buffer and backfill layer that surrounds the container and inhibits groundwater flow and radionuclide transport</li> <li>- Repository model based on one room containing failed container(s)</li> <li>- Linear sequence of 1-D flow tubes that connect the repository to a well. Flow tubes are user-supplied and transport equation is solved considering diffusion, advection/dispersion and sorption, using semi-analytical models</li> <li>- Dose impacts to a farmer household that uses well water, based on conservative model for drinking, immersion, inhalation and ground exposure. Effect of other ingestion pathways is included through a user-supplied multiplier factor</li> <li>- Ability to represent all input parameters with a probability density function and to run Monte-Carlo type simulations</li> <li>- Time-independent material properties and biosphere characteristics</li> <li>- Database of all radionuclides with half-lives longer than 0.1 years and their progeny with half-lives longer than 1 d</li> </ul>

**Table 3.5: HIMv2.0**

<b>Parameter</b>	<b>Comments</b>
Components:	
AMBER	Compartmental Modelling Software, Version 5.5
HIMv2.0	Main Model
Development standard:	Software quality assurance standard is CSA N286.7-99. AMBER is compliant with the TickIt software quality assurance standard.
Key Documentation:	See Appendix C <i>Human Intrusion Model for the Fourth and Fifth Case Studies: HIMv2.0 (Medri 2012)</i>
Main Features:	<ul style="list-style-type: none"> <li>- Branching decay chains</li> <li>- Dose consequences by external, inhalation and ingestion pathways to drill crew member and site resident</li> <li>- Surface contamination decreases with time due to radioactive decay and soil leaching</li> <li>- Time-independent material properties and biosphere characteristics</li> <li>- Includes data for about 90 radionuclides, based on screening calculations.</li> </ul>

### 3.3 SOFTWARE QUALITY ASSURANCE

The Nuclear Waste Management Organization (NWMO) supports the management principles of CSA N286.7, and has defined a managed system that meets this commitment through a hierarchy of governing documents and procedures. These procedures include quality assurance requirements.

Software for use in postclosure safety assessments of a deep geologic repository is being developed and maintained by the NWMO consistent with these governing documents and procedures. For the main system codes and reference datasets used for the Fourth Case Study (SYVAC3-CC4, RSM, HIMv2.0, FRAC3DVS-OPG), this procedure identifies CSA N286.7-99 (CSA 1999) as the relevant software standard.

The CSA N286.7-99 software standard identifies requirements for:

- configuration management and change control,
- documentation, and
- verification.



The configuration management approach selected for the NWMO postclosure safety assessment software is based on controlled access, defined releases, and a formal change request system. Figure 3.2 summarizes the procedure followed for making changes to code and data for all codes and datasets developed by the NWMO.

Documentation requirements include a problem definition, a software plan, requirements specification, design description, verification report, programmers manual, program abstract, theory manual, user manual, validation report and a version tracking record.

The CSA N286.7-99 standard distinguishes between verification and validation testing. Verification is the process of ensuring that each phase of the software development is consistent with the previous phase. For example, it ensures that the source code is consistent with the code design, or that the installed version on a new system is consistent with the archived version. Validation is the process of demonstrating that a model adequately represents the physical system that it is meant to describe. A model is validated when it provides a sufficiently good representation of the actual processes occurring in a real system, consistent with the intended use of the model.

Validation is best achieved by comparing model predictions with field or experimental observations. However, full validation of models for long-term assessment of nuclear fuel disposal is not possible for several reasons, notably the long time periods involved. Consequently, validation is approached through a range of partial tests that collectively provide confidence in the model results.

The types of approaches and tests include:

- comparison with field or experimental data (e.g., short term or accelerated experiments or experiments involving specific processes);
- comparison with natural analogs;
- comparison with independently developed codes and models;
- peer review and acceptance; and
- use of conservative models and parameters.

There is no firm criterion for determining what constitutes an acceptable level of validation or confidence in the results (Flavelle 1987). In part, this is a matter for the program stakeholders (e.g., regulators) to assess. The full safety case for any specific candidate repository is expected to include other arguments besides the results of the postclosure safety assessment model (e.g., the age of groundwater at the repository level). Our approach to validating our computer models is through an ongoing testing effort to continuously improve confidence in the long-term models, using the range of approaches outlined above.

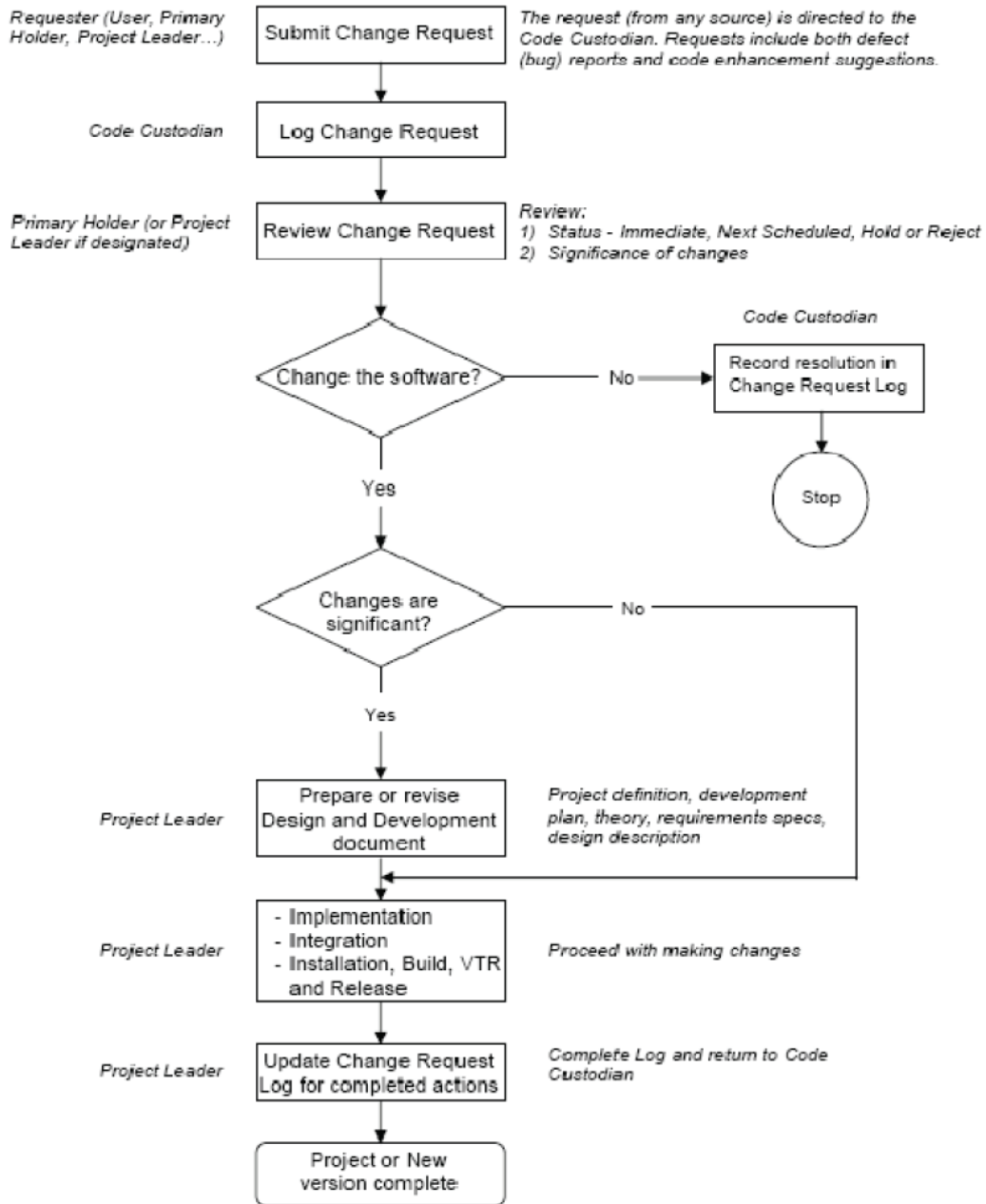


**Figure 3.2: Software change control process followed for the NWMO postclosure safety assessment software and data.**

## 4. USED FUEL DATA

This section describes the used fuel data for the Fourth Case Study. It provides a reference to the source(s) of the data, and a brief justification.

### 4.1 USED FUEL WASTEFORM

The used fuel wasteform is an irradiated natural-uranium UO<sub>2</sub> CANDU fuel bundle after reactor discharge. Reprocessed wastes and other high-level waste forms are not considered. The characteristics of the reference used fuel are summarized in Table 4.1. The repository will contain 4.6x10<sup>6</sup> used fuel bundles, which is the total projected used fuel bundles discharged over the life of the current Canadian CANDU power reactors.

There are presently a few variant CANDU fuel bundles, notably the 28- or 37-element bundle, the standard or long length bundle, and the bundles with or without CANLUB. Sensitivity studies by Tait et al. (2000) indicated that the radionuclide inventory per unit mass of fuel was not sensitive to these factors, and so the standard 37-element (Bruce) fuel bundle is selected as reference. The design of this bundle is summarized in Tait et al. (2000).

The age of the fuel at emplacement in the repository will vary. For example, the earliest CANDU fuel dates to 1970, whereas the repository is unlikely to be open before 2035, leading to some fuel being over 60 years old. The older the fuel, the lower is its residual thermal power and radiation fields. For design purposes, all used fuel is assumed to be 30 years out of the reactor prior to encapsulation in a used fuel container (SNC-Lavalin 2011).

The used fuel irradiation history can be characterized by its power rating and burnup. These are discussed in more detail in Sections 4.2 and 4.3.

**Table 4.1: Used fuel parameters (Tait et al. 2000)**

Parameter	Value	Comments
Waste form	37-element UO <sub>2</sub> fuel bundle	Standard fuel element from Bruce and Darlington stations
Mass U/bundle	19.25 kg	Initial mass (before irradiation)
Mass Zircaloy/bundle	2.2 kg	Includes cladding, spacers, end plates
Initial U-235	0.72 wt%	Natural uranium is used in OPG CANDU fuel.
Burnup	220 MWh/kgU	Highest OPG station-average burnup in Tait et al. (2000).
Power rating	455 kW/bundle	Nominal mid-range value
Fuel age at emplacement	30 years	e.g., 10 years in pools, 20 years in dry storage
Fuel pellet geometric surface area	8.47 cm <sup>2</sup>	Surface area of uncracked pellet (37 element design)

## 4.2 USED FUEL COMPOSITION

Freshly discharged used fuel could contain a few hundred different radionuclides, as well as over 80 stable elements. However, most of these will be present in negligible amounts or will rapidly decay, so they are not a concern for postclosure safety assessment.

The reference dataset used for the Fourth Case Study contains inventory, half-lives, dose coefficients and related data for over 300 radionuclides. All radionuclides with half-lives greater than 0.1 years are included in the dataset. A radionuclide with a half-life longer than 1 day is also included in the dataset, if any parent has a half-life longer than 0.1 years. The dose impacts of radionuclides with half-lives shorter than 1 day are incorporated through the dose coefficients of the parents (Gobien and Garisto 2012).

The analyses for the scenarios discussed in Section 2 start with this full list of radionuclides and chemical elements. However, screening studies are used to reduce the number of nuclides and chemical elements examined in more detail.

For clarity, we do not list data for all the nuclides and chemical elements in the full dataset. Instead, data is presented for only the radionuclides and chemical elements that have been identified as of interest for the Normal Evolution Scenario (and its variants) and the All Containers Fail Scenario, based on the screening results for the Fourth Case Study (NWMO 2012a).

The screening analysis identified 25 radionuclides in the fuel that are of potential concern (NWMO 2012a). However, parents and progeny of the screened in radionuclides are also included to ensure that ingrowth is properly accounted for in the system model. The radionuclide decay chains included in the radiological assessment are shown in Table 4.2.

**Table 4.2: Radionuclides included in the detailed CC4 radiological assessment**

<b>Single Nuclides</b>		Cl-36, I-129, C-14, Cs-135, Ca-41, Ni-59, Se-79
<b>Chain Nuclides</b>	1	Am-241 → Np-237 → Pa-233 → U-233 → Th-229 → Ra-225 → Ac-225
	2	Pu-242 → U-238 → Th-234 → U-234 → Th-230 → Ra-226 → Rn-222 → Pb-210 → Bi-210 → Po-210
	3	Pu-239 → U-235 → Th-231 → Pa-231 → Ac-227 → Th-227 → Ra-223
	4	Pu-240 → U-236 → Th-232 → Ra-228 → Th-228 → Ra-224
	5	Sn-126 → Sb-126

The impacts of potentially chemically hazardous elements in the fuel are also considered in the Fourth Case Study. Therefore, the reference dataset also includes the properties of more than 80 chemical elements, including their inventories in the fuel. A screening study was carried out to screen out the chemical elements in the fuel that would not be of concern in the postclosure safety assessment (NWMO 2012a).

The screening study identified 16 elements of potential concern, where multiple isotopes of an element are considered as one element. In addition, the element As is added for historical reasons, and Cu is included because the repository holds a large quantity of copper that can corrode in the groundwater, albeit slowly (King 2010), releasing Cu into the buffer porewater. However, some of these screened in elements (i.e., Pb, Ag, and Te) are generated by radioactive decay of parent progeny. Consequently, to ensure that in-growth is properly taken into account, these decay chains are also included in the system model chemical hazard assessment. The chemical elements of potential concern along with the required decay chains are shown in Table 4.3.

**Table 4.3: Potentially chemically hazardous elements and radionuclide decay chains included in the CC4 chemical hazard assessment\***

Elements		As, Ce, Cd, Co, Cr, Cu, Eu, Hg, I, La, Nd, P, Pr, Y
Chain Nuclides	1	Pu-242 → U-238 → Th-234 → U-234 → Th-230 → Ra-226 → Rn-222 → Pb-210 → Bi-210 → Po-210 → Pb
	2	Pu-239 → U-235 → Th-231 → Pa-231 → Ac-227 → Th-227 → Ra-223 → Pb
	3	Pu-240 → U-236 → Th-232 → Ra-228 → Th-228 → Ra-224 → Pb
	4	Pd 107 → Ag
	5	Sn-126 → Te

\*Screened-in elements are shown in blue (see text).

Note that it is the total concentration of a potentially chemically hazardous element in the biosphere that is important for the hazardous substance assessment. For example, for uranium, the total concentration in a particular biosphere medium (e.g., soil or well water) is the sum of the concentrations of all the uranium isotopes in that medium.

All the radionuclides and chemical elements that passed the screening analyses are from the UO<sub>2</sub> fuel matrix. That is, all radionuclides and chemical elements released from the Zircaloy fuel sheath were screened out. Consequently, only UO<sub>2</sub> fuel inventories are listed in Section 4.3.

The data used in the postclosure safety assessment for the radionuclides and chemical elements in Table 4.2 and Table 4.3 are presented in this report.

Similarly, in Appendix G, data for the nuclides identified as important for the inadvertent human intrusion calculations (Medri 2012) are presented. Much of the relevant data for the other nuclides considered in the analyses but not listed in the present report are documented in Gobien and Garisto (2012).

### 4.3 NUCLIDE AND ELEMENT INVENTORIES OF UO<sub>2</sub> FUEL

The radionuclide and chemical element inventories in the fuel, at time of emplacement, will depend on how long it has been since the fuel was discharged from the reactor. In particular, there is significant decay of short-lived radionuclides during this initial period after discharge. Based on system schedule considerations (notably the projected start-up of the repository) as well as engineering design considerations (older fuel produces less thermal power), a minimum fuel age of 30 years has been selected as a design basis. Since we do not know the fuel age distribution at present, for safety assessment purposes we conservatively assume that all fuel is 30-years old at the time of emplacement.

The used fuel radionuclide and chemical element inventories for CANDU fuel of various burnups were calculated by Tait et al. (2000, 2001) using ORIGEN-S. The data of Tait et al. are used to calculate the average radionuclide and chemical element inventories in a container with 360 fuel bundles.

The uncertainties in these inventories are discussed below. It should be noted that what is important is the uncertainties in the average inventories in a container. These uncertainties are much smaller than the uncertainties in the inventories of a single fuel bundle, based on the central limit theorem and the large number of fuel bundles in a container.

The total uncertainty in the average inventories in a container is the sum of

- 1)  $\sigma_{OR}$ , the uncertainties/errors in the inventories calculated by ORIGEN-S for a fuel bundle with a specified burnup and power history, which arise due ORIGEN-S model and input data uncertainties, and
- 2)  $\sigma_{PR}$ , the uncertainties in the inventories arising from the uncertainty in average fuel burnup and fuel power rating of the bundles in container (see below).

The validation of the ORIGEN-S code for predicting radionuclide inventories in CANDU fuel is discussed in Appendix D, based on the work of Tait et al. (1995). Generally, the ORIGEN-S calculated inventories agree well with the measured values, with differences generally well within the measurement uncertainties. Consequently, the uncertainties/errors in the inventories calculated by ORIGEN-S,  $\sigma_{OR}$ , for a fuel bundle with a specified burnup and power history, are set equal to the measurement uncertainties, as discussed in Appendix D.

Nuclide inventories generally increase with fuel burnup (Tait et al. 2000). The distribution of fuel burnups for existing fuel bundles (up to September 2006) from all OPG reactors is shown in Figure 4.1. This distribution was obtained using data from Wilk and Cantello (2006). The average burnup is  $\approx 190$  MWh/kgU (initial U), the median burnup is  $\approx 193$  MWh/kgU, the 95<sup>th</sup> percentile burnup is  $\approx 255$  MWh/kgU, and the standard deviation is about 42 MWh/kgU. However, on a station-specific basis, used fuel from the Pickering A Nuclear Generating Station has the highest average burnup of  $\approx 205$  MWh/kgU, and a 95% percentile burnup of  $\approx 282$  MWh/kgU.

The used fuel disposal container in the Fourth Case Study holds 360 fuel bundles. Each bundle inventory depends on its burnup. The total nuclide inventory in a container can be calculated from the average burnup of the bundles inside it. On average, across the entire repository, the average "container burnup" is the same as the average fuel bundle burnup, or 190 MWh/kgU, and the standard deviation in the average container burnup is about  $42/(360)^{1/2}$  or 2.2 MWh/kgU. However, because individual containers may be filled primarily with bundles from

one station (from logistics considerations), the average burnup in a large group of containers may approach 205 MWh/kgU (e.g., fuel bundles from the Pickering A Nuclear Generating Station). For the Fourth Case Study, the reference container inventories are conservatively calculated for a fuel burnup of 220 MWh/kgU (Tait et al. 2000). Consequently, there is no need to account for the uncertainty in the total inventories in a container due to the small uncertainty in the average container burnup.

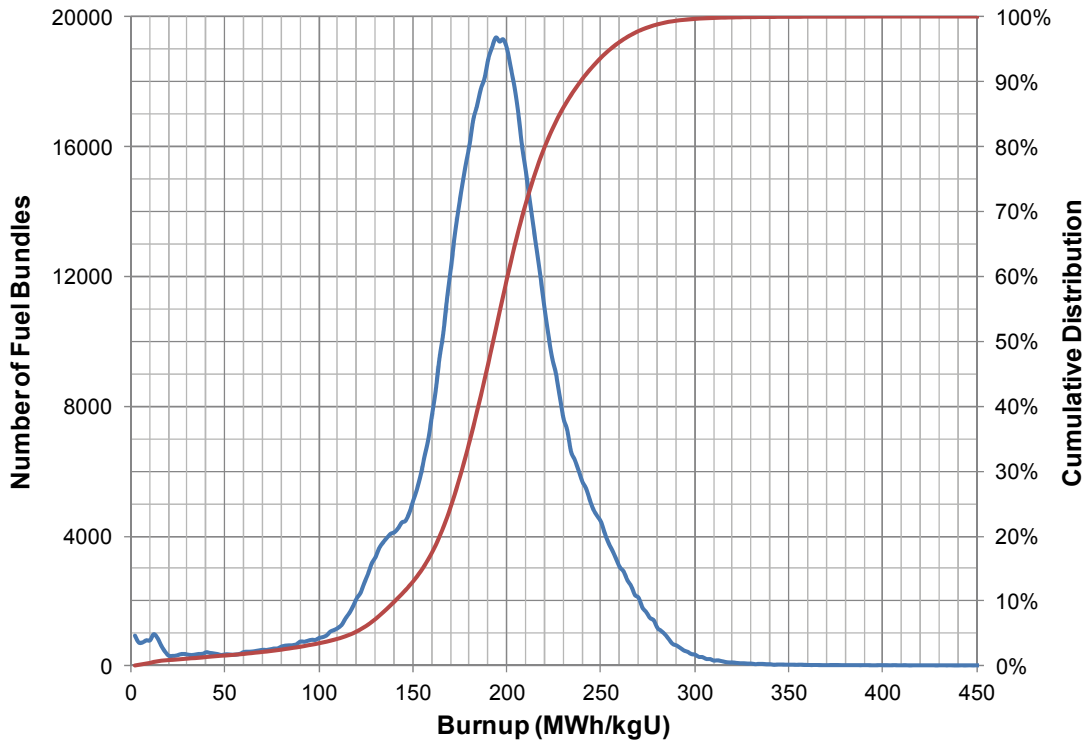


**Figure 4.1: Distribution of burnups and cumulative distribution for all fuel bundles (discharged up to September 2006) for all OPG owned reactors.**

Although the calculated inventories are for a typical fuel power rating of 455 kW/bundle, Tait et al. (2000) show that the inventories of important radionuclides (i.e., the most significant contributors to radiological dose, decay heat or gamma radiation) are not sensitive to this value. In general, the differences in the concentrations of the important radionuclides at the minimum (200 kW/bundle), average (455 kW/bundle) and maximum (900 kW/bundle) powers were less than  $\approx 2\%$ . Thus, based on the central limit theorem, the uncertainty in the total inventory in a container due to the uncertainty in the average fuel power rating (of all bundles in a container),  $\sigma_{PR}$ , would be much smaller.

The radionuclide Cs-135, however, exhibited a substantial inverse dependence on concentration with power. The concentration of Cs-135 at the average power is about 2-fold lower than at the minimum power and about 1.8 times greater than at the maximum power. Since the distribution of bundle power ratings has a standard deviation of approximately 150 kW/bundle (see Figure 4.3), the uncertainty ( $\sigma_{PR}$  in %) in the total inventory of Cs-135 in a

container due to the uncertainty in the average power rating of the fuel bundles in the container is conservatively estimated to be  $150/(360)^{1/2} \cdot 100\%/(455-200) = 3\%$ . This uncertainty is included in the calculation of the total uncertainty in the Cs-135 inventory in a container, as indicated in Table 4.2.

Finally, Tait et al. (2000) calculated inventories using an average bundle burnup calculation. However, elements in each ring of the fuel bundle will see a different neutron flux due to shielding of the surrounding elements, the burnup for each ring will be different. Hence, Tait et al. (2000) examined the differences between the fuel inventories calculated assuming an average fuel bundle burnup and those calculated by summing inventories produced in the individual rings of the fuel bundle. The latter are referred to as the “ring sum” inventories. The analysis indicated that most actinide inventories were under-predicted by the bundle average calculation (Tait et al. 2000, Appendix B). For the actinide radionuclides of most interest (i.e., the most significant contributors to radiological dose, decay heat or gamma radiation), the differences were: Cm-244 ( $\approx 10\%$ ), Am-243 ( $\approx 5\%$ ), Np-239 ( $\approx 5\%$ ), Pu-242 ( $\approx 2\%$ ) and less than 1% higher for the remaining actinides of interest.

The analysis also indicated that for the majority of fission products there was no consistent trend to either under- or over-prediction, and absolute differences between the bundle average and the “ring sum” inventories were  $< 1\%$ .

For the Fourth Case Study, corrections to the inventories calculated by Tait et al. (2000) were made to account for the difference in the bundle average and “ring sum” inventories only if differences exceeded  $+1\%$ . That is, corrections were not made if the bundle average calculation over-predicted the inventory. Corrections were required for the radionuclides Ac-227 (1%), Pa-231 (1.2%), Pu-242 (1.9%) and U-235 (1.7%). A correction was also required for the element Cd (1%).

Table 4.4 lists the radionuclides of interest, their half-lives and their inventories. Table 4.5 lists the chemical elements of interest and their inventories. If an isotope of an element of interest is listed in Table 4.4, then the inventory of the isotope is not included in the inventory of the element listed in Table 4.5. This means that in simulations involving the chemical elements of interest, the isotopes of these elements listed in Table 4.4 must be included in the simulation in order to determine the total element concentration in the environment.

Table 4.4 and Table 4.5 also show the estimated uncertainties in the average inventories in a container arising from the potential differences between ORIGEN-S and measured concentrations,  $\sigma_{OR}$ , which are dominated by the measurement uncertainty, as well as uncertainties arising from the assumptions made by Tait et al. (2000), i.e.,  $\sigma_{PR}$ . Thus, for most nuclides, the overall inventory is modelled as a normal PDF with standard deviation  $\sigma_{Total}$ , and upper and lower bounds set to 5 standard deviations higher and lower than the mean (see Appendix D).

The concentrations of some radionuclides and chemical elements in fuel are affected by the decay of short-lived precursors with relatively large inventories (e.g., Pu-241  $\rightarrow$  Am-241, Pu-238  $\rightarrow$  U-234 and Sm-151  $\rightarrow$  Eu). Since these precursors are not modelled directly in the simulations carried out for the Fourth Case Study, their influence is accounted for by adding the inventory of the precursor to that of the progeny. This affects the inventory of the radionuclides Am-241 and U-234, and the element Eu. Short-lived precursors such as Cm-245 and Am-243 with relatively small inventories are neglected in the simulations.



The inventories of C-14 and Cl-36 in Table 4.4 are not directly from Tait et al. (2000).

The inventory of the activation product C-14 in used fuel was calculated using an N impurity level of 15 µg/g (Tait et al. 2000). The range of measured C-14 concentrations in numerous fuels (Stroes-Gascoyne et al. 1994) is about 0.4 to 1.43 times the ORIGEN-S prediction. Therefore, the C-14 inventory in fuel is described using a uniform distribution with lower and upper bounds equal to 0.4 times and 1.43 times the predicted inventory, and a median value of  $5.6 \times 10^{-6}$  moles/kgU initial.

The inventory of the activation product Cl-36 was calculated using a conservative Cl impurity level of 5 µg/g in used fuel (Tait et al. 2000), leading to an overestimate of the Cl-36 inventory in fuel (Tait et al. 1997). Thus, the Cl-36 inventory is described as a uniform distribution with an upper bound equal to the ORIGEN-S prediction, a lower bound 10 times smaller and a median value of  $5.42 \times 10^{-6}$  moles/kgU initial.

Figure 4.2 shows the total radioactivity of the reference fuel and how it decreases with time. The radioactivity from light element activation and from the Zircaloy cladding is only a small contributor. After a few hundred years, the radioactivity is dominated by the actinides. The radioactivity levels out after about 1 million years. This residual activity is caused by the natural uranium chains remaining in the used fuel.

Radionuclides from the Zircaloy cladding are not included in the Fourth Case Study safety assessment calculations because they were screened out, i.e., their contribution to the total calculated dose rates was small. The low radioactivity in the Zircaloy cladding relative to the fuel itself is demonstrated by the results shown in Figure 4.2.

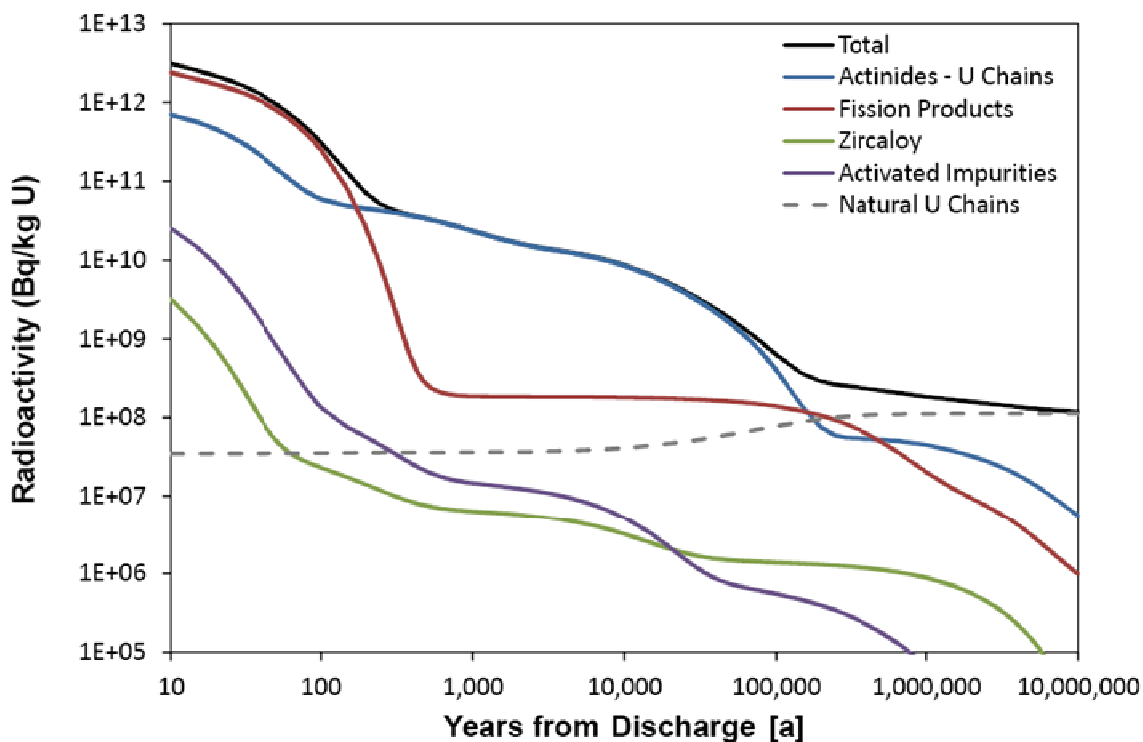


**Figure 4.2: Radioactivity of used fuel (220 MWh/kgU burnup) as a function of time after discharge from reactor. The fission products dominate at short times, but have decayed to low levels after 1000 years. After about 1 million years, the remaining activity is largely that due to the natural uranium content of the fuel.**

Note: The blue line (Actinides – U Chains) shows the radioactivity of all actinides, except the U-238, U-235 and U-234 actinides and their progeny.

**Table 4.4: Inventories of radionuclides of interest in UO<sub>2</sub> fuel for 220 MWh/kgU burnup and 30 years cooling (Tait et al. 2000)**

Nuclide	Half-life <sup>1</sup> [a]	Inventory [moles/kgU initial]	σ <sub>OR</sub> [%]	σ <sub>PR</sub> <sup>2</sup> [%]	σ <sub>Total</sub> <sup>3</sup> [%]
Ac-225	2.738E-02	1.662E-14	-		NA1
Ac-227	2.177E+01	1.573E-11 <sup>#</sup>	2.5		2.5
Am-241	4.326E+02	1.155E-3 <sup>&amp;</sup>	15		15
Bi-210	1.372E-02	5.296E-18	-		NA1
C-14	5.700E+03	5.60E-06	-		NA2
Ca-41	1.020E+05	2.354E-06	7		7.0
Cl-36	3.010E+05	5.42E-06	-		NA2
Cs-135	2.300E+06	2.675E-04	7	3	7.6
I-129	1.570E+07	4.228E-04	7		7.0
Ni-59	7.600E+04	6.438E-06	-		NA3
Np-237	2.144E+06	1.708E-04	20		20
Pa-231	3.276E+04	3.820E-08 <sup>#</sup>	2.5		2.5
Pa-233	7.385E-02	5.901E-12	-		NA1
Pb-210	2.220E+01	8.604E-15	55		55
Pd-107	6.500E+6	6.901E-4	7		7
Po-210	3.789E-01	1.463E-16	-		NA1
Pu-239	2.411E+04	1.123E-02	3		3
Pu-240	6.561E+03	5.339E-03	4		4.0
Pu-242	3.735E+05	4.257E-04 <sup>#</sup>	7		7.0
Ra-223	3.129E-02	2.243E-14	-		NA1
Ra-224	1.002E-02	1.099E-12			NA1
Ra-225	4.079E-02	2.460E-14	-		NA1
Ra-226	1.600E+03	2.354E-12	55		55
Ra-228	5.750	8.370E-13			NA1
Rn-222	1.047E-02	1.541E-17	-		NA1
Sb-126	3.381E-02	2.462E-12	-		NA1
Se-79	2.950E+05	1.762E-05	7		7.0
Sn-126	2.300E+05	5.182E-05	7		7.0
Th-227	5.114E-02	3.620E-14	-		NA1
Th-228	1.912	2.097E-10			NA1
Th-229	7.340E+03	4.783E-09	20		20
Th-230	7.538E+04	1.636E-08	55		55
Th-231	2.911E-03	2.944E-14	-		NA1
Th-232	1.405E+10	2.095E-03	4		4
Th-234	6.598E-02	6.091E-11	-		NA1
U-233	1.592E+05	3.608E-05	20		20
U-234	2.455E+05	2.089E-04 <sup>&amp;</sup>	50		50
U-235	7.038E+08	7.238E-03 <sup>#</sup>	2.5		2.5
U-236	2.342E+07	3.501E-03	4		4
U-238	4.468E+09	4.125E+00	0		0

<sup>#</sup>Median value from Tait et al. increased to account for “ring sum” correction: Ac-227 (1%), Pa-231 (1.2%), Pu-242 (1.9%) and U-235 (1.7%) (Appendix B, Tait et al. 2000).

<sup>&</sup>Includes inventory of short-lived precursor: Am-241 (Pu-241, 2.737E-4 mol/kgU) and U-234 (Pu-238, 2.259E-5 mol/kgU). Since the uncertainty is expressed as a percentage, it is affected by addition of the precursor inventory.

<sup>1</sup>Half-life from ENDF/B VII.1 (Chadwick et al. 2011) converted, if needed, using 365.25 days = 1 year.

<sup>2</sup>Uncertainty in the radionuclide inventory in a container due to uncertainty in power rating of the fuel in a container is important only for Cs-135, as indicated in text.

<sup>3</sup>NA1 = Nuclide assigned a constant inventory because it has a short half-life.

NA2 = Nuclide inventory is assigned a uniform distribution (see text). For C-14, the inventory is between  $2.45 \times 10^{-6}$  and  $8.75 \times 10^{-6}$  moles/kgU and for Cl-36 the inventory is between  $9.86 \times 10^{-7}$  and  $9.86 \times 10^{-6}$  moles/kgU. Table shows the median value, which is not from Tait et al. (2000).

NA3 = Nuclide assigned a constant inventory because it is formed by activation of impurity in the fuel, and impurity levels were assigned high values in Tait et al. (2000).

**Table 4.5: Inventories of chemical elements of interest in UO<sub>2</sub> fuel for 220 MWh/kgU burnup and 30 years cooling (Tait et al. 2000)**

Element or Nuclide	Main Source <sup>1</sup> or Half-life [a]	Inventory <sup>2</sup> [moles/kgU initial]	$\sigma_{OR}$ [%]	$\sigma_{PR}$ <sup>3</sup> [%]	$\sigma_{Total}$ <sup>4</sup> [%]
Ag	FP	3.348E-4	7		7.0
As	Imp	4.024E-5	-		NA1
Cd	FP	1.928E-4 <sup>#</sup>	7		7.0
Ce	FP	4.766E-3	7		7.0
Co	Imp	3.099E-4			NA1
Cr	Imp	9.635E-4	-		NA1
Eu	FP	1.895E-4 <sup>&amp;</sup>	6.5		6.5
Hg	Imp	6.719E-6	-		NA1
I	FP	1.144E-4	7		7.0
La	FP	2.459E-03	7		7.0
Nd	FP	7.562E-03	7		7.0
P	Imp	1.935E-3	-		NA1
Pb	Imp	4.824E-4	-		NA
Pr	FP	2.181E-3	7		7.0
Te	FP	1.048E-3	7		7.0
Y	FP	1.327E-3	7		7.0

<sup>&</sup>Inventory of short-lived precursor added to that of progeny: Eu (Sm-151, 1.455E-5). Since the uncertainty is expressed as a percent, it is affected by addition of the precursor inventory.

<sup>#</sup>Median value in Tait et al. increased to account for "ring sum" correction: Cd (1%).

<sup>1</sup>Source of chemical element in fuel is either fission product (FP) or impurity in fuel (Imp).

<sup>2</sup>Inventory does not include the inventory of isotopes of the element listed in Table 4.4.

<sup>3</sup>Uncertainty in the inventory of a chemical element in a container due to the uncertainty in the power rating of the fuel in a container is small, as indicated in text.

<sup>4</sup>NA1 = Nuclide assigned a constant inventory because it is formed by activation of impurity in the fuel, and impurity levels were assigned high values in Tait et al. (2000).

#### 4.4 INSTANT RELEASE FRACTION

Radionuclides are released from used fuel by two processes - instant release and congruent dissolution release. Instant release is the rapid release of nuclides on contact of the used fuel with water. Congruent dissolution is the slower release of nuclides as the matrix material itself (either the  $\text{UO}_2$  fuel or the Zircaloy cladding) dissolves.

The instant release process considers any radionuclide (or chemical element) inventory in the fuel-cladding gap or in the  $\text{UO}_2$  fuel grain boundaries to be quickly exposed to water and to dissolve into the water. The degree of segregation of the various radionuclides (or chemical elements) is highly dependent on fuel operating parameters such as linear power rating and burnup, as well as on the properties of the radionuclides (or chemical elements).

The amount of a chemical element (or radionuclide) that is susceptible to instant release is defined as a fraction of the total inventory of that chemical element (or radionuclide) within the fuel. The IRF data are given in Table 4.6. The range of values in the data allow for uncertainties. Radionuclides of the same element are all assumed to have the same IRF. The sources of the IRF data are described below.

The instant release fraction (IRF) data for key elements such as I, Sr, and Cs, are based on the work of Stroes-Gascoyne (1996). The IRFs of these key elements were reviewed for the Fourth Case Study, including the possible implications of newer non-CANDU data (Johnson et al. 2004, 2005; SKB 2010). However, for CANDU fuel, Stroes-Gascoyne (1996) remains the best data source.

Stroes-Gascoyne (1996) found that the IRF for Cs can be described using a normal distribution with mean 0.039 and standard deviation 0.019. The IRF for I can be described using a normal distribution with mean 0.036 and standard deviation 0.024. This is higher than the IRF used by SKB for LWR fuel (SKB 2010).

The fuels used in the experiments of Stroes-Gascoyne (1996) had burnups and (peak) linear power ratings (LPRs) that were generally higher than those expected for typical CANDU fuel. For example, about 14% of CANDU fuel bundles have peak LPRs greater than 42 kW/m (see Figure 4.3, data from Wilk and Cantello 2006), whereas in the work of Stroes-Gascoyne 57% of the fuels had peak LPRs greater than 42 kW/m. Thus, her measured IRFs should be conservative, based on the relationship between fission gas releases and LPR, as described below.

Generally fission (noble) gas releases from CANDU fuel bundles are low if the peak linear power rating of the fuel is less than about 42 kW/m, and increase with LPR for LPR values above 42 kW/m (Floyd et al. 1992), as illustrated in Figure 4.4. (A threshold for fission gas release has also been found for BWR fuel (Kamimura 1992).)

For LWR fuel, fission gas releases are independent of fuel burnup for burnups less than about 1000 MWh/kgU and then increase with burnup (Johnson et al. 2004). Since CANDU burnups are much lower than 1000 MWh/kgU and there is no correlation between fuel burnup and LPR, fission gas releases from CANDU fuels are not correlated to fuel burnup.

**Table 4.6: Instant release fractions for CANDU fuel**

Element	PDF Type	PDF Attributes*	PDF Bounds
Ac	constant	0.	n/a
Ag	uniform	(0.0,0.001)	n/a
Am	constant	0.	n/a
As	normal	(0.006,0.0015)	0.0023, 0.03
Bi	normal	(0.006,0.0015)	0.0023, 0.03
C	normal	(0.027, 0.016)	0.0005, 0.075
Ca	constant	0.	n/a
Cd	normal	(0.006,0.0015)	0.0023, 0.03
Ce	constant	0.	n/a
Cl	normal	(0.06, 0.01)	0.01, 0.2
Co	uniform	(0.0,0.001)	n/a
Cr	constant	0.0	n/a
Cs	normal	(0.04, 0.01)	0.015, 0.20
Eu	constant	0.	n/a
Hg	normal	(0.04, 0.01)	0.015, 0.20
I	normal	(0.04, 0.01)	0.015, 0.20
La	constant	0.	n/a
Nd	constant	0.	n/a
Ni	uniform	(0.0,0.001)	n/a
Np	constant	0.	n/a
P	normal	(0.006,0.0015)	0.0023, 0.03
Pa	constant	0.	n/a
Pb	normal	(0.006,0.0015)	0.0023, 0.03
Pd	lognormal	(0.01, 2)	0.0005, 0.05
Po	normal	(0.04, 0.01)	0.015, 0.20
Pr	constant	0.	n/a
Pu	constant	0.	n/a
Ra	normal	(0.025, 0.008)	0.001, 0.05
Rn	normal	(0.04, 0.01)	0.015, 0.20
Sb	normal	(0.006,0.0015)	0.0023, 0.03
Se	normal	(0.006,0.0015)	0.0023, 0.03
Sn	uniform	(0.0,0.001)	n/a
Te	normal	(0.006,0.0015)	0.0023, 0.03
Th	constant	0.	n/a
U	constant	0.	n/a
Y	constant	0.	n/a

\*PDF attributes are (mean, standard deviation) for the normal PDF, and (geometric mean, geometric standard deviation) for the lognormal PDF and (lower limit, upper limit) for the uniform PDF.

Since iodine and cesium behave like the noble gases (Iglesias et al. 2011), the I and Cs gap inventories should depend similarly on the fuel LPR. This is illustrated by the plotting the IRFs for I and Cs (i.e., the sum of the gap and grain boundary inventories) versus the peak LPR, as shown in Figure 4.5. Because of the scarcity of data at low LPRs, no attempt was made to calculate an average Cs (or I) IRF for the 360 fuel bundles in a fuel container from the distribution of bundle linear powers. Rather, the mean IRFs derived by Stroes-Gascoyne (1996), i.e., using unweighted averages, are used in the assessment. These are expected to be conservative given the relatively large number of high peak LPR fuels used by Stroes-Gascoyne (compare Figures 4.3 and 4.5).

The standard deviations in the IRFs found by Stroes-Gascoyne (1996) reflect mainly the differences between the 14 different fuels used in her experiments. For a large quantity of fuel (i.e., the 360 fuel bundles in a used fuel container), the standard deviation for the average IRF would be much smaller. For example, the standard deviation for the IRF of I associated with having 360 bundles in a container, assuming that the measured variability is randomly distributed between fuel bundles, is  $0.024/(360)^{1/2} = 0.0013$ . However, the measured variability may include systematic biases and not just random measurement uncertainty; therefore, the standard deviation for the average IRF for the fuel in a container has been set to a nominal value of 0.01.

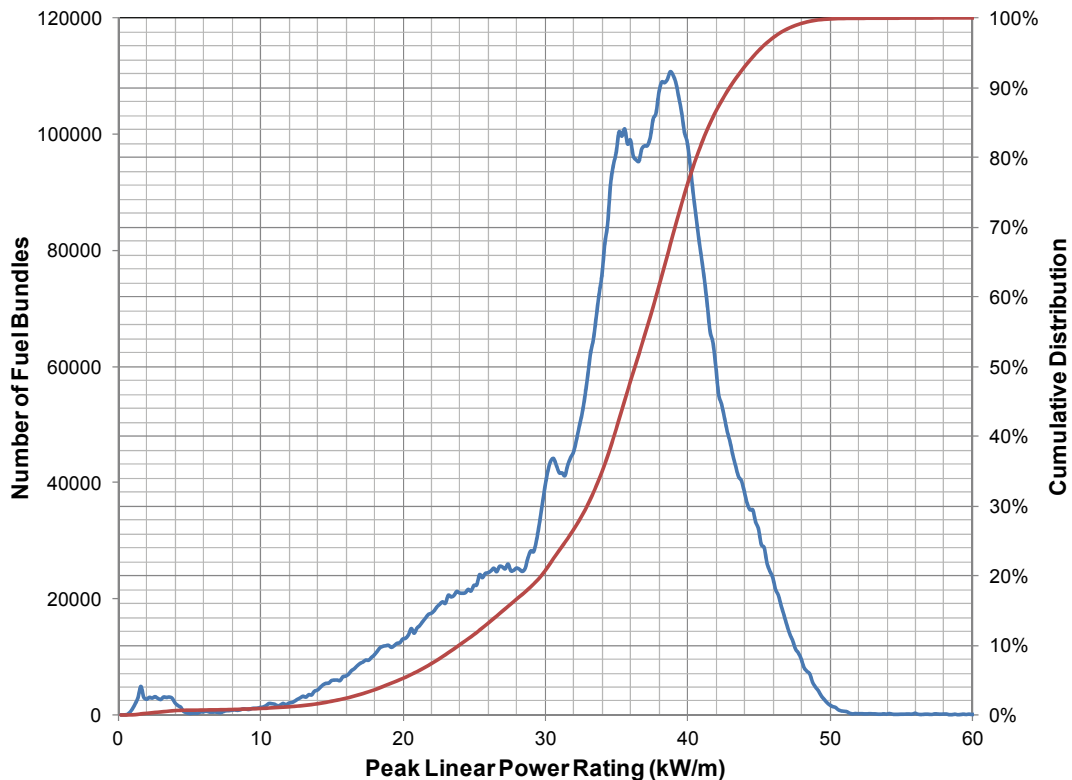


**Figure 4.3: Distribution of maximum linear power ratings and cumulative distribution for all fuel bundles (discharged up to September 2006) from all OPG owned reactors. The standard deviation of the distribution is approximately 7.7 kW/m or, for a Bruce bundle, approximately 140 kW/bundle.**

In summary, for the Fourth Case Study, we assume that the IRF for Cs and I are described by a normal distribution with mean 0.04 and standard deviation 0.01. The limits of the distribution are set at 0.015 to 0.20. The minimum value corresponds approximately to the smallest IRF measured by Stroes-Gascoyne (1996) and the maximum value corresponds approximately to the calculated fission gas release from a high power rating/high burnup fuel (Iglesias et al. 2011).

The IRF for Cl is derived from the Cl-36 release data of Tait et al. (1997), who suggest that most of the Cl-36 in the fuel originates from the fuel-cladding gap and that little is present in the grain boundaries. The IRF for Cl increases with both the peak LPR and burnup (BU) of the fuel (see Figure 4.6). Thus, one could in theory use the relationship in Figure 4.6 along with the distribution of peak LPRs (Figure 4.3) to obtain the average expected Cl-36 IRF from all fuel bundles. However, the data of Tait et al. are limited (i.e., most data are for low LPR, low BUs or for high LPR, high BU fuels) and so the relationship shown in Figure 4.6 may not be generally applicable. Hence, a conservative estimate of the Cl-36 IRF was made assuming, based on Tait et al. (1997), that fuels with low peak LPR (< 40 kW/m), low BU (<190 MWh/kgU); intermediate LPR, intermediate BU; and high LPR (> 43 kW/m) or high BU (> 230 MWh/kgU) have Cl-36 IRFs of 0.7%, 4.5% and 15%, respectively. Using the distribution of fuel LPR and burnup data for the Pickering Nuclear Generating Station (for which LPRs and, hence, IRFs are the highest), the calculated Cl-36 IRF is 0.06. Therefore, the IRF for Cl-36 is described as a normal distribution with mean 0.06 and standard deviation of 0.01. This standard deviation accounts for the large quantity of fuel in a used fuel container, as discussed above for I and Cs. The limits of the distribution are set at 0.01 to 0.2, the approximate limits of the IRF data measured by Tait et al. (1997).

Sr-90 is not a radionuclide of concern for the Forth Case Study (NWMO 2012a). However, Sr is used as a chemical analog for other alkaline earth elements (e.g., Ca) so its IRF is relevant. Stroes-Gascoyne (1996) measured releases of Sr-90 from crushed CANDU fuel samples to derive the IRF of Sr-90. The IRF of Sr-90 was independent of the fuel power or burnup. Based on her data, the IRF of Sr can be described by a normal distribution with a mean of 0.025, a standard deviation of 0.008, and a maximum IRF of about 0.05.

Since Sr is mainly dissolved in the fuel matrix (Kleykamp 1985), segregation of Sr to the grain boundaries of the fuel is not expected. The measurements show otherwise. Segregation of the short-lived parents of Sr-90 has been proposed to explain why segregation of Sr-90 occurs in fuel (Stroes-Gascoyne 1996).

For CANDU fuel, Stroes-Gascoyne et al. (1994) measured C-14 releases from crushed fuel samples. No correlation of total C-14 release with fuel burnup or power rating was observed. The mean release from the fifteen fuel samples was 0.027, with a standard deviation of 0.016.

Technetium is used as an analog for other elements so its instant release fraction is important for the Fourth Case Study. Technetium is not soluble in the UO<sub>2</sub> fuel and is present in used fuel in metallic form, typically in alloy inclusions (Kleykamp 1985). The results of leaching studies indicate that Tc gap and grain boundary releases are generally small, i.e., < 0.002 (Johnson and Tait 1997, Garisto and Gierszewski 2002). This may be due to the insolubility of the alloy inclusions in which Tc is found. The highest Tc releases, up to 5%, were observed in studies involving leaching of CANDU fuel that was oxidized in air to U<sub>3</sub>O<sub>8</sub> powder (Stroes-Gascoyne and Sellinger 1986). Although such conditions are not representative of fuel under repository conditions, they may provide a better estimate of the total grain boundary inventory of Tc.



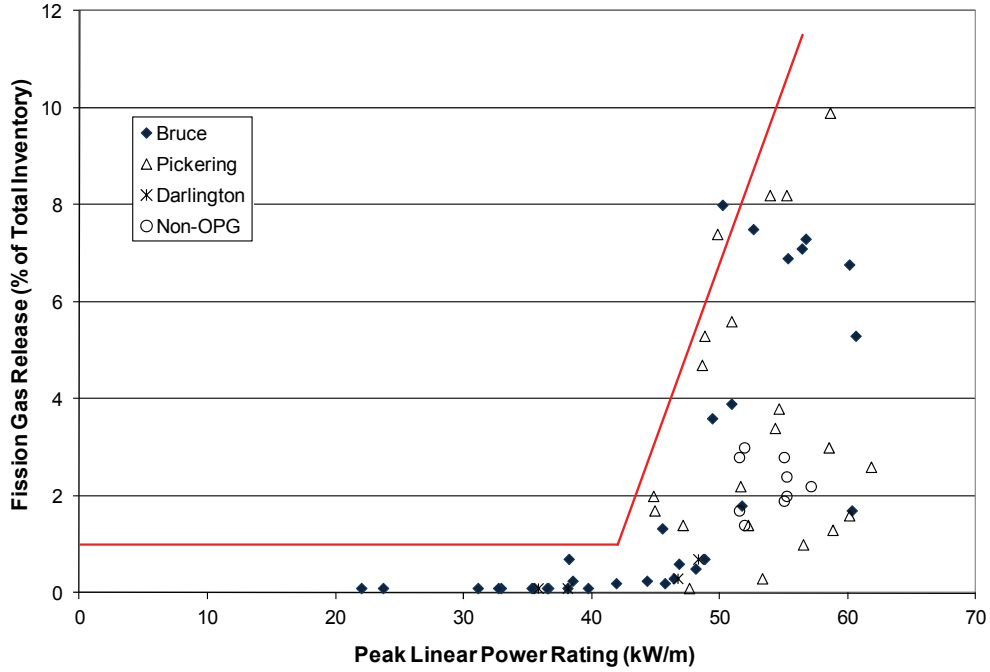


Figure 4.4: Fission gas (gap) release as a function of peak linear power rating for CANDU fuels with burnups less than 400 MWh/kgU

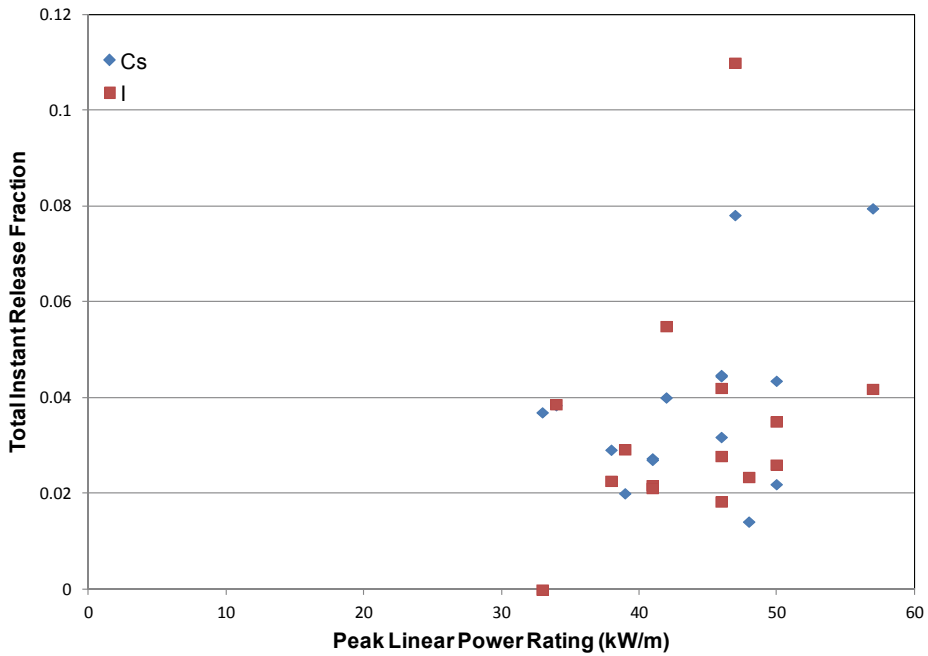
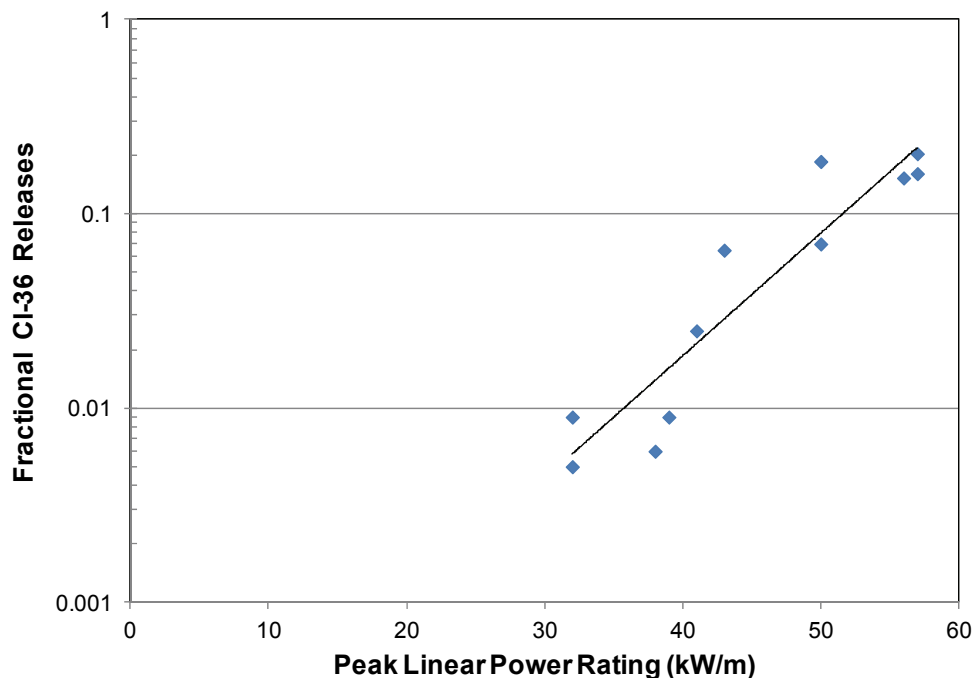


Figure 4.5: Total instant release fractions (=gap + grain boundary inventories) for iodine and cesium (data from Stroes-Gascoyne 1996)



**Figure 4.6: CI-36 releases from CANDU fuel (data from Tait et al. 1997)**

The Tc IRF is taken from the review of Garisto and Gierszewski (2002). Their Tc IRF is lognormally distributed with a geometric mean of 0.01 and a geometric standard deviation of 2. This IRF is larger than that used by SKB in their SR-Site safety assessment (SKB 2010) since it is based on results of leaching experiments with both slightly preoxidized ( $\text{UO}_{2+x}$ ,  $x < 0.25$ ) and non-oxidized CANDU fuels. This larger value was selected to account for the uncertainty in the amount of Tc that could be leached from the fuel grain boundaries over hundreds of years.

The IRFs of all actinides and lanthanides are taken to be zero, as in other studies (Johnson et al. 2004), since they form non-volatile oxides that are dissolved within the  $\text{UO}_2$  fuel matrix.

The IRFs for the elements Sn and Se have not been measured for CANDU fuels. Wilson (1990a, 1990b) attempted to measure the IRFs of Se-79 and Sn-126 for LWR fuels. However, the amount leached was less than the detection limit. From the “less than” data reported by Wilson, it is possible to infer maximum IRFs (Johnson et al. 2004, SKB 2010).

For Se, a semi-volatile element that is non-soluble in the  $\text{UO}_2$  fuel, the maximum IRF is less than 15% of the fission gas release. Such a low IRF suggests that Se is not volatile in the fuel. Perhaps Se forms alloys in the fuel, e.g., BaSe, as suggested by Iglesias et al. (2011). For the Fourth Case Study, the IRF of Se is set equal to 15% of the IRF of I and Cs (following SKB 2010). Thus, the IRF for Se is described by a normal distribution with mean 0.006 and standard deviation 0.0015. The limits of the distribution are set at 0.0023 to 0.03.

For Sn, a non-volatile element that is expected to be present as a metallic precipitate in used fuel (Kleykamp 1985), the maximum IRF, based on the “less than” values from Wilson (1990a, 1990b) is low, i.e., less than 0.0001. Given the uncertainties in the experiments, the differences between CANDU and LWR fuels and the fact that Sn is used as an analog for other elements

(see below), it is conservatively assumed in the Fourth Case Study that the IRF for Sn is described by a uniform distribution from 0.0 to 0.001, with a median value of 0.0005.

For the many chemical elements for which leaching measurements are not available, the only basis for estimating the IRFs are the diffusion coefficients of the elements in fuel and the chemistry of the elements in fuel. For example, an understanding of which elements form solid solutions with  $\text{UO}_2$  and which elements form metallic or oxide precipitates in fuel would be important (Kleykamp 1985). This methodology is used to conservatively estimate the IRFs of elements for which measured data are not available.

Generally, fission products can be classified into 4 groups (Kleykamp 1985):

1. Gases and other volatiles:  
Kr, Xe, Br, I
2. Fission products forming metallic precipitates:  
Mo, Tc, Ru, Rh, Pd, Ag, Cd, In, Sn, Sb, Te
3. Fission products forming oxide precipitates (often referred to as the "grey phase"):  
Rb, Cs, Ba, Zr, Nb, Mo, Te
4. Fission products dissolved in the fuel matrix:  
Sr, Zr, Nb, Rare Earths, Y, La, Ce, Pr, Nd, Pm, Sm

Some elements fall into two categories. There is a continuous transition between categories 2 and 3 due to the similar oxygen potential of some fission product oxides and fuel, which changes composition during irradiation. Transitions can also occur between categories 3 and 4 due to the burnup dependent distribution of cations in both oxide phases. Furthermore, some fission products can react without participation of oxygen (e.g.,  $\text{Cs}_2\text{Te}$ ,  $\text{CsI}$ , etc.).

The key thermodynamic factor that influences the chemical state of the fission products in fuel is the oxygen potential, which in turn depends on the stoichiometry of the fuel, the temperature and burnup. The fuel is initially stoichiometric, i.e., the oxygen potential is very low (Lindemer and Besmann 1985), but burnup raises the O/U value because the  $\text{O}_2$  released by fission of uranium cannot be completely bonded by the generated fission products (Cordfuncke and Konings 1988). For near-stoichiometric fuels, the oxidation potential in the fuel may be buffered by the Mo/ $\text{MoO}_2$  couple (Kleykamp 1985, Cubicciotti and Sanecki 1978), since this couple has an oxidation potential that is similar to that of slightly hyperstoichiometric fuel and the fission yield of Mo is relatively high.

The oxidation potential for formation of the oxide of each element, relative to the oxidation potential of the fuel, was used to assess the chemical state of the elements in fuel (Kleykamp 1985) and, thence, to estimate the instant release fractions of the elements for which no measured values are available. For an element for which measured IRFs are not available, the rationale for the selected instant release fraction is provided in Table 4.7.

**Table 4.7: Rationale for selection of instant release fractions for elements with no measured data**

Element	Chemical State of Element in Fuel	Element Boiling Point (K)	Rationale for Selected Instant Release Fraction
Ac, Am, Np, Pa, Pu, Th, U	Oxides dissolved in the fuel matrix	-----	Actinides are present in solid solution in the fuel matrix. Assume IRF=0 for all actinides (Johnson and Tait 1997)
Ag	Metallic precipitate alloyed with other noble metals such as Cd and Sn (Kleykamp 1985).	2435	Boiling point of Ag is similar to that of Sn (2875 K). Since Ag is likely alloyed with Sn and other similar metals in fuel, assume IRF for Ag is the same as that for Sn.
As	In elemental form in fuel	887	Boiling point of As is similar to that of Se (958 K), so assume IRF of As is that same as that of Se.
Bi	Metallic precipitate in fuel	1837	Boiling point of Bi is lower than that of Sn (2875 K) and higher than that of Se (958 K). For conservatism, assume IRF is same as that of Se.
Ca	Oxide in fuel. CaO is soluble in fuel matrix	-----	CaO is likely present in solid solution in the UO <sub>2</sub> fuel matrix, so the IRF of Ca is set to zero.
Cd	Metallic precipitate in fuel, alloyed with, e.g., Ag, Sn and Pd.	1040	Boiling point of Cd is similar to that of Se (958 K), so assume IRF of Cd is that same as that of Se.
Ce, Eu, La, Nd, Pr	Oxides dissolved in the fuel matrix	-----	Lanthanides are present in solid solution in the fuel matrix. Assume IRF=0 for all lanthanides (Johnson and Tait 1997)
Co	Metallic precipitate in fuel.	3200	Boiling point of Co is somewhat higher than that of Sn (2875 K); but, for conservatism, assume IRF for Co is the same as that for Sn.
Cr	Oxide in fuel, Cr <sub>2</sub> O <sub>3</sub> , with limited solubility in UO <sub>2</sub> (0.06 wt% at 1600°C).	-----	The amount of Cr in fuel does not exceed the solubility limit of Cr <sub>2</sub> O <sub>3</sub> in fuel; therefore Cr is likely present in solid solution in the UO <sub>2</sub> fuel matrix and so the IRF of Cr is set to zero.
Hg	Metallic precipitate in fuel, alloyed with other elements	630	The volatility of Hg is quite high at the temperature of fuel in the reactor; therefore, assume IRF is similar to that of noble gases such as Rn.
Ni	Metallic precipitate in fuel.	3186	Boiling point of Ni is somewhat higher than that of Sn (2875 K); but, for conservatism, assume IRF for Ni is the same as that for Sn.
P	Chemistry of P in fuel is uncertain. Phosphates could form in fuel, perhaps in the grey phase (Kleykamp 1985).	-----	Assume P behaves like As, another Group VB element, in fuel; so, IRF of P is set equal to that of As.

Pb	Metallic precipitate in fuel	2022	Boiling point of Pb is lower than that of Sn (2875 K) and higher than that of Se (958 K). For conservatism, assume IRF is same as that of Se.
Pd	Metallic precipitate alloyed with a wide variety of metals in fuel, e.g., found in epsilon particles with Tc, Ru, Rh and Mo.	3236	Assume same IRF of Pd is the same as for Tc, since found in grain boundaries of fuel alloyed with Tc in epsilon particles.
Po	Chemistry is similar to that of Bi and Te.	-----	Po has only short-lived isotopes, so for conservatism assume that IRF of Po is the same as for noble gases such as Rn.
Ra	Oxide in fuel.	-----	Ra is likely dissolved in the fuel matrix. However, for conservatism, assume Ra behaves like Sr in fuel, since both are alkaline earth elements. Thus, assume IRF of Ra is the same as that of Sr.
Rn	Non-reactive gas	-----	Rn is a noble gas. The IRFs of the Cs, I and the noble gases are similar. Therefore, IRF for Rn is set equal to that of Cs or I.
Sb	Metallic precipitate alloyed with Pd, Sn and other metals	1860	Boiling point of Sb is lower than that of Sn (2875 K) and higher than that of Se (958 K). For conservatism, assume IRF is same as that of Se.
Te	Chemistry of Te is complex – it dissolves in UO <sub>2</sub> , forms alloys with Pd and Sn, forms oxide precipitates (e.g., BaTeO <sub>3</sub> ) and forms non-oxide compounds (e.g., Cs <sub>2</sub> Te) (Kleykamp 1985).	1261	Assume Te behaves similarly to Se in the fuel. Therefore, the IRF of Te is set equal to that of Se.
Y	Oxide in fuel, dissolved in UO <sub>2</sub> fuel matrix	-----	Y is present in solid solution in the fuel matrix. Assume IRF=0 for Y (Johnson and Tait 1997)

## 4.5 FUEL DISSOLUTION RATE

The UO<sub>2</sub> ceramic fuel matrix is durable, and dissolves slowly in water. The most important factor in the rate of dissolution of UO<sub>2</sub> in water is the redox conditions in the surrounding groundwater. Reducing conditions are expected to prevail in and around the container under the influence of the reducing groundwater, and consumption of any residual oxygen by reaction with the copper and steel container materials or with ferrous and organic material in the sealing materials. Under these reducing conditions, the UO<sub>2</sub> fuel would dissolve very slowly.

However, the conditions at the used fuel surface are likely to be oxidizing for a long time due to the production of oxidants in the water from radiolysis (Poinsot et al. 2005). (This water would have reached the fuel only after failure of the container and fuel cladding.) Radiolysis of the groundwater would be caused by the  $\alpha$ -,  $\beta$ -, and  $\gamma$ -radiations emitted by the used fuel, at rates that depend on the radiation type and that generally decrease with time as the radiation field strengths decrease (Garisto et al. 2009).

For the Fourth Case Study, an empirical model for radiolysis-driven dissolution is used. In this approach, the rates of dissolution of the used fuel matrix due to  $\alpha$ -,  $\beta$ - and  $\gamma$ -radiolysis are assumed proportional to the corresponding dose rates, i.e.,

$$R_{\alpha} = A_{\text{cont}} G_{\alpha} f_{\alpha} [D_{\alpha}(t+t_C)]^{a\alpha} \quad (4.1)$$

$$R_{\beta} = A_{\text{cont}} G_{\beta} f_{\beta} [D_{\beta}(t+t_C)]^{a\beta} \quad (4.2)$$

$$R_{\gamma} = A_{\text{cont}} G_{\gamma} f_{\gamma} [D_{\gamma}(t+t_C)]^{a\gamma} \quad (4.3)$$

with the exponents  $a\alpha = a\beta = a\gamma = 1$ . The total matrix dissolution rate,  $R_{\text{TOT}}$ , is given by

$$R_{\text{TOT}} = R_{\alpha} + R_{\beta} + R_{\gamma} + R_{\text{ch}} * A_{\text{cont}} \quad (4.4)$$

where

- $R_{\alpha}$ ,  $R_{\beta}$ , and  $R_{\gamma}$  are the dissolution rates ( $\text{mol}_U \cdot \text{a}^{-1}$ ) due to  $\alpha$ -,  $\beta$ - and  $\gamma$ -radiation;
- $R_{\text{ch}}$  is the chemical fuel dissolution rate, i.e., the dissolution rate of the fuel in the absence of radiolysis ( $\text{mol}_U \cdot \text{m}^{-2} \cdot \text{a}^{-1}$ );
- $R_{\text{TOT}}$  is the total dissolution rate ( $\text{mol}_U \cdot \text{a}^{-1}$ );
- $D_{\alpha}(t+t_C)$ ,  $D_{\beta}(t+t_C)$  and  $D_{\gamma}(t+t_C)$  are the time-dependent dose rates ( $\text{Gy} \cdot \text{a}^{-1}$ );
- $t$  is the time after placement of the fuel in the repository;  $t_C$  is the age of the fuel at the time of placement in the repository (i.e., the time between fuel removal from reactor and its placement in the repository) (years);
- $G_{\alpha}$ ,  $G_{\beta}$  and  $G_{\gamma}$  are empirical rate constants for fuel dissolution in the presence of alpha, beta and gamma radiation fields, respectively ( $\text{mol}_U \cdot \text{m}^{-2} \cdot \text{Gy}^{-1}$ );
- $f_{\alpha}$ ,  $f_{\beta}$  and  $f_{\gamma}$  are the alpha, beta and gamma dose variability factors; and
- $A_{\text{cont}}$  is the effective surface area of the dissolving fuel, per container ( $\text{m}^2$ ).

The model and the derivation of the model parameter values are described in more detail in Appendix E. The parameter values recommended for the Fourth Case Study are summarized in Table 4.8 and Table 4.9.

**Table 4.8: Radiation doses at fuel surface (220 MWh/kgU)<sup>#</sup>**

Time After Fuel Discharge (years)	Alpha Dose Rate (Gy/a)	Beta Dose Rate (Gy/a)	Gamma Dose Rate (Gy/a)
10	1.42E+06	3.77E+06	7.11E+05
20	1.72E+06	2.82E+06	5.30E+05*
30	1.89E+06	2.20E+06	3.95E+05*
40	1.99E+06	1.72E+06	2.95E+05*
50	2.03E+06	1.35E+06	2.20E+05
60	2.05E+06	1.06E+06	1.74E+05*
75	2.04E+06	7.38E+05	1.23E+05*
100	2.00E+06	4.04E+05	6.87E+04
150	1.88E+06	1.24E+05	2.16E+04*
200	1.77E+06	3.96E+04	6.80E+03
300	1.58E+06	6.66E+03	1.02E+03*
500	1.30E+06	2.69E+03	22.8
1,000	9.03E+05	1.53E+03	15.5
10,000	3.21E+05	3.78E+02	16.5
100,000	1.80E+04	1.68E+02	28.4
1,000,000	6.24E+03	1.49E+02	38.4
10,000,000	4.19E+03	1.15E+02	35.8

<sup>#</sup>Data from Garisto et al. (2009)

\*Interpolated values assuming exponentially decaying function.

**Table 4.9: Used fuel dissolution rate parameters (see Appendix E)**

<b>Parameter</b>	<b>Best-estimate or median value</b>	<b>PDF<sup>1</sup></b>
Fuel surface area per container	1570 m <sup>2</sup>	Lognormal PDF with GM=1570 m <sup>2</sup> , GSD = 3, bounds of 340 and 7860 m <sup>2</sup>
Alpha, beta and gamma dose rates	Table 4.8	Variability included separately through the $f_{\alpha}$ , $f_{\beta}$ and $f_{\gamma}$ factors
Alpha dose rate variability factor, $f_{\alpha}$	1.0	Triangular PDF with bounds of 0.80 and 1.20
Beta dose rate variability factor, $f_{\beta}$	1.0	Triangular PDF with bounds of 0.80 and 1.20
Gamma dose rate variability factor $f_{\gamma}$ factor	1.0	Triangular PDF with bounds of 0.80 and 1.20
Age of fuel at time of emplacement, $t_c$	30 years	Design basis
$G_{\alpha}$	$1.4 \times 10^{-10}$ mol·m <sup>-2</sup> ·Gy <sup>-1</sup>	Lognormal PDF with GM= $1.4 \times 10^{-10}$ mol·m <sup>-2</sup> ·Gy <sup>-1</sup> , GSD = 6.0, bounds of $3.5 \cdot 10^{-12}$ and $2.1 \cdot 10^{-9}$ mol·m <sup>-2</sup> ·Gy <sup>-1</sup>
$G_{\beta}$ and $G_{\gamma}$	$1.1 \times 10^{-9}$ mol·m <sup>-2</sup> ·Gy <sup>-1</sup>	Loguniform PDF with bounds of $3.7 \times 10^{-11}$ and $3.3 \times 10^{-8}$ mol·m <sup>-2</sup> ·Gy <sup>-1</sup>
Chemical dissolution rate	$4.0 \times 10^{-7}$ mol·m <sup>-2</sup> ·a <sup>-1</sup>	Loguniform PDF with bounds of $4.0 \times 10^{-8}$ and $4.0 \times 10^{-6}$ mol·m <sup>-2</sup> ·a <sup>-1</sup>

<sup>1</sup> GM = Geometric mean, GSD = Geometric standard deviation.



## 5. CONTAINER

### 5.1 CONTAINER DIMENSIONS

The used fuel container design is illustrated in Figure 5.1. The main properties needed here are summarized in Table 5.1 and Table 5.2. The Fourth Case Study reference container design has changed to the IV-25 container which holds 360 bundles as opposed to the IV 324-hex design used in the Third Case Study.

The outer container shell is made from oxygen-free low-phosphorous copper. The main structural support is provided by a thick carbon steel inner vessel. Inside this vessel are carbon steel baskets holding the used fuel bundles.

**Table 5.1: Container internal parameters**

Parameter	Reference Value	Comments
Total number of fuel bundles in container	360	SNC Lavalin (2011)
Mass U in container	6.93 Mg	360 bundles x 19.25 kgU/bundle (pre-irradiation value) (Tait et al. 2000)
Inner vessel diameters	1.195 and 0.990 m, outer and inner	SNC Lavalin (2011)
Inner vessel length	3.700 and 3.360 m, outer and inner	SNC Lavalin (2011)
Inner vessel internal volume	2.59 m <sup>3</sup>	Volume is $(\pi \cdot 0.990^2 / 4) \cdot (3.360) = 2.59 \text{ m}^3$
Internal void volume	1.58 m <sup>3</sup>	Inner vessel volume 2.59 m <sup>3</sup> minus 0.9 m <sup>3</sup> fuel volume, minus 0.11 m <sup>3</sup> basket volume
Internal porosity fraction	0.61	(Internal void volume)/(Internal volume)

**Table 5.2: Container external parameters**

Parameter	Value	Comments
Container outer diameter	1.247 m	Outer copper shell (SNC Lavalin, 2011)
Container length	3.842 m	SNC Lavalin (2011)
Copper shell thickness	0.025 m	SNC Lavalin (2011)

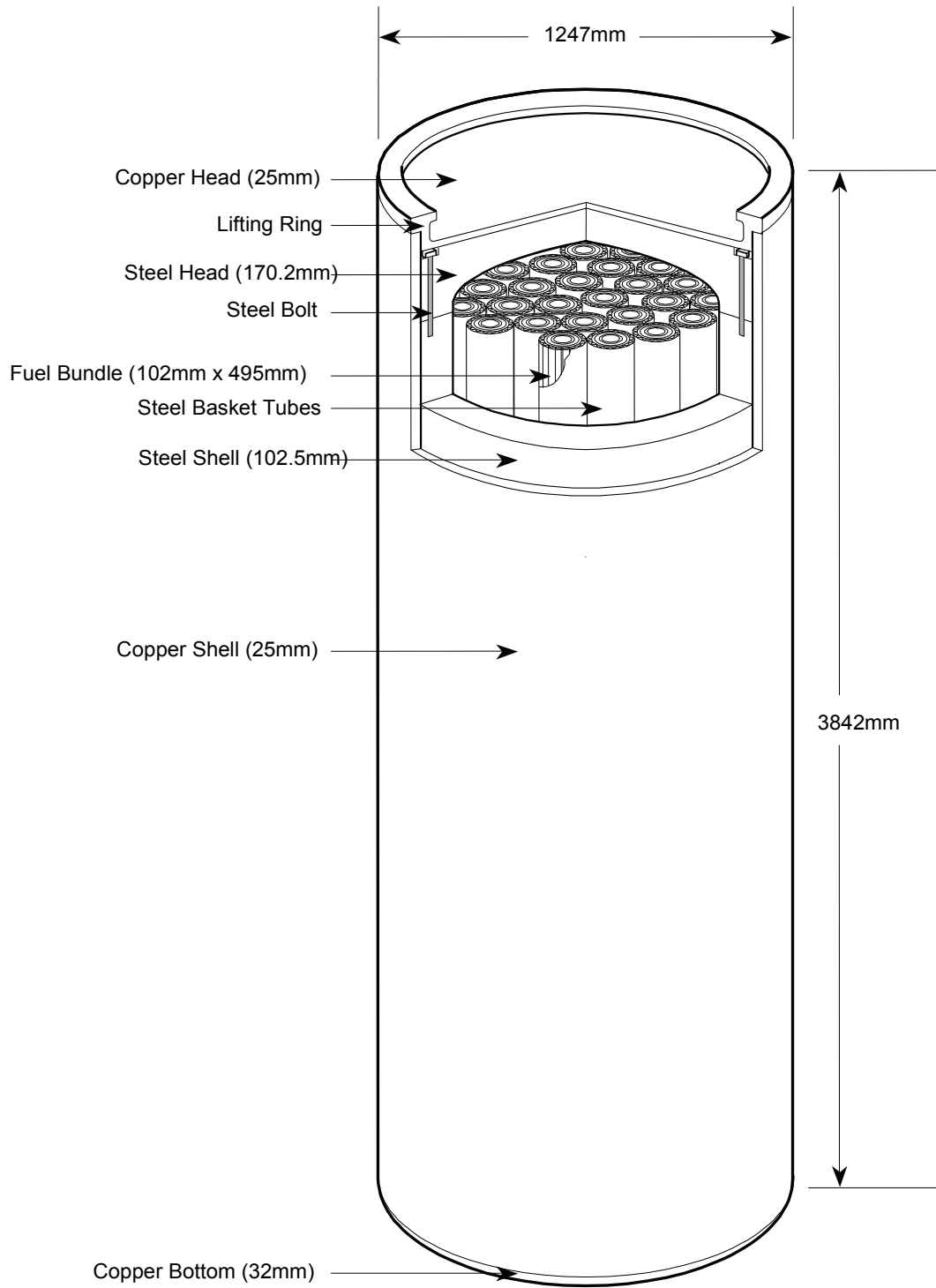


**Figure 5.1: Container design showing copper outer shell, inner steel vessel, and fuel assemblies inside support tubes.**

## 5.2 DEFECTIVE CONTAINER

In the Normal Evolution Scenario of the Fourth Case Study, we assume that some containers are unknowingly placed in the repository with a small, undetected through-wall defect. After the repository has saturated, this defect allows groundwater to enter the container and corrode the used fuel, and permits transport of radionuclides out of the container and into the buffer. The parameters used to describe this failure mode are listed in Table 5.3, and discussed further below.

**Table 5.3: Defective container scenario parameters**

Parameter	Reference Value	Comment
Probability of early failure	$2 \cdot 10^{-4}$ per container	Lognormal PDF with $GM=2 \cdot 10^{-4}$ and $GSD=2$ , bounds of $10^{-4}$ to $10^{-3}$ per container (Maak et al. 2001)
Container Release Time	100 a	Conservative minimum time from emplacement of container in repository until a water pathway exists for transport of nuclides out of container (including time for sealing material saturation, water to enter container, breach cladding and reach the fuel).
Defect radius	1 mm	Triangular PDF from 0.2 to 2 mm
Defect length	25 mm	Radial thickness of container copper shell (Table 5.2)
Groundwater temperature in and near container	70°C	Temperature decreases with time from peak value of around 100°C, to nominal host rock temperature of 20°C. For timescales of most interest, temperatures will be intermediate. Normal PDF with mean of 70°C, standard deviation of 10°C, and bounds of 20°C and 100°C.

The probability of early failure is expected to be small because of the careful manufacturing, inspection and handling process. The probability has been estimated based on an evaluation of early failure rates for various nuclear components as being in the range of  $10^{-4}$  to  $10^{-3}$  per container, with a best-estimate of  $2 \times 10^{-4}$  per container (Maak et al. 2001).

If the probability of such a failure per container is  $p_f$ , then the probability of  $N_f$  failed containers out of  $N_t$  total containers is given by the binomial distribution, and would have a best-estimate value of  $p_f \cdot N_t$ . For 12,778 containers, this means that statistically there would be between two and three containers in the repository with defects. The Fourth Case Study safety assessment will pessimistically assume 3 containers with defects are placed in the repository for the reference case.

In comparison, SKB has fabricated over 20 test containers as part of their fabrication development program, with generally similar dimensions albeit 50-mm thick. Their latest safety assessment concludes that the probability of a defect between 10 and 20 mm deep is 1 per

thousand and the probability of a defect greater than 20-mm long is negligible (SKB 2011, Section 5.4.2), i.e., there are no containers with initial through-wall defects.

For the Fourth Case Study, in the absence of a specific review for the reference Canadian container, we assume the failure rate is small but not negligible, and describe the distribution as lognormal with a GM of  $2 \cdot 10^{-4}$  and a GSD of 2.

The defect cannot be too large or it would be readily noticed during inspection. The SKB SR-Can assessment considered a circular defect with a radius of 2 mm ( $12.6 \text{ mm}^2$ ) (SKB 2006). This value was described as rather large given the observed distribution of pore sizes from friction stir welding (SKB 2006) and will be considered a bounding upper value in the Fourth Case Study. Larger defects would be readily visible. The Fourth Case Study assumes the defect radius has a lower limit of 0.2 mm. This is similar to the lower limit of 0.15 assumed in the Second Case Study (Johnson et al. 1996).

**Table 5.4: Free water diffusivity (at 25°C)**

Element	Reference Value <sup>1,2</sup> (m <sup>2</sup> /a)	Element	Reference Value <sup>1,2</sup> (m <sup>2</sup> /a)
Ac	0.032	Ni	0.021
Ag	0.053	Np	0.032
Am	0.032	P	0.067 <sup>#</sup>
As	0.067 <sup>#</sup>	Pa	0.032
Bi	0.067 <sup>#</sup>	Pb	0.067 <sup>#</sup>
C	0.038	Pd	0.032
Ca	0.025 <sup>*</sup>	Po	0.067 <sup>#</sup>
Cd	0.023	Pr	0.067 <sup>#</sup>
Ce	0.067 <sup>#</sup>	Pu	0.032
Cl	0.063	Ra	0.028
Co	0.022	Rn	0.067 <sup>#</sup>
Cr	0.067 <sup>#</sup>	Sb	0.032
Cs	0.067	Se	0.032
Cu	0.053 <sup>*</sup>	Sn	0.067 <sup>#</sup>
Eu	0.032	Te	0.067 <sup>#</sup>
Hg	0.067 <sup>#</sup>	Th	0.032 <sup>*</sup>
I	0.063	U	0.032
La	0.067 <sup>#</sup>	Y	0.067 <sup>#</sup>
Nd	0.067 <sup>#</sup>		

<sup>1</sup>Values are assumed to be normally distributed with a standard deviation of 0.01 and upper and lower bounds of 0.01 and 0.1 respectively

<sup>2</sup>Ohlsson and Neretnieks (1997), unless otherwise stated.

<sup>#</sup>Value conservatively assumed to be the same as for Cs.

<sup>\*</sup>Values for Ca, Cu and Th set equal to Sr, Ag and U values in Ohlsson and Neretnieks, respectively.

Radionuclides will escape out of the failed container by diffusion through the defect, given the small dimensions of the defect and the surrounding impermeable clay buffer. The free water diffusivity of various ions ranges from 0.025 to 0.067 m<sup>2</sup>/a at 25°C (Ohlsson and Neretnieks 1997). The values are listed in Table 5-4. For Th, the free-water diffusivity in Ohlsson and

Neretnieks seemed unusually low, and therefore its diffusivity was set equal to that for the other actinides such as U. Values for elements not listed in Ohlsson and Neretnieks were conservatively assumed to be the same as for cesium ( $0.067 \text{ m}^2/\text{a}$ ).

Diffusivities would increase by a factor of about 1.5 at  $40^\circ\text{C}$  and 2.7 at  $70^\circ\text{C}$  (assuming that the diffusivity can be scaled by the temperature/viscosity ratio, according to Rohsenow and Choi 1961, p.383). The free-water diffusivity therefore ranges from  $0.025 \text{ m}^2/\text{a}$  ( $0.79 \times 10^{-9} \text{ m}^2/\text{s}$ ) to  $0.18 \text{ m}^2/\text{a}$  ( $5.7 \times 10^{-9} \text{ m}^2/\text{s}$ ), depending on the species and on the container temperature when the release occurs.

### 5.3 WATER COMPOSITION

The groundwater composition around the repository would need to be determined for any specific site. The range of measured groundwater compositions in Canadian Shield rock mass are described in McMurry (2004). A reference crystalline rock groundwater, CR-10, has been defined for the Fourth Case Study host rock based on the groundwaters found at a depth of around 500 m. Its composition is listed in Table 5.5. It is a reducing Na-Ca-Cl groundwater, with total dissolved solids (TDS) of about 11.6 g/L.

**Table 5.5: Contact water composition (Duro et al 2010)**

Composition	CR-10 Equilibrated	CR-10 Bentonite-Iron Equilibration
pH	7.1	8.7
Environment	Reducing	Reducing
Eh (mV)	-194	-575
<b>Solutes (mg/L)</b>		
Na	1,899	6,255
K	15	80
Ca	2,217	870
Mg	60	182
HCO <sub>3</sub>	50	4
SO <sub>4</sub>	1,243	4,314
Cl	6,099	6,059
Br	-	-
Sr	25	25
Li	-	-
F	2	2
I	-	-
B	-	-
Si	5	10
Fe	8	7
NO <sub>3</sub>	1	1
PO <sub>4</sub>	1	1
TDS	11,625	17,810

The composition of the water actually reaching the used fuel will be that of the surrounding host rock groundwater but conditioned by passage through the backfill, buffer and container. In particular, the concentrations of the species in the water reaching the used fuel will be affected by ion exchange with the bentonite buffer (e.g., calcium ions in the groundwater may be exchanged for sodium ions in the bentonite as the groundwater passes through the bentonite), the presence of the iron-canister, as well as the dissolution of the minor mineral components of the buffer, such as gypsum and calcite, which could lead to higher carbonate and sulphate concentrations in the contact water (Duro et al. 2010).

The composition of the contact water is also shown in Table 5.5. This was calculated by Duro et al. (2010) by equilibrating the selected CR-10 reference groundwater (see Table 5.5) for the Fourth Case Study site (which is on the Canadian Shield) with the bentonite buffer minerals and the steel canister. The assumed initial  $E_h$  of the groundwater is approximately -200mV but this is expected to decrease to approximately -560mV after equilibration of the groundwater with the carbon steel canister insert.

#### 5.4 SOLUBILITY LIMITS

After container failure, water can contact the fuel, and cause the release of contaminants. The rate at which contaminants are released from the fuel is determined by the used fuel dissolution model. In theory, the concentrations of a contaminant in the water in the container could reach the solubility limit for that element. Consequently, precipitation of contaminants could occur, especially within or near the container where concentrations are highest.

The SYVAC3-CC4 model can calculate the solubility of several elements given the composition of the contact water. However, this feature of the model is not utilized in the Fourth Case Study. Instead, the solubility limits are calculated externally and incorporated into the SYVAC3-CC4 model calculations through the input data.

The element solubilities are listed in Table 5.6. These solubilities were calculated for 25°C and the reference water compositions in Table 5-5. Many solubility limits are temperature sensitive and the vault temperature is expected to be higher than 25°C (approximately 70°C) for thousands of years after repository closure. Despite this, solubility limits were calculated at 25°C since very little thermodynamic data exists for temperatures outside of 25°C. The solubility limits can also be quite sensitive to the groundwater composition which is also likely to vary somewhat throughout the repository due to non-homogeneities in mineral composition of the granitic rock and perhaps the buffer material. To account for uncertainties in the solubility due to the higher temperatures in the repository and the groundwater composition, the solubility values listed in Table 5-6 are increased by a factor of 10 for use in the safety assessment calculations.

For most elements, i.e., Am, Bi, C, Np, Pa, Pb, Pd, Pu, Ra, Se, Sn, Th, U, and Zr, the solubilities were calculated by Duro et al (2010) using PHREEQC and the ThermoChimie v7b database. ThermoChimie includes the thermodynamic data compiled by the NEA, when available, and uses the specific ion theory (SIT) activity corrections (Guillaumont et al. 2003). Due to uncertainty in the thermodynamic data as well as variability in the geochemical conditions at repository depth, the solubility limit is described using a lognormal distribution. For elements in which the thermodynamic data is well defined or the solubility limit is relatively insensitive to repository conditions, a lognormal distribution with a GSD of 3.2 is assumed. This

GSD corresponds to the 95% confidence bounds being with a factor of 10 of the GM. Conversely for Pa, for which the solubility is highly uncertain, a GSD of 10 is used.

The elements Ag, Cd, Co, Ni and Sb are also expected to have limited solubilities on the basis of thermodynamic stabilities and observed behaviour in natural and experimental systems. The solubilities of these elements in the two groundwaters listed in Table 5-5 were calculated using PHREEQC (version v2.18.5570) and the ThermoChimie database (v.7.d June 2011) that comes with PHREEQC. The higher of these two calculated solubility values is used in the assessment and is listed in Table 5.6.

The solubilities for Ce, Eu, La, Nd, and Pr were taken from Johnson et al. 1996.

The remaining elements (Ac, As, Ca, Cl, Cr, Cs, Hg, I, P, Po, Rn, Te, and Y) are assigned a very high constant solubility ( $2000 \text{ mol/m}^3$ ) to ensure that precipitation does not occur. These elements are either expected to be highly soluble, or to have a low inventory in the fuel, or to exist only as short-lived radionuclides, or to be gaseous (i.e., they do not precipitate), or to have complex chemistries so that their solubility limit is highly uncertain.

**Table 5.6: Element solubilities used in the Fourth Case Study<sup>1</sup>**

Element	Value <sup>2</sup> (mol/m <sup>3</sup> )	GSD	Distribution Type	Comments
Ac	2000	-	Constant	No solubility limit
Ag	1.1x10 <sup>-2</sup>	3.2	Lognormal	Calculated, AgCl(s) controlling solid
Am	2.2x10 <sup>-2</sup>	3.2	Lognormal	Duro et al. (2010)
As	2000	-	Constant	No solubility limit
Bi	1.2x10 <sup>-2</sup>	3.2	Lognormal	Duro et al. (2010)
C	8.3x10 <sup>-1</sup>	3.2	Lognormal	Duro et al. (2010)
Ca	2000	-	Constant	No solubility limit
Cd	7.6x10 <sup>-2</sup>	3.2	Lognormal	Calculated, CdCO <sub>3</sub> controlling solid
Ce	0.1	3.2	Lognormal	Table 5-4 in Johnson et al. (1996)
Cl	2000	-	Constant	No solubility limit
Co	0.1	3.2	Lognormal	Calculated, CoCO <sub>3</sub> controlling solid
Cr	2000	-	Constant	Low inventory, assigned high value for conservatism
Cs	2000	-	Constant	No solubility limit
Cu	1.4x10 <sup>-5</sup>	3.2	Lognormal	Duro et al. (2010)
Eu	0.1	3.2	Lognormal	Table 5-4 in Johnson et al. (1996)
Hg	2000	-	Constant	No solubility limit
I	2000	-	Constant	No solubility limit
La	0.1	3.2	Lognormal	Table 5-4 in Johnson et al. (1996)
Nd	0.1	3.2	Lognormal	Johnson et al. 1996, Table 5-4
Ni	2.9	3.2	Lognormal	Calculated, Ni(OH) <sub>2</sub> controlling solid
Np	1.1x10 <sup>-6</sup>	3.2	Lognormal	Duro et al. (2010)
P	2000	-	Constant	Low inventory, assigned high value for conservatism
Pa	2.2x10 <sup>-6</sup>	10	Lognormal	Duro et al. (2010)
Pb	8.0x10 <sup>-3</sup>	3.2	Lognormal	Duro et al. (2010), Pb <sub>3</sub> (CO <sub>3</sub> ) <sub>2</sub> controlling solid
Pd	4.1x10 <sup>-3</sup>	3.2	Lognormal	Duro et al. (2010)
Po	2000	-	Constant	No solubility limit
Pr	0.1	3.2	Lognormal	Table 5-4 in Johnson et al. (1996)
Pu	9.1x10 <sup>-5</sup>	3.2	Lognormal	Duro et al. (2010)
Ra	1.6x10 <sup>-4</sup>	3.2	Lognormal	Duro et al. (2010)
Rn	2000	-	Constant	No solubility limit
Sb	5.7x10 <sup>-2</sup>	3.2	Lognormal	Calculated, Sb <sub>2</sub> O <sub>3</sub> controlling solid
Se	1.3x10 <sup>-5</sup>	3.2	Lognormal	Duro et al. (2010)
Sn	9.6x10 <sup>-4</sup>	3.2	Lognormal	Duro et al. (2010)
Te	2000	-	Constant	No solubility limit
Th	2.5x10 <sup>-5</sup>	3.2	Lognormal	Duro et al. (2010)
U	3.5x10 <sup>-6</sup>	3.2	Lognormal	Duro et al. (2010)
Y	2000	-	Constant	Short half-life, assigned high value for conservatism
Zr	1.8x10 <sup>-5</sup>	3.2	Lognormal	Duro et al. (2010)

<sup>1</sup>The solubility value used in the safety assessment calculations is 10-fold larger than those listed here to account for uncertainties, as discussed in the text.

<sup>2</sup>Constant value for the constant distribution function, and geometric mean for the lognormal distribution function.



## 6. REPOSITORY DATA

This section of the report describes the design of the deep geological repository (DGR), comprising the excavations for underground placement of the used fuel containers (UFCs). The design is based on the 'in-floor' placement concept: placement of UFCs within boreholes drilled in the floor of placement rooms. The placement rooms are located at a depth of 500 m.

Dimensions and parameters presented here are consistent with the current repository design (SNC-Lavalin 2011).

### 6.1 PHYSICAL LAYOUT

The DGR repository consists of a system of access tunnels and placement rooms arranged in distinct panels. Figure 6.1 presents the design for the repository layout. The design consists of a total of 160 placement rooms, arranged in panels of between 14 and 24 rooms. Placement rooms will be spaced a minimum of 40 m between centre-lines, based on thermal modelling of the repository (Guo 2009); the 40 m-spacing is to prevent UFCs from reaching surface temperatures of over 100°C.

The repository is designed for a total capacity of 12,778 UFCs or 4,600,000 used fuel bundles. Assuming an ideal site, the minimum footprint of the underground repository would be approximately 1.5 km by 2.3 km (SNC Lavalin 2011). These dimensions do not account for any adaptations that may be required at an actual site to accommodate local conditions (e.g., specific rock structures, faults, or stress anomalies).

Each placement room will contain an average of approximately 80 UFCs. As shown in Figure 6.2, UFCs will be placed with a minimum axial separation of 4.2 m, based on thermal modelling (Guo 2009). The design provides for approximately one tenth of UFC boreholes to be left unused for quality assurance reasons, resulting in an average of 89 boreholes excavated in each placement room.

The placement room is designed with an elliptical cross-section, as shown in Figure 6.3 (SNC Lavalin 2011). The voids around the UFC and the placement room itself are filled with engineered sealing materials of various compositions and densities.

Placement room parameters are listed in Table 6.1; as-placed properties of the engineered sealing materials are listed in Table 6.2.

The rings of highly compacted 100% bentonite (HCB) can be fabricated separately. The specifications for the HCB rings are similar to those demonstrated for the SKB KBS-3V buffer rings (SKB 2009). The 5-cm placement tolerance around UFCs is filled with dense bentonite pebbles, with sufficient compaction to ensure the final post-saturation buffer density is high enough to maintain unfavourable conditions for microbial activity. The as-placed gapfill parameters specified in Table 6.2 are consistent with placement trials (Kjartanson et al. 2003).

**Table 6.1: Placement room parameters**

<b>Parameter</b>	<b>Value</b>	<b>Comment</b>
Borehole diameter	1968 mm	UFC diameter is 1247 mm (see Table 5.2)
pellets, inner annulus	50 mm	50 mm of bentonite pellets around O.D. of the UFC I.D.: 1347 mm, O.D.: 1868 mm 50 mm of bentonite pellets around borehole O.D.
bentonite ring	260.5 mm	
pellets, outer annulus	50 mm	
Borehole depth	6918 mm	measuring from the rock floor accommodating 14 blocks/rings of clay-based sealing materials
2 dense backfill blocks	1000 mm	
4 bentonite blocks	2000 mm	
8 bentonite rings	3918 mm	
Volume of clay materials in borehole	16.27 m <sup>3</sup>	closed hollow cylinder: borehole volume – UFC volume
Dense backfill	2.74 m <sup>3</sup>	
Bentonite blocks	5.48 m <sup>3</sup>	
Bentonite rings	5.15 m <sup>3</sup>	
Bentonite pellets	2.89 m <sup>3</sup>	
Axial spacing between containers	4.2 m	as per thermal analysis (Guo 2009)
Placement room spacing	40 m	as per thermal analysis (Guo 2009)
Number of containers in repository	12,778	4.6 million bundles, 360 bundles/container
Number of placement rooms	160	arranged in panels
Containers per placement room	80	12,778 UFCs distributed across 160 placement rooms means an average of 80 UFCs/room  on average, approximately 10% of boreholes are expected to be rejected for QA purposes
Boreholes per placement room	89	
Placement room		
Width	5500 mm	assumes elliptical cross section, less chamfers (0.25 m × 0.25 m)
Height	5500 mm	
Cross-sectional area	23.70 m <sup>2</sup>	
Length	395.6 m	length includes straight section, excludes 78.5 m entrance curve
Area of backfill	23.70 m <sup>2</sup>	
Inner dense backfill blocks	19.00 m <sup>2</sup>	corresponds with an average 264 mm-thick shell of light backfill pellets surrounding the dense backfill blocks
Outer light backfill pellets	4.70 m <sup>2</sup>	
Length of concrete bulkhead	12 m	12 m concrete bulkhead extends 6 m into curved portion of entranceway (SNC Lavalin 2011)
Volume of concrete	284.4 m <sup>3</sup>	
Key length	6.0 m	clay-based sealing materials keyed into rock to interrupt EDZ, filled with compacted bentonite and gapfill bentonite pellets
Key depth at floor	2.0 m	
Key depth in roof and walls	1.3 m	

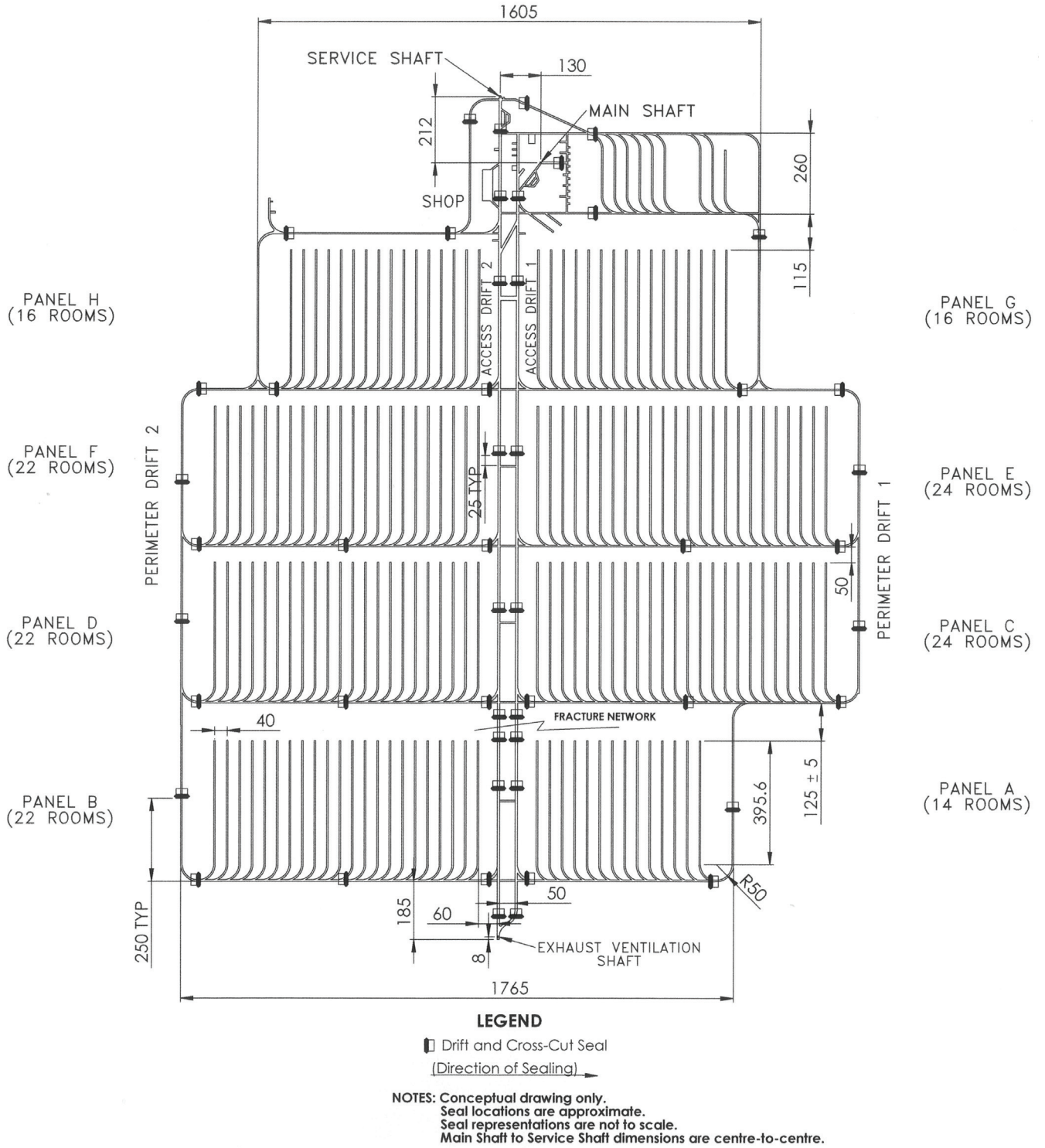


Figure 6.1: Plan view of underground repository

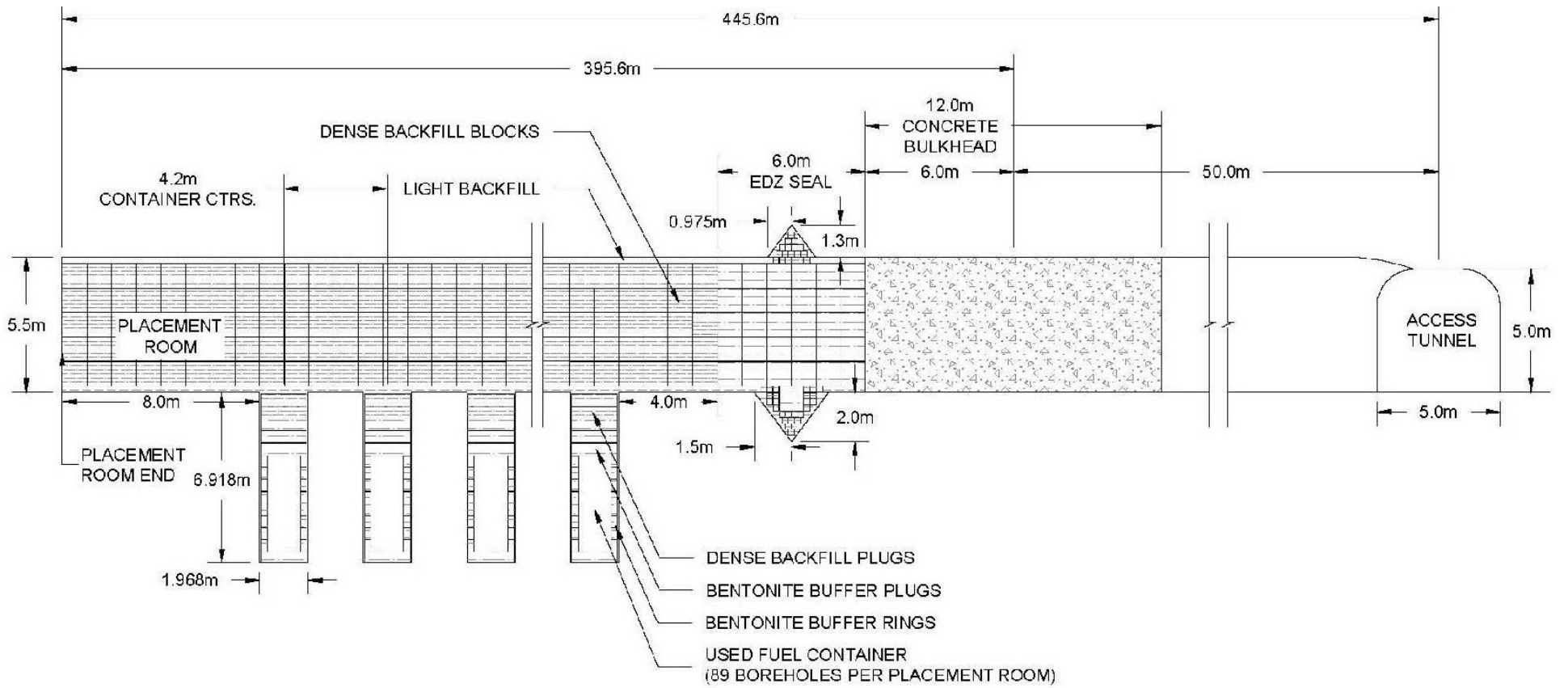
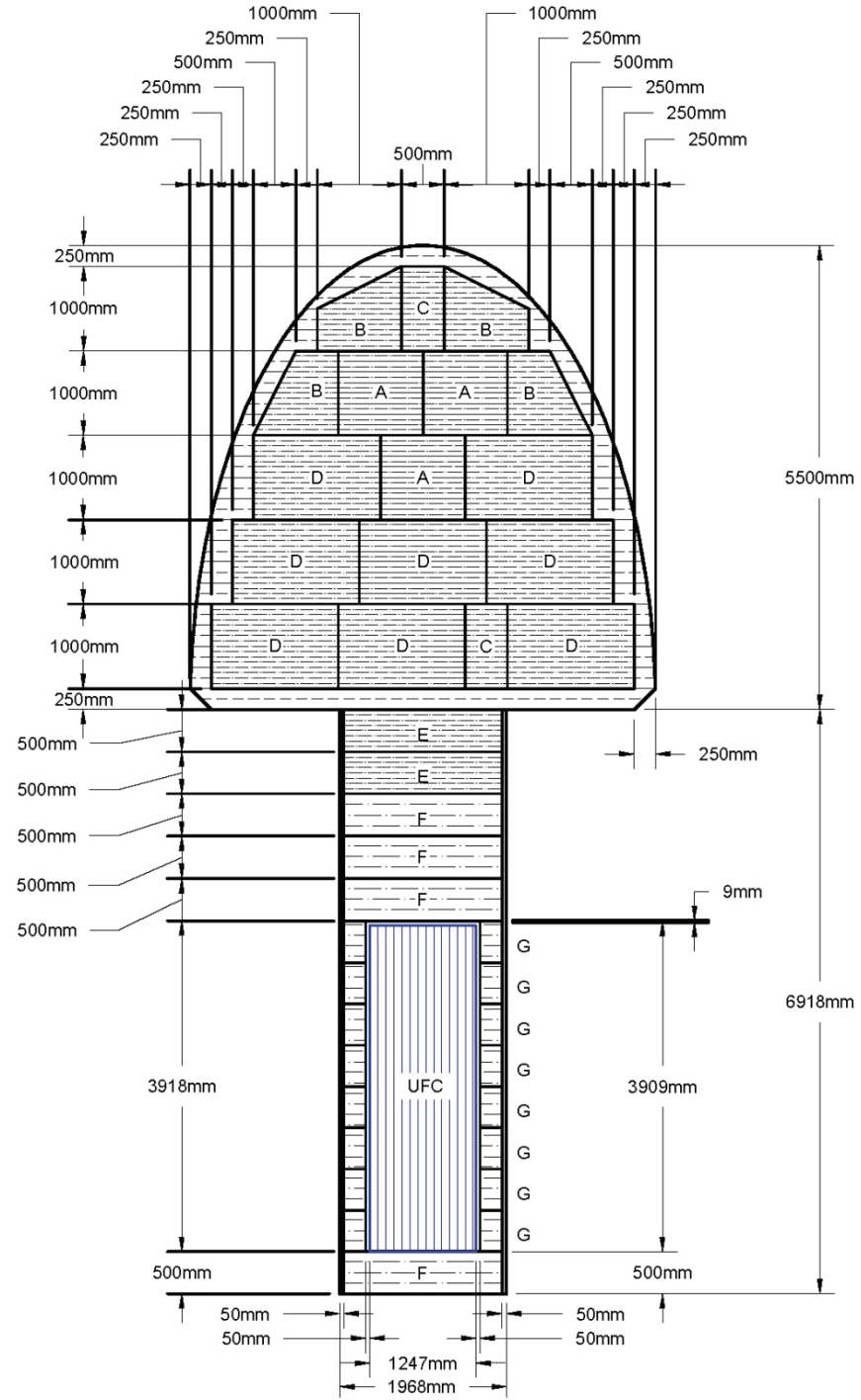


Figure 6.2: Longitudinal view of placement room



- LEGEND:**
- DENSE BACKFILL (DBF)
  - COMPACTED BENTONITE (HCB)
  - BENTONITE PELLETS (LBF)

**Figure 6.3: Cross-sectional view of placement room**

**Table 6.2: Properties of as placed materials in the repository**

	Dry density [kg/m <sup>3</sup> ]	Saturation [%]	Porosity [%]	Bulk density [kg/m <sup>3</sup> ]	Thermal conductivity [W/m·K]	Heat capacity [J/kg·K]
UFC (design IV-25)	-	-	0	7800	300	500
Compacted bentonite (100% bentonite)	1610	65	41.3	1880	1	1280
Gapfill pellets (100% bentonite)	1410	6	48.6	1439	0.4	870
Light backfill pellets (50:50 bentonite:granite sand)	1240	33	53.7	1418	0.7	1240
70% bentonite (70:30 bentonite:silica sand, used for shaft seals)	1600	80	41.1	1930	0.94	1360
Dense backfill (5:25:70 bentonite:clay:aggregate)	2120	80	19.4	2276	2.0	1060
Concrete	N/A	50	5	2425	1.67	900
Asphalt	N/A	N/A	2	1960	N/A	N/A

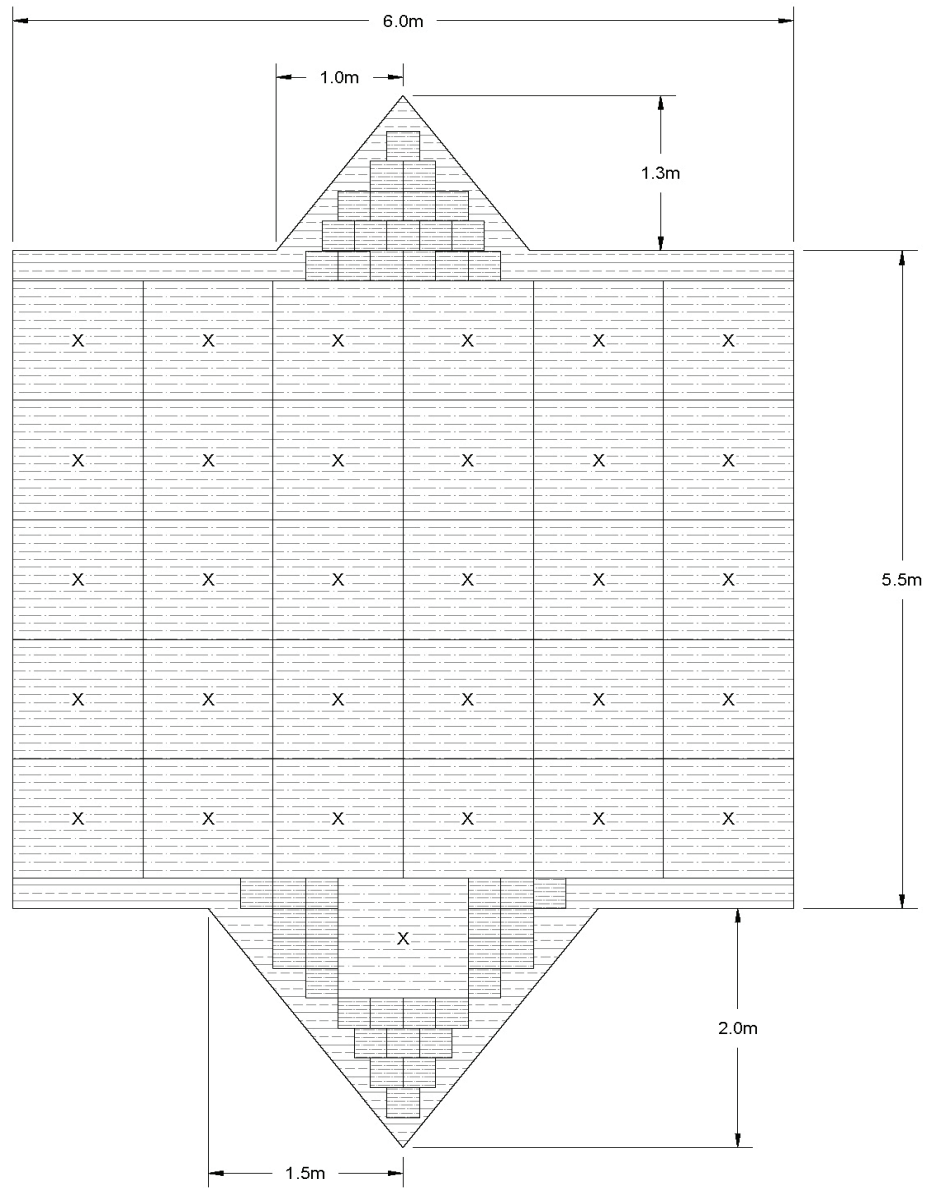
N.B. These data assume relative solid densities of 2.75, 2.67, 2.65, and 2.62 for MX-80 bentonite (80% montmorillonite), non-montmorillonite clay, silica sand, and granite (aggregate), respectively. The density of water having 10 g/L salinity is 1005.8 kg/m<sup>3</sup> at 20°C. Dry densities and saturations of the clay-based sealing materials are taken from SNC Lavalin (2011); other properties are determined using calculations illustrated in Baumgartner (2006). The concrete bulk density, thermal conductivity and heat capacity are from Didry et al. (2000).

Due to the excavation process, there will be a ring of damaged rock surrounding all the tunnels. This Excavation Damage Zone (EDZ) is more porous and has a higher hydraulic conductivity than the surrounding host rock. In order to minimize hydraulic flow between the rooms and access tunnels along the EDZ, bentonite clay will be keyed into the rock to interrupt the EDZ transport path (see Figure 6.4).

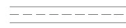


Figures 6.2 and 6.3 show the major material components and Table 6.2 summarizes their as-placed composition and physical properties. These properties will change with time as the materials saturate. Properties relevant to contaminant transport are described below.

The repository design includes three shafts: main shaft, service shaft and ventilation shaft (see Figure 6.1). The excavated diameter of the main shaft is 8 m and the excavated diameter of the service and ventilation shafts is 7.5 m. However, removal of the excavation damage zone, which will take place during decommissioning of the repository, will result in a nominal postclosure diameter of 9 m for the main shaft and 8.5 m for the service and ventilation shafts.

The shafts will be backfilled primarily with a 70% bentonite (70:30 bentonite:silica sand) seal (NWMO 2012a). Concrete will be placed as a monolith at the base of the shafts, and at specific bulkheads or caps within the shaft. A layer of asphalt (or highly-compacted bentonite) may be included also as a redundant seal. The shaft seal conceptual design is described in Table 6.3.



**LEGEND:**

-  LBF
-  HCB (BLOCKS)
-  HCB (BRICKS)

**Figure 6.4: Longitudinal view of the placement room seal**

**Table 6.3: Shaft seal design**

Depth	Comment
0 - 20 m	Low Heat High Performance Concrete (LHHPC) cap at surface
20 - 150 m	70:30 bentonite:sand seal
150 – 170 m	LHHPC bulkhead – keyed in
170 – 330 m	70:30 bentonite:sand seal
330 – 380 m	Asphalt seal
380 – 480 m	70:30 bentonite:sand seal
480 – 500 m	LHHPC monolith

## 6.2 BUFFER

The containers are surrounded by rings of highly compacted 100% bentonite (HCB). Upon placement, the buffer placed around the containers consists of a 0.26 m-thick ring of HCB, plus an additional 0.05 m of 100% bentonite pebbles to fill the gap between the buffer and container, and the gap between the buffer and borehole wall. The HCB has a dry density of 1.61 Mg/m<sup>3</sup>, and its Equivalent Montmorillonite Dry Density (EMDD) is about 1.465 Mg/m<sup>3</sup> based on an 80% montmorillonite content in the bentonite clay.

The as-placed gapfill buffer has a dry density of 1.41 Mg/m<sup>3</sup> and an EMDD of about 1.26 Mg/m<sup>3</sup>. The hydraulic conductivity of the gapfill buffer at saturation is 3.7x10<sup>-13</sup> m/s, based on calculations illustrated in Baumgartner (2006).

With saturation, the bentonite will swell and expand into the gapfill region, equilibrating into a buffer layer of uniform density. After saturation, this 0.36-m layer of bentonite will have a porosity of 42.8%, a saturated density of 2.0 Mg/m<sup>3</sup>, and an EMDD of 1.425 Mg/m<sup>3</sup>. The properties of compacted bentonite at saturation are listed in Table 6.4.

The saturated buffer layer is essentially impermeable to groundwater flow since the dense bentonite would have a very low permeability, even for groundwater salinities up to 50 g/L (Dixon et al. 2002). Thus, the exact value of the saturated bentonite permeability is not critical since transport will be diffusion-dominated in the buffer; a value of 1.4x10<sup>-20</sup> m<sup>2</sup> is conservatively selected (Dixon et al. 2001, 2002). The conversion factor from permeability to hydraulic conductivity varies from 1.0x10<sup>7</sup> (m/s)/m<sup>2</sup> at 20°C, to 1.4x10<sup>7</sup> (m/s)/m<sup>2</sup> at 40°C, and 2.4x10<sup>7</sup> (m/s)/m<sup>2</sup> at 70°C.



**Table 6.4: Compacted bentonite properties at saturation**

	Value	Comment
Dry density	1571 kg/m <sup>3</sup>	The compacted bentonite and bentonite gapfill pellets have equilibrated at saturation. The equilibrated dry density is the average of the compacted bentonite and bentonite gapfill pellets, weighted according to their relative volumes around the UFC: compacted bentonite, 10.63 m <sup>3</sup> and neighbouring bentonite gapfill pellets, 2.59 m <sup>3</sup> .
Porosity	43%	Averaged
Hydraulic conductivity	1.4×10 <sup>-13</sup> m/s 3.4×10 <sup>-13</sup> m/s	20°C value 70°C value
Intrinsic permeability	1.4×10 <sup>-20</sup> m <sup>2</sup>	
Swelling pressure	6.1 MPa	Saturated

N.B. Data listed are derived using calculations illustrated in Baumgartner (2006).

The rock wall of the boreholes is expected to reach a maximum temperature of approximately 65°C around 30 years after the used fuel containers are placed within them; the springline along the placement rooms is expected to reach a maximum temperature of approximately 57°C around 3,000 years after placement (Guo 2009). In the Fourth Case Study groundwater and transport simulations, the overall repository temperature is assumed constant, at 20°C, while the temperature within the boreholes is assumed to be constant, at 70°C. This is considered a reasonable reflection of the impact of the relatively brief thermal transient on mass transport since for I-129, a nonsorbing radionuclide that is the dominant contributor to the total dose rate, the peak mass flux into the surface biosphere occurs approximately 100,000 years after closure of the repository.

### **Diffusion coefficients**

The diffusive transport of contaminants is described, in part, by their effective (or intrinsic) diffusivity in the medium ( $D_e$ ). The measured effective diffusivity of contaminants in dense buffer materials under reducing conditions varies from about 10<sup>-12</sup> to 10<sup>-9</sup> m<sup>2</sup>/s (Oscarson et al. 1995; Yu and Neretnieks 1997; JNC 2000, Section 5.3.1). These compilations also indicate that the diffusivity increases by a factor of 2 to 3 as the temperature increases from room temperature to 60 to 80°C.

Some nuclides are expected to be present in the buffer as anionic species, notably I and Cl (and possibly Se and Po as well, though not accounted for in this work). For these species, repulsion by the nominally negative surface charge on the clay particles results a lower effective porosity and, consequently, a lower effective diffusivity than for neutral or cationic species (Wersin and Schwyn 2004, Yu and Neretnieks 1997). The effective buffer porosity for anions is 0.169, based on the anion porosity (0.174) from SKB (2010) and the ratio of the porosities of the buffers in the SKB (0.44) and Fourth Case Study (0.428) repositories.

Effective diffusivities for the engineered clay-based sealing materials are listed in Table 6.5 and are described by a triangular PDF. These values, which account for the possible effects of ion exclusion or surface diffusion on diffusive transport, are taken from the SKB (2010), in which the different elements are sorted into three categories: anionic elements, non-charged and

hydrolyzable cationic elements, and cesium. The values listed for bentonite are sufficiently representative of all clay-based sealants in the repository design, except for dense backfill.

The effective diffusivity of a contaminant,  $D_e$ , can be expressed in terms of the free-water diffusivity  $D_o$ , the porosity  $\varepsilon$  and tortuosity factor  $\tau$ , where  $D_e = \varepsilon \cdot \tau \cdot D_o$ . Using the effective buffer diffusivities and free water diffusivities in Table 6.5 and the effective porosity (0.169 for anions and 0.43 for non-anions), it is found that the buffer tortuosity is 0.033 for anions and in the range 0.15 to 0.49 for non-anions.

### **Sorption coefficients**

Sorption coefficients are listed in Table 6.6. The sorption coefficients are described by a triangular probability density function (with the lower and upper bounds equal to the pessimistic and optimistic values, respectively, and the peak value equal to the reference value).

Where available, sorption coefficients are taken from Vilks (2011); otherwise, values for the highly-compacted bentonite buffer material are taken from SKB (2010). The SKB sorption coefficients are based on a comprehensive review of sorption data by Ochs and Talerico (2004). Both Vilks (2011) and SKB (2010) report the uncertainties and/or ranges in the sorption coefficient values.

Several sorption values are defined by use of chemical analogs: Ac by Am (trivalent actinides); Ca, Cd, Co, Cr, and Sb by Sr (alkali earth metals or similar chemistry); La, Nd, Pr, and Y by Ce (lanthanides or similar chemistry); and Te by Se (chalcogens).

Based on its likely speciation (as  $\text{HCO}_3^-$ ), the sorption coefficient of carbon has been set to zero, i.e., carbon is not expected to sorb strongly onto any of the sealing materials. Also, data could not be found for Hg and P, so their sorption coefficients are set to zero for conservatism.

The sorption coefficients for several elements have changed only slightly (e.g., Cl, Cs, I and Rn) from those used in the Third Case Study. Other sorption coefficients have generally increased. The sorption coefficient for Pb, in particular, has increased by several orders of magnitude. Ochs and Talerico (2004) cite several studies reporting consistent values for lead sorption on clay, leading to the conclusion that, for reducing conditions, the  $K_d$  for Pb would be within the range 12 - 457  $\text{m}^3/\text{kg}$ .

The values listed for bentonite are sufficiently representative of all clay-based sealants in the repository design, except for dense backfill which is described in next section.

### **Capacity factor**

The sorption properties of the buffer can also be described by a capacity factor,  $\text{CF} = \varepsilon + \rho \cdot K_d$ , where  $\varepsilon$  is the porosity of the buffer,  $\rho$  is the dry bulk density, and  $K_d$  is the sorption coefficient. Capacity factors are listed in Table 6.7 and are described by a triangular PDF over the indicated range.

**Table 6.5: Effective diffusivities for bentonite and dense backfill at 25°C**

	Free Water Diffusivities		Effective Diffusivities					
	(m <sup>2</sup> /year)		Bentonite			Dense Backfill		
	Reference Case		Upper Limit	Lower Limit	Reference Case	Upper Limit	Lower Limit	
Ac	0.032	4.4E-03	6.6E-03	2.9E-03	1.6E-03	2.5E-03	6.6E-04	
Ag	0.053	4.4E-03	6.6E-03	2.9E-03	1.6E-03	2.5E-03	6.6E-04	
Am	0.032	4.4E-03	6.6E-03	2.9E-03	1.6E-03	2.5E-03	6.6E-04	
As	0.067	4.4E-03	6.6E-03	2.9E-03	1.6E-03	2.5E-03	6.6E-04	
Bi	0.067	4.4E-03	6.6E-03	2.9E-03	1.6E-03	2.5E-03	6.6E-04	
C	0.038	4.4E-03	6.6E-03	2.9E-03	1.6E-03	2.5E-03	6.6E-04	
Ca	0.025	4.4E-03	6.6E-03	2.9E-03	1.6E-03	2.5E-03	6.6E-04	
Cd	0.023	4.4E-03	6.6E-03	2.9E-03	1.6E-03	2.5E-03	6.6E-04	
Ce	0.067	4.4E-03	6.6E-03	2.9E-03	1.6E-03	2.5E-03	6.6E-04	
Cl	0.063	3.5E-04	1.9E-03	1.9E-05	1.3E-04	4.1E-04	4.1E-05	
Co	0.022	4.4E-03	6.6E-03	2.9E-03	1.6E-03	2.5E-03	6.6E-04	
Cr	0.067	4.4E-03	6.6E-03	2.9E-03	1.6E-03	2.5E-03	6.6E-04	
Cs	0.067	1.3E-02	1.3E-02	3.0E-03	4.1E-03	4.1E-03	6.6E-04	
Cu	0.053	4.4E-03	6.6E-03	2.9E-03	1.6E-03	2.5E-03	6.6E-04	
Eu	0.032	4.4E-03	6.6E-03	2.9E-03	1.6E-03	2.5E-03	6.6E-04	
Hg	0.067	4.4E-03	6.6E-03	2.9E-03	1.6E-03	2.5E-03	6.6E-04	
I	0.063	3.5E-04	1.9E-03	1.9E-05	1.3E-04	4.1E-04	4.1E-05	
La	0.067	4.4E-03	6.6E-03	2.9E-03	1.6E-03	2.5E-03	6.6E-04	
Nd	0.067	4.4E-03	6.6E-03	2.9E-03	1.6E-03	2.5E-03	6.6E-04	
Ni	0.021	4.4E-03	6.6E-03	2.9E-03	1.6E-03	2.5E-03	6.6E-04	
Np	0.032	4.4E-03	6.6E-03	2.9E-03	1.6E-03	2.5E-03	6.6E-04	
P	0.067	4.4E-03	6.6E-03	2.9E-03	1.6E-03	2.5E-03	6.6E-04	
Pa	0.032	4.4E-03	6.6E-03	2.9E-03	1.6E-03	2.5E-03	6.6E-04	
Pb	0.067	4.4E-03	6.6E-03	2.9E-03	1.6E-03	2.5E-03	6.6E-04	
Pd	0.032	4.4E-03	6.6E-03	2.9E-03	1.6E-03	2.5E-03	6.6E-04	
Po	0.067	4.4E-03	6.6E-03	2.9E-03	1.6E-03	2.5E-03	6.6E-04	
Pr	0.067	4.4E-03	6.6E-03	2.9E-03	1.6E-03	2.5E-03	6.6E-04	
Pu	0.032	4.4E-03	6.6E-03	2.9E-03	1.6E-03	2.5E-03	6.6E-04	
Ra	0.028	4.4E-03	6.6E-03	2.9E-03	1.6E-03	2.5E-03	6.6E-04	
Rn	0.067	4.4E-03	6.6E-03	2.9E-03	1.6E-03	2.5E-03	6.6E-04	
Sb	0.032	4.4E-03	6.6E-03	2.9E-03	1.6E-03	2.5E-03	6.6E-04	
Se	0.032	4.4E-03	6.6E-03	2.9E-03	1.6E-03	2.5E-03	6.6E-04	
Sn	0.067	4.4E-03	6.6E-03	2.9E-03	1.6E-03	2.5E-03	6.6E-04	
Te	0.067	4.4E-03	6.6E-03	2.9E-03	1.6E-03	2.5E-03	6.6E-04	
Th	0.032	4.4E-03	6.6E-03	2.9E-03	1.6E-03	2.5E-03	6.6E-04	
U	0.032	4.4E-03	6.6E-03	2.9E-03	1.6E-03	2.5E-03	6.6E-04	
Y	0.067	4.4E-03	6.6E-03	2.9E-03	1.6E-03	2.5E-03	6.6E-04	

N.B. Effective diffusivities are defined using triangular probability density functions. Values for bentonite are adopted from the SR-Site data report (SKB TR-10-52); values for the dense backfill are adopted from the SR-Can data report (SKB TR-06-25). The values listed for bentonite are sufficiently representative of all clay-based sealants included in the vault design, except for dense backfill.

**Table 6.6: Sorption coefficients for bentonite, dense backfill and concrete**

	Adsorption Coefficients, $K_d$ ( $m^3/kg$ )								
	Bentonite			Dense Backfill			Concrete		
	Reference Case	Upper Limit	Lower Limit	Reference Case	Upper Limit	Lower Limit	Reference Case	Upper Limit	Lower Limit
Ac	61	380	10	19	110	3.2	80	300	20
Ag	0	15	0	0.0035	4.5	0.0007	0	0	0
Am	61	380	10	19	110	3.2	80	300	20
As	0.3	0.3	0.3	0	0	0	0	0	0
Bi	35	50	25	2.5	28	0.31	0	0	0
C	0	0	0	0	0	0	0	0	0
Ca	0.0045	0.027	0.00075	0.0015	0.0097	0.00028	0.001	0.001	0.0007
Cd	0.0045	0.027	0.00075	0.0015	0.0097	0.00028	0.001	0.001	0.0007
Ce	8	93	0.8	2.4	28	0.24	80	300	20
Cl	0	0	0	0	0	0	0.005	0.007	0.003
Co	0.0045	0.027	0.00075	0.0015	0.0097	0.00028	0	0	0
Cr	0.0045	0.027	0.00075	0.0015	0.0097	0.00028	0.001	0.001	0.0007
Cs	0.093	0.56	0.015	0.036	0.19	0.0061	0.0005	0.0007	0.0003
Cu	0.022	0.26	0.007	0	0	0	0	0	0
Eu	8	93	0.8	2.5	28	0.31	80	300	20
Hg	0	0	0	0	0	0	0	0	0
I	0	0	0	0	0	0	0	0	0
La	8	93	0.8	2.4	28	0.24	80	300	20
Nd	8	93	0.8	2.4	28	0.24	80	300	20
Ni	0.3	3.3	0.03	0.091	0.99	0.0096	0	0	0
Np	63	1100	4	19	330	1.2	80	300	20
P	0	0	0	0	0	0	0	0	0
Pa	3	45	0.2	0.97	14	0.095	0.1	0.1	0.07
Pb	74	460	12	22	140	3.6	0.5	0.7	0.3
Pd	5	75	0.3	1.5	23	0.09	0	0	0
Po	0.06	0.5	0.008	0	0	0	0	0	0
Pr	8	93	0.8	2.4	28	0.24	80	300	20
Pu	63	1100	4	19	330	1.3	80	300	20
Ra	0.0045	0.027	0.00075	0	0	0	0.05	0.07	0.03
Rn	0	0	0	0	0	0	0	0	0
Sb	0.0045	0.027	0.00075	0.0015	0.0097	0.00028	0.001	0.001	0.0007
Se	0	0	0	0.00007	0.00035	0.000035	0.03	0.04	0.02
Sn	63	1800	2.3	19	530	0.69	10	30	2
Te	0	0	0	0.00007	0.00035	0.000035	0.03	0.04	0.02
Th	63	700	6	19	210	1.9	80	300	20
U	63	1100	3.6	19	330	1.2	2	2	1
Y	8	93	0.8	2.4	28	0.24	80	300	20

N.B. Adsorption coefficients are defined using triangular probability density functions, with the exception of a lognormal distribution for bismuth sorption on bentonite (geometric mean of 35, geometric standard deviation of 1.6, ranging from 25 to 50). The bentonite values are also used for light backfill and 70% bentonite.

### 6.3 BACKFILL

In the repository design, backfill does not surround the container so it is not present in the CC4 model of the repository. However, backfill is present in the FRAC3DVS-OPG models of the repository (NWMO 2012a).

Placement rooms are backfilled with blocks of dense backfill, composed of 5 wt% bentonite, 25 wt% glacial clay, 70 wt% crushed granite aggregate (Dixon et al. 2001). To fill the gaps around the dense backfill blocks, pellets of light backfill are blown in; light backfill pellets are 50 wt% crushed granite and 50% bentonite (Dixon et al. 2001). The as-placed densities are given in Table 6.2 and the saturated densities are given in Table 6.8 and Table 6.9. These densities correspond to 376 kg/m<sup>3</sup> EMDD for dense backfill and 692 kg/m<sup>3</sup> EMDD for light backfill.

The permeability of dense backfill blocks is calculated to be about  $9.0 \times 10^{-18} \text{ m}^2$  at saturation and is insensitive to the groundwater salinity up to approximately 100 g/L (Dixon et al. 2001, 2002). The permeability of the light backfill, however, is expected to be sensitive to salinity. The light backfill permeability is estimated at  $10^{-19}$  to  $10^{-18} \text{ m}^2$  under fresh water conditions,  $10^{-18}$  to  $10^{-16} \text{ m}^2$  for 35-60 g/L total dissolved solids (TDS) and about  $10^{-15} \text{ m}^2$  at 100 g/L TDS (Dixon et al. 2002).

The light and dense backfills are expected to equilibrate at saturation as a homogenous backfill. The equilibrated dry density is calculated as the average, weighted according to the cross sectional areas of light and dense backfill in the placement room. The calculated density is shown in Table 6.10.

The permeability of the homogenous backfill is defined using a lognormal PDF with a geometric mean of  $1.8 \times 10^{-18} \text{ m}^2$ , a geometric standard deviation of 3.2, and bounds of  $10^{-19} \text{ m}^2$  and  $10^{-15} \text{ m}^2$ . This distribution respects the range in possible values, but weights the higher salinity cases as less likely, with 95% of the values within  $10^{-19}$  and  $10^{-17} \text{ m}^2$ .

In the Fourth Case Study groundwater and transport simulations, the overall repository temperature, including the backfill, is assumed constant, at 20°C (see Section 6.2). The conversion factor from permeability to hydraulic conductivity is  $1.0 \times 10^7 \text{ (m/s)/m}^2$  at 20°C.

For consistency with the intact rock values (see Section 7.4), the longitudinal dispersivity in the backfill is set to 10 m, reflecting shorter path lengths through the backfill than the rock. The transverse dispersivity is 10% of the longitudinal value.

The shaft seal design calls for a sealing material comprised of 70% bentonite and 30% aggregate. Its properties at saturation are provided in Table 6.11. On average, the 70% bentonite sealing material is not expected to be subject to elevated temperatures for significant periods of time.

**Table 6.7: Capacity factors for bentonite and dense backfill**

	Capacity Factors (—)					
	Bentonite			Dense Backfill		
	Reference Case	Upper Limit	Lower Limit	Reference Case	Upper Limit	Lower Limit
Ac	96000	590000	16000	37000	210000	6200
Ag	0.43	24000	0.43	7.1	8800	1.6
Am	96000	590000	16000	37000	210000	6200
As	470	470	470	0.26	0.26	0.26
Bi	55000	79000	39000	4900	54000	600
C	0.43	0.43	0.43	0.26	0.26	0.26
Ca	7.5	43	1.6	3.2	19	0.81
Cd	7.5	43	1.6	3.2	19	0.81
Ce	13000	150000	1300	4700	54000	470
Cl	0.17	0.17	0.17	0.1	0.1	0.1
Co	7.5	43	1.6	3.2	19	0.81
Cr	7.5	43	1.6	3.2	19	0.81
Cs	150	880	24	70	370	12
Cu	35	410	11	0.26	0.26	0.26
Eu	13000	150000	1300	4900	54000	600
Hg	0.43	0.43	0.43	0.26	0.26	0.26
I	0.17	0.17	0.17	0.1	0.1	0.1
La	13000	150000	1300	4700	54000	470
Nd	13000	150000	1300	4700	54000	470
Ni	470	5200	48	180	1900	19
Np	99000	1700000	6300	37000	640000	2300
P	0.43	0.43	0.43	0.26	0.26	0.26
Pa	4700	71000	310	1900	27000	190
Pb	120000	720000	19000	43000	270000	7000
Pd	7900	120000	470	2900	45000	180
Po	95	790	13	0.26	0.26	0.26
Pr	13000	150000	1300	4700	54000	470
Pu	99000	1700000	6300	37000	640000	2500
Ra	7.5	43	1.6	0.26	0.26	0.26
Rn	0.43	0.43	0.43	0.26	0.26	0.26
Sb	7.5	43	1.6	3.2	19	0.81
Se	0.43	0.43	0.43	0.4	0.94	0.33
Sn	99000	2800000	3600	37000	1000000	1300
Te	0.43	0.43	0.43	0.4	0.94	0.33
Th	99000	1100000	9400	37000	410000	3700
U	99000	1700000	5700	37000	640000	2300
Y	13000	150000	1300	4700	54000	470

N.B. Capacity factors are defined using triangular probability density functions, with the exception of a lognormal distribution for bismuth (geometric mean of 55 000, geometric standard deviation of 1.6, ranging from 39 000 to 79 000). The bentonite values are also used for light backfill and 70% bentonite.

### **Diffusion coefficients**

For anionic species, repulsion by the nominally negative surface charge on the clay particles results a lower effective porosity and, consequently, a lower effective diffusivity than for neutral or cationic species. The effective backfill porosity for anions is taken to be 0.104, based on the anion porosity (0.174) from SKB (2010) and the ratio of the porosities of the buffer (0.44) in the SKB repository (0.44) and the backfill (0.264) in the Fourth Case Study repository.

Effective diffusivities for the backfill are listed in Table 6.5 and are described by a triangular PDF. These values, which account for the possible effects of ion exclusion or surface diffusion on diffusive transport, are taken from the SKB (2006), in which elements are essentially sorted into three categories: anionic elements, non-charged and hydrolysable cationic elements and cesium.

Using the effective backfill diffusivities and free water diffusivities in Table 6.5, and the effective porosity (0.104 for anions and 0.26 for non-anions), it is found that the backfill tortuosity is 0.02 for anions and in the range 0.092 to 0.29 for non-anions.

### **Sorption coefficients**

Backfill sorption coefficients are listed in Table 6.6. The sorption coefficients are described by a triangular probability density function (with the lower and upper bounds equal to the pessimistic and optimistic values, respectively, and the peak value equal to the reference value).

Sorption coefficients are generally taken from SKB (2006), which are based on a comprehensive review of sorption data by Ochs and Talerico (2004). However, for conservatism, the sorption coefficients of C and Ra are set to zero. Many sorption values are defined by use of chemical analogs: Ac by Am (trivalent actinides); Ca, Cd, Co, Cr, and Sb by Sr (alkali earth metals or similar chemistry); La, Nd, Pr, and Y by Ce (lanthanides or similar chemistry); Bi by Eu; and Te by Se (chalcogens). Finally, for As, Cu, Hg, P and Po, data are not available so the backfill sorption coefficient is conservatively set to zero.

The sorption properties of the backfill can also be described by a capacity factor. Capacity factors are listed in Table 6.7 and are described by a triangular PDF over the indicated range.

**Table 6.8: Properties of light backfill pellets at saturation**

<b>Property</b>	<b>Value</b>	<b>Comment</b>
Dry density	1240 kg/m <sup>3</sup>	
Porosity	54%	
Hydraulic conductivity	1.2×10 <sup>-11</sup> m/s	20°C value
Intrinsic permeability:	1.3×10 <sup>-18</sup> m <sup>2</sup>	
Swelling pressure	188 kPa	

N.B. Data listed are derived using calculations illustrated in Baumgartner (2006).

**Table 6.9: Properties of dense backfill blocks at saturation**

Property	Value	Comment
Dry density	2120 kg/m <sup>3</sup>	
Porosity	20%	
Hydraulic conductivity	8.8×10 <sup>-11</sup> m/s	20°C value
Intrinsic permeability:	9.0×10 <sup>-18</sup> m <sup>2</sup>	
Swelling pressure	42 kPa	

N.B. Data listed are derived using calculations illustrated in Baumgartner (2006).

**Table 6.10: Properties of backfill at saturation assuming homogenization of light backfill pellets and dense backfill blocks**

Property	Value	Comment
Dry density	1945 kg/m <sup>3</sup>	CC4 assumes a homogenous backfill, where the light and dense backfills equilibrate at saturation. The equilibrated dry density is calculated as the average, weighted according to the cross sectional areas of light and dense backfill in the placement room: dense backfill blocks, 19.0 m <sup>2</sup> ; light backfill pellets, 4.7 m <sup>2</sup> .
Porosity	26%	
Hydraulic conductivity	1.8×10 <sup>-11</sup> m/s	20°C value
Intrinsic permeability:	1.8×10 <sup>-18</sup> m <sup>2</sup>	
Swelling pressure	142 kPa	

N.B. Data listed are derived using calculations illustrated in Baumgartner (2006).

**Table 6.11: Properties of 70% bentonite / 30% sand at saturation**

Property	Value	Comment
Dry density	1600 kg/m <sup>3</sup>	
Porosity	41%	
Hydraulic conductivity	4.8×10 <sup>-13</sup> m/s	20°C value
Intrinsic permeability:	4.9×10 <sup>-20</sup> m <sup>2</sup>	
Swelling pressure	2.30 MPa	

N.B. Data listed are derived using calculations illustrated in Baumgartner (2006).

## 6.4 CONCRETE

The reference concrete is a Low-Heat High-Performance Concrete (LHPC) that is designed to minimize effects on the adjacent clay (Dixon et al. 2001). Transport modelling assumes degraded concrete properties from the time of closure, to account for degradation of concrete over tens of thousands of years (Quintessa and Geofirma 2011). The relevant properties of this concrete are summarized in Table 6.12.



The effective diffusivity of all contaminants in concrete is taken to be  $3.9 \times 10^{-3} \text{ m}^2/\text{a}$  (Quintessa and Geofirma 2011).

Sorption coefficients for concrete are from NAGRA (2004), where available, and are provided in Table 6.6. Many sorption values are defined by use of chemical analogs: Ca, Cd, Cr, and Sb by Sr (alkali earth metals or similar chemistry); Ce, La, Nd, Pr, and Y by Eu (lanthanides or similar chemistry); and Te by Se (chalcogens). For Ag, As, Bi, Hg, P, Pd and Rn, data are not available for concrete so the sorption coefficient is set to zero for conservatism.

Except for the bulkheads, all concrete will be removed from the placement rooms prior to backfilling and sealing. Concrete bulkheads are expected to be subject to raised temperatures, with a peak of approximately  $40^\circ\text{C}$  around 1,500 years after closure of the repository (Guo 2009). As described in Section 6.2, the overall repository temperature (which includes the concrete bulkheads) is assumed to be at  $20^\circ\text{C}$ ; this is considered a reasonable reflection of the impact of the relatively brief thermal transient on mass transport.

**Table 6.12: Properties of concrete at saturation**

Property	Value	Comment
Bulk density	$2491 \text{ kg/m}^3$	
Porosity	10%	
Hydraulic conductivity	$1 \times 10^{-10} \text{ m/s}$	$20^\circ\text{C}$ value
Intrinsic permeability:	$1 \times 10^{-17} \text{ m}^2$	
Effective diffusivity	$1.25 \times 10^{-10} \text{ m}^2/\text{s}$	Value assumes degraded concrete properties to account for degradation over tens of thousands of years.

## 6.5 ASPHALT

The shaft seal design concept includes a 50 m thick asphalt layer, as shown in Table 6.3 (SNC-Lavalin 2011). This provides a redundant low-permeable seal material. The reference asphalt mastic mix is the same as proposed for use in the Waste Isolation Pilot Plant (WIPP 2009). It contains 70% (by weight) silica sand, 20% asphalt and 10% hydrated lime. The high sand content provides a mechanical framework, the high asphalt content relative to conventional (road) asphalt provides this mixture with more plasticity, and the hydrated lime helps to stabilize the mixture and minimize microbial activity.

The relevant properties of the asphalt layer are provided in Table 6.13.

The effective diffusivity of all contaminants in asphalt is  $3.16 \times 10^{-6} \text{ m}^2/\text{a}$  (Quintessa and Geofirma 2011).

Owing to a lack of sorption data, and due to the small porosity and small physical extent of this material, all sorption coefficients for the asphalt shaft seal are conservatively taken to be zero.

**Table 6.13: Properties of asphalt at saturation**

<b>Property</b>	<b>Value</b>	<b>Comment</b>
Bulk density	1960 kg/m <sup>3</sup>	
Porosity	2%	
Hydraulic conductivity	1×10 <sup>-12</sup> m/s	20°C value
Effective diffusivity	1×10 <sup>-13</sup> m <sup>2</sup> /s	Based on reported experimental results, this is a conservative estimate (Quintessa and Geofirma 2011).

## 7. GEOSPHERE DATA

### 7.1 GENERAL SITE DESCRIPTION

The repository in the Fourth Case Study is located at a hypothetical but plausible Canadian Shield site. The Fourth Case Study and Third Case Study repository sites are in the same regional watershed. However, the repository depth (500 m) and location are different in the Fourth Case Study (NWMO 2012a).

The surface topography of the ~200 km<sup>2</sup> subregional watershed area around the site is relatively flat, as illustrated in Figure 7.1. A major river passes through the watershed, which is bounded by topographic highs to the north and south. The reference repository location is near the centre of this area.

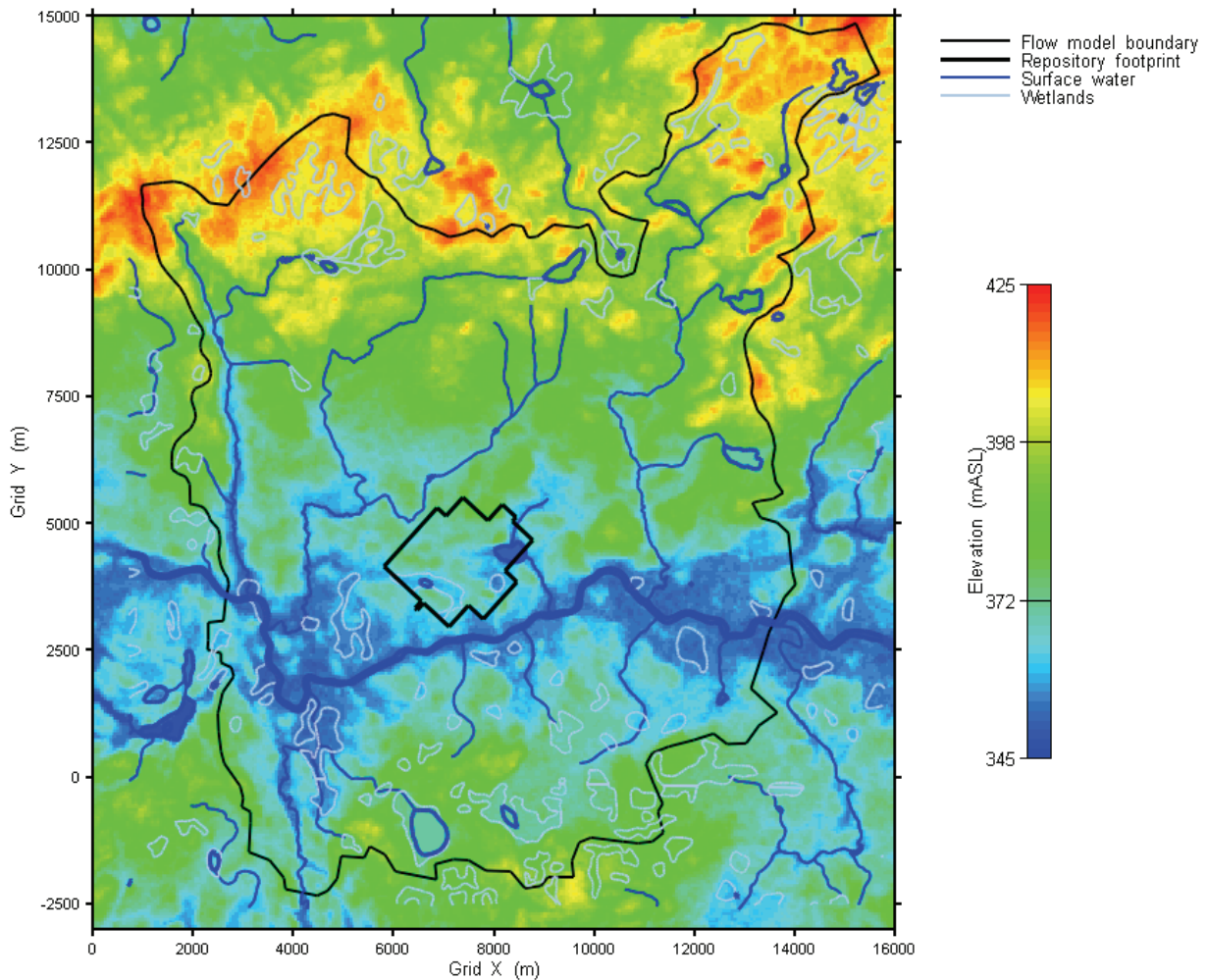


**Figure 7.1: The hypothetical subregional surface topography, indicating major lakes and rivers and repository location. The topography is relatively flat.**

Since the surface elevation varies, an absolute co-ordinate system has been defined relative to sea level. The ground surface above the repository is at approximately 360 m Above Sea Level (mASL) and the repository is located at -140 mASL.

For the hypothetical Fourth Case Study site, a set of major fractures (500 m or longer) was defined across the entire ~200 km<sup>2</sup> subregional area down to a depth of 1500 m (Srivastava 2002). The fracture network is illustrated in Figure 7.2. This figure illustrates the complexity of the fracture network at the subregional level. Although not obvious from this figure, the network consists of a large number of intersecting features within the first few hundred meters depth, and much fewer larger and more vertical features extending to greater depths.

The bedrock around the site is Canadian Shield granite, extending up to close to the surface. The properties of this granite are largely based on the properties of granite at the Whiteshell (Manitoba) and Atikokan (Ontario) Research Areas (Stevenson et al. 1996, Ophori and Chan 1996).

## **7.2 HYDRAULIC CONDUCTIVITY**

The rock mass (hydraulic) conductivity is represented as a series of horizontally uniform layers with isotropic conductivity, and with conductivity decreasing with depth.

For the Fourth Case Study, the uncertainty in the conductivity is represented by considering several cases of conductivity versus depth, as shown in Table 7.1 and Figure 7.3. Also shown in Figure 7.3, for comparison, are deep borehole data from two research locations on the Canadian Shield, Whiteshell and Atikokan.

The Reference Case and Sensitivity Cases 1 to 3 conductivity profiles range between a sparsely fractured granitic rock and a more permeable rock. The conductivity profile for the Reference Case represents a medium permeability rock. The impact of higher conductivity values is examined by using the Sensitivity Case 1 conductivity profile in which the rock conductivity is 10-fold larger than in the Reference Case for depths greater than 10 m. Sensitivity Cases 2 and 3 examine the influence of rock conductivity values lower than those used in the Reference Case.

Thermal models of the repository indicate that the thermal loading from the used fuel would create a region of somewhat elevated temperature around the repository, with a somewhat higher hydraulic conductivity, for around 10,000 years (Guo 2009). This transient temperature pulse is not expected to greatly affect the contaminant transport results, given that for I-129 (a mobile radionuclide that is the dominant contributor to the total dose rate) the peak mass flux to the surface biosphere occurs 100,000 years after repository closure, i.e., well after dissipation of the thermal pulse. Thus, the transient temperature pulse is neglected in the Fourth Case Study.

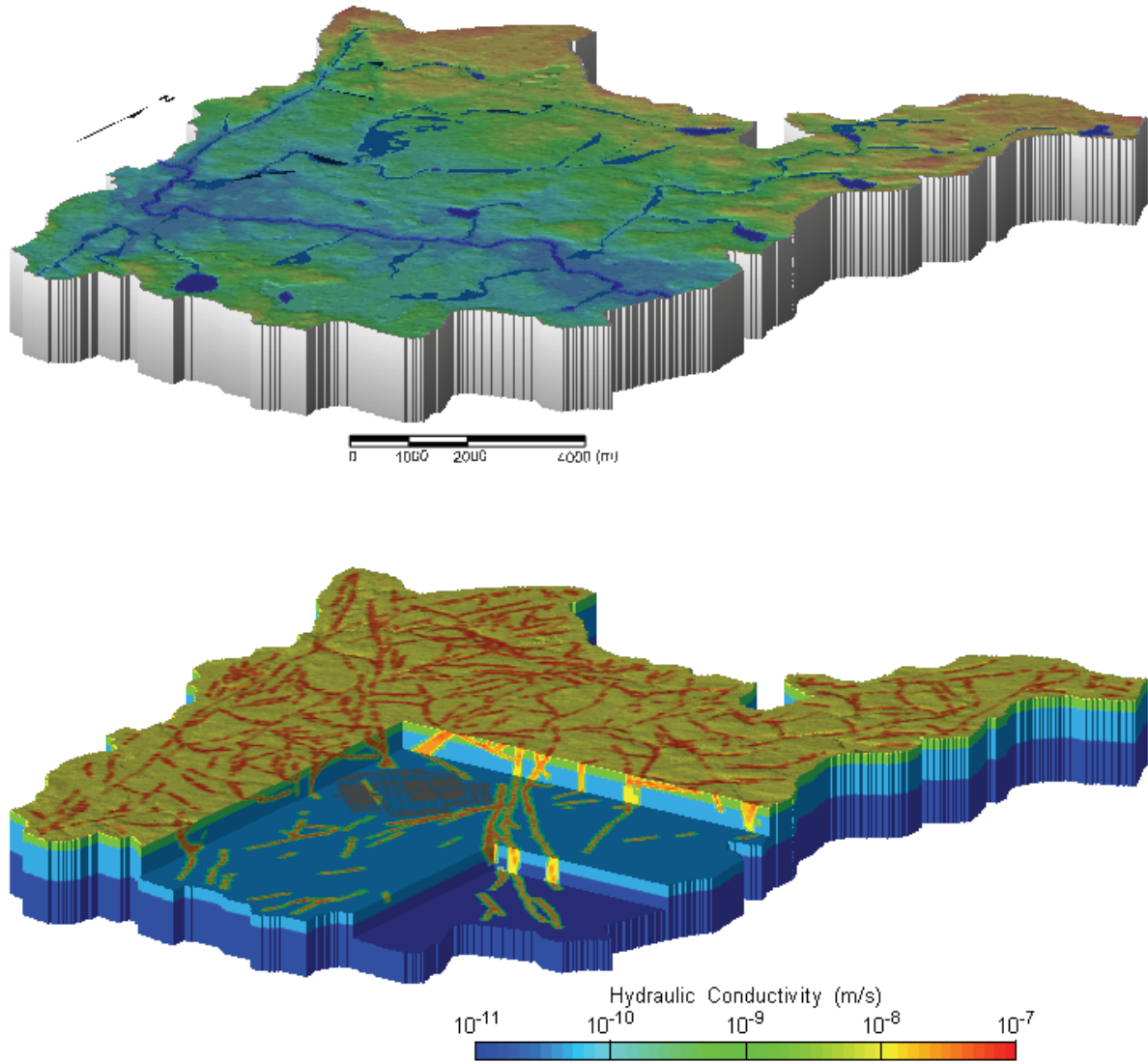


**Figure 7.2: Perspective view of 200 km<sup>2</sup> subregional area. Top figure shows surface lineaments and surface water features. Bottom figure shows fracture network at repository level (500 m depth) and location of the repository.**

Table 7.1: Geosphere conductivity profile

Depth (m)	Reference Case (m/s)	Sensitivity Case 1 (m/s)	Sensitivity Case 2 (m/s)	Sensitivity Case 3 (m/s)	Fracture (m/s)
0 – 10 (sediment)	$1 \times 10^{-5}$	$1 \times 10^{-5}$	$1 \times 10^{-5}$	$1 \times 10^{-5}$	-
0 – 10 (overburden)	$1 \times 10^{-8}$	$1 \times 10^{-8}$	$1 \times 10^{-8}$	$1 \times 10^{-8}$	-
10 - 150	$2 \times 10^{-9}$	$2 \times 10^{-8}$	$2 \times 10^{-10}$	$2 \times 10^{-11}$	$1 \times 10^{-6}$
150 - 700	$4 \times 10^{-11}$	$4 \times 10^{-10}$	$4 \times 10^{-12}$	$4 \times 10^{-13}$	$1 \times 10^{-6}$
700 - 1500	$1 \times 10^{-11}$	$1 \times 10^{-10}$	$1 \times 10^{-12}$	$1 \times 10^{-13}$	$1 \times 10^{-6}$

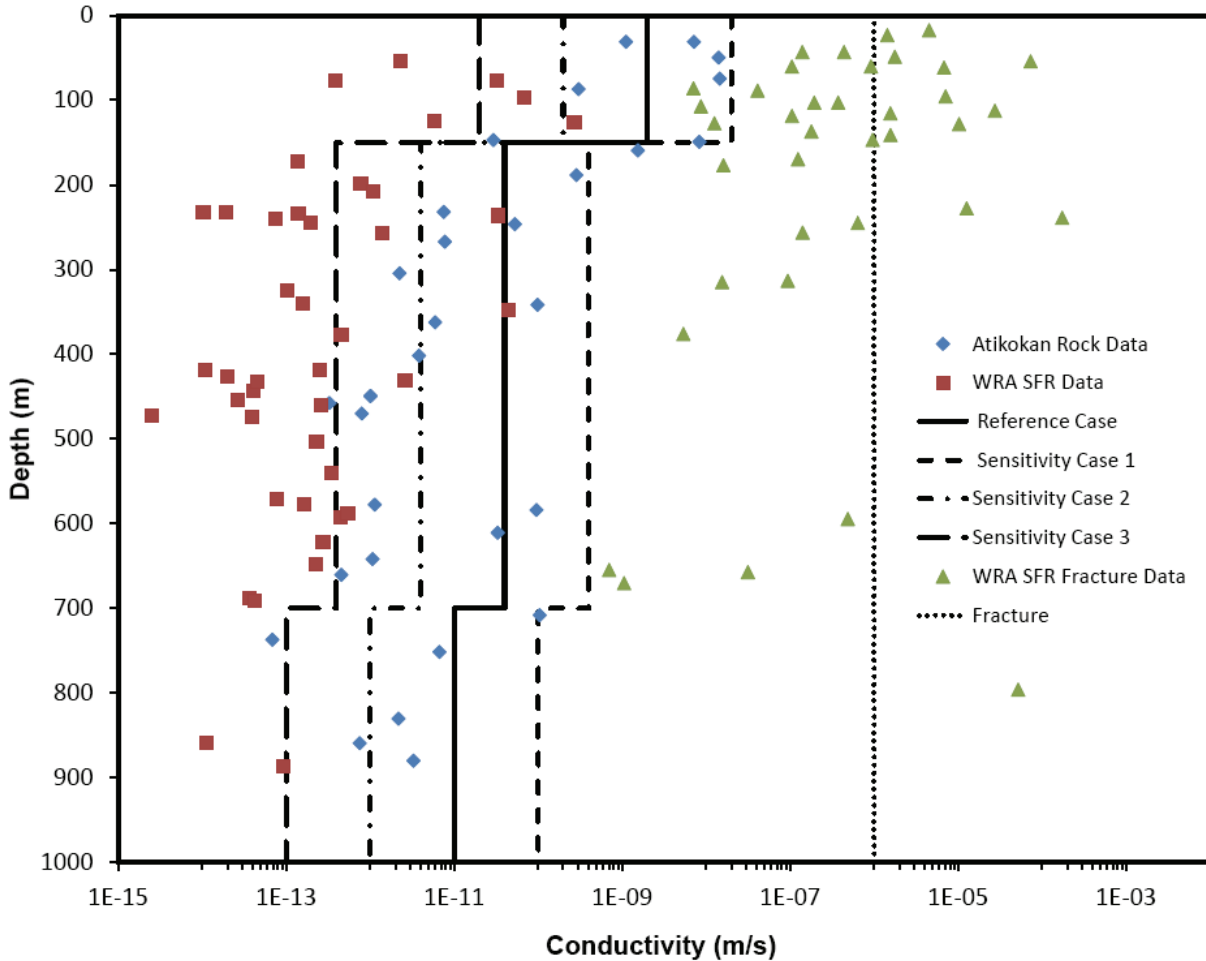


Figure 7.3: The conductivity versus depth profiles of the rock mass and fracture used for Fourth Case Study geosphere. Data from the Whiteshell (Manitoba) and Atikokan (Ontario) Research Areas on the Canadian Shield are shown, illustrating both the typical scatter in data and the trend for lower permeability with depth.

The fractures identified in Figure 7.2 are conservatively assumed to have a high conductivity of  $1 \times 10^{-6}$  m/s as indicated in Figure 7.3. The fractures are assumed to have an effective thickness of 1 m and a porosity of 0.1.

In general, there may be layers of overburden (e.g., sand, clay) and sediment on top of the bedrock. For the Fourth Case Study, the overburden thickness is characterized by a lognormal PDF with a GM of 4 m, a GSD of 1.7 m, and range from 0 to 20 m, based on field experience with support from Singer and Cheng (2002). In the EIS, Davison et al. (1994, p.415) indicate that the sediment thickness under Canadian Shield lakes can be described as a lognormal PDF with GM = 3.7 m, GSD = 2.2 m. This PDF is used in the Fourth Case Study, but with bounds of 0.3 to 10 m. The mean sediment thickness underneath the large river near the repository was further reduced by a factor of 10 due to its higher flow rate.

At the Fourth Case Study site it is assumed that the bedrock is close to the surface. Specifically, we limit the combined thickness of the sediment and overburden to 10 m (to reflect the geosphere conductivity profile in Table 7.1), with the overburden thickness adjusted as needed. The overburden and sediment conductivities given in Table 7.1 are based on measurements at the Whiteshell site (Davison et al. 1994, Appendix D).

### 7.3 PHYSICAL AND CHEMICAL CHARACTERISTICS

Table 7.2 and Table 7.3 summarize the assumed physical and chemical characteristics of the geosphere zones at the Fourth Case Study site.

The tortuosity  $\tau$  is defined in such a way that the effective diffusivity is given by  $D_e = \varepsilon \cdot \tau \cdot D_o$ . This definition of tortuosity is different from that used in the TCS. The relationship is  $\tau = 1/\tau_{TCS}^2$ . Values of  $\tau$  for the different geosphere zones were calculated from the values of  $\tau_{TCS}$  (which were based on Davison et al. 1994, Appendix D) and are given in Table 7.2. In the case of the Deep Rock Zone, Davison et al. (1994) defined  $\tau_{TCS}$  using a triangular distribution with minimum 2, mode 3 and maximum 8. The distribution for  $\tau$  has been approximately fitted here with a lognormal PDF. For the fracture and overburden zones,  $\tau_{TCS}$  is constant and equal to one. For the sediment,  $\tau_{TCS}$  is defined by a lognormal PDF with GM=1.2 and GSD=1.1, over the range 1 to 1.4. Because the range of  $\tau_{TCS}$  values is narrow, the sediment  $\tau$  values are defined to be uniformly distributed from 0.5 to 1.

Note that the oxidation state in Table 7.2 is an indication of the most likely oxidation conditions; the depth of the redox divide (see Table 7.3) determines the oxidation conditions of the rock zones.

The rock around the perimeter of the repository will tend to become unsaturated after excavation, since water will be removed by seepage pumps and air ventilation until containers are placed and the placement rooms, tunnels and shafts are backfilled. The extent of this partially saturated zone depends on the operating characteristics of the repository (e.g., time delay from excavation to room sealing). However, for groundwater transport of contaminants, the rock will have returned to saturation and so the properties of saturated rock would be applicable.

**Table 7.2: Physical characteristics of geosphere zones**

Geosphere Zone	Depth [m]	Density [kg/m <sup>3</sup> ]	Porosity [-]	Tortuosity [-]	Oxidation State
Overburden	0 - 10	1537	0.42	1	Oxidizing
Sediment (lake or river)	0 - 10	1250	0.5	0.75	Oxidizing
Shallow Rock Zone	10-150	2700	0.003	1	Oxidizing
Intermediate or Deep Rock Zone	150+	2700	0.003	0.06	Reducing
Shallow Fracture Zone	0-150	2400	0.1	1	Oxidizing
Intermediate or Deep Fracture Zone	150+	2400	0.1	1	Reducing

**Table 7.3: Chemical characteristics of geosphere zones**

Geosphere Zone	Mineral Content			
	Mineral	Density (g/cm <sup>3</sup> )	Mean Mineral Fraction	Standard Deviation <sup>1</sup>
Overburden	Clay	2.65	0.7	0.28
	Slit	2.65	0.2	0.3
	Sand	2.65	0.1	0.5
Sediment (lake or river)	Organics	2.5	1	-
Rock Zones	Granite	2.7	1	-
Fracture Zones	Granite	2.7	1	-

<sup>1</sup>Mineral composition fractions are described by normal distributions, with bounds from 0 to 1, except for granite and sediment which are defined as one composition.

In the Fourth Case Study, the groundwater flow models assume steady-state flow of constant density groundwater, i.e., the impact of variable density groundwater (i.e., salinity) on groundwater flow is not addressed.

The rock temperature around the repository will vary with time as the heat load from the used fuel is dissipated into the rock. Preliminary analysis of the heat generated by the repository shows that the heat is largely contained within the repository itself and the heat does not extend any appreciable distance into the nearby rock. It is assumed that the rock is at ambient temperature over time frames of interest for contaminant transport.

Available evidence shows that the concentrations of natural colloids are low in the Canadian Shield (Davison et al. 1994, p.337), probably in the order of 0.04-4 mg/L. An additional potentially important source of colloids will be from the clay materials in the engineered barriers in the repository. However, while these concentrations could be on the order of 40 mg/L in low



salinity water, the concentrations will be much lower for the expected salinities at the site (11.6 g/L, see Table 5.5), with values lower than 0.14 mg/L (Vilks and Miller 2007). In the Fourth Case Study, a total colloid concentration in the range 0.034 – 3.4 mg/L, from all sources, is assumed.

The nature of the colloids at the site is uncertain. For present purposes, we assume the colloids are primarily montmorillonite as a basis for estimating their sorption characteristics, as indicated in Table 7.4. (It is plausible that the colloids could be natural organics, which would imply that the colloid sorption properties would be similar to those for sediments). Furthermore, it is assumed that these same colloids continue to be dominant in the upper fracture and rock zones. As these zones are less saline, it is plausible that any bentonite colloids that reach the upper fracture zones will remain as colloidal particles rather than agglomerate. Although these colloids could be diluted by other natural colloids present in the upper zones, this possibility is neglected.

The colloid itself may move either with the groundwater or at a different rate characterized by the so-called colloid retardation factor. In the Reference Case of the Fourth Case Study, it is assumed that the colloids are not retarded and move with the groundwater, i.e., the colloid retardation factor = 1 (see Table 7.5).

#### **7.4 GEOSPHERE TRANSPORT PARAMETERS**

The physical transport parameters through the host sparsely-fractured rock are described here.

##### Effective Diffusivity

The effective or intrinsic diffusivity of contaminants in groundwater in saturated rock can be expressed in terms of the free-water diffusivity  $D_o$ , rock transport porosity  $\varepsilon$  and tortuosity factor  $\tau$ , where  $D_e = \varepsilon \cdot \tau \cdot D_o$ . Ohlsson and Neretnieks (1997) indicate that surface diffusion and anion exclusion are not important in granite under saline conditions (i.e., total dissolved solid concentrations over 10 g/L).

The selected free water diffusivities are from Ohlsson and Neretnieks (1997) and are the same as those in Table 5.4. Porosity and tortuosity values are listed in Table 7.2. These properties are defined at 25°C. This is higher than the host rock ambient temperature of about 11°C (Table 7.4). Since the rock is not expected to heat up significantly on timescales relevant to transport (see Section 7.2), no further temperature scaling is provided.

The calculated effective diffusivity values are shown in Table 7.5.

**Table 7.4: Geochemistry parameters**

<b>Parameter</b>	<b>Reference Case</b>	<b>Comment</b>
Redox divide elevation at repository	150 mASL	Normal PDF assumed with mean 150, a standard deviation of 75 m, and range from 50 to 300 m. Based on Whiteshell data (Gascoyne 2004). Note that surface elevation at repository location is approximately 360 mASL.
Ambient temperature at repository horizon	11°C	Consistent with a 5°C average surface temperature and 0.012°C/m geothermal gradient.
Colloid concentration	0.34 mg/L	Average colloid concentration in Whiteshell area is 0.34 mg/L (Davison et al. 1994, p.337). Range assumed 10-fold smaller to 10-fold higher, so colloid concentration described using loguniform PDF from 0.034–3.4 mg/L. Colloid grain density assumed to be 2700 kg/m <sup>3</sup> .
Colloid transport retardation factor	1	Lognormal PDF with GM = 1.0, GSD = 5.0, bounds = 0.9 to 100.
Colloid Sorption Coefficient	See Table 6-7	Reference Case K <sub>d</sub> value for element on bentonite used. All sampled values are directly correlated with bentonite sorption values.

**Table 7.5: Effective diffusivities in geosphere zones [m<sup>2</sup>/a]**

<b>Element</b>	<b>Deep or Intermediate Rock</b>	<b>Shallow Rock</b>	<b>Fracture</b>	<b>Overburden</b>	<b>Sediment</b>
Ac	5.8x10 <sup>-6</sup>	9.6x10 <sup>-5</sup>	3.2x10 <sup>-3</sup>	1.3x10 <sup>-2</sup>	1.2x10 <sup>-2</sup>
Ag	9.5x10 <sup>-6</sup>	1.6x10 <sup>-4</sup>	5.3x10 <sup>-3</sup>	2.2x10 <sup>-2</sup>	2.0x10 <sup>-2</sup>
Am	5.8x10 <sup>-6</sup>	9.6x10 <sup>-5</sup>	3.2x10 <sup>-3</sup>	1.3x10 <sup>-2</sup>	1.2x10 <sup>-2</sup>
As	1.2x10 <sup>-5</sup>	2.0x10 <sup>-4</sup>	6.7x10 <sup>-3</sup>	2.8x10 <sup>-2</sup>	2.5x10 <sup>-2</sup>
Bi	1.2x10 <sup>-5</sup>	2.0x10 <sup>-4</sup>	6.7x10 <sup>-3</sup>	2.8x10 <sup>-2</sup>	2.5x10 <sup>-2</sup>
C	6.8x10 <sup>-6</sup>	1.1x10 <sup>-4</sup>	3.8x10 <sup>-3</sup>	1.6x10 <sup>-2</sup>	1.4x10 <sup>-2</sup>
Ca	4.5x10 <sup>-6</sup>	7.5x10 <sup>-5</sup>	2.5x10 <sup>-3</sup>	1.1x10 <sup>-2</sup>	9.4x10 <sup>-3</sup>
Cd	4.1x10 <sup>-6</sup>	6.9x10 <sup>-5</sup>	2.3x10 <sup>-3</sup>	9.7x10 <sup>-3</sup>	8.6x10 <sup>-3</sup>
Ce	1.2x10 <sup>-5</sup>	2.0x10 <sup>-4</sup>	6.7x10 <sup>-3</sup>	2.8x10 <sup>-2</sup>	2.5x10 <sup>-2</sup>
Cl	1.1x10 <sup>-5</sup>	1.9x10 <sup>-4</sup>	6.3x10 <sup>-3</sup>	2.6x10 <sup>-2</sup>	2.4x10 <sup>-2</sup>
Co	4.0x10 <sup>-6</sup>	6.6x10 <sup>-5</sup>	2.2x10 <sup>-3</sup>	9.2x10 <sup>-3</sup>	8.3x10 <sup>-3</sup>
Cr	1.2x10 <sup>-5</sup>	2.0x10 <sup>-4</sup>	6.7x10 <sup>-3</sup>	2.8x10 <sup>-2</sup>	2.5x10 <sup>-2</sup>
Cs	1.2x10 <sup>-5</sup>	2.0x10 <sup>-4</sup>	6.7x10 <sup>-3</sup>	2.8x10 <sup>-2</sup>	2.5x10 <sup>-2</sup>
Cu	4.5x10 <sup>-6</sup>	7.5x10 <sup>-5</sup>	2.5x10 <sup>-3</sup>	1.1x10 <sup>-2</sup>	9.4x10 <sup>-3</sup>
Eu	5.8x10 <sup>-6</sup>	9.6x10 <sup>-5</sup>	3.2x10 <sup>-3</sup>	1.3x10 <sup>-2</sup>	1.2x10 <sup>-2</sup>
Hg	1.2x10 <sup>-5</sup>	2.0x10 <sup>-4</sup>	6.7x10 <sup>-3</sup>	2.8x10 <sup>-2</sup>	2.5x10 <sup>-2</sup>
I	1.1x10 <sup>-5</sup>	1.9x10 <sup>-4</sup>	6.3x10 <sup>-3</sup>	2.7x10 <sup>-2</sup>	2.4x10 <sup>-2</sup>
La	1.2x10 <sup>-5</sup>	2.0x10 <sup>-4</sup>	6.7x10 <sup>-3</sup>	2.8x10 <sup>-2</sup>	2.5x10 <sup>-2</sup>
Nd	1.2x10 <sup>-5</sup>	2.0x10 <sup>-4</sup>	6.7x10 <sup>-3</sup>	2.8x10 <sup>-2</sup>	2.5x10 <sup>-2</sup>
Ni	3.8x10 <sup>-6</sup>	6.3x10 <sup>-5</sup>	2.1x10 <sup>-3</sup>	8.8x10 <sup>-3</sup>	7.9x10 <sup>-3</sup>
Np	5.8x10 <sup>-6</sup>	9.6x10 <sup>-5</sup>	3.2x10 <sup>-3</sup>	1.3x10 <sup>-2</sup>	1.2x10 <sup>-2</sup>
P	1.2x10 <sup>-5</sup>	2.0x10 <sup>-4</sup>	6.7x10 <sup>-3</sup>	2.8x10 <sup>-2</sup>	2.5x10 <sup>-2</sup>
Pa	5.8x10 <sup>-6</sup>	9.6x10 <sup>-5</sup>	3.2x10 <sup>-3</sup>	1.3x10 <sup>-2</sup>	1.2x10 <sup>-2</sup>
Pb	1.2x10 <sup>-5</sup>	2.0x10 <sup>-4</sup>	6.7x10 <sup>-3</sup>	2.8x10 <sup>-2</sup>	2.5x10 <sup>-2</sup>
Pd	5.8x10 <sup>-6</sup>	9.6x10 <sup>-5</sup>	3.2x10 <sup>-3</sup>	1.3x10 <sup>-2</sup>	1.2x10 <sup>-2</sup>
Po	1.2x10 <sup>-5</sup>	2.0x10 <sup>-4</sup>	6.7x10 <sup>-3</sup>	2.8x10 <sup>-2</sup>	2.5x10 <sup>-2</sup>
Pr	1.2x10 <sup>-5</sup>	2.0x10 <sup>-4</sup>	6.7x10 <sup>-3</sup>	2.8x10 <sup>-2</sup>	2.5x10 <sup>-2</sup>
Pu	5.8x10 <sup>-6</sup>	9.6x10 <sup>-5</sup>	3.2x10 <sup>-3</sup>	1.3x10 <sup>-2</sup>	1.2x10 <sup>-2</sup>
Ra	5.0x10 <sup>-6</sup>	8.4x10 <sup>-5</sup>	2.8x10 <sup>-3</sup>	1.2x10 <sup>-2</sup>	1.1x10 <sup>-2</sup>
Rn	1.2x10 <sup>-5</sup>	2.0x10 <sup>-4</sup>	6.7x10 <sup>-3</sup>	2.8x10 <sup>-2</sup>	2.5x10 <sup>-2</sup>
Sb	5.8x10 <sup>-6</sup>	9.6x10 <sup>-5</sup>	3.2x10 <sup>-3</sup>	1.3x10 <sup>-2</sup>	1.2x10 <sup>-2</sup>
Se	5.8x10 <sup>-6</sup>	9.6x10 <sup>-5</sup>	3.2x10 <sup>-3</sup>	1.3x10 <sup>-2</sup>	1.2x10 <sup>-2</sup>
Sn	1.2x10 <sup>-5</sup>	2.0x10 <sup>-4</sup>	6.7x10 <sup>-3</sup>	2.8x10 <sup>-2</sup>	2.5x10 <sup>-2</sup>
Te	1.2x10 <sup>-5</sup>	2.0x10 <sup>-4</sup>	6.7x10 <sup>-3</sup>	2.8x10 <sup>-2</sup>	2.5x10 <sup>-2</sup>
Th	5.8x10 <sup>-6</sup>	9.6x10 <sup>-5</sup>	3.2x10 <sup>-3</sup>	1.3x10 <sup>-2</sup>	1.2x10 <sup>-2</sup>
U	5.8x10 <sup>-6</sup>	9.6x10 <sup>-5</sup>	3.2x10 <sup>-3</sup>	1.3x10 <sup>-2</sup>	1.2x10 <sup>-2</sup>
Y	1.2x10 <sup>-5</sup>	2.0x10 <sup>-4</sup>	6.7x10 <sup>-3</sup>	2.8x10 <sup>-2</sup>	2.5x10 <sup>-2</sup>

### Dispersion Length

The dispersion length is a parameter that approximates the spreading of a contaminant plume due to inherent variability in the local rock or fracture permeability. As a general rule of thumb a dispersion length is roughly 5-10% of the total path length. For the present repository, the path length of interest for the contaminant plume (i.e., when it reaches the surface) ranges from 400 m (the shortest direct distance from the repository to the bottom of the well) to 500 m (shortest direct distance from repository to surface based). Since a lower dispersion results in less spreading of the contaminant plume, the current study assumes a constant longitudinal dispersion length of 20 m or 5% of the 400 m total path length. The transverse dispersion length was assumed to be 10% of the longitudinal dispersion length or 2 m (uniform distribution with a lower bound of 1.6 m and an upper bound of 2.4 m).

## **7.5 EDZ TRANSPORT PARAMETERS**

In the Fourth Case Study, the excavation of the shafts, tunnels, placement rooms and boreholes will create zones of disturbed rock in which there is significantly increased porosity and flow permeability. These zones are referred to as excavation damage zones (EDZ). The extent and severity of the EDZ is dependent on the excavation method, size of the excavation, localized rock stress and residual heat generated by the fuel. Beyond the EDZ, the rock may be disturbed with respect to stress redistribution, but no significant change to the flow and transport properties of the rock is expected.

The selected EDZ parameters used in the Fourth Case Study are summarized in Table 7.6 and Table 7.7, and are described below.

### EDZ Thickness

The shafts, placement rooms (with a half-ellipse cross section, see Figure 6.3), and tunnels are assumed to be excavated by a controlled drill-and-blast technique resulting in an EDZ in the rock around the periphery of the shafts and tunnels. However, by considering the stress state in the host rock, by use of the half-ellipse shape, and by appropriate control of the excavation, the extent of the EDZ can be minimized.

The in-floor boreholes are assumed to be mechanically excavated. Therefore, the EDZ around the boreholes is initially expected to be much narrower than around the shafts and tunnels. However, use of circular boreholes within the stress fields anticipated in the Canadian Shield results in high local stress fields around the borehole, possibly leading to near-surface cracking around the boreholes. Furthermore, after the placement rooms are completed and the used fuel containers are placed in the repository, the heat generated by the used fuel will contribute additional thermal stresses that will increase the porosity and flow permeability of the EDZ around the boreholes.

Martino (2000) and Chan et al. (1999) provide reviews of EDZ properties in Canadian Shield granite, including measurements made in the Mine-by Tunnel and Tunnel Sealing Experiments at the AECL Underground Research Laboratory. Bäckblom (2008) summarizes the results of several international experiments. These reviews focus on drill-and-blast excavated tunnels but include some limited discussion of tunnels excavated by a tunnel boring machine or mechanical excavation. The reports concluded that the severity of the EDZ significantly decreases the further away from tunnel surface. Based on these reviews, in the Fourth Case Study, the

damaged zone around the boreholes, placement rooms, access tunnels and shafts are divided into three regions, a thermally damaged zone (TDZ), an inner excavation damage zone and an outer excavation damage zone (see Figure 7.4).

The thermal damage zone is a region of high permeability created in the floor of the placement room by the heat generated by the used fuel. The resulting temperatures are high enough to spall the rock and create numerous small fractures. Thermal modelling shows that this region will be triangular in shape and extend 0.7m below the floor of the placement room.

As in the TCS, the inner excavation damage zone is assumed to be relatively narrow, extending out 0.3 m from the walls and roof of tunnels, access tunnels and below the thermal damage zones in the floor of the placement rooms. The damage will be most severe within 0.1 m of the surface; however, it is conservatively assumed that the entire inner EDZ (0.3 m depth) has the same properties as this most highly damaged zone.

The outer EDZ extends an additional 1 m from the inner EDZ and has very similar properties to the host rock. Although some experiments observed a stress disturbed zone out to 3 m from the tunnel surface, the transport properties in that region were unchanged from those of the host rock.

For the boreholes, the EDZ is expected to be much narrower than in the tunnel. For the present study, only a single EDZ layer is considered, with a best-estimate thickness of 0.08 m and a range of 0.01 to 0.3 m.

At the end of each placement room, a bentonite seal will be keyed into the rock with the intent of restricting flow through the excavation damage zone (see Figure 6.2). The room seal will be carefully excavated to reduce the likelihood of an additional EDZ forming. However, it is possible a thin layer of EDZ could form around the seal. In the Fourth Case Study, this additional room seal EDZ is included in the detailed modelling. It is assumed to be 0.1 m thick and is assigned the transport properties consistent with the inner EDZ defined above.

Shafts in the Fourth Case Study scenario are roughly circular and the local stress field around the shafts is expected to be high. Martino (2000) states that significant stress changes occur within approximately two tunnel radii of the center. As a result, the shaft EDZ is conservatively assumed to have an inner EDZ extending 4.75 m (or 1 shaft radius) into the rock and an outer EDZ extending an additional 4.75 m into the rock. The inner and outer shaft EDZs are assigned the same porosity and flow permeability as the inner and outer EDZ surrounding the placement rooms and tunnels. The shaft design includes several bulkheads that serve the same purpose as the room seals. The bulkheads are designed to interrupt any continuous flow paths along the shaft EDZ with an impermeable layer. However, as is the case for the room seals, a thin 0.1 m thick inner EDZ is assumed to form around these bulkheads.

### EDZ Permeability

EDZ measurements in Canadian Shield granite at the AECL Underground Research Laboratory indicated that the transmissivity of the inner EDZ was about two to three orders of magnitude higher than of the intact rock (Martino 2000). EDZ tests at other sites report a 1 to  $10^5$  times increase over the host rock permeability for the TDZ, inner EDZ, and outer EDZ (Chan et al. 1999, Appendix A; Bäckblom 2008).

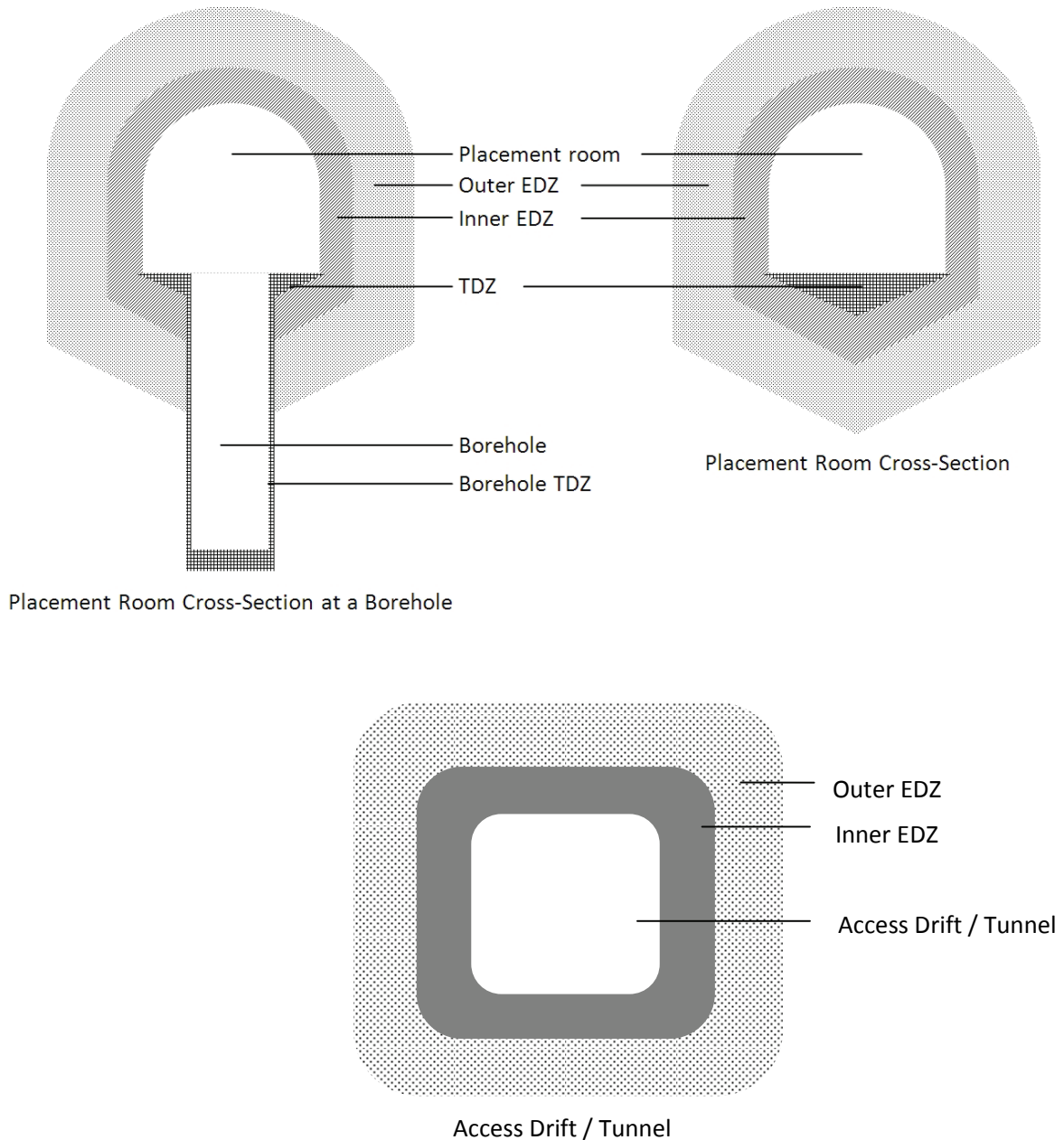


**Figure 7.4: Illustration (not to scale) of distinct regions of the EDZ in: (top) the placement rooms and (bottom) access drifts or tunnels.**

Seepage measurements along the floor of the AECL Mine-by Tunnel experiment gave permeability values of  $10^{-13} \text{ m}^2$  occurring in a small  $0.004 \text{ m}^2$  area, while similar tests in the Tunnel Sealing Experiment floor gave values of  $2.5 \times 10^{-15} \text{ m}^2$ , occurring over  $0.2 \text{ m}^2$  (Martino 2000). This is consistent with other observations in tunnels in highly stressed rock where "notches" at the roof or floor have greater rock damage and corresponding increased permeability.

Some of these seepage measurements also explored the axial connectivity of the EDZ permeability. In the AECL Room 209 tests over a 6-m floor section, it was found that the EDZ did not form a continuous path beyond one blast round (about 3 m) (Martino 2000). However, in the Mine-by Tunnel, no drop in permeability was noted over 1 to 4 m (Martino 2000). For the Fourth Case Study, it is conservatively assumed that the EDZ permeability is axially connected along each borehole and around the tunnels and drifts.

For this study, the reference value for the axial inner EDZ permeability is selected to be 100 times the host rock permeability. Since values range from 10 to 1000 times the intact rock permeability, the EDZ permeability is defined by a lognormal PDF with a geometric mean of 100 times the intact rock permeability and a geometric standard deviation (GSD) of 3.2, so that 95% of the values of the distribution are within 10 to 1000 times the intact rock permeability. Bounds are set at 10 and 1000 times the intact rock permeability. The inner EDZ permeability is also assumed to be correlated to the porosity of the inner EDZ with a correlation coefficient of 0.8 (higher porosity implies higher permeability). The inner EDZ permeability in the radial direction is set to 0.1 times the axial value.

A best-estimate value for the outer EDZ permeability is 10 times the host rock permeability with lower and upper limits of 1 and 100 times the host rock permeability, respectively.

With respect to a room center thermal damage zone, the best-estimate TDZ permeability is  $10^4$  times the host rock permeability.

#### EDZ Dispersion length

The axial-flow EDZ dispersion length is defined parallel (longitudinal) or transverse to the room axis direction. Although the room length is about 300 m, we expect that the contaminant path length through the EDZ will normally be less than 100 m, considering that the failed container location can vary and that contaminants can also move radially.

The SCS used a fit to dispersion data from a range of laboratory and field studies that gives a 14 m (best estimate) to 45 m (95% confidence bound) dispersion length for axial transport along a 100-m path (i.e., 14 to 45% of the path length) (Johnson et al. 1996, p.181). Flow measurements in the EDZ in the Mine-by Tunnel indicated a dispersion length of 0.60 m for a test region of 1.5 m, i.e., 40% of the scale length. Results from the TRUE tracer tests on a 3-m scale implied a 10% dispersion length (SKB 2001, p.99, p.161).

Thus, in the Fourth Case Study CC4 model calculations, the longitudinal dispersion length for axial transport in the EDZ is described by a uniform PDF from 10 to 40 m, corresponding to 10 to 40% of a 100-m path length. However, in the FRAC3DVS-OPG calculations, the longitudinal dispersion coefficient in the EDZ is selected to be 10 m based on Quintessa and Geofirma (2011) to avoid unrealistic transport results, i.e., large upstream dispersion. Upstream dispersion does not occur in the CC4 geosphere transport model (NWMO 2012b).

The SCS suggests that the transverse dispersion is about 1% of the longitudinal dispersion (Johnson et al. 1996, p.181), whereas other "rules of thumb" suggest 10% (Chan et al. 1999). For the Fourth Case Study, these give a transverse dispersion length range of either 0.1 to 0.4 m, or 1 to 4m. Since the EDZ radial thickness is about 0.3 m, the transverse dispersion length is selected to be 1% of the longitudinal dispersion length. Thus, in the CC4 model calculations,

the EDZ transverse dispersion length is described by a uniform PDF from 0.1 to 0.4 m and in the FRAC3DVS-OPG calculations the EDZ transverse dispersion length is 0.1 m.

In the CC4 model, a radial flow component is separately modelled and assigned its own longitudinal and transverse dispersion lengths. These are set to 1% of the corresponding longitudinal and transverse dispersion lengths for axial flow.

### EDZ Porosity

It is expected that the porosity of the EDZ is comparable to or larger than that of the host rock. Two measurements along the tunnel floor in the AECL Mine-by Tunnel experiment (Chan et al. 1999, Appendix A) indicated a transport porosity of around 3%, compared to the intact rock porosity of about 0.3%. However, these tests also indicated very high permeabilities, and so it is likely that the measured porosity represents the porosity of the bottom EDZ notch rather than the bulk EDZ porosity. In the AECL EDZ study (Chan et al. 1999), the porosity of the inner EDZ was modelled as 0.5%, and the center notches were treated as either 0.5% or 3%, compared with the rock porosity of 0.3%.

For the Fourth Case Study, the best-estimate porosity of the intact rock is 0.3%. The best-estimate porosity is 0.6% for the thermal damage zones, 0.6% for the borehole and tunnel inner EDZ, and 0.3% for the tunnel outer EDZ. However, in CC4, only the EDZ around the borehole can be modelled (see Figure 7.4). To account for this, the EDZ porosity is described by a lognormal PDF with a geometric mean of 0.6%, a geometric standard deviation of 3.2, and bounding values of 0.06% and 6%. Furthermore, the EDZ porosity is positively correlated with the EDZ permeability, so that the porosities are large when the permeability is large. Although there is no specific data, it is judged that this should be a fairly tight correlation - a correlation coefficient of 0.8 is used.

### EDZ Tortuosity

As previously noted, the tortuosity,  $\tau$ , used in the Fourth Case Study is defined so that the effective diffusivity is given by  $D_e = \varepsilon \cdot \tau \cdot D_o$ . This definition is different from that used the TCS. The relationship is  $\tau = 1/\tau_{TCS}^2$ .

In the AECL EDZ study (Chan et al. 1999), the EDZ tortuosity was assumed to be equivalent to  $\tau_{TCS} = 3.2$ , the same as for the intact rock, but ranging from 1.3 to 4.1. For the Third Case Study, the best-estimate value for the inner EDZ tortuosity was equal to the tortuosity of the intact rock, but a smaller range was considered because of the higher EDZ porosity. Specifically,  $\tau_{TCS}$  for the EDZ layer was described by a normal PDF with mean 3.2, a standard deviation 1, and bounds of 1.5 and 4.

For the Fourth Case Study, the inner EDZ tortuosity from the TCS is used to calculate the corresponding PDF for  $\tau$ , the inner EDZ tortuosity used in the Fourth Case Study. The inner EDZ tortuosity is described by a lognormal PDF with GM = 0.1, GSD = 1.7 and bounds from 0.06 to 0.44.

For the more highly damaged TDZ and bulkhead EDZ, the tortuosity is set equal to the maximum tortuosity value used for the inner EDZ tortuosity, i.e., 0.44.



**Table 7.6: Properties of the different excavation damage zones**

EDZ Zone	Thickness [m]	Permeability Ratio <sup>1</sup> [K <sub>edz</sub> /K <sub>rock</sub> ]	Range [K <sub>edz</sub> /K <sub>rock</sub> ]	Porosity <sup>2</sup> [-]	Tortuosity [-]
<b>Placement rooms</b>					
Floor TDZ	0.7	10 <sup>4</sup>	10 <sup>3</sup> -10 <sup>5</sup>	2×rock	0.44
Borehole TDZ	0.08	10 <sup>4</sup>	10 <sup>3</sup> -10 <sup>5</sup>	2×rock	0.10
Inner EDZ	0.3	100	10-10 <sup>3</sup>	2×rock	0.1
Outer EDZ	1	10	1-100	1×rock	0.1
Room Seal EDZ	0.1	100	10-10 <sup>3</sup>	2×rock	0.1
<b>Drifts &amp; tunnels</b>					
Inner EDZ	0.3	100	10-10 <sup>3</sup>	2×rock	0.1
Outer EDZ	1	10	1-100	1×rock	0.1
<b>Shafts</b>					
Inner EDZ (xy)	4.75	100	10-10 <sup>3</sup>	2×rock	0.1
Inner EDZ (z)	4.75	1000	10-10 <sup>3</sup>	2×rock	0.1
Outer EDZ	4.75	10	1-100	1×rock	0.1
Bulkhead EDZ	0.1	100	10-10 <sup>3</sup>	2×rock	0.44

<sup>1</sup>Host rock conductivity is listed as  $4 \times 10^{-11}$  m<sup>2</sup> at 500m repository depth (Table 7.1).

<sup>2</sup>Host rock porosity is listed as 0.003 (Table 7.2).

**Table 7.7: Transverse, radial, and axial EDZ properties<sup>1</sup>**

Parameter	Reference Value	Comment
Axial flow, axial dispersion length	25 m	Uniform PDF from 10 m to 40 m. (In FRAC3DVS-OPG, the axial dispersion length is set at 10 m to avoid unrealistic transport, i.e., upstream dispersion.)
Axial flow, transverse dispersion length	0.25 m	Uniform PDF from 0.1 to 0.4 m. (In FRAC3DVS-OPG, transverse dispersion length is set to 10% of longitudinal value or 1 m.)
Radial flow, ratio of radial to axial dispersion length	0.01	Same as TCS
Radial flow, ratio of radial to axial transverse dispersion length	0.01	Same as TCS
Ratio of radial EDZ permeability to axial EDZ permeability	0.1	Same as TCS

## 7.6 GEOSPHERE SORPTION PARAMETERS

Chemical species will, to different degrees, interact with the mineral surfaces surrounding the pores in the rock. Sorption of a radionuclide in the geosphere, may be modelled using a linear relation (justified by the expected low radionuclide concentrations) between the concentration of the sorbed species and the aqueous concentration. The proportionality constant is called the sorption coefficient  $K_d$  ( $m^3/kg$ )

Sorption properties of the rock depend on a number of factors, such as groundwater chemical composition, groundwater redox potential, rock type, degree of fracturing, etc. Many of the factors controlling radionuclide sorption onto the host rock are site-specific, and experimental data obtained for other conditions may not be applicable or may need to be adapted. At present, many of the site-specific conditions are unknown and, therefore, the sorption data used are partly generic.

Radionuclide sorption during transport through the geosphere is incorporated in SYVAC-CC4 using a retardation factor  $R$  given by

$$R = 1 + [\rho_s(1-\varepsilon)/\varepsilon] K_{d,in} \quad (7.1)$$

where  $\rho_s$  is the material grain density,  $\varepsilon$  is the porosity of the geological material and  $K_{d,in}$  is the radionuclide sorption coefficient for intact rock.  $K_{d,in}$  and  $R$  are element dependent.

In order to correct from experimentally measured sorption data on crushed rock samples to those for intact rock, a normalization factor is applied to the experimental sorption coefficient  $K_d$  (Vandergraaf 1997, Vandergraaf and Ticknor 1994) to account for the larger sorption area of the crushed rock, i.e.,

$$K_{d,in} = [(1-\varepsilon_{expt})/\varepsilon_{expt}] [(1-\varepsilon)/\varepsilon]^{-1} K_d \quad (7.2)$$

where  $\varepsilon_{expt}$  is the porosity of the unconsolidated material used in the experimental measurement of  $K_d$ . SKB also uses such a normalization factor (Crawford et al. 2006), but that used in Equation 7.2 (Vandergraaf and Ticknor 1994) is more conservative, i.e., generates smaller  $K_{d,in}$  values. Substituting Equation (7.2) into Equation (7.1) leads to the following expression for the retardation factor

$$R = 1 + [\rho_s(1-\varepsilon_{expt})/\varepsilon_{expt}] K_d \quad (7.3)$$

Table 7.8 lists values of  $[\rho_s(1-\varepsilon_{expt})/\varepsilon_{expt}]$  for various geological materials (Vandergraaf and Ticknor 1994).

In general, the geosphere includes an overburden on top of the bedrock, and the compacted (deep) sediment layer at the bottom of lakes. The normalization factors for the overburden materials were calculated with Equation 7.2 assuming a solid density of 2.65 kg/L and a porosity of 0.42 (Davison et al. 1994, p. 366). For the compacted sediment, a density of 2.5 kg/L (Davis et al. 1993, p. 82) and a porosity of 0.5 (Davison et al. 1994, p. 366) were used. For granite, a density of 2.7 kg/L (Davison et al. 1994) and a porosity of 0.5 (Davison et al. 1994) were used

**Table 7.8: Values of  $[\rho_s(1-\epsilon_{\text{expt}})/\epsilon_{\text{expt}}]$  for several geological materials**

<b>Geological Material</b>	<b><math>\rho_s(1-\epsilon_{\text{expt}})/\epsilon_{\text{expt}}</math> (kg/m<sup>3</sup>)</b>
granite	2700
sand	3660
silt	3660
clay	3660
sediment	2500

In the CC4 model, the experimental  $K_d$  values are input into the code and then the normalization factor is applied within the model. A complete list of  $K_d$  values are shown in Table 7.9. The  $K_d$  values are generally described using a lognormal probability density function. No distinction is made between sorption values for the bulk granite and for fracture materials, given the limited data available for fracture materials.

The  $K_d$  values are taken from Crawford et al. (2006), when available. The GM of the distribution is set equal to their recommended  $K_d$  value, and the GSD was calculated assuming that the lower limit selected by SKB is 3 standard deviations from the GM.

The  $K_d$  values for sand, silt, clay and sediment in the overburden are taken from Thibault et al. (1990) and Davis et al. (1993) for sand, loam, clay and organic soils, respectively, with updates for Cl, I, Np, Ra and U, as described in Section 8. (Note that CSA (2008) has also adopted the soil  $K_d$  values of Thibault et al. (1990) and Davies et al. (1993).) The same values are used for oxidizing or reducing conditions. The soil  $K_d$  values are generally described by a lognormal distribution with a geometric standard deviation of 10; thus, the same PDF is used for sand, silt, clay and sediment.

**Table 7.9: Reference values of  $K_d$  for fractures and crushed rock<sup>1,2</sup>**

Element	Distribution	GM [m <sup>3</sup> /kg]	GSD [-]	Lower Limit [m <sup>3</sup> /kg]	Upper Limit [m <sup>3</sup> /kg]
Ac	Lognormal	3	1.4	1	5
Ag	Lognormal Lognormal	Non Saline 0.5 Saline 0.05	Non Saline 1.7 Saline 1.7	Non Saline 0.1 Saline 0.01	Non Saline 1 Saline 0.1
Am	Lognormal	13	3.9	0.22	190
As <sup>5</sup>	Constant	0		-	
Bi <sup>4</sup>	Lognormal	0.001	2.2	0.0001	0.01
C	Lognormal	0.001	1.3	5x10 <sup>-4</sup>	2x10 <sup>-3</sup>
Ca <sup>6</sup>	Lognormal Lognormal	Non Saline 1.3x10 <sup>-2</sup> Saline 9.8x10 <sup>-5</sup>	Non Saline 2.4 Saline 1.9	Non Saline 1x10 <sup>-3</sup> Saline 1.4x10 <sup>-5</sup>	Non Saline 6.1x10 <sup>-1</sup> Saline 5x10 <sup>-4</sup>
Cd	Lognormal Lognormal	Non Saline 0.1 Saline 0.02	Non Saline 1.3 Saline 1.3	Non Saline 0.05 Saline 0.01	Non Saline 0.5 Saline 0.1
Ce <sup>6</sup>	Lognormal	2	1.3	1	5
Cl	Constant	0		-	
Co	Lognormal Lognormal	Non Saline 0.1 Saline 0.02	Non Saline 1.3 Saline 1.3	Non Saline 0.05 Saline 0.01	Non Saline 0.5 Saline 0.1
Cr <sup>6</sup>	Lognormal	2	1.3	1	5
Cs	Lognormal Lognormal	Non Saline 0.18 Saline 0.042	Non Saline 4.7 Saline 4.7	Non Saline 1.7x10 <sup>-3</sup> Saline 4x10 <sup>-4</sup>	Non Saline 9.6 Saline 2.0
Cu <sup>6</sup>	Lognormal Lognormal	Non Saline 1.3x10 <sup>-2</sup> Saline 9.8x10 <sup>-5</sup>	Non Saline 2.4 Saline 1.9	Non Saline 1x10 <sup>-3</sup> Saline 1.4x10 <sup>-5</sup>	Non Saline 6.1x10 <sup>-1</sup> Saline 5x10 <sup>-4</sup>
Eu	Lognormal	2	1.3	1	5
Hg <sup>5</sup>	Constant	0		-	
I	Constant	0		-	
La <sup>6</sup>	Lognormal	2	1.3	1	5
Nd <sup>6</sup>	Lognormal	2	1.3	1	5
Ni	Lognormal Lognormal	Non Saline 0.12 Saline 0.01	Non Saline 1.9 Saline 1.7	Non Saline 1.8x10 <sup>-2</sup> Saline 2.0x10 <sup>-3</sup>	Non Saline 5.4x10 <sup>-1</sup> Saline 8.7x10 <sup>-2</sup>
Np (V) Np (IV) <sup>3</sup>	Lognormal Lognormal	Oxidizing 0.018 Reducing 0.96	Oxidizing 2.1 Reducing 2.7	Oxidizing 2.0x10 <sup>-3</sup> Reducing 4.7x10 <sup>-2</sup>	Oxidizing 2.2x10 <sup>-1</sup> Reducing 20
P <sup>4</sup>	Constant	0		-	

Pa	Lognormal	1	1.3	$5 \times 10^{-1}$	5
Pb <sup>4</sup>	Lognormal Lognormal	Non Saline 0.12 Saline 0.01	Non Saline 1.9 Saline 1.7	Non Saline 0.018 Saline 0.002	Non Saline 0.54 Saline 0.087
Pd	Lognormal Lognormal	Non Saline 0.1 Saline 0.01	Non Saline 2.2 Saline 2.2	Non Saline 0.01 Saline 0.001	Non Saline 0.5 Saline 0.05
Po <sup>7</sup>	Lognormal	0.1	2.2	0.01	1
Pr <sup>6</sup>	Lognormal	2	1.3	1	5
Pu	Lognormal	5	1.7	1	10
Ra <sup>2</sup>	Lognormal Lognormal	Non Saline 1.3 Saline 2.1	Non Saline 2.7 Saline 6.9	Non Saline $6.3 \times 10^{-2}$ Saline $6.4 \times 10^{-4}$	Non Saline 11 Saline 2.6
Rn <sup>5</sup>	Constant	0	-		
Sb <sup>5</sup>	Constant	0	-		
Se	Lognormal	0.001	1.3	$5 \times 10^{-4}$	$5 \times 10^{-3}$
Sn	Lognormal	$1 \times 10^{-3}$	4.6	0	$1 \times 10^{-2}$
Te <sup>5</sup>	Constant	0	-		
Th	Lognormal	1	1.3	$5 \times 10^{-1}$	10
U (VI) U (IV) <sup>3</sup>	Lognormal Lognormal	Oxidizing 0.0063 Reducing 6.3	Oxidizing 2.3 Reducing 5.1	Oxidizing $5.0 \times 10^{-4}$ Reducing $4.8 \times 10^{-2}$	Oxidizing $1.2 \times 10^{-1}$ Reducing 280
Y <sup>6</sup>	Lognormal	2	1.3	1	5

<sup>1</sup>K<sub>d</sub> values for granite are from Crawford et al. (2006, Table 7.1-7.3), except as noted.

<sup>2</sup>Saline groundwater in Crawford et al (2006) is defined as [Cl<sup>-</sup>] > 500 mg/L, and non-saline otherwise. In the Fourth Case Study, the groundwater has a [Cl<sup>-</sup>] of 6000 mg/L (see Table 5.5). Salinity was not found to affect the K<sub>d</sub> for other elements

<sup>3</sup>Oxidizing values used in geosphere zones above redox divide, see Table 7.4.

<sup>4</sup>K<sub>d</sub> values are from Ticknor and Vandergraaf (1999).

<sup>5</sup>K<sub>d</sub> values are assumed to be zero.

<sup>6</sup>K<sub>d</sub> values are based on chemical analogue. Ca and Cu are assumed to have the same K<sub>d</sub> as Sr from Crawford et al (2006), Cr is assumed to have the same K<sub>d</sub> as Ce, as suggested by Ticknor and Vandergraaf (1996), and several of the lanthanides (Ce, La, Nd, Pr, and Y) are assumed to have the same K<sub>d</sub> as Eu from Crawford et al. (2006).

<sup>7</sup>K<sub>d</sub> value for Po is from Baston et al. (1999).

## 7.7 WELL LOCATION AND DEPTH

An important pathway for human exposure to contaminants released from the repository is through a well, which can supply water for drinking, domestic use and irrigation. As a conservative assumption for safety assessment, the location and depth of the well are selected so as to maximize the possibility that the well water becomes contaminated. However, this must be tempered with the knowledge that some well locations would be unrealistic. For instance, the water could be unacceptably saline or the rock might not be sufficiently permeable to provide the amount of water required.

For the EIS, a survey of wells drilled around the Whiteshell Research Area was used to derive a statistical distribution of well depths. The results were described by a lognormal PDF with geometric mean of 37 m, geometric standard deviation of 2.2 m, and a range from 0 to 200 m (Davison et al. 1994, p.386). The wells were judged to draw all or part of their water from weathered and fractured bedrock.

The FRAC3DVS-OPG groundwater flow modelling requires a specific well location and depth. For the Fourth Case Study, a reference well location and depth was defined. The location was selected based on preliminary FRAC3DVS-OPG calculations so as to intercept the contaminant plume from the repository. A reference (bottom) well depth of about 100 m was chosen as a plausible but conservative value for the following reasons:

- The well could be located along the centerline of the contaminant plume from the defective containers (which were located at the repository location with the shortest groundwater transit time to the surface);
- The well intersected a fracture, ensuring good water supply;
- Salinity increases with depth, making the water less suitable for use; and
- This well depth is about twice as deep as typical Canadian Shield practice, according to the EIS data.

The well was analytically tested to be capable of supplying a range of well demands of interest. If the well is not capable of supplying all the water needed by the critical group, then it is assumed that the water demand that cannot be satisfied by the well is taken from the Lake. More information on the well location, and on the groundwater flow around the well, is provided in NWMO (2012a).

Table 7.10 summarizes the reference well properties (well demand is discussed in Section 8).

**Table 7.10: Well model geosphere parameters**

<b>Parameter</b>	<b>Reference Value</b>	<b>Comment</b>
Well depth	100 m	Bottom of well, relative to ground surface
Well casing radius	0.0508 m	75% of wells on Canadian Shield are 0.0508 m radius while 25% are 0.0762 m radius (4 or 6 inches diameter). (Davison et al. 1994, p.416)
Well bypass discharge minimum fraction	1.0	Minimum fraction for the reduction of the discharge area associated with the well bypass. Set to one representing no reduction of the discharge area due to well demand.
Well divergent break point A	911 m <sup>3</sup> /a	Break Points A, B, and C (BP <sub>a</sub> , BP <sub>b</sub> , and BP <sub>c</sub> ) are used for segments leading away from divergent nodes that exhibit changes in flow amounts due to different well demands. The break point values are used in combination with the change of the fractional flow per unit well demand for the three ranges (Appendix F).
Well divergent break point B	1500 m <sup>3</sup> /a	
Well divergent break point C	2500 m <sup>3</sup> /a	
Well demand maximum	2500 m <sup>3</sup> /a	For well demands above BP <sub>c</sub> the divergent fraction is estimated to increase at the same slope as the range from BP <sub>b</sub> to BP <sub>c</sub> . The initial source fractions for divergent segments are based on the zero well condition.  If the well demand is estimated to exceed this value, the CC4 code generates a warning indicating the effects of this well demand are estimates and beyond the verified range of the groundwater flow fields for which the geosphere transport model was developed.

## 7.8 OTHER GEOSPHERE PARAMETERS

Table 7.11 lists values of other miscellaneous parameters used by the CC4 geosphere model.

**Table 7.11: Other properties**

Parameter	Reference Value	Comment
Water density $\rho_0$ at 25°C for density equation	997.1 kg/m <sup>3</sup>	Value used in calculation of density at other temperatures. (CRC 1993).
Compressibility of water $\beta_{\text{water}}$ at 25°C for the density equation	4.57x10 <sup>-10</sup> Pa <sup>-1</sup>	CRC (1993) <sup>1</sup>
Coefficient <b>a</b> for density equation	-3.17x10 <sup>-4</sup> K <sup>-1</sup>	CRC (1993) <sup>1</sup>
Coefficient <b>b</b> for density equation	-2.56x10 <sup>-6</sup> K <sup>-2</sup>	CRC (1993) <sup>1</sup>
Coefficient <b>a</b> for viscosity equation	1.27x10 <sup>-6</sup> kg/m·s	CRC (1993) <sup>2</sup>
Coefficient <b>b</b> for viscosity equation	1.97x10 <sup>3</sup> K	CRC (1993) <sup>2</sup>
Reference water density	1000 kg/m <sup>3</sup>	Reference water density used for input hydraulic head data. Value corresponds to freshwater at atmospheric pressure and 6°C.
Reference water viscosity	1.472x10 <sup>-3</sup> kg/m·s	Reference water viscosity used for input hydraulic conductivity data. Value corresponds to freshwater at atmospheric pressure and 6°C.
0°C	273.15 K	Used in °C to K conversion

<sup>1</sup>Density of water =  $\rho_0 (1 + \beta_{\text{water}} \Delta p + \mathbf{a}(\Delta T) + \mathbf{b}(\Delta T)^2)$ , where  $\Delta T = T[^\circ\text{C}] - 25^\circ\text{C}$  and  $\Delta p = \text{head difference from hydrostatic [Pa]}$ . Calculated densities match values in CRC (1993) within 1% over the range 0-100°C.

<sup>2</sup>Viscosity of water =  $\mathbf{a} \cdot e^{(\mathbf{b}/T[\text{K}])}$ . Calculated viscosities match values in CRC (1993) within 5% over the range 0-70°C.

## 7.9 GEOSPHERE NODE DATA

The geosphere is represented by either 3-D finite-element models in FRAC3DVS-OPG, or as a network of 1-D transport paths in SYVAC3-CC4.

The FRAC3DVS-OPG representations typically involve over 1 million nodes, and are not included here. Further details about these detailed models are given in NWMO (2012a). The SYVAC3-CC4 geosphere transport model uses a simplified representation of the FRAC3DVS-OPG groundwater flow field. The input parameters used in this latter model are described in Appendix F of this report.



## **8. BIOSPHERE DATA**

The Fourth Case Study repository is located in the same area of the Canadian Shield as the repository in the Third Case Study (Gierszewski et al. 2004b). Thus, many of the biosphere parameter values are unchanged from those used in the TCS, although some values have been updated where better data were available.

In particular, CSA N288.1 (CSA 2008) values were used to update biosphere model parameter values when available. In addition, biosphere parameters for I, Cl, Np, U, Rn and Ra were also updated based on the recommendations of Sheppard et al. (2002, 2004a, 2004b, 2005a and 2005b, respectively).

The following sections summarize the biosphere parameter values used in the Fourth Case Study and provide links to the original sources of the data.

### **8.1 SITE AND SURFACE WATER**

The Fourth Case Study is based on a hypothetical but plausible Canadian Shield site. The surface topography of this site is relatively flat, as illustrated in Figure 7.1. The sub-regional watershed containing the repository is bounded by topographic highs to the north and south; a major east-west river crosses through the sub-regional watershed area. The repository is approximately in the centre of this area.

A close-up view of the area around the repository is shown in Figure 8.1. The surface water features closest to the repository are the large river, the lake (above the north east corner of the repository) and wetlands north of the river. All water drainage from this area eventually reaches the river.

The biosphere characteristics are typical of the Canadian Shield. A general description of the Canadian Shield biosphere is provided in Davis et al. (1993).

### **8.2 DISCHARGE ZONES**

Contaminants released from the repository can eventually move through the geosphere and, if they do not decay first, reach the biosphere. In general, they will reach the biosphere at specific discharge zones that will depend upon details of the repository location, geosphere properties, and surface topography. Typically, these discharge zones are topographic low areas and often are associated with bodies of water.

Transport modelling results shown in Figure 8.2 indicate that the main discharge areas for contaminants released from the repository are three wetland areas (referred to as the West Wetland, the Central Wetland and the East Wetland), the river and the lake. The discharges to the West Wetland are relatively small and, generally, the travel times from the repository to the West Wetland are much longer than for the other discharge locations. Therefore, the biosphere model specifically considers only four discharge zones, which are referred to as the River, Lake, East Wetland, and Central Wetland in further discussion. Discharges that would have gone to the West Wetland are instead directed to the River discharge location.

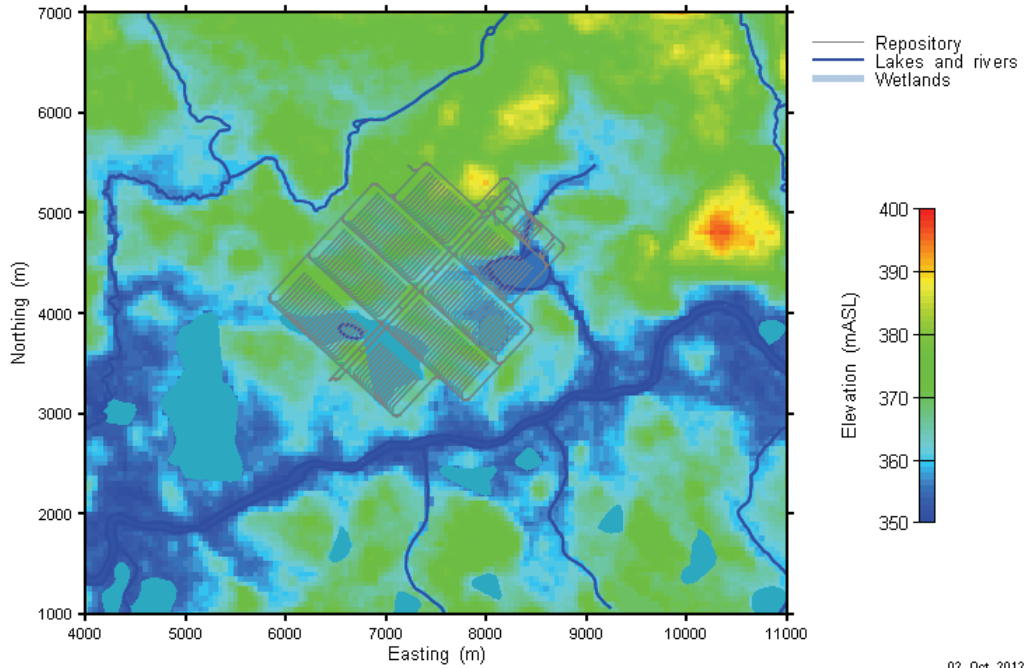


**Figure 8.1: Close-up of the area around the repository site, showing the major water bodies (lakes, rivers and streams) and wetlands. The projected location of the repository at surface is also shown.**

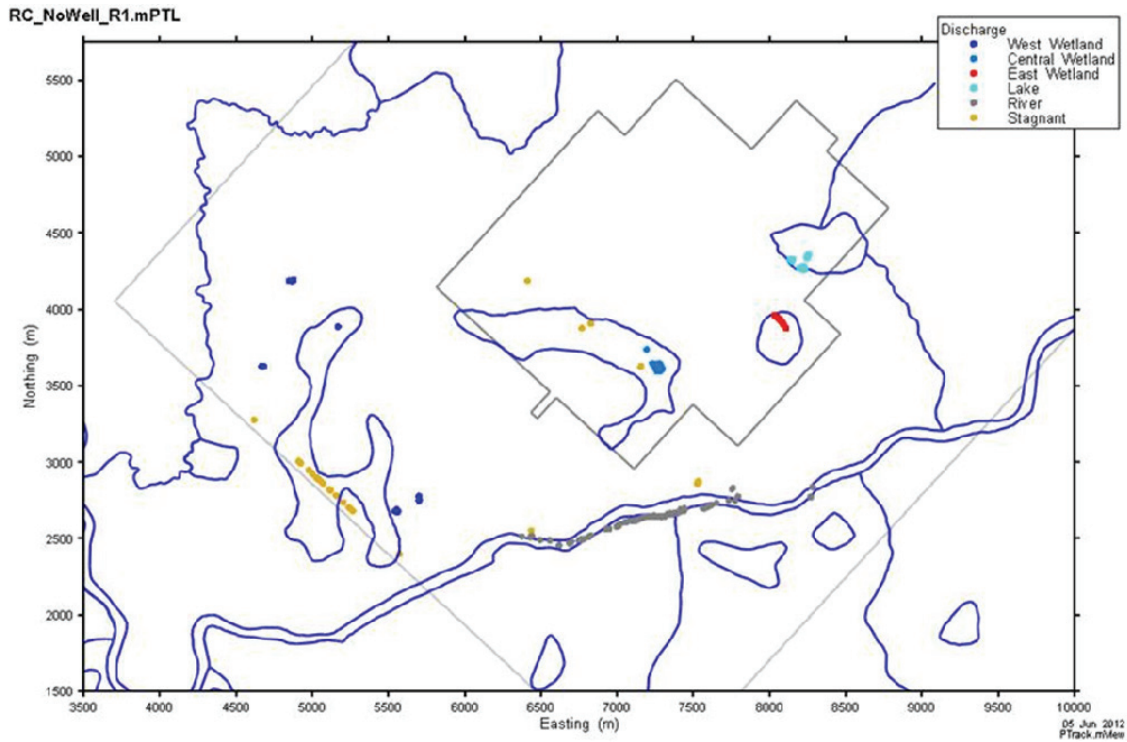


**Figure 8.2: Discharge points of particle track released from repository (plan view). Surface water features, including wetlands, are outlined in blue. These tracks are based on the no-well case.**

The discharge areas are used as various fields by the critical group. The fields are assigned to the discharge areas in the following order: River, Lake, East Wetland and Central Wetland, based on the fraction of particle tracks arriving at these discharge locations when the well used by the critical group is operating.

Ultimately, contaminants released into the biosphere at these discharge locations are either trapped in deep sediments under these water bodies, or transported out of the local watershed through the River. People living near the River, downstream from the repository, could be exposed to all the contaminants that reach the surface. However, there would be significant dilution since this River drains a large watershed area upstream of the repository.

### Lake and River Watershed Areas

The Lake and River watershed areas were calculated based on detailed topographic maps of the area. The Lake and River watershed areas are approximately 4 km<sup>2</sup> and 2300 km<sup>2</sup>, respectively. These values, which are assumed to be constant in time, are used to calculate the water flow rate through the Lake and River, based on the precipitation and runoff values defined in the next section.

In the Fourth Case Study safety assessment, we consider a human critical group living close to the well location, which is in the vicinity of the Central Wetland discharge. We also assume that all discharged contaminants flow into the Lake (even if they are captured by the well) in order to conservatively estimate contaminant concentrations in surface waters and to account for runoff of contaminated water (from, for example, farm fields irrigated with well water). The Lake is selected for this purpose because contaminants would be much less diluted in the Lake than the River, due to the much higher flow rate through the River.

The characteristics of the Lake are summarized in Table 8.1.

### River discharge area

Based on the particle transport modelling from the repository shown in Figure 8.2 (for the now well case) and accounting for lateral dispersion of the contaminant plume, the River discharge area is conservatively estimated to be  $7.9 \times 10^4$  m<sup>2</sup>. However, the discharge areas may change with time, due to natural changes and climate change. Since exposure will likely occur at some time in the future, the future River discharge area is uncertain. Therefore, the River discharge area is described by a loguniform distribution with lower and upper bounds of  $2.6 \times 10^4$  m<sup>2</sup> and  $1.6 \times 10^5$  m<sup>2</sup>, respectively. The lower bound was estimated by neglecting lateral dispersion and the upper bound was estimated from the nominal extent of the surface concentration plumes calculated with FRAC3DVS-OPG, assuming contaminant releases from all containers in the repository.

The transport results in Figure 8.2, suggest that a large fraction of the discharges near the River location emerge onto the land adjacent to the River rather than under the River itself. For the River discharge, the terrestrial discharge fraction is estimated to be about 66% of the total River discharge area.

**Table 8.1: Lake properties**

<b>Parameter</b>	<b>Reference Value</b>	<b>Comment</b>
Lake watershed area	$4 \times 10^6 \text{ m}^2$	Estimated based on topographical map (about 2 km x 2 km).
Lake surface area	$150,000 \text{ m}^2$	Lognormal PDF with GM= $150,000 \text{ m}^2$ , GSD=7.4, and bounds of 10,000 to $800,000 \text{ m}^2$ . Correlated to mean lake depth with a 0.5 correlation coefficient.
Mean lake depth	4.6 m	Lognormal PDF with GM=4.6 m, GSD=2.0, and bounds of 1.0 to 10 m (Davis et al. 1993, p. 97, except for the upper bound). Upper bound is limited by topography of the area around the lake.
Sedimentation rate	0.16 $\text{kg}_{\text{dry sed.}}/\text{m}^2\text{a}$	Lognormal PDF with GM= $0.16 \text{ kg}/(\text{m}^2\cdot\text{a})$ , GSD=2.5, and bounds of 0.01 and $15 \text{ kg}/(\text{m}^2\cdot\text{a})$ (Davis et al. 1993, p.99)
General sediment layer thickness	Lake 3.7 m	Lognormal PDF with GM=3.7 m, GSD=2.2 and bounds of 0.3 and 10 m, based on Davison et al. (1994, p. 415), but with a smaller range.
	River 0.4 m	The thickness of river sediments is assumed to be 1/10th that of lake sediments because of the faster water flows. Lognormal PDF with GM=0.4 m, GSD=2.2 and bounds of 0.03 to 1.
Mixed sediment thickness	0.01-0.1 m	Uniform PDF over 0.01-0.1 m (Davis et al. 1993, p. 99). This is the thickness of the top mixed sediment layer.
Thickness of sediment removed for use in fields	0.3 m	Set to minimum value of 0.3 m allowed by CC4
Sediment dry bulk density	$125 \text{ kg}/\text{m}^3$	(Davis et al. 1993, p.100)

### Lake discharge area

Using the particle track results shown in Figure 8.2 (for the no well case) and accounting for lateral dispersion, the Lake discharge area is conservatively estimated to be  $2.8 \times 10^4 \text{ m}^2$ . However, the discharge area may change with time, due to natural changes and climate change. Thus, the Lake discharge area is described by a loguniform distribution with lower and upper bounds of  $1.1 \times 10^4 \text{ m}^2$  and  $1.4 \times 10^5 \text{ m}^2$ , respectively. The lower bound was estimated by neglecting lateral dispersion and the upper bound was estimated from the nominal extent of the surface concentration plumes calculated with FRAC3DVS-OPG, assuming contaminant releases from all containers in the repository.

A large fraction of the discharges near the Lake location emerge under the lake. It is estimated that the aquatic discharge area is about 75% of the total Lake discharge area.

### East Wetland discharge area

The East Wetland discharge area is estimated from the particle track results in Figure 8.2 (for the no well case). The East Wetland discharge area is estimated to be  $2.2 \times 10^4 \text{ m}^2$ , if lateral dispersion is taken into account. However, the discharge areas may change with time, due to natural changes and climate change. Therefore, the East Wetland discharge area is described by a loguniform distribution with lower and upper bounds of  $5.2 \times 10^3 \text{ m}^2$  and  $7.8 \times 10^4 \text{ m}^2$ , respectively. The lower bound was estimated by neglecting lateral dispersion and the upper bound was estimated from the extent of the surface concentration plumes calculated with FRAC3DVS-OPG, assuming contaminant releases from all containers in the repository.

The East Wetland discharge emerges in a wetland. Therefore, the discharge area is classified as 100% terrestrial for modelling purposes, i.e., the entire East Wetland discharge area can, in theory, house farms or forage fields.

### Central Wetland discharge area

The Central Wetland discharge area, for current day conditions (with no well), is illustrated by the particle tracks in Figure 8.2. Using these results, and accounting for the lateral dispersion of the contaminant plume, it is estimated that this discharge area is  $2.9 \times 10^4 \text{ m}^2$ . However, the discharge areas may change with time, due to natural changes and climate change. Therefore, the Central Wetland discharge area is described by a loguniform distribution with lower and upper bounds of  $1.3 \times 10^4 \text{ m}^2$  and  $6.0 \times 10^4 \text{ m}^2$ , respectively. The lower bound was estimated by mostly neglecting lateral dispersion and the upper bound was estimated from the extent of surface concentration plumes calculated with FRAC3DVS-OPG, assuming contaminant releases from all containers in the repository.

The Central Wetland discharge emerges in a wetland. Therefore, the discharge area is classified as 100% terrestrial for modelling purposes.

Table 8.2 summarizes the discharge zone values.

**Table 8.2: Discharge zone areas**

<b>Discharge zone</b>	<b>Reference area of discharge zone [m<sup>2</sup>]</b>	<b>Range of discharge zone area<sup>#</sup> [m<sup>2</sup>]</b>	<b>Aquatic discharge fraction [-]</b>	<b>Terrestrial discharge fraction [-]</b>
River	$7.9 \times 10^4$	$2.6 \times 10^4 - 1.6 \times 10^5$	0.34	0.66
Lake	$2.8 \times 10^4$	$1.1 \times 10^4 - 1.4 \times 10^5$	0.75	0.25
East Wetland	$2.2 \times 10^4$	$5.2 \times 10^3 - 7.8 \times 10^4$	0.0	1.0
Central Wetland	$2.9 \times 10^4$	$1.3 \times 10^4 - 6.0 \times 10^4$	0.0	1.0

<sup>#</sup>Discharge area is described by a loguniform distribution.

### **8.3 CLIMATE AND ATMOSPHERE**

The climate and atmospheric parameters are summarized in Table 8.3. These values reflect CSA (2008) values when available for a Canadian Shield site; otherwise the values are taken from Davis et al. (1993), as was done for the TCS (Garisto et al. 2004b). The variation in these parameter values represents the natural variation across the Canadian Shield for present-day climate conditions.

### **8.4 SOILS AND SEDIMENT**

#### Soil Physical Characteristics

The physical characteristics of the soil at the hypothetical site are described in Table 8.4. These reflect mostly the values in CSA (2008), where available. Otherwise, the values from the TCS are retained (Garisto et al. 2004b).

In SYVAC3-CC4, two soil models are considered: an upland soil and a shallow soil. For the upland soil, which is more typical, the water table is a reasonable distance below the ground surface. For the shallow soil, the water table extends into the surface soil on a regular and extended basis. The distinction between these two cases is important in determining how readily contaminated groundwater can reach the surface. In the upland soil case, it must be transported by processes such as capillary action. In the shallow soil case, the groundwater is directly discharged into the soil layer.

For the upland soil model, a simple approach is used to account for upward movement of contaminated groundwater into the surface soil. Specifically, the model requires information on the surface soil moisture content, and parameters describing the downward flow rate of surface water (precipitation and irrigation) and upward flow rate of groundwater. The water leaching fraction is the fraction of net precipitation or irrigation, after evapotranspiration, which penetrates deep into the soil rather than running off along the surface. On exposed bedrock, the fraction would be small. However, it is assumed that any farming would be on locations with suitable soil, and so a higher fraction would be expected. Since the specific value is uncertain, a large range from 0.1 to 1 is assumed.

Other soil model characteristics are also shown in Table 8.4.

**Table 8.3: Climate and atmosphere parameters**

Parameter	Reference Value	Comment
Annual total precipitation	0.76 m/a	Geometric mean of annual averages from 1983 to 2006 in Geraldton (ON), which was identified as having a climate representative of the Canadian Shield. Normal PDF with a SD of 0.12 and bounds of 0.28 and 1.92 m/a (CDCD 2006). Lower and upper bounds represent half the minimum and double the maximum annual precipitation.
Annual average runoff	0.31 m/a	This is the balance between total precipitation and evapotranspiration, and includes surface runoff as well as infiltration into the water table (CSA 2008). Normal PDF with mean of 0.31 m/a, standard deviation of 0.08 m/a, and bounds of 0.01 and 0.71 m/a. Correlated to total precipitation with a correlation coefficient of 0.80 (Davis et al. 1993, p.151, 279).
Average wind speed <sup>1</sup>	2.36 m/s	Normal PDF with mean of 2.36 m/s (8.5 km/h), standard deviation of 0.64 m/s, and bounds of 0.44 and 6 m/s. (Davis et al. 1993, p.196).
Average temperature <sup>1</sup>	17°C July - 15°C Jan.	Mean daily temperatures observed on Canadian Shield (Fisheries and Environmental Canada 1978).
Climate state	Temperate	Current climate.
Dry deposition velocity <sup>2</sup>	0.006 m/s	Lognormal PDF with geometric mean of 0.006 m/s and geometric standard deviation of 2 (Amiro 1992).
Atmospheric dust load <sup>2</sup>	$3.2 \times 10^{-8}$ kg <sub>drysoil</sub> / m <sup>3</sup> <sub>air</sub>	Lognormal PDF with GM calculated from suspended particulate matter concentrations in ON, NB, QC and SK during years 1996 to 2002. GSD of 1.7 with bounds of $7.0 \times 10^{-9}$ and $7.5 \times 10^{-8}$ kg <sub>drysoil</sub> /m <sup>3</sup> <sub>air</sub> . (NAPS, 1996 to 2002)
Atmospheric aerosol load <sup>2</sup>	$2.9 \times 10^{-10}$ m <sup>3</sup> <sub>water</sub> / m <sup>3</sup> <sub>air</sub>	Lognormal PDF with geometric mean of $2.9 \times 10^{-10}$ m <sup>3</sup> <sub>water</sub> /m <sup>3</sup> <sub>air</sub> , and geometric standard deviation of 1.41. Based on estimate for sea salt aerosol over oceans (Davis et al. 1993, p.191).
Washout Ratio	630 000	CSA (2008) washout ratio for deposition to plants for all elements other than noble gases and iodine. This value is conservative for iodine. CSA (2008) recommends 200 000 for elemental and 8400 for organic iodine.

<sup>1</sup>Davis et al. (1993) values are judged more representative for a site on the Shield than the CSA (2008) values.

<sup>2</sup>Values for these parameters are not available in CSA (2008).

**Table 8.4: Soil properties**

Parameter	Reference Value	Comment
Soil types	Sandy	On the Canadian Shield soil types are distributed as follows: 57% sand, 14% organic, 24% clay, and 5% loam (Davis et al. 1993, p.146).
Surface soil bulk density	1500 kg dry soil/m <sup>3</sup> soil (sandy soil)	The densities of the four soil types are as follows: 1500, 1300, 1400 and 400 kg dry soil/m <sup>3</sup> soil for sand, loam, clay and organic soils, respectively (CSA 2008).
Active surface soil depth	0.2 m	This is the active or root zone layer for which nuclide concentrations in the soil are determined (CSA 2008).
Soil Depth to water table	1.5 m	Normal PDF, 1.5 m mean, 0.5 m standard deviation, and bounds of 0.01 to 2.5 m. (Davis et al. 1993, p.148)
Minimum soil depth to water table for upland soil model	0.5 m	This is the minimum depth-to-water-table at which the upland soil model is used. For smaller depths, a shallow soil model is used that allows for flooding of the surface soil by contaminated groundwater. (Davis et al. 1993, p.137.)
Upland soil leach rate fraction	0.55	Fraction of net precipitation (precipitation + irrigation - evapotranspiration) that infiltrates into soil. Uniform PDF from 0.1 to 1.
Fraction of runoff entering the overburden	0.10	Uniform distribution with a lower bound of 0.03 and an upper bound of 0.17 (Singer and Cheng 2002).
Surface soil moisture content fraction	0.1 (0.05-0.13) sand 0.2 (0.15-0.27) loam 0.3 (0.25-0.42) clay 0.4 (0.3-0.56) organic	Triangular PDF assumed, with the bracketed numbers correspond to the upper and lower bounds. The lower bound is the average wilting point (Beals 1985) and the upper bound is the average field capacity (Beals 1985). The most probable values are from CSA (2008), except for organic soils for which the most probable value is set to the mid range between the wilting point and average field capacity.
Surface soil summer water deficit	0.20 m/a	Climate-based parameter. Value is from water budget data for various locations in the Ontario portion of the Canadian Shield.
Groundwater upflow exponent	3	Value is based on data for a fine sandy loam (Hillel 1980), and so likely overestimates upward flow for other soil types.
Bioturbation rate	0 /a	Not significant in Canadian Shield podzolic soils.



### Plant/Soil Concentration Ratio

Table 8.5 lists the plant/soil concentration ratios for the different elements and the source of the data. The SYVAC3-CC4 biosphere model distinguishes between "garden" plants grown for human consumption, and "forage" plants which are used for animal consumption. Specifically, the model allows for different plant/soil concentration ratios for these different plants.

Plant/soil concentration ratios are inconsistently recorded on a dry or fresh weight basis. Conversion between the two is inaccurate unless the dry/fresh weight ratio is known. For consistency in the values reported herein, a dry/fresh weight ratio of 0.53 and 0.35 are used for forage and garden crops, respectively. These values were calculated from the dry/fresh weight ratios given in CSA (2008). The dry/fresh weight ratio for forage crops is the average of the dry/fresh weight ratio of 0.19 for forage (e.g., fresh grass) and 0.86 for feed (e.g., grains), and assumes that animals eat 50% forage and 50% feed over the year. Similarly, the dry/fresh weight ratio for garden crops is calculated assuming that the critical group plant intake is 1/3 grain (dry/fresh weight ratio of 0.86) and 2/3 fruits and vegetables (dry/fresh weight ratio of 0.1).

The CSA (2008) plant/soil concentration ratios, which are expressed on a dry weight basis, were converted to a fresh weight basis using the dry/fresh weights shown above. The plant/soil concentration data in Davis et al. (1993) are expressed in a plant fresh-weight basis, and were obtained from the original data using a plant dry/fresh weight ratio of 0.25. For consistency, the Davis et al. (1993) values were converted to a fresh weight basis using the dry/fresh weight ratios selected for this study.

The plant/soil concentration ratio is described using a lognormal PDF with the geometric mean given in Table 8.5 and a geometric standard deviation (GSD) of 5.7 for most elements (unless otherwise specified), as recommended by BEAK (2002).

### Soil Distribution Coefficient ( $K_d$ )

Table 8.6 provides the soil  $K_d$  values. The geometric mean values for Cl, I, Np, Ra and U are from Sheppard et al. (2002, 2004a, 2004b, 2005a and 2005b, respectively). All other geometric means are from CSA (2008); except those for Ac, Bi, Ca, Cd, Pb, Pd and Po which are from Davis et al. (1993, p. 155); and Cu and Rn which are from Gobien and Garisto (2012). The soil  $K_d$  values are described using a lognormal distribution (except for Rn, for which the  $K_d$  values are zero). The GSD assigned is 10, as per Davis et al. (1993), except for I in organic soil for which the GSD = 22 (Sheppard et al. 2002), Ra in all soils for which the GSD = 4.9 (Sheppard et al. 2005a) and U in all soils for which the GSD = 20 (Sheppard et al. 2005b).

There is a strong inverse correlation between plant uptake of elements and the soil  $K_d$  values. Therefore, the  $K_d$  values are correlated to the plant/soil concentration ratio values (Table 8.5) with a correlation coefficient of -0.7 (Sheppard et al. 2010).

### Lake Sedimentation Rate

Table 8.6 provides data for the sedimentation rate of the different chemical elements in lakes. This parameter is defined as the fraction of the element in the water column that is lost to the lake sediments per unit time. It is the net rate of sedimentation, accounting for any resuspension of sediments back into the water column.

The lake sedimentation rates were calculated from the equation (CSA 2008):

$$\lambda_{lake} = \frac{DR \cdot \rho \cdot A \cdot K_d}{V}$$

where:

- $\lambda_{lake}$  is the lake sedimentation rate (1/a);
- $DR$  is the sediment accumulation rate, 1 mm/a (CSA 2008);
- $\rho$  is the sediment density, 400 kg<sub>dw</sub>/m<sup>3</sup> (CSA 2008);
- $A$  is the area of the lake, m<sup>2</sup> (see Table 8.1)
- $K_d$  is the solid-to-liquid partition coefficient, m<sup>3</sup>/kg<sub>dw</sub>; and
- $V$  is the lake volume (m<sup>3</sup>) (see Table 8.1)

CSA (2008) recommends setting the solid-to-liquid partition coefficient to be 5 times the  $K_d$  of loam. Values of the lake sedimentation rate are lognormally distributed with GM values shown in Table 8.6 and the GSD equal to that for the loam  $K_d$  values. Namely, a GSD of 10 except for I in organic soils (GSD=22), Ra in all soils (GSD=4.9) and U in all soils (GSD=20).

**Table 8.5: Plant/soil concentration ratios**

Element	Garden <sup>1</sup> (Bq/kg wet)/ (Bq/kg drysoil)	Forage <sup>1</sup> (Bq/kg wet)/ (Bq/kg dry soil)	Reference
Ac	0.0012	0.0019	Davis et al. (1993)
Am	0.00022	0.00034	CSA (2008)
Bi	0.0046 (2)	0.01 (2)	Sheppard et al. (2009)
C	7.7	11	CSA (2008)
Ca	0.022	0.025 (5.6)	Sheppard et al. (2010)
Cl	3.7	4.2	Sheppard et al. (2004a)
Cs	0.018	0.028	CSA( 2008)
I	0.005 (10)	0.027 (10)	Sheppard et al. (2002)
Ni	0.17	0.25	CSA( 2008)
Np	0.0006 (6.7)	0.0046 (10)	Sheppard et al. (2004b)
Pa	0.013	0.02	CSA( 2008)
Pb	0.00084 (2.5)	0.0012 (2.5)	Sheppard et al. (2010)
Po	0.00088	0.0013	Davis et al. (1993)
Pu	0.000049	7.40E-05	CSA( 2008)
Ra	0.0041 (7.5)	0.017 (11)	Sheppard et al. (2005a)
Rn	0	0	Davis et al. (1993)
Sb	0.00053	0.0008	CSA( 2008)
Se	0.15	0.23	CSA( 2008)
Sn	0.14	0.22	CSA( 2008)
Th	0.0012	0.0018	CSA( 2008)
U	0.00079 (6.3)	0.0027 (8.4)	Sheppard et al. (2005b)

<sup>1</sup>Values are lognormally distributed, with GM as listed and GSD = 5.7, with exceptions shown in brackets.

**Table 8.6: Soil  $K_d$  values<sup>1</sup> [L/kg] and lake sedimentation rates [1/a]**

	<b>Sand</b>	<b>Loam</b>	<b>Clay</b>	<b>Organic</b>	<b>Lake Sedimentation Rate</b>
Ac	450	1500	2400	5400	0.65
Ag	90	120	180	15000	0.052
Am	2000	9600	8100	110 000	4.2
As	1.0	6.0	10	10	0.0026
Bi	100	450	600	1500	0.20
C	5	20	1	70	0.0087
Ca	5	30	50	90	0.013
Cd	80	40	560	800	0.60
Ce	490	8100	20000	3000	3.5
Cl	0.10	0.10	0.10	2200	4.30E-05
Co	60	1300	540	990	0.57
Cr	67	30	1500	270	0.013
Cs	270	4400	1800	270	1.9
Cu	30	100	160	370	0.043
Eu	120	430	650	1500	0.19
Hg	16	55	84	194	0.024
I	8.0	18	12	76	0.0078
La	170	580	880	2000	0.25
Nb	160	550	900	2000	0.24
Ni	400	300	670	1100	0.13
Np	2.5	13	21	530	0.0057
P	9	30	49	110	0.013
Pa	540	1800	2700	6600	0.78
Pb	270	16 000	550	22 000	7.0
Pd	55	180	270	670	0.078
Po	150	400	3000	7300	0.17
Pr	100	360	550	1300	0.16
Pu	540	1200	4900	1800	0.52
Ra	47	47	47	47	0.02
Rn	0.0	0.0	0.0	0.0	0
Sb	45	150	240	540	0.065
Se	150	490	740	1800	0.21
Sn	130	450	670	1600	0.200
Te	130	500	720	1900	0.22
Th	3000	3300	5400	89 000	1.4
U	42	220	180	2200	0.096
Y	170	720	1000	2600	0.31

<sup>1</sup>Values are lognormally distributed with GM as stated and GSD=10, except for I in organic soil with GSD=22, Ra in all soils with GSD=4.9 and U in all soils with GSD=20.

## 8.5 FARMING YIELDS

Table 8.7 summarizes the properties relevant for determining the productivity of the area used for farming and building purposes. The data are from CSA (2008), if available; otherwise the data are from Davis et al. (1993).

**Table 8.7: Farming yield data**

Parameter	Reference Value	Comment
Forest renewal time	50 a	This is the average time for a forest to regenerate, used in estimating woodlot size. Normal PDF with mean 50 a, standard deviation 10 a, and bounds of 25 and 100 a. EIS used a fixed value of 50 a (Davis et al. 1993).
Forest yield in fire	2.2 kg/m <sup>2</sup>	Lognormal PDF with geometric mean of 2.2 kg/m <sup>2</sup> and geometric standard deviation of 1.6 (Davis et al. 1993, p.260). Note only small fraction of the forest mass is consumed in a fire.
Forest yield for wood	10.5 kg/m <sup>2</sup>	Fixed value (Davis et al. 1993, p.260).
Soil contamination of plants	5x10 <sup>-4</sup> kg <sub>drysoil</sub> /kg <sub>wetbio</sub>	Fixed value (Davis et al. 1993, p.258).
Plant yield (plant)	0.8 kg <sub>fw</sub> /m <sup>2</sup>	The yield per harvest of plant used to feed people. Corresponds to a plant human diet of 2/3 fruits and vegetables and 1/3 grain as per CSA (2008, Table G.5). Normal PDF with bounds 0.1 to 8 and standard deviation of 1, calculated using grain (winter wheat, spring wheat, fall rye, buckwheat, oats, barley, mixed grain, canola and coloured beans) data from OMAFRA (2012) and fruits and vegetable data from OMAFRA (2011a, 2011b).
Plant yield (milk)	0.6 kg <sub>fw</sub> /m <sup>2</sup>	The yield per harvest of plants used to feed milk and meat producing animals, such as dairy cattle, beef cattle and chicken. Assume all animals eat generic feed crop (CSA 2008, Table G.5). Normal PDF with bounds of 0.1 to 4 and standard deviation of 1.3, where bounds and standard deviation were determined using the yield from 2001 to 2011 for grain corn, soybeans, dry white beans, fodder corn from OMAFRA (2012).
Plant yield (meat)	0.6 kg <sub>fw</sub> /m <sup>2</sup>	
Plant yield (bird)	0.6 kg <sub>fw</sub> /m <sup>2</sup>	

## 9. DOSE PATHWAYS DATA

### 9.1 HUMAN LIFESTYLE CHARACTERISTICS

For the present-day temperate climate, the reference human group or "critical group" for dose assessment purposes is defined as a self-sufficient farm household living near the repository. Davis et al. (1993, p.274) indicated that up to 50% of rural residents in Ontario used wells; therefore, lakes and wells were equally likely sources of water within the probabilistic safety analyses. In the Fourth Case Study, the critical group is conservatively assumed to use a well, since contaminant concentrations should be higher in well water than in surface waters due to lower dilution.

The number of people living in the reference household was modelled based on the 1987 Canadian census data, which considers households of up to 36 people, and the 1996 Canadian census data, which lumps households of 6 people and more into the same count. The data follows a lognormal distribution with upper and lower bounds of 1 to 12 people per household. This distribution was fitted by a piece-wise uniform distribution so that only an integer number of people per household would be considered. According to the 1996 Canadian census, the average Ontario farm had 3.2 people per farm (Statistics Canada 2002). Since the models are to be applied for long time frames, we judge that this piece-wise distribution, with a best-estimate of 3 persons per household, and a large PDF range, is a reasonable estimate for the critical group size.

Table 9.1 summarizes the lifestyle characteristics that describe the reference farm household.

As noted in Table 9.1, vegetable crops in general would be more likely to be irrigated than forage crops. Furthermore, they are also likely to receive a larger amount of water. The amount of irrigation water required also depends on the soil type - sandy soils in particular are distinctly different in terms of the amount of water they can store for crop use. The recommended irrigation amounts are listed in Table 9.2. These were largely based on 30-year irrigation data from northern Ontario as summarized in Sheppard (1985). The data is represented by a normal PDF, where the standard deviation was calculated using the 95<sup>th</sup> percentile from Coligado (1968). The lower limit of 0.02 m/a is recommended based on the argument that, when irrigation is invoked, this represents the minimum amount of water that would be applied. The upper bound was set at approximately three standard deviations beyond the mean.

The amount of irrigation water will be strongly inversely correlated to the amount of precipitation. The preferred measure would be the effective precipitation, the amount that actually infiltrates the soil. However, total precipitation is the input parameter in SYVAC3-CC4. Therefore, the irrigation rate is correlated to total annual precipitation with a negative correlation coefficient of -0.9.

**Table 9.1: Human lifestyle characteristics for farm household**

<b>Parameter</b>	<b>Reference Value</b>	<b>Comment</b>
People per household	3	Piece-wise uniform PDF from 1 to 12 people per household (Statistics Canada 1996; Davis et al. 1993, p.270).
Domestic water demand per person	110 m <sup>3</sup> /a	Lognormal PDF with geometric mean 110 m <sup>3</sup> /a, GSD of 2 and bounds of 40 and 240 m <sup>3</sup> /a. Calculated from data in Environment Canada (2007)
Man's air inhalation rate	8400 m <sup>3</sup> /a	95 <sup>th</sup> percentile from CSA (2008)
Man's water ingestion rate	840 L/a	90 <sup>th</sup> percentile from CSA (2008)
Man's total energy need	18744 kJ/d	90 <sup>th</sup> percentile from CSA (2008).
Man's meat ingestion rate	103 g/d	Median intakes for male adult (CSA 2008, Table G.9a). Defined as lognormal PDF with GM equal to median and GSD=1.65 (Zach and Sheppard 1992). For a total energy intake of 18744kJ/d, this intake is prorated to 249 g/d.
Man's milk ingestion rate	283 g/d	Median intakes for male adult (CSA 2008, Table G.9a). Defined as lognormal PDF with GM equal to median and GSD=1.35 (Zach and Sheppard 1992). For a total energy intake of 18744kJ/d, this intake is prorated to 685 g/d.
Man's plant ingestion rate	796 g/d	Median intakes for male adult (CSA 2008, Table G.9a). Defined as lognormal PDF with GM equal to median and GSD=1.65 (Zach and Sheppard 1992). For a total energy intake of 18744 kJ/d, this intake is prorated to 1928 g/d.
Man's poultry ingestion rate	53 g/d	Median intakes for male adult (CSA 2008, Table G.9a). Defined as lognormal PDF with GM equal to median and GSD=1.65 (Zach and Sheppard 1992). For a total energy intake of 18744 kJ/d, this intake is prorated to 128 g/d.
Man's fish ingestion rate	7.9 g/d	Median intakes for male adult (CSA 2008, Table G.9a). Defined as lognormal PDF with GM equal to median and GSD=4.48 (Zach and Sheppard 1992). For a total energy intake of 18744 kJ/d, this intake is prorated to 19 g/d.
Soil ingestion rate	0.12 kg/a	95 <sup>th</sup> percentile value from CSA (2008).
Probability of irrigation	0.9 garden, 0.02 forage	Fixed value (Davis et al. 1993, p.157). Probability of irrigating woodlot and peat bog are set to zero.
Irrigation period	100 a	Lognormal PDF with GM = 100 a, GSD = 4, and bounds of 50 and 10000 a (Davis et al. 1993, p.158).
Probability of using fresh lake sediments on fields	0.01	Fixed value. This is uncommon in the Canadian Shield. Infilled lakes are not included in this category, but are considered normal organic-soil fields (Davis et al. 1993, p.158).
Dredged sediment thickness	0.2 m	Fixed value. Thickness of lake sediment used as surface soil for farming, same value as soil thickness.

Cropping frequency	1/a garden 1/a forage 1/50 a woodlot 0 peat bog	Fixed value (Davis et al. 1993, p.137)
Cropping period, non-irrigated fields	50 a	Fixed value (Davis et al. 1993, p. 137). Period over which non-irrigated fields are farmed.
Cropping soil contaminant loss fraction	0.05	Fixed value (Davis et al. 1993, p.157).
Annual energy consumption per household	$10^5$ MJ/a	Normal PDF with GM of $1.2 \times 10^5$ MJ/a, standard deviation of $8 \times 10^3$ MJ/a and bounds of $10^5$ MJ/a and $1.3 \times 10^5$ MJ/a (Natural Resources Canada 2011).
Probability of burning peat for energy	1%	Fixed value (Davis et al. 1993, p.196). Burning peat as a fuel is not common in Canada.
Household lifetime	50 a	Fixed value (Garisto et al. 2004b). Average duration for household to farm a particular area. Only used to estimate peat fuel requirements.
Building width	9.7 m	Lognormal PDF with GM = 9.7 m, GSD = 1.2, bounds of 8.4 and 24 m (Davis et al. 1993, p.197).
Building height	2.4 m	Fixed value for single-story house (Davis et al. 1993, p.197).
Building volume	$228 \text{ m}^3$	Lognormal PDF with GM = $228 \text{ m}^3$ , GSD = 1.42, bounds of 168 and $1382 \text{ m}^3$ , based on Height * (Width) <sup>2</sup> . Fully correlated with building width.
Building occupancy factor	0.8	Fixed value (CSA, 2008).
Building air infiltration rate	0.35 /hr	Fixed value (CSA 1989), minimum recommendation for tightly-sealed house.
Building wake plume entrainment factor	2	Fixed value (Davis et al. 1993, p.198). Value is conservatively set to maximize entrainment.
Probability of being located downwind from energy fires	0.25	Fixed value (Davis et al. 1993). This factor represents how much exposure a person has to nuclides released from a chimney due to burning contaminated wood or peat fuel.
Outdoor or ground exposure factor	0.2	Fixed value (CSA 2008)
Water immersion occupancy factor	0.042	Fixed value (CSA 2008).
Frequency of agricultural fires	1/a	Fixed value (Davis et al. 1993, p.180).
Frequency of land-clearing fires	1/(50 a)	Fixed value (Davis et al. 1993, p. 183).

**Table 9.2: Irrigation rate parameters<sup>1</sup>**

	<b>Mean irrigation rate [m/a]</b>	<b>Standard deviation [m/a]</b>	<b>Lower bound [m/a]</b>	<b>Upper bound [m/a]</b>
<b>Garden</b>				
Sandy soil	0.2	0.06	0.02	0.4
Other soils	0.1	0.05	0.02	0.25
<b>Forage field</b>				
Sandy soil	0.1	0.06	0.02	0.3
Other soils	0.06	0.09	0.02	0.3

<sup>1</sup> Normal PDF.

Table 9.3 summarizes various timing-related parameters.

For example, the fish holdup time is the time between catching a fish and consuming the fish. Davis et al. (1993) state that locally caught fish are generally consumed within one day, while commercially processed fish are stored for an average of 10 days. A self-sufficient farmer would furthermore store food for the winter, so one might further expect that some of the fish consumed would be 3 to 6 months old. A shorter time minimizes decay, while a longer time maximizes ingrowth. Thus, a holdup time of 0.5 d is recommended.

Similarly, the building holdup time allows for any decay of radionuclides from soil or tree equilibrium levels till occupancy of the building. The values used in Davis et al. (1993) for these holdups were set to 1 or 6 months for soil and wood, respectively. Since buildings would likely have lifetimes on the order of 100 years, during which the radionuclides would be decaying, the decay is minimized.

Whether decay or ingrowth is more important, and so whether a shorter or longer time is more conservative, depends on the nuclide. For the long-lived radionuclides that tend to dominate the postclosure safety assessments, for example, a holdup of even 100 years is not an important factor. On the other hand, many biosphere models do not take credit for these holdup delays at all (e.g., CSA 2008). Since these holdups are likely to be of low importance, we set these values to those recommended by Davis et al. (1993).



**Table 9.3: Timing parameters**

Parameter	Reference Value	Comment
Fish holdup time	0.5 d	Time between catching and eating fish (Davis et al. 1993, p.249). Conservatively assume that the critical group eats local fish which is eaten within a day of being caught.
Plant holdup time	1 d	Time between plant absorbing nuclides and being consumed by man (Davis et al. 1993, p.248). Conservatively assume that the critical group eats local produce which is consumed 1 day after harvesting.
Animal feed holdup time	1 d milk, 1 d bird, 5 d meat	Time between removal of feed or forage from a field and the consumption of animal food types by man. (Davis et al. 1993, p.249). Conservatively assume that, in addition to the plant hold-up time (1d), the critical group consumes fresh milk and birds (0 d) and that they age their meat slightly (4d).
Animal drinking water holdup time	0 milk, 0 bird, 4 d meat	Time between water being consumed by animal, and animal (or milk) being consumed by man (Davis et al. 1993, p.249). Because animals drink fresh water from the lake or well, there is no delay between consumption of water and slaughter/milking of animals. Conservatively assume that the critical group consumes fresh milk and birds (0 d) and that they age their meat slightly (4d).
Animal air holdup time	0 milk, 0 bird, 4 d meat	Time between air inhaled by animal and animal (or milk) being consumed by man (Zach et al. 1996, p.36). Because animals inhale fresh air, there is no delay between inhalation and slaughter/milking of animals. Conservatively assume that the critical group consumes fresh milk and birds (0 d) and that they age their meat slightly (4d).
Animal soil holdup time	0 milk, 0 bird, 4 d meat	Time between soil being consumed by animal and animal (or milk) being consumed by man (Davis et al. 1993, p.249). Because animals ingest soil while grazing, there is no delay between ingestion of soil and slaughter/milking of animals. Conservatively assume that the critical group consumes fresh milk and birds (0 d) and that they age their meat slightly (4d).
Food exposure time	100 d plant 50 d milk, 100 d bird, 50 d meat	Time that plants consumed by people or by domestic animals are exposed to possible contamination (Davis et al. 1993, p.250).
Man's water holdup time	0 d	Time between removing water from source and its consumption by man (Davis et al. 1993, p.250).
Inorganic building material holdup time	30 d	Time between inorganic material (e.g. sand, clay, rock) being removed from ground and placed into building occupied by man (Davis et al. 1993, p.250). Conservatively assume that these materials are handled relatively rapidly.
Wood building	180 d	Time between wood being harvested from woodlot and

material holdup time		placed into building occupied by man (Davis et al. 1993, p.250). Normal holdup time is approximate half a year (for harvesting, processing, transporting, storing and building).
Tree age when harvested for building material	60 a	Time from seedling to mature tree. Mean rotation ages for Canadian spruces and firs (typical trees for building materials) from Bowles and Prickett (2001).
Element removal rate from vegetation	12 d	Half-life for physical loss of an element from exposed plant material (leaves), other than radioactive decay. Lognormal PDF with GM=12 d and GSD=2 (Davis et al. 1993, p.251). Bounds of 0.01 and 400 d.

## 9.2 HUMAN PHYSICAL CHARACTERISTICS

Table 9.4 summarizes the physical characteristics of the reference (adult) human used for dose calculations.

**Table 9.4: Human physical characteristics**

Parameter	Reference Value	Comment
Hydrogen concentration in tissue	105 g/kg	Hydrogen content of bulk soft tissue is 10.5% by mass (ICRP 2002, Table 13.2)
Carbon content of soft tissue	16.0 kg	Carbon content of bulk soft tissue is 25.6% by mass (ICRP 2002, Table 13.2)
Chlorine content of soft tissue	0.13 kg	Chlorine content of bulk soft tissue is 0.2% by mass (ICRP 2002, Table 13.2).
Mass of soft tissue	62.5 kg	Difference between mass of reference man and mass of skeletal system ICRP (2002)
Mass of thyroid	0.020 kg	Fixed value (ICRP 2002).
Stable iodine content of thyroid	$1.2 \times 10^{-5}$ kg	Fixed value (Sheppard et al. 2002).

## 9.3 AIR CONCENTRATION PARAMETERS

The dispersion of contaminants into the atmosphere is characterized by several parameters. For contaminants that become airborne as fine particulates, the air concentration due to suspension of particulates from water bodies (i.e., aerosols) is calculated from  $C_{air}^w = A_{DL,w} \cdot C_w$ , and the air concentration due to suspension of dust particulates from land is calculated from  $C_{air}^t = A_{DL,t} \cdot C_s$ , where  $A_{DL,w}$  is the aerosol load ( $m^3$  water/ $m^3$  air),  $A_{DL,t}$  is the atmospheric dust load ( $kg/m^3$ ), and  $C_w$  and  $C_s$  are the radionuclide concentrations in water ( $mol/m^3$ ) and surface soil ( $mol/kg$ ) (see Table 8.3).

In addition, for potentially gaseous nuclides (e.g., Rn-222, I-129, and C-14), additional volatilization terms are considered from both terrestrial sources (soils) and surface waters. The contributions of these sources to the nuclide concentrations in air are calculated as the product of the flux of the radionuclide from the source (i.e., a soil layer or a water body) and an atmospheric dispersion factor. These atmospheric dispersion factors are dependent on the source type (i.e., soil or water).

Aquatic degassing for all nuclides is defined by the following equation:

$$C_{air,AG}^i = \frac{\lambda_{vol}^i}{3.15 \times 10^7 s/a} C_L^i Z_L D_L \quad (8.1)$$

where

$\lambda_{vol}^i$  is the water-to-air loss rate constant for nuclide  $i$  for surface water [ $a^{-1}$ ],  
 $C_L^i$  is the concentration of the nuclide  $i$  in lake water [ $mol\ m^{-3}$ ],  
 $Z_L$  is the depth of the lake [m] (see Table 8.1), and  
 $D_L$  is the semi-empirical dispersion parameter over water described by equation (8.4) [ $m^2_{water}\ m^{-3}_{air}$ ]

No empirical data is available for values of  $\lambda_{vol}^i$  for Rn and I. Therefore, the following equations were used to determine values of  $\lambda_{vol}^i$  for I and Rn:

$$\lambda_{vol}^{Rn} = \frac{K_{water}^{Rn} 3.15 \times 10^7 s/a}{Z_L} \quad (8.2)$$

$$\lambda_{vol}^{I129} = \frac{I_{MLA} 3.15 \times 10^7 s/a}{Z_L D_L} \quad (8.3)$$

where

$K_{water}^{Rn}$  is the radon transfer coefficient from fresh water to air,  $6.7 \times 10^{-6}$  ( $mol/m^2s$ )/( $mol/m^3$ ) (Sheppard et al. 2002),  
 $I_{MLA}$  is the iodine aquatic mass-loading parameter described by equation (8.5) [ $m^3_{water}\ m^{-3}_{air}$ ],  
 and  
 $D_L$  and  $I_{MLA}$  are calculated as follows:

$$D_L = \frac{u_s}{u_{ref}} e^{5 \ln(\ln A_L) - 9} \left[ \frac{s}{m} \right] \quad (8.4)$$

$$I_{MLA} = \frac{F_i k_v \sqrt{A_L}}{u_s Z_a} \quad [-] \quad (8.5)$$

where

$u_{ref}$  is the annual wind speed across the Canadian shield (m/s) (see Table 8.3),  
 $u_s$  is the annual wind speed at the repository site, assumed to be the same as  $u_{ref}$  (m/s),  
 $A_L$  is the area of the lake ( $m^2$ ) (see Table 8.1),  
 $F_i$  is a correction factor (=0.80) to account for ice and lower temperatures in the winter months  
 $k_v$  is the iodine volatilization constant =  $8.8 \times 10^{-3}$  m/a (Connan et al. 2008), and  
 $Z_a$  is the height of the air compartment = 2 m.

The values for these and other dispersion parameters are listed in Table 9.5.

**Table 9.5: Volatilization parameters**

Parameter	Reference Value	Comment
Degassing rate from lake water	0.92/a for C, 4.23x10 <sup>-3</sup> /a for I, 45.9/a for Rn, 0 for others	Value for C from Davis et al. (1993). Value for I is calculated from Equation 8.3 using parameter values described in the text. Value for Rn is calculated from Equation 8.2 using parameter values described in the text.
Gas evasion (degassing) rate from soil	13.6/a for C, 9.47x10 <sup>-4</sup> /a for Cl, 2.11x10 <sup>-2</sup> /a for I, 3.16x10 <sup>-2</sup> /s for Se, 0 for others	Only C, I, Cl and Se are considered volatile. Rn is treated separately. Lognormal PDF with GM as given on left and GSD of 3.3 for C (Zach et al. 1996) and GSD of 10 for Cl (Sheppard et al. 2004a), I (Sheppard et al. 2002) and Se (Davis et al. 1993).
Radon emission rate from soil	2.7x10 <sup>-9</sup> (mol/m <sup>2</sup> .s) / (mol/kg)	Lognormal PDF with GM=2.7x10 <sup>-9</sup> (mol <sub>Rn222</sub> /m <sup>2</sup> .s) / (mol <sub>Ra226</sub> /kg <sub>dry soil</sub> ), GSD = 2.16 (Sheppard et al. 2005b).
Radon indoor transfer coefficient	1.0x10 <sup>-5</sup> (mol/m <sup>3</sup> ) / (mol/kg)	Lognormal PDF with GM =1.0x10 <sup>-5</sup> (mol <sub>Rn222</sub> /m <sup>3</sup> <sub>air</sub> ) / (mol <sub>Ra226</sub> /kg <sub>dry soil</sub> ), GSD = 2.6 (Sheppard et al. 2005b).
Release fraction from indoor water use	Varies by element	Most elements are not volatile under domestic water conditions of E <sub>h</sub> and pH (particularly Cl and I). Values are as follows (Zach et al. 1996, p.14): Rn, Xe, Ar, Kr - Triangular PDF with most probable value of 0.52 and range from 0.3 to 0.9 C - uniform PDF from 0.25 to 1.0 All others - loguniform PDF from 0.00052 to 0.052
Release fraction from agricultural fires	Varies by element	Set to 0.2 for all elements, except for Ar, C, Cl, H, I, Kr, Rn, and Xe for which value is 1 (Davis et al. 1993, p.195).
Release fraction from energy fires	Varies by element	Set to 0.2 for all elements, except for Ar, C, Cl, H, I, Kr, Rn, and Xe for which value is 1 (Davis et al. 1993, p.195).
Release fraction from land clearing (or forest) fires	1	These fires can burn hotter than energy and agricultural fires (Davis et al. 1993, p.195).

## 9.4 MISCELLANEOUS PHYSICAL PARAMETERS

The miscellaneous physical parameters used in the biosphere model are listed in Table 9.6. The physical properties of the various human foods are given in Tables 9.7 and 9.8.

**Table 9.6: Physical parameters**

Parameter	Reference Value	Comment
Hydrogen content of water	112,000 g/m <sup>3</sup>	Mass H = 1.00794, mass O = 15.994, density of water at 16°C = 999 kg/m <sup>3</sup> .
Energy content of peat	5 MJ/kg	Fixed value. Based on average 10 MJ/kg for milled peat, used in wood stove with 50% efficiency (Davis et al. 1993, p.194).
Energy content of wood	5.5 MJ/kg	Fixed value. Based on average 11 MJ/kg for Canadian wood, used in wood stove with 50% efficiency (Davis et al. 1993, p.194).
Hydrogen content of wood	63 g/kg	Average for hardwoods and softwoods in Table 3 of Ragland and Aerts (1991)
Plant interception fractions for food	0.05 irrigation, 1.0 atmospheric	Fraction of the aerial nuclide deposition (wet or dry) that is retained on exposed plant parts and consumed by humans or animals (Davis et al. 1993, p.258).
Plant interception fractions for wood	1.0	This is the fraction of the aerial nuclide deposition that is retained on wood used for building material (Davis et al. 1993, p.259).
Soil to building density conversion factor	1	No change in density of inorganic materials between natural form and as used in building materials (Davis et al. 1993, p.264).
Dry/wet soil conversion factor	0.95	(Davis et al. 1993, p.263)
Wet/dry wood conversion factor	1.7	(Davis et al. 1993, p.264)

**Table 9.7: Food energy and water content**

Parameter	Reference Value	Comment
Carbohydrate fuel value	16.3 kJ/g	CSA (2008) Table G.8
Fat fuel value	37.7 kJ/g	CSA (2008) Table G.8
Protein fuel value	16.7 kJ/g	CSA (2008) Table G.8

**Table 9.8: Nutrient content of foods<sup>1</sup>**

	<b>Plant</b>	<b>Milk</b>	<b>Meat</b>	<b>Bird</b>	<b>Fish</b>
Carbohydrate content [g/kg]	169	32.0	5.4	3.2	0.0
Fat content [g/kg]	25.6	191	203	43.9	62.6
Protein content [g/kg]	49.4	114	170	198	178

<sup>1</sup>CSA (2008), Table G.8. Units are per kg of wet biomass for plant, meat, bird and fish, and per L for milk.

## 9.5 ANIMAL CHARACTERISTICS

The feeding rates of the various domestic animals are given in Table 9.9.

The animal feed ingestion rate corresponds to the allometric feed intake from Table G.6 of CSA (2008), converted to a wet weight basis using the dry/wet weight ratio of 0.53 for forage plants, described in Section 8.4. The animal water consumption rate corresponds to the allometric water intake from Table G.6 of CSA (2008). The inhalation rate corresponds to the allometric inhalation rate from CSA (2008). The soil ingestion rate is calculated from CSA (2008) values assuming that half the soil load is from grazed feed and the other half from harvest feed, in addition to soil from “other contaminated sources”, as reported in CSA (2008). The standard deviation and bounds are from Davis et al. (1993) and are prorated to match the mean derived from the CSA (2008) values. Human food yields are from Davis et al. (1993).

**Table 9.9: Domestic animal data<sup>1</sup>**

	<b>Bird</b>	<b>Dairy cow</b>	<b>Beef cow</b>
Human food yield [Quantity/a/animal]	2.03 kg/a	4600 L/a	145 kg/a
Animal feed consumption rate [kg <sub>wet weight</sub> /d]	Normal PDF m=0.2 sd=0.047 min=0.047 max=0.42	Normal PDF m=37 sd=9.3 min=9.3 max=84	Normal PDF m=25 sd=6.2 min=6.2 max=56
Animal water consumption rate [L/d], with 0.75 correlation with animal feed consumption	Normal PDF m=0.1 sd=0.03 min=0.03 max=0.18	Normal PDF m=75 sd=19 min=19 max=130	Normal PDF m=31 sd=8 min=8 max=54
Animal soil ingestion rate [kg/d], with 0.75 correlation with animal feed consumption	Normal PDF m=0.013 sd=0.003 min=0.003 max=0.029	Normal PDF m=1.6 sd=0.4 min=0.4 max=3.6	Normal PDF m=0.56 sd=0.14 min=0.14 max=1.3
Animal air inhalation rate [m <sup>3</sup> <sub>air</sub> /d], with 0.75 correlation with animal feed consumption	Normal PDF m=1 sd=0.3 min=0.3 max=2.3	Normal PDF m=87 sd=22 min=21 max=198	Normal PDF m=87 sd=22 min=22 max=196

<sup>1</sup>m=mean, sd=standard deviation.

Table 9.10 summarizes the mean values for the animal food ingestion transfer coefficients. These values describe the amount of a contaminant in the animal's daily food intake that appears in their produce as used for human food. For example, in the case of dairy cattle, it is the amount of contaminant (mol/kg) in the cow food intake (kg/d) that appears in the milk (mol/L) and has units of (mol/L)/(mol/kg \* kg/d) = (d/L).

**Table 9.10: Animal ingestion transfer coefficients**

Element	Milk [d/L]	Meat (beef) [d/kg <sub>wetbio</sub> ]	Bird (poultry) [d/kg <sub>wetbio</sub> ]	Freshwater fish [L/kg <sub>wetbio</sub> ]
Ac	$2.0 \times 10^{-5}$	$2.5 \times 10^{-5}$	$2.5 \times 10^{-3}$	$2.5 \times 10^1$
Am	$1.1 \times 10^{-6}$	$1.6 \times 10^{-5}$	$1.2 \times 10^{-3}$	$3.0 \times 10^1$
Bi	$5.0 \times 10^{-4}$	$4.0 \times 10^{-4}$	$4.0 \times 10^{-2}$	$1.5 \times 10^1$
C	$2.8 \times 10^{-2}$	$8.8 \times 10^{-2}$	$8.5 \times 10^0$	$5.7 \times 10^3$
Ca	$1.1 \times 10^{-2}$	$1.6 \times 10^{-3}$	$4.4 \times 10^{-1}$	$4.0 \times 10^1$
Cl	$1.5 \times 10^{-2}$	$2.0 \times 10^{-2}$	$2.0 \times 10^0$	$5.0 \times 10^1$
Cs	$7.5 \times 10^{-3}$	$3.7 \times 10^{-2}$	$4.4 \times 10^0$	$3.5 \times 10^3$
I	$7.6 \times 10^{-3}$	$1.2 \times 10^{-2}$	$7.5 \times 10^0$	$6.0 \times 10^0$
Ni	$1.7 \times 10^{-2}$	$5.0 \times 10^{-3}$	$3.1 \times 10^{-1}$	$1.0 \times 10^2$
Np	$5.0 \times 10^{-6}$	$2.0 \times 10^{-4}$	$2.0 \times 10^{-2}$	$1.5 \times 10^2$
Pa	$5.0 \times 10^{-6}$	$1.1 \times 10^{-5}$	$2.0 \times 10^{-3}$	$1.0 \times 10^1$
Pb	$2.6 \times 10^{-4}$	$4.0 \times 10^{-4}$	$4.0 \times 10^{-2}$	$3.0 \times 10^2$
Po	$3.4 \times 10^{-4}$	$4.5 \times 10^{-3}$	$4.5 \times 10^{-1}$	$5.0 \times 10^2$
Pu	$6.0 \times 10^{-7}$	$2.1 \times 10^{-5}$	$9.2 \times 10^{-4}$	$3.0 \times 10^1$
Ra	$6.2 \times 10^{-4}$	$9.0 \times 10^{-4}$	$1.3 \times 10^{-1}$	$5.0 \times 10^1$
Rn	0.0	0.0	0.0	0.0
Sb	$7.0 \times 10^{-5}$	$4.4 \times 10^{-4}$	$1.0 \times 10^{-1}$	$1.5 \times 10^1$
Se	$1.0 \times 10^{-2}$	$1.0 \times 10^{-1}$	$9.0 \times 10^0$	$2.0 \times 10^2$
Sn	$1.1 \times 10^{-3}$	$1.1 \times 10^{-2}$	$1.2 \times 10^0$	$3.0 \times 10^3$
Th	$2.4 \times 10^{-5}$	$1.2 \times 10^{-4}$	$1.0 \times 10^{-2}$	$1.0 \times 10^2$
U	$3.7 \times 10^{-4}$	$4.0 \times 10^{-4}$	$1.2 \times 10^0$	$5.0 \times 10^1$

The Cl, I, Np, Ra and U values are from Sheppard et al. (2002, 2004a, 2004b, 2005a and 2005b, respectively). The remaining values are preferentially taken from CSA (2008, Table G.3), and supplemented with values from Davis et al. (1993, p.233) for Ac, Bi, Ca, Pb and Po. The CSA values for milk were expressed in d/kg and these were converted to d/L using a milk density of 1.032 L/kg (Wong et al. 1999). For all elements, except those listed below, a lognormal distribution with a GSD of 3.2 was recommended in Davis et al. (1993), reflecting the natural variability in both animals and their feed. For I in milk, a GSD of 2.9 was recommended by Sheppard et al. (2002); for Cl in birds, milk and meat, a GSD of 2.2 was recommended by Sheppard et al. (2004a); and for Ra in birds, a GSD of 7 was recommended by Sheppard et al. (2005a).

Table 9.10 also lists the geometric mean (GM) values for the transfer coefficients for freshwater fish. This is the bioaccumulation factor, or the ratio between the nuclide concentrations in fish flesh (mol/kg<sub>wet biomass</sub>) to that in water (mol/L). The GSD is 12 for all elements. The sources of

these data are the same as discussed above for the animal food ingestion transfer coefficients, except that they are from Table A.25a in CSA (2008).

Table 9.11 provides the geometric mean values for terrestrial animal inhalation transfer coefficients - the amount of contaminant in the animal's daily intake by inhalation that appears in the animal produce used by humans for food. A GSD of 5.2 is used for all elements (Zach et al. 1996). The data sources are the same as those for the ingestion transfer coefficients above, except that for the data from CSA (2008), the ingestion transfer coefficients from Table 9.10 were multiplied by the inhalation/ingestion ratios given in Table G.7 of CSA (2008).

**Table 9.11: Animal inhalation transfer coefficients**

Element	Dairy cattle (milk) [d/L]	Beef cattle (meat) [d/kg <sub>wetbio</sub> ]	Bird (poultry or eggs) [d/kg <sub>wetbio</sub> ]
Ac	$1.0 \times 10^{-2}$	$1.3 \times 10^{-2}$	$1.3 \times 10^0$
Am	$2.7 \times 10^{-4}$	$3.9 \times 10^{-3}$	$2.9 \times 10^{-1}$
Bi	$5.5 \times 10^{-3}$	$4.4 \times 10^{-3}$	$4.4 \times 10^{-1}$
C	$5.6 \times 10^{-4}$	$1.8 \times 10^{-3}$	$1.7 \times 10^{-1}$
Ca	$1.3 \times 10^{-2}$	$1.9 \times 10^{-3}$	$5.3 \times 10^{-1}$
Cl	$1.7 \times 10^{-2}$	$8.0 \times 10^{-2}$	$8.0 \times 10^0$
Cs	$4.7 \times 10^{-3}$	$2.3 \times 10^{-2}$	$2.8 \times 10^0$
I	0.0	0.0	0.0
Ni	$2.1 \times 10^{-1}$	$6.3 \times 10^{-2}$	$3.9 \times 10^0$
Np	$7.5 \times 10^{-5}$	$8.3 \times 10^{-4}$	$8.3 \times 10^{-2}$
Pa	$1.2 \times 10^{-3}$	$2.7 \times 10^{-3}$	$4.8 \times 10^{-1}$
Pb	$7.8 \times 10^{-4}$	$1.2 \times 10^{-3}$	$1.2 \times 10^{-1}$
Po	$1.9 \times 10^{-3}$	$2.5 \times 10^{-2}$	$2.5 \times 10^0$
Pu	$1.4 \times 10^{-4}$	$5.1 \times 10^{-3}$	$2.2 \times 10^{-1}$
Ra	$5.6 \times 10^{-4}$	$1.3 \times 10^{-3}$	$1.3 \times 10^{-1}$
Rn	0.0	0.0	0.0
Sb	$1.2 \times 10^{-4}$	$7.5 \times 10^{-4}$	$1.7 \times 10^{-1}$
Se	$7.5 \times 10^{-3}$	$7.5 \times 10^{-2}$	$6.8 \times 10^0$
Sn	$2.6 \times 10^{-2}$	$2.7 \times 10^{-1}$	$2.9 \times 10^1$
Th	$2.3 \times 10^{-3}$	$1.2 \times 10^{-2}$	$1.0 \times 10^0$
U	$4.1 \times 10^{-3}$	$2.2 \times 10^{-3}$	$1.3 \times 10^{-1}$



## 9.6 DOSE COEFFICIENTS

The International Commission on Radiological Protection (ICRP) 2007 recommendations are considered to be the best estimate of dose response for humans (ICRP 2007) and replace the 1990 recommendations (ICRP 1991). The new recommendations do not lead to changes in dose limits.

The recommendations are based on the Linear No-Threshold model, although account was taken of dose and dose-rate effects in their derivation.

In the Fourth Case Study, radiological exposures to humans are converted to dose rates using dose coefficients based on the 1990 ICRP recommendations (ICRP 1991), since dose coefficients based on the 2007 recommendations are not yet available. However, dose coefficients are not expected to change substantially (Wrixon 2008).

### Adult Ingestion Dose Coefficients

The adult human ingestion dose coefficients are presented in Table 9.12 and are taken from Garisto (2002). They are based on ICRP 72 (ICRP 1996). Garisto (2002) included in the dose coefficients of parent radionuclides the contributions from progeny with half-lives less than 1-day. That is, the dose coefficients assume that an amount of progeny in secular equilibrium with the parent is eaten (the ICRP values only account for ingrowth of progeny within the body). Since the present study does not explicitly model radionuclides with half-lives less than one day, this ensures that doses from these short-lived nuclides are fully included in any dose calculations involving their parent.

The biosphere model also includes a groundwater limit to the internal I-129, Cl-36 and C-14 human doses (NWMO 2012b, Section 5.6). The groundwater dose limit for I-129 is attained when the ratio of I-129 to total iodine in the thyroid is equal to that in groundwater (well water or water discharging into the lake). For Cl-36 (or C-14), the groundwater dose limits are attained when the ratio of Cl-36 to stable chlorine (or C-14 to stable carbon), in the soft tissue of man's body is equal to that in groundwater. These limits reflect that the human body does not distinguish between isotopes when incorporating these elements into its tissue, and in particular will not concentrate the radioisotopes.

The calculation of the groundwater internal dose limits requires data on the concentration of stable I, Cl and C in groundwater and on the human internal dose conversion factors for I-129, Cl-36 and C-14. The values for these parameters are listed in Table 9.13. For I-129, the internal dose conversion factor is based on the thyroid specific-activity model described above; for Cl-36 and C-14, the internal dose conversion factors are on a soft tissue specific activity model.

### Adult Inhalation Dose Coefficients

The adult inhalation dose coefficients are presented in Table 9.12, and are from Garisto (2002). These were based on the values in ICRP 72 (ICRP 1996). The dose coefficients of parent nuclides include contributions from daughters with half-lives less than 1-day, so that doses from these short-lived nuclides are included in any dose calculations involving their parent.

**Table 9.12: Adult human dose coefficients**

Radio-nuclide	Air immersion (Sv/a)/ (Bq/m <sup>3</sup> )	Ground exposure (Sv/a)/ (Bq/kg soil)	Building exposure (Sv/a)/ (Bq/kg dry material)	Water immersion (Sv/a)/ (Bq/m <sup>3</sup> )	Ingestion (Sv/Bq)	Inhalation (Sv/Bq)
Ac-225*	3.26E-07	3.20E-07	0.00E+00 <sup>#</sup>	6.96E-10	2.43E-08	8.53E-06
Ac-227*	1.12E-09	7.97E-10	1.17E-06	2.39E-12	1.10E-06	5.50E-04
Am-241	2.13E-08	1.00E-08	4.70E-08	4.86E-11	2.00E-07	9.60E-05
Bi-210	8.14E-09	1.47E-09	0.00E+00 <sup>#</sup>	9.40E-12	1.30E-09	9.30E-08
C-14	8.20E-11	2.97E-12	0.00E+00	9.09E-14	5.80E-10	5.80E-09
Ca-41	0.00E+00	0.00E+00	0.00E+00	0.00E+00	1.90E-10	1.80E-10
Cl-36	5.24E-09	6.72E-10	5.70E-10	6.15E-12	9.30E-10	7.30E-09
Cs-135	3.00E-10	8.68E-12	0.00E+00	3.28E-13	2.00E-09	8.60E-09
I-129	8.87E-09	2.58E-09	2.00E-08	2.07E-11	1.10E-07	3.60E-08
Ni-59	0.00E+00	0.00E+00	2.00E-12	0.00E+00	6.30E-11	4.40E-10
Np-237	2.80E-08	1.88E-08	6.47E-07	6.28E-11	1.10E-07	5.00E-05
Pa-231	4.95E-08	4.77E-08	1.10E-07	1.08E-10	7.10E-07	1.40E-04
Pa-233	2.70E-07	2.54E-07	0.00E+00 <sup>#</sup>	5.90E-10	8.70E-10	3.90E-09
Pb-210	1.41E-09	5.35E-10	4.05E-09	3.28E-12	6.90E-07	5.60E-06
Po-210	1.23E-11	1.33E-11	0.00E+00 <sup>#</sup>	2.66E-14	1.20E-06	4.30E-06
Pu-239	1.10E-10	7.12E-11	2.40E-10	2.47E-13	2.50E-07	1.20E-04
Pu-240	1.08E-10	3.04E-11	2.60E-10	2.52E-13	2.50E-07	1.20E-04
Pu-242	9.15E-11	2.68E-11	2.20E-10	2.13E-13	2.40E-07	1.10E-04
Ra-223*	4.11E-07	3.76E-07	0.00E+00 <sup>#</sup>	8.76E-10	1.00E-07	8.71E-06
Ra-224	2.41E-06	2.62E-06	0.00E+00 <sup>#</sup>	5.21E-09	7.13E-08	3.62E-06
Ra-225	7.57E-09	2.33E-09	0.00E+00 <sup>#</sup>	1.66E-11	9.90E-08	7.70E-06
Ra-226	8.96E-09	7.88E-09	6.32E-06	1.97E-11	2.80E-07	9.50E-06
Ra-228	1.42E-06	1.53E-06	3.97E-06	3.06E-09	6.90E-07	1.60E-05
Rn-222*	2.63E-06	2.86E-06	0.00E+00 <sup>#</sup>	5.71E-09	2.50E-10	3.50E-09
Sb-126	4.04E-06	4.34E-06	0.00E+00 <sup>#</sup>	8.77E-09	2.40E-09	3.20E-09
Se-79	1.24E-10	4.14E-12	0.00E+00	1.37E-13	2.90E-09	6.80E-09
Sn-126	2.27E-06	2.39E-06	6.76E-06	4.93E-09	4.74E-09	2.80E-08
Th-227	1.40E-07	1.30E-07	0.00E+00 <sup>#</sup>	3.06E-10	8.80E-09	1.00E-05
Th-228	2.56E-09	1.94E-09	0.00E+00 <sup>#</sup>	5.68E-12	7.20E-08	4.00E-05
Th-229	1.06E-07	7.83E-08	9.67E-07	2.36E-10	4.90E-07	2.40E-04
Th-230	4.67E-10	2.89E-10	1.00E-09	1.05E-12	2.10E-07	1.00E-04
Th-231	1.45E-08	8.68E-09	2.90E-08	3.19E-11	3.40E-10	3.30E-10
Th-232	2.28E-10	1.23E-10	5.20E-10	5.18E-13	2.30E-07	1.10E-04
Th-234*	5.65E-08	4.21E-08	9.50E-08	1.03E-10	3.40E-09	7.70E-09
U-233	4.48E-10	3.42E-10	8.90E-10	9.94E-13	5.10E-08	9.60E-06
U-234	1.93E-10	9.29E-11	4.60E-10	4.39E-13	4.90E-08	9.40E-06
U-235	2.04E-07	1.78E-07	4.40E-07	4.51E-10	4.70E-08	8.50E-06
U-236	1.22E-10	4.80E-11	3.00E-10	2.81E-13	4.70E-08	8.70E-06
U-238	7.89E-11	2.15E-11	1.90E-10	1.85E-13	4.50E-08	8.00E-06

\*Identifies radionuclides whose dose coefficients include contributions from secular-equilibrium progeny with half-lives less than one day.

<sup>#</sup>The building dose coefficient is set to zero for short-lived nuclides for which the building dose coefficient is added to the building dose coefficient of a longer lived parent.

### Adult Ground Exposure and Air Immersion Dose Coefficients

The adult ground exposure and air immersion dose coefficients are presented in Table 9.12, and are from Garisto (2002). These were based on the values in Eckerman and Leggett (1996), which are consistent with ICRP 60 (ICRP 1991). Garisto (2002) included in the dose coefficient of parent nuclides contributions from any progeny with half-lives less than 1 day.

### Adult Water Immersion Dose Coefficients

Eckerman and Leggett (1996) calculate adult water immersion dose coefficients based on the recommendations in ICRP 60 (ICRP 1991). These data were selected for use in the Fourth Case Study unless otherwise stated. The values are presented in Table 9.12.

The dose coefficients in Eckerman and Leggett (1996) do not include any contributions from progeny. Although radionuclides with half-lives less than one day are not explicitly modelled in the Fourth Case Study, their contribution to the total water immersion dose is accounted for by adding their water immersion dose coefficient or a fraction thereof (depending on the decay scheme) to that of the parent radionuclide, to derive effective water immersion dose coefficients for the parent, as was done for other dose coefficients (Garisto 2002).

### Adult Building Exposure Dose Coefficients

Whole body building dose coefficients were derived from Holford (1989), who lists building dose coefficients, in units of (Sv/a)/(Bq/kg), for three building types: concrete, wood-log and wood-frame house.

The building dose coefficients in Holford (1989) are based on ICRP26/28 recommendations. However, MacDonald and Laverock (1996) compare air, water and soil external dose coefficients based on the ICRP26/28 and ICRP60 recommendations. Thus, the ICRP60 whole body building dose coefficients, for each building type, were estimated by dividing the ICRP26/28 dose coefficients from Holford (1989) for a nuclide by the smallest value of the ICRP26/28-to-ICRP60 dose coefficient ratio listed in MacDonald and Laverock (1996) for that particular nuclide.

Radionuclides with half-lives less than one day are not explicitly modelled in the Fourth Case Study assessment. Instead, their contribution to the total building exposure dose rate is accounted for by adding their building dose coefficient or a fraction thereof (depending on the decay scheme) to that of the parent radionuclide to derive an effective building dose coefficient for the parent.

However, the CC4 biosphere model does not simulate the ingrowth of radionuclides in building materials. This may be a nonconservative approximation if the building dose coefficient of the progeny is higher than that of the parent and ingrowth contributes significantly to the progeny concentration in building materials. Hence, radionuclides with half-lives less than 2 years are assumed to be in secular equilibrium with their parents in all building materials, and their contribution to the total building exposure dose rate is accounted for by adding their effective building dose coefficient to that of the parent radionuclide. In this case, the building dose coefficient of the short-lived progeny is set to zero (see Table 9.12).

For each nuclide, the largest of the building dose coefficients for the three building types was conservatively chosen for use in the Fourth Case Study. The effective building dose coefficients are presented in Table 9.12.

**Table 9.13: Parameters for human specific activity models**

<b>Parameter</b>	<b>Units</b>	<b>Reference Value</b>	<b>Comment</b>
Stable iodine concentration in groundwater	kg/L	$7.0 \times 10^{-9}$	GM of lognormal PDF with GSD of 8.0 and bounds of $1.0 \times 10^{-10}$ to $4.0 \times 10^{-7}$ (Sheppard and Gascoyne 1997).
Stable chlorine concentration in groundwater	kg/L	$3.0 \times 10^{-5}$	GM of lognormal PDF with GSD of 6.0 and bounds of $8.0 \times 10^{-7}$ to $1.0 \times 10^{-3}$ (Sheppard and Gascoyne 1997).
Stable carbon concentration in groundwater	kg/L	$4.0 \times 10^{-5}$	GM of lognormal PDF with GSD of 3.0 and bounds of $4.0 \times 10^{-6}$ to $2.0 \times 10^{-4}$ (Sheppard and Gascoyne 1997). Upper bound set to maximum observed concentration.
$^{129}\text{I}$ internal dose conversion factor (based on thyroid specific activity model)	(Sv/a)/ (Bq/kg thyroid)	$1.6 \times 10^{-8}$	Zach et al. (1996, p.32)
$^{36}\text{Cl}$ internal dose conversion factor (based on specific activity model)	(Sv/a)/ (Bq/kg soft tissue)	$1.38 \times 10^{-6}$	Zach et al. (1996, p.31)
$^{14}\text{C}$ internal dose conversion factor (based on specific activity model)	(Sv/a)/ (Bq/kg soft tissue)	$2.50 \times 10^{-7}$	Davis et al. (1993)
$^3\text{H}$ internal dose conversion factor (based on specific activity model)	(Sv/a)/ (Bq/kg soft tissue)	$2.9 \times 10^{-8}$	Davis et al. (1993)

No-Effect Concentrations for Non-Human Biota

Potential radiological impacts on non-human biota will be assessed using the No-Effect Concentrations (NECs) listed in Table 9.15. These values correspond to the upper estimate for a Southern Canadian Deciduous Forest environment from Garisto et al. (2008) (Tables 20 a-d).

**Table 9.14: No-effect concentrations for non-human biota**

Radionuclide	Media			
	Water (Bq L <sup>-1</sup> )	Soil (Bq kg <sup>-1</sup> )	Sediment (Bq kg <sup>-1</sup> )	Groundwater (Bq L <sup>-1</sup> )
C-14	2.4×10 <sup>-1</sup>	3.5×10 <sup>2</sup>	2.8×10 <sup>5</sup>	1.6×10 <sup>6</sup>
Cl-36	3.1×10 <sup>0</sup>	5.0×10 <sup>0</sup>	4.1×10 <sup>4</sup>	3.0×10 <sup>5</sup>
Zr-93	1.8×10 <sup>0</sup>	2.8×10 <sup>5</sup>	5.0×10 <sup>6</sup>	5.9×10 <sup>6</sup>
Nb-94	1.6×10 <sup>-2</sup>	1.3×10 <sup>2</sup>	2.6×10 <sup>4</sup>	3.6×10 <sup>4</sup>
I-129	3.2×10 <sup>0</sup>	1.9×10 <sup>4</sup>	1.2×10 <sup>6</sup>	9.0×10 <sup>5</sup>
Ra-226	5.9×10 <sup>-4</sup>	2.8×10 <sup>2</sup>	9.3×10 <sup>2</sup>	5.9×10 <sup>2</sup>
Np-237	5.8×10 <sup>-2</sup>	5.0×10 <sup>1</sup>	1.1×10 <sup>3</sup>	5.8×10 <sup>2</sup>
U-238	2.3×10 <sup>-2</sup>	4.9×10 <sup>1</sup>	6.6×10 <sup>4</sup>	5.6×10 <sup>2</sup>
Pb-210	5.0×10 <sup>0</sup>	3.7×10 <sup>3</sup>	6.3×10 <sup>3</sup>	1.8×10 <sup>5</sup>
Po-210	7.0×10 <sup>-3</sup>	3.0×10 <sup>1</sup>	1.1×10 <sup>5</sup>	5.4×10 <sup>2</sup>

Chemical Hazard

The proposed values for protection of humans and non-human biota from potentially chemically hazardous elements are listed in Table 9.15 and are based on Canadian guideline values for concentrations in environmental media relevant to human health and environmental protection, supplemented as needed.

**Table 9.15: Proposed acceptance criteria for protection of humans and non-human biota from non-radiological impacts**

Chemical Element	Ground-water ( $\mu\text{g L}^{-1}$ )	Note	Surface Water ( $\mu\text{g L}^{-1}$ )	Note	Soil ( $\mu\text{g g}^{-1}$ )	Note	Sed ( $\mu\text{g g}^{-1}$ )	Note
Ag	0.3	a	0.1	b, c	0.5	a	0.5	a
As	13	a	5	b, c	11	a	5.9	d
Cd	0.5	a	0.017	c	1	a	0.6	a
Ce	-	-	22	f	53	f	19000	f
Co	3.8	a	0.9	b	19	a	50	a
Cr	11	a,h	1	b,i	0.4	e, i	26	a,h
Cu	5	a	1	b	62	a	16	a
Eu	-	-	10.1	g	50	g	4700	g
Hg	0.1	a	0.004	c,j	0.16	a	0.17	d
I	-	-	100	b	4	e	-	-
La	-	-	10.1	f	50	e	4700	f
Nd	-	-	1.8	f	50	g	7500	f
P	-	-	4	c	-	-	-	-
Pb	1.9	a	1	b, c	45	a	31	a
Pr	-	-	9.1	f	50	g	5800	f
Te	-	-	20	k	250	e, l	-	-
U	8.9	a	5	b	1.9	a	-	-
Y	-	-	6.4	f	50	g	1400	h

- a 'Full Depth Background Site Condition Standard' for Ontario from MoE (2011). Used 'Agricultural or Other Property Use' values for soil.
- b Lowest available Provincial Water Quality Objective(PWQO)/Interim PWQO from MoEE (1994).
- c Freshwater value from CCME (2007).
- d Freshwater values from CCME (2002).
- e Lowest available for each media from ODEQ (2001).
- f Maximum Permissible Concentration (MPC) from Sneller et al. (2000).
- g Value for La used.
- h Values for total chromium used.
- i Values for Cr VI used.
- j Values for methylmercury used.
- k Based on oral mouse LD50 value for Te.
- l Converted from soil solution concentration to soil concentration using  $K_d$  for sand of  $0.125 \text{ m}^3/\text{kg}$ .
- No value available.

## 10. SUMMARY

For the Fourth Case Study, several codes were used to support the safety assessment. The data and codes used for this project have been maintained under configuration management and have been documented according to the NWMO software procedure. This report briefly describes the codes and data. For further details, references to the original documentation are provided.

Most of the model parameters are the same as the Canadian dataset developed as part of the Third Case Study (Gierszewski et al. 2004a). The notable model parameters changes are:

- new repository site location;
- repository depth of 500 m;
- revised repository design, with in-floor container emplacement, and larger container with capacity to hold 360 fuel bundles;
- repository shafts seal material data included;
- revised geosphere transport network, based on the new site geosphere model;
- changes in groundwater discharge areas, resulting from new site geosphere model and new repository location;
- main groundwater discharge from repository is to a stream rather than a lake;
- revised  $\text{UO}_2$  corrosion rate model and data;
- revised solubility data, based on thermodynamic calculations with PHREEQC and a selected groundwater composition;
- revised sorption coefficients for engineered barriers (buffer and backfill) and geosphere, based on latest available data;
- updated biosphere and dose pathway data to reflect current CSA N288.1 standard (CSA 2008);
- addition of No-Effect Concentrations for non-human biota;
- addition of acceptance criteria for protection of humans and non-human biota from potentially chemically hazardous elements; and
- updated biosphere values for Cl, I, Np, Ra, Rn and U recommended by Sheppard et al. (2002, 2004a, 2004b, 2005a and 2005b, respectively).

## REFERENCES

- AECL (Atomic Energy of Canada Limited). 1994. Environmental impact statement on the concept for disposal of Canada's nuclear fuel waste. Atomic Energy of Canada Limited Report AECL-10711, COG-93-1. Pinawa, Canada.
- Amiro, B.D. 1992. The atmosphere submodel for the assessment of Canada's nuclear fuel waste management concept. Atomic Energy of Canada Limited Report, AECL-9889, COG-91-199. Pinawa, Canada.
- Bäckblom, G. 2008. Excavation damage and disturbance in crystalline rock – results from experiments and analyses. SKB Technical Report TR-08-08. Stockholm, Sweden.
- Baston, G.M.N., J.A. Berry, M. Brownsword, T.G. Heath, D.J. Ilett, R. McCrohon, C.J. Tweed and M. Yui. 1999. The sorption of polonium, actinium and protactinium onto geological materials. Mat. Res. Soc. Symp. Proc. 556, 1107-1114.
- Baumgartner, P. 2006. Generic thermal-mechanical-hydraulic (THM) data for sealing materials – Volume 1: Soil-water relationships. Ontario Power Generation Report 06819-REP-01300-10122-R00. Toronto, Canada.
- BEAK International. 2002. Guidance for calculation of Derived Release Limits for radionuclides in airborne and liquid effluents from Ontario Power Generation Nuclear Facilities - Appendices. Ontario Power Generation Report N-REP-03482-10000-R00. Toronto, Canada.
- Beals, D.I. 1985. Soil and climate parameters for post-closure biosphere assessment of nuclear fuel waste disposal. Atomic Energy of Canada Limited Technical Record, TR-285. Pinawa, Canada.
- Bowles, I.A. and G.T. Prickett. 2001. Footprints in the Jungle. Oxford University Press. NY, USA. p137
- CCME (Canadian Council of Ministers of the Environment). 2002. Canadian Sediment Guidelines for the Protection of Aquatic Life, Summary tables. 2002 update. Accessed through website of the Canadian Environmental Quality Guidelines: <http://st-ts.ccme.ca/>
- CCME (Canadian Council of the Ministers of the Environment). 2007. Canadian Water Quality Guidelines for the Protection of Aquatic Life, Summary Tables. 2007 update. Accessed through website of the Canadian Environmental Quality Guidelines: <http://st-ts.ccme.ca/>
- CDCCD (Canadian Daily Climate Data). 2006. National Climate Data and Information Archive. Retrieved online at: <ftp://arcdm20.tor.ec.gc.ca/pub/dist/CDCCD/>
- Chadwick, M.B., M. Herman, P. Obložinský, M.E. Dunn, Y. Danon, A.C. Kahler, D.L. Smith, B. Pritychenko, G. Arbanas, R. Arcilla, R. Brewer, D.A. Brown, R. Capote, A.D. Carlson, Y.S. Cho, H. Derrien, K. Guber, G.M. Hale, S. Hoblit, S. Holloway, T.D. Johnson, T. Kawano, B.C. Kiedrowski, H. Kim, S. Kunieda, N.M. Larson, L. Leal, J.P. Lestone, R.C. Little, E.A. McCutchan, R.E. MacFarlane, M. MacInnes, C.M. Mattoon, R.D. McKnight, S.F. Mughabghab, G.P.A. Nobre, G. Palmiotti, A. Palumbo, M.T. Pigni, V.G. Pronyaev, R.O. Sayer, A.A. Sonzogni, N.C. Summers, P. Talou, I.J. Thompson, A. Trkov, R.L.



- Vogt, S.C. van der Marck, A. Wallner, M.C. White, D. Wiarda, P.G. Young. 2011. ENDF/B-VII.1 Nuclear data for science and technology: Cross section, covariances, fission product yields, and decay data. *Nuclear Data Sheets*: 112-12, 2887-2996 (2011).
- Chan, T., M. Kolar, P.A. O'Connor, N.W. Scheier and F.W. Stanchell. 1999. Finite-element sensitivity analysis of effects of an excavation damage zone on  $^{129}\text{I}$  transport from a used CANDU fuel waste disposal repository. Ontario Hydro Report 06819-REP-01200-0022-R00. Toronto, Canada.
- Coligado, M.C., W. Baier and W.K. Sly. 1968. Risk Analyses of Weekly Climatic Data for Agricultural and Irrigation Planning, Kapuskasing, Ontario, Technical Bulletin 31, Canada Land Inventory, Dept of Forestry and Rural Development, Agriculture Canada, p8.
- Connan, O., E. Tessier, D. Maro, D. Amouroux, D. Hebert, M. Rozet, C. Vaiseux and L. Solier. 2008. Water to atmosphere fluxes of  $^{131}\text{I}$  in relation with alkyl-iodide compounds from the Sein Estuary (France). *J. Environ. Radioactivity* 99, 1102-1110.
- Cordfunke, E.H.P. and R.J.M. Konings. 1988. Chemical interactions in water-cooled nuclear fuel: A thermodynamic approach. *J. Nucl. Mat.* 152, 301-309.
- Crawford, J., I. Neretnieks and M. Malmström. 2006. Data and uncertainty assessment for radionuclide  $K_d$  partitioning coefficients in granitic rock for use in SR-Can calculations. SKB Research Report R-06-75. Stockholm, Sweden.
- CRC. 1993. CRC Handbook of chemistry and physics, 73rd ed. CRC Press, Ann Arbor, USA.
- CSA (Canadian Standards Association). 1999. Quality assurance of analytical, scientific, and design computer programs for nuclear power plants. Canadian Standards Association Standard CSA N286.7-99. Toronto, Canada.
- CSA (Canadian Standards Association). 2008. Guidelines for calculating derived release limits for radioactive material in airborne and liquid effluents for normal operation of nuclear facilities. Canadian Standards Association Report CSA-N288.1-08. Toronto, Canada.
- CSA (Canadian Standards Association). 1989. Residential mechanical ventilation requirements. Canadian Standards Association Preliminary Standard F326.1-M1989. Toronto, Canada.
- Cubicciotti, D. And J.E. Sanecki. 1978. Characterization of deposits on inside surfaces of LWR cladding. *J. Nucl. Mat.* 78, 96-111.
- D'Andrea, A. 2001. Radionuclide Screening Model (RSM) Version 1.1 User Manual. Ontario Power Generation Report 06819-REP-01300-10026-R00. Toronto, Canada.
- Davis, P.A., R. Zach, M.E. Stephens, B.D. Amiro, G.A. Bird, J.A.K. Reid, M.I. Sheppard and M. Stephenson. 1993. The disposal of Canada's nuclear fuel waste: The biosphere model, BIOTRAC, for postclosure assessment. Atomic Energy of Canada Limited Report AECL-10720. Pinawa, Canada.
- Davison, C.C., T. Chan, A. Brown, M. Gascoyne, D. Kamineni, G. Lodha, T. Melnyk, B.W. Nakka, P. O'Connor, D. Ophori, N. Scheier, N. Soonawala, F. Stanchell, D. Stevenson,

- G. Thorne, T. Vandergraaf, P. Vilks and S. Whitaker. 1994. The disposal of Canada's nuclear fuel waste: The geosphere model for postclosure assessment. Atomic Energy of Canada Limited Report AECL-10719, COG-93-9. Pinawa, Canada.
- Didry, O., M.N. Gray, A. Cournut and J. Graham. 2000. Modelling the early age behaviour of a low heat concrete bulkhead sealing an underground tunnel. Canadian Journal of Civil Engineering 27. 112-124.
- Dixon, D.A., N.A. Chandler and P. Baumgartner. 2002. The influence of groundwater salinity and interfaces on the performance of potential backfilling materials. Proc. 5th Inter. Workshop on Design and Construction of Final Repositories, Brussels, Belgium.
- Dixon, D.A., N.A. Chandler and P.M. Thompson. 2001. The selection of sealing system components in AECL's 1994 Environmental Impact Statement. Ontario Power Generation Report 06819-REP-01200-10074-R00. Toronto, Canada.
- Duro, L., V. Montoya, E. Colàs and D. García. 2010. Groundwater equilibration and radionuclide solubility calculations. Nuclear Waste Management Organization Technical Report NWMO TR-2010-02. Toronto, Canada.
- Eckerman, K.F. and R.W. Leggett. 1996. DCFPAK: Dose Coefficients Data File Package for Sandia National Laboratory. Oak Ridge National Laboratory Report ORNL/TM-13347. Oak Ridge, US. (<http://homer.hsr.ornl.gov/vlab/VLcodeDF.html>)
- Environment Canada. 2007. Municipal Water Use 2004 Statistics. Ontario, Canada.
- Fisheries and Environment Canada. 1978. Hydrological atlas of Canada. Department of Fisheries and Environment Canada, Printing and Publishing Supply Services Canada. Ottawa, Canada.
- Flavelle, P. 1987. Regulatory perspectives of concept assessment. In Proceedings of the Conference on Geostatistical, Sensitivity, and Uncertainty Methods for Ground-Water Flow and Radionuclide Transport Modeling, San Francisco, USA. Battelle Press, USA. p.111-119.
- Floyd, M.R., J. Novak and P.T. Truant. 1992. Fission-gas release in fuel performing to extended burnups in Ontario Hydro Nuclear Generating Stations. Proceedings of a Technical Committee Meeting on Fission Gas Release and Fuel Rod Chemistry Related to Extended Burnup, Pembroke, Ontario, Canada, 28 April – 1 May 1991. IAEA-TECDOC-697, p. 53. Vienna, Austria.
- Garisto, F. 2001. Radionuclide Screening Model (RSM) version 1.1 verification and validation. Ontario Power Generation Report 06819-REP-01300-10029-R00. Toronto, Canada.
- Garisto, F. 2002. Radionuclide and element specific data for the Radionuclide Screening Model version 1.1. Ontario Power Generation Report 06819-REP-01200-10038-R01. Toronto, Canada.
- Garisto, F. and P. Gierszewski. 2001. Summary of verification and validation studies for SYVAC3-PR4 and its submodels. Ontario Power Generation Report 06819-REP-01200-10043-R00. Toronto, Canada.

- Garisto, F. and P. Gierszewski. 2002. Technetium-99: Review of properties relevant to a Canadian geologic repository. Ontario Power Generation Report 06819-REP-01200-10081-R00. Toronto, Canada.
- Garisto, F., A. D'Andrea, P. Gierszewski and T. Melnyk. 2004b. Third Case Study - Reference Data and Codes. Ontario Power Generation Report 06819-REP-01200-10107-R00. Toronto, Canada.
- Garisto, F., J. Avis, N. Calder, A. D'Andrea, P. Gierszewski, C. Kitson, T. Melnyk, K. Wei and L. Wojciechowski. 2004a. Third Case Study - Defective Container Scenario. Ontario Power Generation Report 06819-REP-01200-10126-R00. Toronto, Canada.
- Garisto, F., J. Avis, N. Calder, P. Gierszewski, C. Kitson, T. Melnyk, K. Wei and L. Wojciechowski. 2005a. Horizontal borehole concept case study. Ontario Power Generation Report 06819-REP-01200-10139-R00. Toronto, Canada.
- Garisto, F., J. Avis., T. Chshyolkova, P. Gierszewski, M. Gobien, C. Kitson, T. Melnyk, J. Miller, R. Walsh and L. Wojciechowski. 2010. Glaciation scenario: Safety assessment for a deep geological repository for used fuel. Nuclear Waste Management Organization Technical Report NWMO TR-2010-10. Toronto, Canada.
- Garisto, F., D.H. Barber, E. Chen, A. Ingot and C.A. Morrison. 2009. Alpha, beta and gamma dose rates in water in contact with used CANDU fuel. Nuclear Waste Management Organization Technical Report NWMO TR-2009-27. Toronto, Canada.
- Garisto, F., T. Kempe, P. Gierszewski, K. Wei, C. Kitson, T. Melnyk, L. Wojciechowski, J. Avis and N. Calder. 2005b. Horizontal borehole concept case study: Chemical toxicity risk. Ontario Power Generation Report 06819-REP-01200-10149-R00. Toronto, Canada.
- Garisto, N.C., F. Cooper and S. L. Fernandes. 2008. No-effect concentrations for screening assessment of radiological impacts on non-human biota. Nuclear Waste Management Organization Technical Report NWMO TR-2008-02. Toronto, Canada.
- Gascoyne, M. 2004. Hydrogeochemistry, groundwater ages and sources of salts in a granitic batholith on the Canadian Shield, southeastern Manitoba. *Appl. Geochem.* 19, 519-560.
- Gierszewski, P., J. Avis, N. Calder, A. D'Andrea, F. Garisto, C. Kitson, T. Melnyk, K. Wei and L. Wojciechowski. 2004a. Third Case Study - Postclosure Safety Assessment. Ontario Power Generation Report 06819-REP-01200-10109-R00. Toronto, Canada.
- Gierszewski, P., M. Jensen, P. Maak and A. Vorauer. 2004b. Third Case Study - Site and design description. Ontario Power Generation Report 06819-REP-01200-10124-R00. Toronto, Canada.
- Gobien, M. and F. Garisto. 2012. Data for radionuclide and chemical element screening. Nuclear Waste Management Organization Technical Report NWMO TR-2012-11. Toronto, Canada.
- Goodwin, B.W., T. Andres, W. Hajas, D. LeNeveu, T. Melnyk, J. Szekely, A. Wikjord, D. Donahue, S. Keeling, C. Kitson, S. Oliver, K. Witzke and L. Wojciechowski. 1996. The Disposal of Canada's Nuclear Fuel Waste: A study of postclosure safety of in-room

- emplacement of used CANDU fuel in copper containers in permeable plutonic rock. Volume 5: Radiological Assessment. Atomic Energy of Canada Limited Report AECL-11494-5, COG-95-552-5. Pinawa, Canada.
- Goodwin, B.W., P. Gierszewski and F. Garisto. 2001. Radionuclide Screening Model (RSM) Version 1.1 - Theory. Ontario Power Generation Report 06819-REP-01200-10045-R00. Toronto, Canada.
- Goodwin, B.W., D. McConnell, T. Andres, W. Hajas, D. LeNeveu, T. Melnyk, G. Sherman, M. Stephens, J. Szekely, P. Bera, C. Cosgrove, K. Dougan, S. Keeling, C. Kitson, B. Kummern, S. Oliver, K. Witzke, L. Wojciechowski and A. Wikjord. 1994. The disposal of Canada's nuclear fuel waste: Postclosure assessment of a reference system. Atomic Energy of Canada Limited Report AECL-10717, COG-93-7. Pinawa, Canada.
- Guillaumont, R., J. Fanghänel, V. Neck, J. Fuger, D.A. Palmer, I. Grenthe, and M.H. Ran. 2003. Chemical Thermodynamics 5. Update on the Chemical Thermodynamics of Uranium, Neptunium, Plutonium, Americium and Technetium. NEA OECD, Elsevier, Amsterdam.
- Guo, R. 2009. Application of numerical modelling in choosing container spacing, placement-room spacing and placement-room shape for a deep geological repository using the in-floor borehole placement method. Nuclear Waste Management Organization Technical Report NWMO TR-2009-28. Toronto, Canada.
- Hillel, D. 1980. Application of Soil Physics. Academic Press, Toronto, Canada.
- Holford, R.M. 1989. Supplement to dose conversion factors for air, water, soil and building materials. Atomic Energy of Canada Limited Report AECL-9825-1. Pinawa, Canada.
- ICRP (International Commission on Radiological Protection). 1991. 1990 recommendations of the International Commission on Radiological Protection. Annals of the ICRP 21 (1-3), ICRP Publication 60. Pergamon Press, Oxford, UK.
- ICRP (International Commission on Radiological Protection). 1996. Age-dependent doses to members of the public from intake of radionuclides: Part 5, Compilation of ingestion and inhalation dose coefficients. Annals of the ICRP 26 (1), ICRP Publication 72. Pergamon Press, Oxford, UK.
- ICRP (International Commission on Radiological Protection). 2002. Basic Anatomical and Physiological Data for Use in Radiological Protection Reference Values. Ann. ICRP 32 (3-4), 2002. Vienna, Austria.
- ICRP (International Commission on Radiological Protection). 2007. The 2007 recommendations of the International Commission on Radiological Protection. Annals of the ICRP 37(2-4), ICRP Publication 103. Pergamon Press, Oxford, UK.
- Iglesias, F., M. Kaye and B. Lewis. 2011. Estimate of instant release fractions using ORIGEN-S and FEMAXI. Nuclear Waste Management Organization Technical Report NWMO TR-2011-19. Toronto, Canada.
- JNC. 2000. H12: Project to establish the scientific and technical basis for HLW disposal in Japan; Supporting Report 3; Safety assessment of the geological disposal system.

- Japan Nuclear Cycle Development Institute Report JNC TN1410 2000-004. Tokai, Japan.
- Johnson, L., C. Ferry, C. Poinssot and P. Lovera. 2005. Spent fuel radionuclide source-term model for assessing spent fuel performance in geological disposal. Part I: Assessment of the instant release fraction. *J. Nucl. Mat.* 346, 56-65.
- Johnson, L., C. Poinssot, C. Ferry and P. Lovera. 2004. Estimates of the instant release fractions for UO<sub>2</sub> and MOX fuel at t=0. NAGRA Technical Report NTB 04-08. Wetingen, Switzerland.
- Johnson, L.H. and J.C. Tait. 1997. Release of segregated nuclides from spent fuel. SKB Technical Report SKB TR 97-18. Stockholm, Sweden.
- Johnson, L.H., D.M. LeNeveu, F. King, D.W. Shoesmith, M. Kolar, D.W. Oscarson, S. Sunder, C. Onofrei, and J.L. Crosthwaite. 1996. The disposal of Canada's nuclear fuel waste: A study of postclosure safety of in-room emplacement of used CANDU fuel in copper containers in permeable plutonic rock, Volume 2: Vault model. Atomic Energy of Canada Limited Report AECL-11494-2. Pinawa, Canada.
- Kamimura, K. 1992. FP gas release behaviour of high burn-up MOX fuels for thermal reactors. Proceedings of a Technical Committee Meeting on Fission Gas Release and Fuel Rod Chemistry Related to Extended Burnup, Pembroke, Ontario, Canada, 28 April – 1 May 1991. IAEA-TECDOC-697, p. 82. Vienna, Austria.
- King, F. 2010. Critical review of the literature on the corrosion of copper by water. SKB Technical Report TR-10-69. Stockholm, Sweden.
- King, F. 2002. Status of the copper corrosion model for a deep geologic repository. Ontario Power Generation Report 06819-REP-01300-10043-R00. Toronto, Canada.
- King, F. and M. Kolar. 2006. Simulation of the consumption of oxygen in long-term in situ experiments and in the Third Case Study repository using the Copper Corrosion Model CCM-UC.1.1. Ontario Power Generation Report 06819-REP-01300-10084-R00. Toronto, Canada.
- Kitson, C., T. Melnyk, P. Gierszewski and L. Wojciechowski. 2012. SYVAC3-CC4 User Manual. Nuclear Waste Management Organization Technical Report NWMO TR-2012-21. Toronto, Canada.
- Kjartanson, B.H., D.A. Dixon and P. Baumgartner. 2003. Concepts and technologies for backfilling a nuclear fuel waste repository. Ontario Power Generation Report 06819-REP-01200-10103-R00. Toronto, Canada.
- Kleykamp, H. 1985. The chemical state of the fission products in oxide fuels. *J. Nucl. Mat.* 131, 221-246.
- Lindemer, T.B. and T.M. Besmann. 1985. Chemical thermodynamic representation of <UO<sub>2±x</sub>>. *J. Nucl. Mat.* 130, 473-488.

- Maak, P., P. Gierszewski and M. Saiedfar. 2001. Early failure probability of used-fuel containers in a deep geologic repository. Ontario Power Generation Report 06819-REP-01300-10022 R00. Toronto, Canada.
- Macdonald, C.R. and M. Laverock. 1996. External ICRP 60 dose conversion factors for air and water immersion, groundshine and soil. Atomic Energy of Canada Limited Report TR-739. Pinawa, Canada.
- Martino, J. 2000. A review of excavation damage studies at the Underground Research Laboratory and the results of the excavation damage zone study in the Tunnel Sealing Experiment. Ontario Power Generation Report 06819-REP-01200-10018-R00. Toronto, Canada.
- McMurry, J. 2004. Reference water compositions for a deep geologic repository in the Canadian Shield. Ontario Power Generation Report 06819-REP-01200-10135-R01. Toronto, Canada.
- Medri, C. 2012. Human Intrusion Model for the Fourth and Fifth Case Studies: HIMv2.0. Nuclear Waste Management Organization Technical Report NWMO TR-2012-04. Toronto, Canada.
- Mishra, S. 2002. Assigning probability distributions to input parameters of performance assessment models. SKB Technical Report TR-02-11. Stockholm, Sweden.
- MOE (Ministry of the Environment). 2011. Soil, groundwater, sediment standards for use under Part Xv.1 of the Environmental Protection Act. Ontario, Canada.
- MoEE (Ministry of the Environment and Energy). 1994. Provincial water quality objectives. Policy guidelines of the Ministry of the Environment and Energy. Ontario, Canada.
- NAGRA. 2004. Project Opalinus Clay – Integrated approach for the development of geochemical databases used for safety assessment. NAGRA Technical Report 03-06. Wettingen, Switzerland.
- NAPS (National Air Pollution Surveillance). 1996-2002. NAPS network annual data summaries. Retrieved online at: [http://www.etc-cte.ec.gc.ca/publications/naps/naps\\_lib\\_e.html](http://www.etc-cte.ec.gc.ca/publications/naps/naps_lib_e.html)
- Natural Resources Canada. 2011. Office of Energy Efficiency Comprehensive Energy Use Database Table. Retrieved online at: [http://oee.nrcan.gc.ca/corporate/statistics/neud/dpa/tablestrends2/res\\_ca\\_2\\_e\\_3.cfm?attr=0](http://oee.nrcan.gc.ca/corporate/statistics/neud/dpa/tablestrends2/res_ca_2_e_3.cfm?attr=0)
- NWMO (Nuclear Waste Management Organization). 2012a. Used fuel repository conceptual design and postclosure safety assessment in crystalline rock. Nuclear Waste Management Organization Technical Report NWMO TR-2012-16. Toronto, Canada.
- NWMO (Nuclear Waste Management Organization). 2012b. SYVAC3-CC4 Theory Manual. Nuclear Waste Management Organization Technical Report NWMO TR-2012-22. Toronto, Canada.

- Ochs., M. and C. Talerico. 2004. SR-Can. Data and uncertainty assessment – Migration parameters for the bentonite buffer in the KBS-3 concept. SKB Technical Report TR-04-18. Stockholm, Sweden.
- ODEQ (Oregon Department of Environmental Quality). 2001. Guidance for ecological risk assessments: Levels I, II, III and IV. (Level II screening benchmark values updated 2001). Portland, USA.
- Ohlsson, Y. and I. Neretnieks. 1997. Diffusion data in granite. Recommended values. SKB Technical Report TR 97-20. Stockholm, Sweden.
- OMAFRA (Ontario Ministry of Agriculture, Food and Rural Affairs). 2011a. Area, production and farm value of specified commercial fruit crops, Ontario, 2009 - 2010. Retrieved online at: [http://www.omafra.gov.on.ca/english/stats/hort/fruit\\_all09-10.htm](http://www.omafra.gov.on.ca/english/stats/hort/fruit_all09-10.htm)
- OMAFRA (Ontario Ministry of Agriculture, Food and Rural Affairs). 2011b. Area, production and farm value of specified commercial vegetable crops, Ontario, 2009 - 2010. Retrieved online at: [http://www.omafra.gov.on.ca/english/stats/hort/veg\\_all09-10.htm](http://www.omafra.gov.on.ca/english/stats/hort/veg_all09-10.htm)
- OMAFRA (Ontario Ministry of Agriculture, Food and Rural Affairs). 2012. Estimated area, yield, production and farm value of specified field crops, Ontario, 2001-2011. (Metric Units). Retrieved online at: [http://www.omafra.gov.on.ca/english/stats/crops/estimate\\_metric.htm](http://www.omafra.gov.on.ca/english/stats/crops/estimate_metric.htm).
- Ophori, D.U. and T. Chan. 1996. Regional groundwater flow in the Atikokan Research Area: Model development and calibration. Atomic Energy of Canada Limited Report AECL-11081. Pinawa, Canada.
- Oscarson, D.W., N.G. Sawatsky, W.-J. Cho and J.-W. Choi. 1995. Compacted clays as barriers to radionuclide transport. In 5th Inter. Conf. on Radioactive Waste Management and Environmental Remediation, Berlin Germany, p.751-754.
- Parkhurst, D.L. and C.A.J. Appelo. 1999. User's guide to PHREEQC (version 2). A computer program for speciation, batch reaction, one dimensional transport and inverse geochemical calculations. U. S. Department of the Interior. U. S. Geological Survey, Water Resources Investigations. Reston, Virginia, USA.
- Poinssot, C., C. Ferry, M. Kelm, B.Grambow, A. Martinez-Esparza, L. Johnson, Z.Andriambololona, J. Bruno, C. Cachoir, J-M. Cavendon, H. Christensen, C.Corbil, C. Jegou, K.Lemmens, A. Loida, P. Lovera, F. Miserque, J. de Pablo, A. Poulesquen, J. Quinones, V. Rondinella, K. Spahiu and D.Wegen. 2005. Final report of the European project spent fuel stability under repository conditions. European Commission Report CEA-R-6093. Brussels, Belgium.
- Quintessa. 2009a. AMBER 5.3 Reference guide. Quintessa Ltd. report QE-AMBER-1, Version 5.3. Henley-on-Thames, UK.
- Quintessa. 2009b. AMBER 5.3 Getting started. Quintessa Ltd. report QE-AMBER-2, Version 5.3. Henley-on-Thames, UK.

- Quintessa Ltd. and Geofirma Engineering Ltd. 2011. Postclosure safety assessment: Data. Nuclear Waste Management Organization Report NWMO DGR-TR-2011-32 R000. Toronto, Canada.
- Ragland, K.W. and D.J.Aerts. 1991. Properties of wood for combustion analysis. *Bioresource Technology* 37, 161-168.
- Rohsenow, W. and H. Choi. 1961. Heat, mass and momentum transfer. Prentice-Hall, Englewood Cliffs, USA.
- Sheppard, M.I., S.C. Sheppard and B. Sanipelli. 2002. Recommended biosphere model values for iodine. Ontario Power Generation Report 06819-REP-01200-10090. Toronto, Canada.
- Sheppard, M.I., S.C. Sheppard and B. Sanipelli. 2004a. Recommended biosphere model values for chlorine. Ontario Power Generation Report 06819-REP-01200-10119-R00. Toronto, Canada.
- Sheppard, M.I., S.C. Sheppard and B. Sanipelli. 2004b. Recommended biosphere model values for neptunium. Ontario Power Generation Report 06819-REP-01200-10120-R00. Toronto, Canada.
- Sheppard, M.I., S.C. Sheppard and B. Sanipelli. 2005a. Recommended biosphere model values for uranium. Ontario Power Generation Report 06819-REP-01200-10088-R00. Toronto, Canada.
- Sheppard, M.I., J.C. Tait, B.L. Sanipelli and S.C. Sheppard. 2005b. Recommended biosphere model values for radium and radon. Ontario Power Generation Report 06819-REP-01200-10144-R00. Toronto, Canada.
- Sheppard, S. 1985. Use of the food chain model FOOD III and the soil model SCEMR to assess irrigation as a biosphere pathway. Atomic Energy of Canada Limited Report AECL-8380. Pinawa, Canada.
- Sheppard, S.C. and M. Gascoyne. 1997. Supplement to the database of groundwater iodine, chlorine and carbon concentrations. Ontario Hydro Report 06819-REP-01200-0005. Toronto, Canada.
- Sheppard, S.C., J.Long and B. Sanipelli. 2009. Field Measurements of the transfer factors for iodine and other trace elements. Nuclear Waste Management Organization Technical Report NWMO TR-2009-35. Toronto, Canada.
- Sheppard, S.C., J.M.Long, B.Sanipelli. 2010. Plant/soil concentration ratios for paired field and garden crops, with emphasis on iodine and the role of soil adhesion. *Journal of Environmental Radioactivity* 101, 1032-1037.
- Singer, S.N. and C.K. Cheng. 2002. An assessment of the groundwater resources of Northern Ontario. Ontario Ministry of the Environment, Environmental Monitoring and Reporting Branch, Report: Hydrogeology of Ontario Series (Report 2). Toronto, Ontario.



- SKB (Svensk Kärnbränslehantering AB). 2001. First TRUE stage - Transport of solutes in an interpreted single fracture. Proc. 4th Inter. Seminar Aspö, September 2000. Swedish Nuclear and Waste Management Company Technical Report SKB TR-01-24. Stockholm, Sweden.
- SKB (Svensk Kärnbränslehantering AB). 2006. Data report for the safety assessment SR-Can. SKB Technical Report TR-06-25. Stockholm, Sweden.
- SKB (Svensk Kärnbränslehantering AB). 2009. Design premises for a KBS-3V repository based on the results from the safety assessment SR-Can and some subsequent analyses. SKB Technical Report SKB TR-09-22. Stockholm, Sweden.
- SKB (Svensk Kärnbränslehantering AB). 2010. Data report for the safety assessment SR-Site. SKB Technical Report SKB TR-10-52. Stockholm, Sweden.
- SKB (Svensk Kärnbränslehantering AB). 2011. Long-term safety for the final repository for spent fuel at Forsmark. Main report of the SR-Site project. SKB Technical Report SKB TR-11-01. Stockholm, Sweden.
- SNC-Lavalin Nuclear Inc. 2011. APM conceptual design and cost estimate update. Deep geological repository design report, crystalline rock environment copper used fuel container. Nuclear Waste Management Organization Report APM-REP-00440-0001. Toronto, Canada.
- Sneller, F.E.C, D.F. Kalf, L. Weltje and A.P. Van Wezel. 2000. Maximum permissible concentrations and negligible concentrations for rare earth elements (REEs). Nederland National Institute of Public Health and the Environment, RIVM Report 601501011. Bilthoven, The Netherlands.
- Srivastava, R.M. 2002. The discrete fracture network model in the local scale flow system for the Third Case Study. Ontario Power Generation Technical Report 06819-REP-01300-10061-R00. Toronto, Canada.
- Statistics Canada. 2002. Web pages: Private household by size data tables (1996 census) in [www.statcan.ca/english/census96/oct14/hou.htm](http://www.statcan.ca/english/census96/oct14/hou.htm); Ontario farm population data tables in [www.statcan.ca/english/census96/apr26/ont3.htm](http://www.statcan.ca/english/census96/apr26/ont3.htm). Statistics Canada. Ottawa, Canada.
- Statistics Canada. 1996. Private households by size, showing structural type of dwelling, for Canada, Provinces and Territories, 1996 Census – 20% Sample data. Retrieved online at: <http://www.statcan.gc.ca/c1996-r1996/oct14-14oct/household-menages-eng.pdf>
- Stevenson, D.R., E.T. Kozak, C.C. Davison, M. Gascoyne and R.A. Broadfoot. 1996. Hydrogeologic characteristics of domains of sparsely fractured rock in granitic Lac du Bonnet batholith, southeastern Manitoba, Canada. Atomic Energy of Canada Limited Report AWCL-11558. Pinawa, Manitoba.
- Stroes-Gascoyne, S. 1996. Measurements of instant release source terms for Cs-137, Sr-90, I-129, Tc-99 and C-14 in used CANDU fuel. J. Nucl. Mat. 238, 264-277.

- Stroes-Gascoyne, S. and D.M. Sellinger. 1986. The effect of fuel power on the leaching of cesium and iodine from used CANDU fuel. *In* Proceedings of the International Conference on CANDU Fuel, Chalk River, Canada, p. 383.
- Stroes-Gascoyne, S., J.C. Tait, R.J. Porth, J.L. McConnell and W.J. Lincoln. 1994. Release of  $^{14}\text{C}$  from the gap and grain-boundary regions of used CANDU fuels to aqueous solutions. *Waste Management* 15, 385-392.
- Tait, J.C. and S. Hanna. 2001. Characteristics and radionuclide inventories of used fuel from OPG Nuclear Generating Stations, Volume 3 - Radionuclide inventory data. Decay times 10 to 300 years. Ontario Power Generation Report 06819-REP-01200-10029-R00. Toronto, Canada.
- Tait, J.C., I. Gauld and A.H. Kerr. 1995. Validation of the ORIGEN-S code for predicting radionuclide inventories in used CANDU fuel. *J. Nucl. Mat.* 223, 109-121.
- Tait, J.C., H. Roman and C.A. Morrison. 2000. Characteristics and radionuclide inventories of used fuel from OPG Nuclear Generating Stations. Volume 1 - Main report; and Volume 2 - Radionuclide inventory data. Ontario Power Generation Report 06819-REP-01200-10029-R00. Toronto, Canada.
- Tait, J.C., R.J.J. Cornett, L.A. Chant, J. Jirovec, J. McConnell and D.L. Wilkin. 1997. Determination of Cl impurities and  $^{36}\text{Cl}$  instant release from used CANDU fuels. *Mat. Res. Soc. Symp. Proc.* 465, 503-510.
- Therrien, R., R. G. McLaren, E. A. Sudicky, S.M. Panday, and, V. Guvanasen. 2010. FRAC3DVS-OPG: A three-dimensional numerical model describing subsurface flow and solute transport. User's guide. Groundwater Simulations Group, University of Waterloo. Waterloo, Canada.
- Thibault, D.H., M.I. Sheppard and P.A. Smith. 1990. A critical compilation and review of default soil solid/liquid partition coefficients,  $K_d$ , for use in environmental assessments. Atomic Energy of Canada Limited Report AECL-10125. Pinawa, Canada.
- Ticknor, K.V. and T.T. Vandergraaf. 1996. A revised compilation of sorption coefficients for use in geosphere models in performance assessments of used fuel disposal in granitic environments. Atomic Energy of Canada Limited Report AECL-11343, COG-96-71 Pinawa, Canada.
- Vandergraaf, T.T. 1997. The sorptive capacity of sparsely and moderately fractured rock. Atomic Energy of Canada Limited Technical Record TR-752. Pinawa, Canada.
- Vandergraaf, T.T. and K.V. Ticknor. 1994. A compilation and evaluation of sorption coefficients used in the geosphere model of SYVAC for the 1990 assessment of the Whiteshell Research Area. Atomic Energy of Canada Limited Report AECL-10546, COG-92-59. Pinawa, Canada.
- Vilks, P. 2011. Sorption of selected radionuclides on sedimentary rocks in saline conditions - Literature review. Nuclear Waste Management Organization Technical Report NWMO TR-2011-12. Toronto, Canada.

- Vilks, P. and N.H. Miller. 2006. Laboratory bentonite colloid migration experiments to support the Aspo Colloid Project. Ontario Power Generation Report 06819-REP-01300-10123. Toronto, Canada.
- Wersin, P. and B. Schwyn. 2004. Project Opalinus Clay - Integrated approach for the development of geochemical databases used for safety assessment. NAGRA Technical Report 03-06. Wettingen, Switzerland.
- Wilk, L. and G. Cantello. 2006. Used fuel burnups and power ratings for OPG owned used fuel. Ontario Power Generation Report 06819-REP-01300-10121. Toronto, Canada.
- Wilson, C.N. 1990a. Results from NNWSI series 2 bare fuel dissolution tests. Pacific Northwest Laboratory Report PNL-7169. Richland, USA.
- Wilson, C.N. 1990b. Results from NNWSI series 3 spent fuel dissolution tests. Pacific Northwest Laboratory Report PNL-7170. Richland, USA.
- WIPP. 2009. Waste isolation pilot plant hazardous waste facility permit renewal application September 2009: Appendix I2, Appendix A, Material specification shaft sealing system compliance submittal design report. Waste Isolation Pilot Plant, U.S. Department of Energy, Carlsbad, USA.
- Wong, N.P., R. Jenness, M. Keeney, and E.H. Marth. 1999. Fundamentals of Dairy Chemistry (3<sup>rd</sup> Edition). Springer-Verlag.
- Wrixon, A.D. 2008. New ICRP recommendations. J. Radiol. Prot. 28, 161-168.
- Yu, J.-W. and I. Neretnieks. 1997. Diffusion and sorption properties of radionuclides in compacted bentonite. SKB Technical Report TR 97-12. Stockholm, Sweden.
- Zach, R. and S.C. Sheppard. 1992. The food-chain and dose submodel, CALDOS, for the assessment of Canada's nuclear fuel waste management concept. Atomic Energy of Canada Limited Report, AECL-10165, COG-91-195. Pinawa, Canada.
- Zach, R., B.D. Amiro, G.A. Bird, C.R. Macdonald, M.I. Sheppard, S.C. Sheppard and J.G. Szekely. 1996. The disposal of Canada's nuclear fuel waste: A study of postclosure safety of in-room emplacement of used CANDU fuel in copper containers in permeable plutonic rock, Volume 4: Biosphere model. Atomic Energy of Canada Limited Report AECL-11494-4. Pinawa, Canada.



## **APPENDIX A: COMPUTER PROGRAM ABSTRACT FOR SYVAC3-CC4**

### **A.1 PURPOSE**

This document summarizes the SYVAC3-CC4 system code, version SCC409.

SYVAC3-CC4 is a system model for the safety assessment of a deep geologic repository for nuclear fuel waste. It is primarily intended for disposal concepts based on a CANDU used fuel bundle waste form, durable containers, saturated engineering barrier materials around the container, a stable geosphere, and a nearby self-sufficient farming household in a temperate biosphere. SYVAC3-CC4 can carry out multiple simulations, including selection of input parameters from various types of probability density functions, in order to estimate a distribution of consequences.

### **A.2 PROGRAM ORIGIN AND STATUS**

The first version of the executive code SYVAC3 (Version SV309), the CC3 system model of the repository (Version CC305) and the Modelling Algorithm Library (Version ML303), were developed and used by AECL in support of the Environmental Impact Statement on their concept for disposal of Canada's nuclear fuel waste (Goodwin et al. 1994). The coding was carried out under extensive quality assurance.

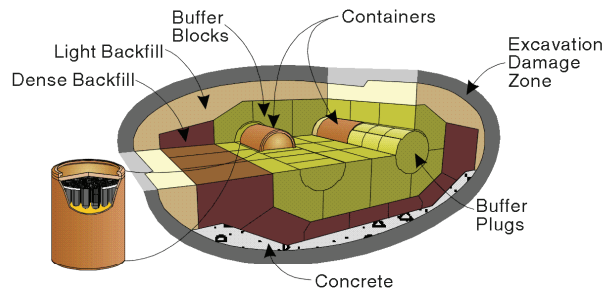
Subsequently, AECL made further changes to both the system model and SYVAC3. The revised codes were named PR401 and SV310, respectively. The new combined code, SYVAC3-PR4, was used to evaluate a second hypothetical repository with different design assumptions, i.e., the Second Case Study (Wikjord et al. 1996). Figures A-1 to A-3 illustrate the vault, geosphere and biosphere as simulated by SYVAC3-PR4 in this Second Case Study.

Control of SYVAC3-PR4 was turned over to Ontario Hydro in 1997. The code was subsequently managed through the Ontario Hydro (and then Ontario Power Generation) software configuration management and change control systems, which are compliant with CSA N286.7-99.

In 2000/2001, this code package was improved through completing a number of quality assurance tasks and minor code cleanup items, including a review and disposition of the open change requests in the AECL change request archives (pre 1997). The system code was then named CC402, reflecting that it was now considered the reference Canadian Concept code, and no longer considered "PRototype".

On January 1<sup>st</sup> 2009 the Nuclear Waste Management Organization (NWMO) officially separated from OPG and control of the SYVAC3-CC4 software package was transferred to the NWMO. The NWMO continues to maintain and develop the SYVAC3-CC4 system model with AECL implementing new features and additional modeling capabilities. The present version is SYVAC3-CC4, Version SCC409.

a) Physical Layout of Disposal Room



b) Model Geometry

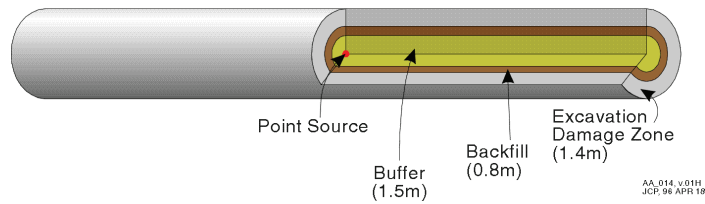


Figure A.1: Illustration of the vault sector model simulated by SYVAC3-PR4 for the AECL Second Case Study.

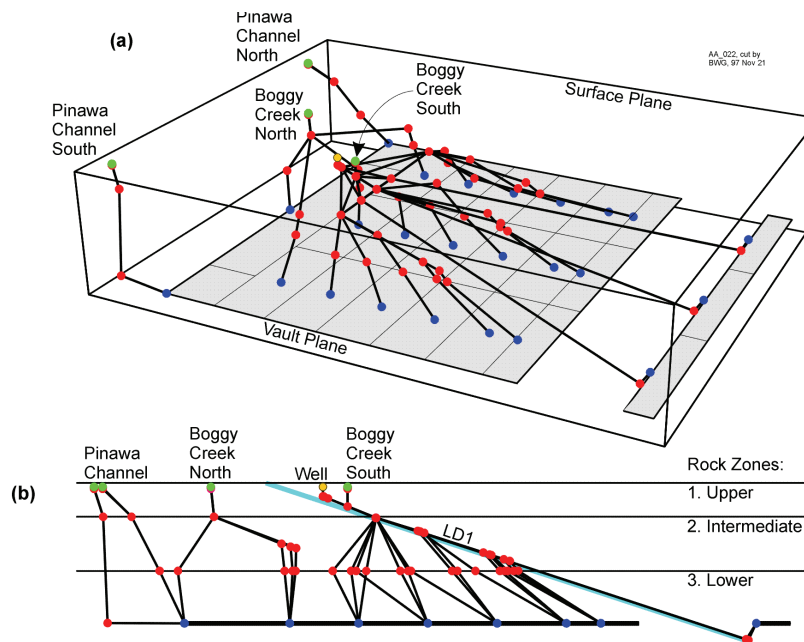
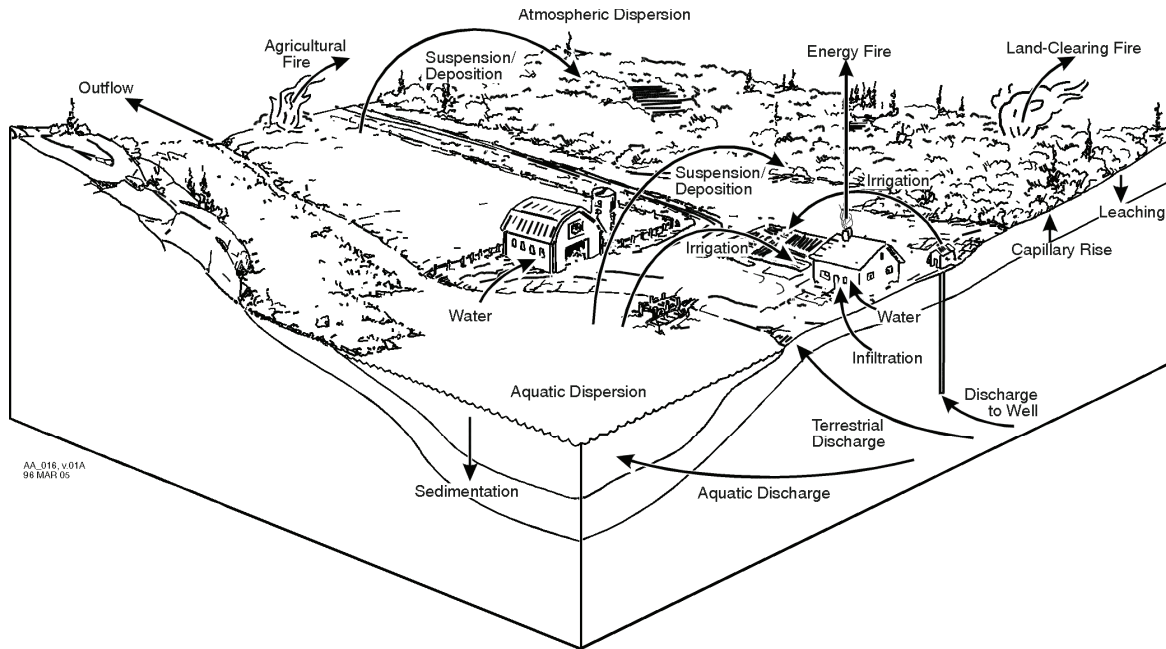


Figure A.2: Illustration of the geosphere model simulated by SYVAC3-PR4 for the AECL Second Case Study.



**Figure A.3: Illustration of the biosphere model simulated by SYVAC3-PR4 for the AECL Second Case Study.**

### A.3 OPERATING REQUIREMENTS

SYVAC3-CC4 is ANSI FORTRAN 90 compliant. It uses some FORTRAN 77 features that are no longer recommended (e.g. COMMON and EQUIVALENCE), but are still acceptable within FORTRAN 90. While it can be operated on other platforms that support ANSI FORTRAN 90 compilers, the information in this abstract is based on personal computer platforms running under Windows XP.

The hardware requirements for SYVAC3-CC4 depend on the case modelled. For example, a single random run case similar to the temperate case in the glaciation scenario (Garisto et al. 2010) with 40 nuclides, a simulation time of  $10^7$  years, a time series accuracy of 0.001 and only the main output files, took about 2.5 minutes on a 2.99 GHz Pentium D processor with 2 GB RAM. The complete set of output files (CDS, DOS, LPT, NDS, OUT, PAR, SUB) requires about 150 MB of disk space.

### A.4 COMPONENTS

The code consists of four main parts: the SYVAC3 (Version SV312) executive code, the CC409 detailed vault/geosphere/biosphere models, the ML303 Math Library, and the SLATEC Common Mathematical Library, Version 4.1 (which is included as part of the CC409 source code package). The input data are also an important part of system modelling, but are not part of the SYVAC3-CC4 code and are not discussed here.

The SV312 source code is divided into the following packages:

EC	Execution Control
FR	File Reading
IF	Model Interface (templates, help files)
PS	Parameter Sampling
SV	SYVAC general
TS	Time Series management

The CC408 source code is divided into the following packages:

BT	Biosphere Transport code
CC	Common Code
DO	DOse code
F3	Interface code with FRAC3DVS-OPG vault/geosphere transport model
GT	Geosphere Transport code
VT	Vault Transport code Slatec Math subroutines

The ML303 source code is divided into the following packages:

AR	Assorted Routines
FI	Finite Interval response function
SI	Semi-Infinite response function

## A.5 CAPABILITIES

The main capabilities of SYVAC3-CC4 (Version SCC409) are as follows:

- (1) Model transport of multiple nuclides through multiple pathways, with the following features:
  - decay chains, which may include short-lived nuclides in secular equilibrium with a precursor;
  - nuclide release from the waste form by instant release and congruent dissolution of the waste form, where the latter is driven by radiolysis (UO<sub>2</sub> only) or is solubility-limited or is given by a constant corrosion rate;
  - calculation of solubility limits for U, Pu, Th, Tc and Np nuclides based on selected groundwater parameters or can be user specified (solubility limits for all other elements are user-specified);
  - precipitation of nuclides inside a failed container if solubility limits are exceeded, including sharing the solubility limit between isotopes of the same element;
  - durable containers that fail through small defects that penetrate the container walls at user-specified times;
  - radionuclide transport out of the container by diffusion through the defect (hole) in the container;
  - a cylindrical buffer layer that surrounds the container and that limits radionuclide transport to diffusion within the pore space (see Figure A-1);
  - a cylindrical backfill material that isolates the buffer from the surrounding host rock;
  - a cylindrical excavation damage zone surrounding each disposal room;
  - a vault located deep in the geosphere, composed of multiple sectors, each connected to one end of a geosphere transport segment with sector-specific flow and transport properties;



- a user-input geosphere network of 1-D flow tubes that represent the transport pathways from the various vault sectors to the surface, where each flow tube includes diffusive, advective and sorption along the flow path (see Figure A-2);
  - ability to use alternative geosphere discharges to surface from FRAC3DVS-OPG code output instead of that calculated by the VT/GT packages;
  - a one-compartment soil model that includes groundwater and surface source/loss terms; and
  - various exposure pathways in the surface biosphere that lead to dose impacts to a critical human group and generic biota.
- (2) The ability to use a variety of probability density functions to describe uncertain parameter values in the submodels. In each simulation, a set of parameter values is sampled from their distributions and passed to the system model. These values remain constant throughout a simulation. Multiple simulations provide information on how the parameter uncertainties affect the range of consequences.
- (3) The ability to define a number of different states and state dependent parameters allowing significant differences in both the geosphere and biosphere models (e.g. permafrost). Currently state dependent capabilities of SYVAC3-CC4 are used to model glaciation cycles and assess their impact on dose to critical groups and non-human biota.
- (4) The transport equations are solved using semi-analytic and numerical methods. This methodology is robust for large ranges of parameter values.
- (5) The automated management of time series information. This includes the efficient selection of time points such that a time-dependent variable can be accurately described on both short and long time scales, as well as support for arithmetic operations between time-series data. For example, two time series can be added with automatic reselection of new time points to appropriately represent the resultant combined time-series.

## A.6 LIMITATIONS

System model: The model capabilities described in Section A.5 above must be appropriate for the physical systems being simulated. It is intended for disposal concepts based on CANDU used fuel and other waste forms, durable containers, saturated engineering barrier materials around the container, a stable geosphere, and a nearby self-sufficient farming household in a temperate biosphere.

Decay chain: The model can calculate transport through the vault and geosphere for linear decay chains. The model assumes 100% decay to the next nuclide (i.e., no branching).

Groundwater chemistry and actinide solubilities: The container solubility model for U, Np, Pu, Th and Tc assumes thermodynamic equilibrium is achieved, that there are no limitations to the supply of reacting groundwater species (e.g., carbonates), and that the dissolved actinide concentrations are too small to significantly affect the water chemistry. The model and species are intended for application under reducing conditions and assume that solids controlling the solubilities are  $\text{UO}_2(\text{fuel})$  or  $\text{UO}_3(\text{s})$ ,  $\text{PuO}_2(\text{am})$ ,  $\text{ThO}_2(\text{am})$ ,  $\text{NpO}_2(\text{am})$  and  $\text{TcO}_2(\text{s})$ . Under some input conditions, unphysically large solubilities can be calculated.

Time-invariant properties: The input material properties, groundwater flow and biosphere characteristics are time-invariant, although the calculated radionuclide release, transport and accumulation in biosphere, and dose rates to receptors, are time-dependent.

Mass conservation: The vault and geosphere models satisfy strict mass conservation within their numerical accuracy. The biosphere model includes several simplifying but conservative assumptions that can result in the "creation" or multiple counting of radionuclide masses under plausible conditions.

Maximum array sizes: Array sizes are defined through parameter statements in INCLUDE files. The array sizes are adjusted by changing the parameter value and recompiling the source code. For example, the present model can handle a maximum of 40 radionuclides and 25 different chemical elements in one run.

Units: Input parameters must be in the appropriate units, generally SI, as defined for use in the models.

## **A.7 ANALYSIS UNCERTAINTIES**

Numerical operations: The main numerical algorithms are: time series operations, including addition, multiplication, and convolution; solution of a compartment model; evaluation of a semi-infinite response function for transport of a decay chain through a porous medium; and evaluation of a boundary-integral solution for transport of nuclides in the buffer/backfill/excavation damage zone domain. These algorithms have been extensively tested in the EIS and Second Case Studies, as well as a number of other applications, and should provide robust solutions for similar studies. Note that the time-series convergence is based on the time integral of the series, so that there may be large local errors where absolute values are relatively small. Also, while the convergence of an individual time series is to a user-specified tolerance, these errors can build up over a long series of time series combinations.

Inventory calculations: For real decay chains and using secular equilibrium for short-lived nuclides, the accuracy of the solution is on the order of 0.2% at the calculated time points, and somewhat less for interpolated time points depending on the time series accuracy settings. The model does not include spontaneous fission, which could cause a small long-term inventory of short-lived fission products (e.g., about  $10^{-15}$  mol/kgU of Sr-90) (see Goodwin et al. 2002).

Container release rate: The calculated release out through the container defect is up to a factor of two higher than the exact numerical result, except at very short times that are not relevant to used fuel disposal (see Goodwin et al. 2002).

## **A.8 DOCUMENTATION**

### Theory Manuals

The theory for the CC408 system model is described in NWMO (2012b). The theory for the SYVAC3 executive code (system variability approach, parameter sampling and time series) is covered in Andres (2000).

### Validation Reports

Validation of the CC4 system model is being undertaken on a continuous basis. Historic checks are documented in:

- Summary of verification and validation studies for SYVAC3-PR4 and its submodels (Garisto and Gierszewski 2001).
- Validation of four submodels of SYVAC3-CC4, Version SCC402 (Goodwin et al. 2002).

Cross-checks of the CC4 models for near-field and far-field transport are reported in the Third Case Study reports (Garisto et al. 2004, 2005) and the main Fourth Case Study report (NWMO 2012a).

### User Manual

A user manual for the CC408 system model is available (Kitson et al. 2012).

### Programmer Manual

This document is stored in the NWMO software QA archive. Programmer information for SYVAC3 is available in Andres (2000).

### Version Tracking Record

This document is stored in the NWMO software QA archive.

## **A.9 REFERENCES**

Andres, T. 2000. SYVAC3 manual. Atomic Energy of Canada Limited report AECL-10982. Pinawa, Canada.

Garisto, F. and P. Gierszewski. 2001. Summary of verification and validation studies for SYVAC3-PR4 and its submodels. Ontario Power Generation Report 06819-REP-01200-10043-R00. Toronto, Canada.

Garisto, F., J. Avis, N. Calder, A. D'Andrea, P. Gierszewski, C. Kitson, T. Melnyk, K. Wei and L. Wojciechowski. 2004. Third case study - Defective container scenario. Ontario Power Generation Report 06819-REP-01200-10126-R00. Toronto, Canada.

Garisto, F., J. Avis, N. Calder, P. Gierszewski, C. Kitson, T. Melnyk, K. Wei and L. Wojciechowski. 2005. Horizontal borehole concept case study. Ontario Power Generation Report 06819-REP-01200-10139-R00. Toronto, Canada.

Goodwin, B.W., T. Melnyk, F. Garisto, J.D. Garroni, C.I. Kitson, S. Stroes-Gascoyne and L.C. Wojciechowski. 2002. Validation of four submodels of SYVAC3-CC4, Version SCC402. Ontario Power Generation Report 06819-REP-01300-10057-R00. Toronto, Canada.

Goodwin, B., D. McConnell, T. Andres, W. Hajas, D. LeNeveu, T. Melnyk, G. Sherman, M. Stephens, J. Szekely, P. Bera, C. Cosgrove, K. Dougan, S. Keeling, C. Kitson, B. Kummen, S. Oliver, K. Witzke, L. Wojciechowski and A. Wikjord. 1994. The disposal of Canada's nuclear fuel waste: Postclosure assessment of a reference system. Atomic Energy of Canada Limited report, AECL-10717, COG-93-7. Pinawa, Canada.

Kitson, C., T. Melnyk, P. Gierszewski and L. Wojciechowski. 2012. SYVAC3-CC4 user manual. Nuclear Waste Management Org. Technical Report NWMO TR-2012-21. Toronto, Canada.

NWMO (Nuclear Waste Management Organization). 2012a. Used fuel repository conceptual design and postclosure safety assessment in crystalline rock. Nuclear Waste Management Organization Technical Report NWMO TR-2012-16. Toronto, Canada.

NWMO (Nuclear Waste Management Organization). 2012b. SYVAC3-CC4 theory manual. Nuclear Waste Management Organization Technical Report NWMO TR-2012-22. Toronto, Canada.

Wikjord, A., P. Baumgartner, L. Johnson, F. Stanchell, R. Zach and B. Goodwin. 1996. The disposal of Canada's nuclear fuel waste: A study of postclosure safety of in-room emplacement of used CANDU fuel in copper containers in permeable plutonic rock. Volume 1: Summary. Atomic Energy of Canada Limited report, AECL-11494-1, COG-95-552-1. Pinawa, Canada.

## **APPENDIX B: COMPUTER PROGRAM ABSTRACT FOR RSM**

### **B.1 PURPOSE**

RSM Version 1.1 is a Radionuclide Screening Model (RSM) for the safety assessment of a deep geologic repository for used nuclear fuel. Used nuclear fuel contains many different radionuclides arising from fission and neutron activation processes. However, there is considerable variation in the ability of these radionuclides to cause harm to humans and the natural environment due to their characteristics and inventory in used fuel. RSM identifies those radionuclides that would not lead to significant radiological harm and that do not require further evaluation.

More specifically, it simulates the transport and decay of radionuclides in a repository through a simple pathway involving waste form, container, repository, geosphere and biosphere, with peak dose rate as the main output. The transport is modelled by a sequence of semi-analytic solutions to the 1-D advection-diffusion equation. RSM Version 1.1 works with a database covering all nuclides with a half-life greater than 0.1 years. Nuclides with a half-life greater than 1 day are also included in the database if they are progeny of a parent nuclide with a half-life greater than 0.1 years. The RSM database also includes stable elements.

### **B.2 PROGRAM ORIGIN AND STATUS**

RSM 1.0 was developed at Ontario Power Generation (OPG) as a system model to be run under the executive code SYVAC3. The RSM coding was carried out under a CSA N286.7 compliant software development plan. Some RSM modules were obtained from the system model (CC306.1) developed by AECL for their Second Case Study (Wikjord et al. 1996).

The original version of RSM was developed with a 25-nuclide capability. RSM 1.0 was then recompiled to be compatible with a 933-nuclide database (Garisto 2002). The current version, RSM 1.1, was developed from RSM 1.0 and includes some improvements to the models, notably the addition of solubility limits in the container and better treatment of the nuclide concentration in air. It consists of the source code packages SV310.1 (SYVAC3) and RS110 (the specific RSM system model). The combined executable code is designated RSM110.

### **B.3 OPERATING REQUIREMENTS**

RSM 1.1 is ANSI FORTRAN 90 compliant. It was developed using the Compaq FORTRAN 90 compiler. Although it can be operated on other platforms that support ANSI FORTRAN 90 compilers, the information in this Abstract is based on Intel platforms running Windows NT 4.0 and Dec/Compaq ALPHA platforms running UNIX. On the Windows-Intel platform, the program runs in a DOS window.

The hardware requirements for RSM depend on the case modelled. For example, a simulation with 930 nuclides, full decay chains, a simulation time limit of  $10^7$  years, a time series accuracy of 0.001, and full output files needed 12.5 minutes on a 733 MHz Pentium III with 256 MB RAM, and 225 MB disk space.

## B.4 COMPONENTS

The code consists of two components: the RS110 repository/geosphere/biosphere models and the SYVAC3 (Version SV310.1) executive code. The input data are also an important part of the system modelling, but are not part of the RSM code and are not discussed here (see Garisto 2002). Each of the code components consists of a number of FORTRAN modules and INCLUDE files.

The RS110 source code is divided into the following packages:

Bio	Biosphere Transport code, including dose consequences
Com	Common Code
Geo	Geosphere Transport code, including convolution integral calculations
Vlt	Vault (i.e., repository) Transport code, including inventory and decay calculations.

The SV310.1 source code is divided into the following packages:

EC	Execution Control
FR	File Reading
IF	Model Interface (templates, help files)
PS	Parameter Sampling
SV	SYVAC general
TS	Time Series management.

## B.5 CAPABILITIES

The main capabilities of RSM 1.1 are:

1. Model transport of multiple nuclides, including full decay chains, through a linear sequence of steps that include:
  - nuclide release from used fuel via instant release and  $UO_2$  congruent dissolution, and from cladding via Zircaloy congruent dissolution;
  - accumulation within, and release out of, durable containers that fail after some delay time because of small openings (for example, from fabrication defects) that limit radionuclide transport to diffusion through the opening;
  - precipitation within the container based on a user-input elemental solubility limit;
  - a buffer material that surrounds the container in which 1-D transport occurs via diffusion and that sorbs nuclides following a linear isotherm;
  - a backfill material that surrounds the buffer in which 1-D transport occurs via diffusion and advection, and that sorbs nuclides following a linear isotherm;
  - a linear sequence of up to 5 geosphere zones in which 1-D transport occurs via diffusion and advection, and nuclides sorb following a linear isotherm; and
  - nuclide capture via a well that leads to ingestion, air immersion, air inhalation and external groundshine doses to an exposed human.
2. The ability to handle a wide range of nuclides and decay chains; the reference database includes all nuclides with half-lives longer than 0.1 years (and nuclides with a half-life greater than 1 day, if they have a parent with a half-life longer than 0.1 years), and the  $4n$ ,  $4n+1$ ,  $4n+2$  and  $4n+3$  actinide decay chains.

3. The flow transport equations are solved using semi-analytic equations. This methodology is robust for large ranges of parameter values and avoids numerical errors inherent in purely discrete numerical solution techniques.
4. Produces a ranked list of all nuclides according to peak dose rate and a list organized alphabetically by nuclide name.
5. RSM is normally intended to be run in a deterministic mode, but it does have the ability to run multiple simulations in which uncertain input parameters are selected from probability density functions. Multiple simulations provide information on the impact of parameter uncertainties on the consequences.

## B.6 LIMITATIONS

System model: The models as described in the RSM 1.1 Theory Manual (Goodwin et al. 2001) must be relevant to the physical system being simulated. The RSM system model is appropriate for deep geologic repository concepts for used fuel that are similar to the concept considered in the Third Case Study: used fuel bundles; durable containers that fail through small perforations; a saturated clay-based layer surrounding the containers; a saturated, stable, crystalline rock geosphere; a dominant groundwater pathway for contaminant transport from the repository through the geosphere that can be described by an equivalent porous medium approximation and a linear sorption coefficient; and a well-based farming household at the geosphere discharge point.

Decay chains: The model allows linear decay chains of up to 12 members. Branching or converging decay chains must be treated by dividing them into parallel chains, and distributing the initial inventories of any isotope among the chains. The decay chain solutions may lose accuracy if the half-lives range over more than a factor of  $10^{13}$  (on a 15-significant figure processor).

Solubility: Precipitation is only modelled within the container since this is likely the point of maximum concentration. The elemental solubility limit is shared among its isotopes within the container based on the relative (time-dependent) inventories of each isotope. This inventory ratio in the container is approximated by the (time-dependent) ratio of these isotopes in either the original fuel or Zircaloy waste form.

Ruptured containers: The containers are considered to be durable, such that the reference failure mode is through small holes that penetrate the wall. The model for contaminant diffusion out of the container assumes that the hole is small. In the case of large holes, the release rate from the container might still be limited by the resistance of the buffer outside the container, but this is not included in the container release model.

Diffusion: Although different diffusion coefficients are used in the container, buffer, backfill and geosphere to reflect differences in local conditions such as temperature, the model assumes that the same diffusion coefficient applies to all radionuclides. For example, it does not distinguish between anions, cations or neutral species diffusing through the clay.

Sorption: Sorption of radionuclides onto the buffer, backfill and geosphere is modelled using a linear sorption isotherm.

Groundwater flow: The model requires the groundwater flow field as input, and assumes that the user can identify a relevant (e.g., dominant) geosphere transport pathway of interest.

Matrix diffusion: The model is based on a 1-D equivalent-porous-medium model for transport through the geosphere. Matrix diffusion is not modelled.

Biosphere: The biosphere model includes several simplifying assumptions that can result in the same amount of a given nuclide causing doses through multiple exposure paths. The ingestion dose is directly calculated only for drinking water; all other ingestion pathways are accounted for by a drinking-water-dose ingestion multiplier that the user must provide as input. The biosphere model does not include a detailed soil model, and assumes rapid equilibrium of any discharged radionuclides with the biosphere. Except possibly through the user-supplied ingestion multiplier, there is no ingrowth or decay in the biosphere; this may affect predictions of short-lived daughters that might form during typical biosphere transport time scales.

Conservatism: The models used are relatively simple, and also tend to be conservative. The resulting calculated peak dose rates will therefore be larger than expected from more detailed models that use the same input data. However, the absolute degree of conservatism is dependent on the input values supplied by the user. While in most cases, the conservative direction for a given parameter is obvious, the user should be aware that it is not necessarily always so clear - e.g., a conservative choice for diffusion coefficients is not necessarily obvious for decay chain members. The use of multiple runs with probabilistic data sampling is one option for the user to help ensure that conservative conditions have been used.

Relative ranking: The model includes all factors believed to be important for groundwater transport of radionuclides and agricultural biosphere conditions. However, since different nuclides are affected by different factors in the repository design, the model assumptions affect nuclides differently, and so the resulting ranking of nuclides may not be exactly the same as would be found from more detailed models.

Time-invariant properties: The model conditions and physical properties are time-invariant.

Numerical operations: There are three main numerical algorithms: time series operations, including addition and multiplication; solution of a compartment model with inflow, ingrowth, and release; and evaluation of a semi-infinite response function for transport of a decay chain. These algorithms have been extensively tested in the EIS and Second Case Studies, as well as a number of other applications, and should provide robust solutions for RSM. Note that the time-series convergence is based on the time integral of the series, so that there may be large local errors where absolute values are relatively small.

Input: The code uses the SYVAC3 executive code for input file reading, and therefore the input file follows SYVAC3 conventions, which includes strict formatting rules. RSM 1.1 checks a number of input parameters to ensure that they are non-negative or non-zero, but does not completely check for self-consistency of the input data. Users should check all warning messages and confirm that their input data is satisfactory.

Units: Input parameters must be in the appropriate units, generally SI, as defined for use in the models. Time units are in "years" for most parameters.



## **B.7 DOCUMENTATION**

The following documents are available. They are stored in the NWMO software QA archive.

Theory Manual: Goodwin et al. (2001).

Verification and Validation Report: Garisto (2001).

User Manual: A. D'Andrea (2001).

Version Tracking Record: Stored in the NWMO software QA archive.

## **B.8 REFERENCES**

D'Andrea, A. 2001. Radionuclide screening model (RSM) version 1.1: User manual. Ontario Power Generation Report 06819-REP-01300-10026-R0. Toronto, Canada.

Garisto, F. 2002. Radionuclide and element specific data for the radionuclide screening model version 1.1. Ontario Power Generation Report 06819-REP-01200-10038-R01. Toronto, Canada.

Garisto, F. 2001. Radionuclide Screening Model (RSM) version 1.1 verification and validation. Ontario Power Generation Report 06819-REP-01300-10029-R0. Toronto, Canada.

Goodwin, B., P. Gierszewski and F. Garisto. 2001. Radionuclide screening model (RSM) version 1.1 - Theory. Ontario Power Generation Report 06819-REP-01200-10045-R0. Toronto, Canada.

Wikjord, A., P. Baumgartner, L. Johnson, F. Stanchell, R. Zach and B. Goodwin. 1996. The disposal of Canada's nuclear fuel waste: A study of postclosure safety of in-room emplacement of used CANDU fuel in copper containers in permeable plutonic rock. Volume 1: Summary. Atomic Energy of Canada Limited report, AECL-11494-1, COG-95-552-1. Pinawa, Canada.



## **APPENDIX C: COMPUTER PROGRAM ABSTRACT FOR HIMv2.0**

### **C.1 PURPOSE**

HIMv2.0 is a Human Intrusion Model (HIM) for use in the safety assessment of a deep geologic repository for used nuclear fuel. It provides an estimate of the consequences of inadvertent human intrusion into a repository.

Specifically, it considers inadvertent intrusion by a drilled borehole that intersects a container, bringing a portion of used fuel directly to the surface. The dose consequences of this exposure scenario are assessed in terms of the acute doses to the drill crew at the time the material is brought to surface and the chronic dose rate to residents who may live near the site after the intrusion occurred. The model does not calculate the probability of the human intrusion scenario nor the resulting risk.

### **C.2 PROGRAM ORIGIN AND STATUS**

Inadvertent human intrusion calculations were performed as part of the Environmental Impact Statement for a deep geologic repository using the GENIE code (Wuschke 1992, 1996). HIM was developed as a quality-assured model for use in Canadian assessments that would be compatible with the other safety assessment codes and datasets, and to accommodate any changes in the exposure scenarios.

Previous safety assessments examined the impact of human intrusion using HIM V1.1, a model developed under the SYVAC-CC4 framework (D'Andrea and Gierszewski, 2004). HIMv2.0 was developed using a similar set of equations as HIM v1.1, but on the AMBER v5.5 platform.

### **C.3 OPERATING REQUIREMENTS**

HIMv2.0 runs within AMBER v5.5 on Intel Pentium-based computers running Windows XP, Vista or Windows 7 operating systems. For installation and operation directions, see the AMBER Reference Guide (Quintessa, 2011a).

### **C.4 COMPONENTS**

The only component that needs to be installed is the AMBER v5.5 executable developed and licensed by Quintessa Ltd. End users at NWMO do not have access to the AMBER 5.5 source code, only to the HIMv2.0 case file (HIMv20.CSE) which is stored on the NWMO software QA archive.

### **C.5 CAPABILITIES**

The main capabilities of HIMv2.0 are:

- radioactive decay, with linear decay chains;
- interception of a used fuel container by a drill;

- exposure to a drill crew member from contaminated drill slurry (groundshine, external irradiation, inhalation and ingestion pathways); and
- exposure to a resident living in a house on contaminated soil (groundshine, inhalation, soil and plant ingestion).

The dose rate to the drill crew is based on exposure at the time of intrusion. The resident dose rate is calculated based on the time after placement of fuel in the repository, given a specific time delay from placement to the original borehole intrusion. After intrusion and contamination of the soil, radionuclide concentrations in soil can change by both decay (and ingrowth) as well as by leaching due to infiltration through the soil layer.

## C.6 LIMITATIONS

Simple Models: The models used are stylized. They are intended to capture the main exposure paths from intrusion, but are not detailed. The resulting doses will therefore be indicative of doses and of the importance of the various pathways.

Intrusion Probability: The model does not consider the probability of intrusion into the repository. Thus, the results show the impact of intrusion if intrusion occurs, but do not reflect the likelihood of intrusion as a function of time after emplacement.

External Irradiation: The model calculates an effective soil concentration assuming the used fuel is mixed with drilling mud and deposited in a small area around the drill site. From this, the groundshine dose is conservatively calculated using the dose-coefficient for a soil contaminated to an infinite depth. External irradiation exposure to the drill crew from the core sample is modelled using a point-source approximation. Neither groundshine nor external radiation geometry assumptions take into account shielding or finite geometry effects.

Inhalation: The contaminant concentration in dust is based on the local contamination level, and does not include any dilution or dispersion effects from uncontaminated areas.

Closed Borehole: The model emphasis is on the acute consequences of the intrusion. The model assumes that the drill hole is closed and sealed afterwards and does not consider possible long-term leakage through a poorly sealed borehole.

Probabilistic Assessment: The model does not include probabilistic assessments. Only deterministic cases are evaluated.<sup>1</sup>

## C.7 DOCUMENTATION

Medri (2012) includes the theory, requirements specifications, design description, user manual, and verification for HIMv2.0.

Documentation for AMBER v5.5 is provided in Quintessa (2011a and 2011b))

The version tracking record for HIMv2.0 is stored in the NWMO software QA archive.

---

<sup>1</sup>AMBER is capable of probabilistic runs, but HIMv2.0 has not been created using this capability.

## **C.8 REFERENCES**

D'Andrea, A. and P. Gierszewski. 2004. Human intrusion model (HIM) Version 1.1. Ontario Power Generation Report 06819-REP-01300-10085 R00. Toronto, Canada.

Medri, C. 2012. Human Intrusion Model for the Fourth and Fifth Case Studies: HIMv2.0. Nuclear Waste Management Organization Technical Report NWMO-TR-2012-04. Toronto, Canada.

Quintessa Ltd. 2011a. AMBER 5.3 Reference guide. Henley-On-Thames. UK.

Quintessa. 2011b. AMBER 5.5 Verification summary. Henley-On-Thames. UK.

Wuschke, D.M. 1996. Assessment of the long-term risks of inadvertent human intrusion into a proposed Canadian nuclear fuel waste disposal vault in deep plutonic rock - Revision 1. Atomic Energy of Canada Limited Report, AECL-10279 Rev. 1, COG-92-151 Rev. 1. Pinawa, Canada.

Wuschke, D.M. 1992. Assessment of the long-term risks of inadvertent human intrusion into a proposed Canadian nuclear fuel waste disposal vault in deep plutonic rock. Atomic Energy of Canada Limited Report, AECL-10279, COG-92-15. Pinawa, Canada.



## APPENDIX D: USED FUEL INVENTORY UNCERTAINTY

The radionuclide and chemical inventories are presented in Section 4.3, Table 4.4 and Table 4.5. The uncertainties in these inventories are discussed in this Appendix.

The inventories in the container are uncertain due to:

- Variation in the average age of the fuel in each container.
- Uncertainties in the ORIGEN-S calculations due to uncertainties in the data used by ORIGEN-S (e.g., nuclear cross-sections, fission product yields, decay constants, impurity levels, etc.) and perhaps model approximations.
- Variation in the average burnup and power rating of the fuel in each container.

The design basis for the used fuel specifies a minimum fuel age of 30 years at time of emplacement. However, the Fourth Case Study assumes that fuel placed in the repository has cooled for exactly 30 years. This assumption is conservative for short-lived radionuclides such as Sr-90, and does not affect the inventory of the potentially most important dose contributors such as I-129 and Cl-36 because of their long half-lives. Therefore, uncertainty in the nuclide inventories arising from the uncertainty in the average fuel age is neglected.

Validation studies (Tait et al. 1995) indicate that ORIGEN-S predictions generally agree reasonably well with measured actinide and fission product inventories. Furthermore, the residual uncertainty is in many cases related more to the accuracy of the measured nuclide concentrations as shown in Table D.1.

Large deviations are observed between the calculated and measured concentrations for I-129, Tc-99 and Ru-106 (see Table D.1). In each case, the calculated concentrations are significantly larger than the measured concentrations. The discrepancies for these isotopes, which are outside the analytical uncertainty, is attributed to: I-129, losses due to incomplete capture in the off-gas stream; Tc-99, incomplete recovery due to its association with the undissolved metallic residue; and, Ru-106, poor counting (gamma) geometry for the solid metallic residue, as essentially all the Ru-106 is associated with this undissolved residue.

In comparison, more recent comparisons by SKB (2010) for PWR fuel, indicates that the ratio of measured to ORIGEN calculated inventories is 1.01 for U and Pu isotopes; 1.01 for fission products and 1.11 for actinides other than U and Pu. Again, the agreement is good and within the uncertainty of the measured data. Moreover, the results suggest that use of the more recent input data may have improved agreement between measured and ORIGEN calculated inventories.

Following Johnson et al. (1996, Appendix A), the uncertainty in the ORIGEN calculated inventories,  $\sigma_{OR}$ , for most radionuclides and chemical elements was, therefore, estimated as a normal PDF with the predicted inventory as the mean value and the measurement (or analytical) uncertainty ( $\sigma_{meas}$ , see Table D.1) as the standard deviation. Upper and lower bounds were chosen to be 5 standard deviations higher and lower than the mean. If the lower bound was not meaningful, i.e., less than zero, then the lower bound was set to 10 times smaller than the mean. For short lived radionuclides, i.e., half-life < 2 years, the initial inventory is assigned a constant value because, soon after repository closure, the inventory of such short-lived nuclides would be determined by ingrowth from a long-lived parent nuclide or would be negligibly small.

If measurement uncertainties were not available in Tait et al. (1995), then: (1) for progeny of well characterized parents, the PDF and error bounds of the parent were used; or (2) a standard deviation of 7% was used, which is a typical uncertainty for fission products in Tait et al. (1995).

In addition to the measurement uncertainty, uncertainty in average inventories in a container also arise due to the uncertainty in the average burnup and average power rating of the fuel bundles in the container. As discussed in the text, the burnup uncertainty is conservatively treated by using calculated inventories for a burnup of 220 MWh/kgU, whereas the likely maximum average burnup would be about 205 MWh/kgU (for fuel from the Pickering A Nuclear Station). This approach is conservative because radionuclide inventories generally increase with burnup and the standard deviation in the average container burnup is only about  $42/(360)^{1/2}$  MWh/kgU = 2.2 MWh/kgU, which is much smaller than 15 MWh/kgU (= 220 – 205 MWh/kgU), the difference between the burnup for which inventories were calculated and the expected maximum average burnup of fuel bundles in a container. Here, 42 MWh/kgU is the standard deviation in the distribution of bundle burnups (see Figure 4.1).

Nuclide inventories in used fuel bundles could also depend on the power rating of the fuel bundle (Tait et al. 2000). The inventories in Tait et al. (2000) were calculated for a bundle power rating of 455 kW/bundle and a screening analysis was done to determine the effect on the calculated inventories of using lower and higher power ratings. These results were used to estimate inventory uncertainties arising from uncertainties in the average power rating of the bundles in a container.

It is estimated that the distribution of fuel bundle power ratings has a standard deviation of approximately 150 kW/bundle (see Figure 4.3). However, if bundles are selected randomly, the standard deviation in the average power rating for the bundles in a container would be about  $150/360^{1/2}$  or 8 kW/bundle, based on the central limit theorem. Assuming that nuclide inventories are linearly dependent on the power rating, the uncertainty in the nuclide inventory in a container,  $\sigma_{PR}$ , arising from the uncertainty in the average power rating of the bundles in the container could be estimated using the formula

$$\sigma_{PR}(\%) = \frac{8 \text{ kW / bundle}}{(900 - 200) \text{ kW / bundle}} \left[ 100 \frac{I_{PR900} - I_{PR200}}{I_{PR455}} \right] \quad (3.2)$$

where the term in square brackets is the percentage difference in the nuclide inventories for bundle power ratings of 900 and 200 kW/bundle. Values of  $\sigma_{PR}$  are generally small (< 0.1%) for the radionuclides of interest, except for the nuclides Cs-135 (3%) and Pu-238 (0.5%).

In conclusion, the total uncertainty in the inventory of a radionuclide (or chemical element) in a container is dominated by the estimated uncertainty,  $\sigma_{OR}$ , in the calculated ORIGEN inventory of the radionuclide (or chemical element), as shown Table 4.4 and Table 4.5. Consequently, the inventory uncertainties are not correlated.



**Table D.1: ORIGEN-S: Pickering fuel inventory comparison (Tait et al. 1995)**

Isotope	Measured <sup>1</sup> (Bq/kgU)	ORIGEN-S (Bq/kg U)	Ratio (meas./calc.)
Cm-244	7.12E+08 ± 15%	7.44E+08	0.96 ± 0.14
Am-241	1.86E+10 ± 20%	1.92E+10	0.97 ± 0.19
Np-237	1.00E+05 ± 20%	8.51E+05	1.17 ± 0.23
H-3	2.07E+09 ± 7%	2.23E+09	0.92 ± 0.06
Sr-90	4.86E+11 ± 4%	5.03E+11	0.97 ± 0.04
Tc-99	1.08E+08 ± 10%	1.50E+08	0.72 ± 0.07
Ru-106	8.72E+07 ± 5%	2.52E+08	0.35 ± 0.02
Sb-125	2.20E+09 ± 18%	2.56E+09	0.86 ± 0.16
I-129	2.44E+05	3.62E+05	0.67
Cs-134	4.16E+09 ± 7%	4.03E+09	1.03 ± 0.07
Cs-137	8.05E+11 ± 5%	7.88E+11	1.02 ± 0.05
Eu-154	8.14E+09 ± 5%	9.07E+09	0.90 ± 0.04
Eu-155	3.35E+09 ± 8%	3.13E+09	1.07 ± 0.09
Isotope	Measured (g/kg U)	ORIGEN-S (g/ kg U)	Ratio (meas./calc.)
U-233	< 0.01	2.22E-07	--
U-234	0.0339 ± 55%	0.0423	0.8 ± 0.44
U-235	1.64 ± 2.4%	1.64	1.00 ± 0.02
U-236	0.802 ± 3.7%	0.813	0.99 ± 0.04
U-238	983.5 ± 0.01%	983.5	1.00 ± 0.0
Pu-238	0.0058 ± 5.6%	0.0053	1.10 ± 0.06
Pu-239	2.69 ± 2.5%	2.72	0.99 ± 0.03
Pu-240	1.22 ± 37%	1.25	0.98 ± 0.04
Pu-241	0.134 ± 9%	0.142	0.95 ± 0.09
Pu-242	0.094 ± 6.8%	0.0972	0.97 ± 0.07

<sup>1</sup>Analytical or measurement uncertainty,  $\sigma_{\text{meas}}$ , expressed as a percentage.

## REFERENCES

- Johnson, L.H., D.M. LeNeveu, F. King, D.W. Shoesmith, M. Kolar, D.W. Oscarson, S. Sunder, C. Onofrei, and J.L. Crosthwaite. 1996. The disposal of Canada's nuclear fuel waste: A study of postclosure safety of in-room emplacement of used CANDU fuel in copper containers in permeable plutonic rock, Volume 2: Vault model. Atomic Energy of Canada Limited Report AECL-11494-2. Pinawa, Canada.
- SKB (Svensk Kärnbränslehantering AB). 2010. Spent nuclear fuel for disposal in the KBS-3 repository. SKB Technical Report SKB TR-10-13. Stockholm, Sweden.

Tait, J.C., I.C. Gauld and A.H. Kerr. 1995. Validation of the ORIGEN-S code for predicting radionuclide inventories in used CANDU fuel. J. Nucl. Mat. 223, 109-121 (Also AECL-10891, COG-93-346, 1994).

Tait, J.C., H. Roman and C.A. Morrison. 2000. Characteristics and Radionuclide Inventories of Used Fuel from OPG Nuclear Generating Stations, Volume 2 – Radionuclide Inventory Data. Ontario Power Generation Report 06819-REP-01200-10029-R00. Toronto, Canada.

## APPENDIX E: USED FUEL DISSOLUTION MODEL

### E.1 UO<sub>2</sub> DISSOLUTION MODEL

The UO<sub>2</sub> ceramic fuel matrix is durable, and dissolves slowly in water. However, due to the radionuclides trapped within it, the rate of fuel dissolution is important.

The most important factor in the rate of dissolution of UO<sub>2</sub> in water is the redox conditions in the surrounding groundwater. Reducing conditions are expected to prevail in and around the container under the influence of the reducing groundwater, and consumption of any residual oxygen by reaction with the copper and steel container materials or with ferrous and organic material in the sealing materials. Under these reducing conditions, the UO<sub>2</sub> would dissolve very slowly.

However, the conditions at the used fuel surface are likely to be oxidizing for long time due to the production of oxidants in the water from radiolysis (Poinssot et al. 2005). (This water would have reached the fuel only after failure of the container and fuel cladding.) Radiolysis of the groundwater would be caused by the  $\alpha$ -,  $\beta$ -, and  $\gamma$ -radiations emitted by the used fuel, at rates that depend on the radiation type and that decrease with time as the radiation fields decrease.

Shoesmith and Sunder (1991) used an electrochemical approach to predict the effect of  $\alpha$ -,  $\beta$ - and  $\gamma$ -radiolysis on fuel dissolution. In this model, corrosion potential ( $E_{CORR}$ ) measurements as a function of radiation source strength were combined with independent measurements of the fuel dissolution rate as a function of corrosion potential. This model formed the basis of the dissolution model for the Second Case Study (Johnson et al. 1996). However, this approach requires long extrapolations of the measurements at high doses to the low dose conditions expected at the fuel surface.

For the Fourth Case Study, an empirical model for radiolysis-driven dissolution is used. In this approach, the rates of dissolution of the used fuel matrix due to  $\alpha$ -,  $\beta$ - and  $\gamma$ -radiolysis are assumed linear to the corresponding dose rates, i.e.,

$$R_{\alpha} = A_{cont} G_{\alpha} f_{\alpha} [D_{\alpha}(t+t_C)]^{a\alpha} \quad (E.1)$$

$$R_{\beta} = A_{cont} G_{\beta} f_{\beta} [D_{\beta}(t+t_C)]^{a\beta} \quad (E.2)$$

$$R_{\gamma} = A_{cont} G_{\gamma} f_{\gamma} [D_{\gamma}(t+t_C)]^{a\gamma} \quad (E.3)$$

with  $a\alpha = a\beta = a\gamma = 1$ ; and the total matrix dissolution rate is given by

$$R_{TOT} = R_{\alpha} + R_{\beta} + R_{\gamma} + R_{ch} * A_{cont} \quad (E.4)$$

where

- $R_{\alpha}$ ,  $R_{\beta}$ , and  $R_{\gamma}$  are the dissolution rates ( $\text{mol}_U \cdot \text{a}^{-1}$ ) due to  $\alpha$ -,  $\beta$ - and  $\gamma$ -radiation, respectively;
- $R_{ch}$  is the chemical fuel dissolution rate, i.e., the dissolution rate of the fuel in the absence of radiolysis ( $\text{mol}_U \cdot \text{m}^{-2} \cdot \text{a}^{-1}$ );
- $D_{\alpha}(t+t_C)$ ,  $D_{\beta}(t+t_C)$  and  $D_{\gamma}(t+t_C)$  are the time-dependent dose rates ( $\text{Gy} \cdot \text{a}^{-1}$ );

- $t$  is the time after placement of the fuel in the repository;  $t_c$  is the age of the fuel at the time of placement in the repository (i.e., the time between fuel removal from reactor and its placement in the repository) (years);
- $G_\alpha$ ,  $G_\beta$  and  $G_\gamma$  are empirical rate constants for fuel dissolution in the presence of alpha, beta and gamma radiation fields, respectively ( $\text{mol}_U \cdot \text{m}^{-2} \cdot \text{Gy}^{-1}$ );
- $f_\alpha$ ,  $f_\beta$  and  $f_\gamma$  are the alpha, beta and gamma dose variability factors; and
- $A_{\text{cont}}$  is the effective surface area of the dissolving fuel, per container ( $\text{m}^2$ ).

The remainder of this Appendix provides the basis for the values recommended for these parameters in the Fourth Case Study

## E.2 FUEL SURFACE AREA IN A CONTAINER

The surface area of the fuel depends on the fragment size. The minimum possible surface area is that of the intact fuel pellets (about 12 mm diameter), or  $0.043 \text{ m}^2/\text{kg}$ . After irradiation, the fuel pellets may be fragmented. The geometric surface area of used fuel has been estimated to be about  $0.2 \text{ m}^2/\text{kg}$ , based on the size of fuel fragments from a Bruce bundle (Johnson 1982). If the fuel were to be completely broken into small particles of about 0.6 mm, the surface area would be  $1 \text{ m}^2/\text{kg}$ .

The mass of  $\text{UO}_2$  fuel in a container is 7860 kg, based on the 21.84 kg  $\text{UO}_2$  per bundle and 360 bundles. Therefore, based on the range of geometric surface areas given above,  $A_{\text{cont}}$  is described using a lognormal distribution with a geometric mean of  $1570 \text{ m}^2$ , a geometric standard deviation of 3, and lower and upper bounds of 340 and  $7,860 \text{ m}^2$ , respectively.

Note that the effective surface area undergoing dissolution could be somewhat higher than the geometric surface area if the surface is rough. A typical value of the surface roughness factor is 3 (Grambow et al. 2000, p.27; Forsyth 1997 p.77). However, geometric surface areas are used here because the  $G_m$  ( $m = \alpha, \beta$  or  $\gamma$ ) values in Equation (E.1) to (E.3) are derived based on experimental dissolution rates calculated using the geometric surface area of the fuel.

## E.3 FUEL RADIATION FIELDS

The alpha, beta and gamma radiation fields near the surface of a used fuel bundle within a water filled used fuel container have been calculated by Garisto et al. (2009) for the reference fuel burnup of 220 MWh/kg U. These radiation field strengths are presented in Table 4.5.

Based on the variability in alpha stopping power and nuclide inventories, the alpha dose rate variability factor  $f_\alpha$  is described using a triangular probability density function with a most probable value of 1 and bounds of 0.8 to 1.2 (Garisto et al. 2009).

Based on the variability in beta stopping power and nuclide inventories, the beta dose rate variability factor  $f_\beta$  is described using a triangular probability density function with a most probable value of 1 and bounds of 0.8 to 1.2 (Garisto et al. 2009).

Based on the variability in nuclide inventories, the gamma dose rate variability factor  $f_\gamma$  is described using a triangular probability density function with a most probable value of 1 and bounds of 0.8 to 1.2 (Garisto et al. 2009).

#### E.4 $G_\alpha$ , $G_\beta$ and $G_\gamma$ VALUES

The value of  $G_\alpha$  is based on the experimental corrosion rate data compiled by Poinssot et al. (2005) (see also Shoesmith 2007) and plotted in Figure E.1. These corrosion rates are for  $\alpha$ -doped  $UO_2$ , non-doped  $UO_2$  (0.01 MBq/g) and used fuel. Search of the literature indicates that only a few additional experiments have been done since the compilation of Poinssot et al. (2005). The additional data from Muzeau et al. (2009) are also plotted in Figure E.1.

The results in Figure E.1 show a clear trend of increasing corrosion rates with increasing alpha activity. It also seems to show that there is a threshold activity below which no effect of alpha activity is observed (at approximately 1 MBq/g( $UO_2$ )). Below the threshold activity, the corrosion rate of used  $UO_2$  fuel is determined by the chemical dissolution rate  $R_{ch}$  (see Equation E.4).

A line with a slope of one (i.e., the corrosion rate is assumed to vary linearly with the alpha activity) was fitted through the experimental points, as shown in Figure E.1. This line describes the fuel dissolution rate as a function of alpha activity in fuel. The dashed lines show rates that are one order of magnitude lower and higher than the best estimate value. About 80% of the points fall within the two dashed lines.

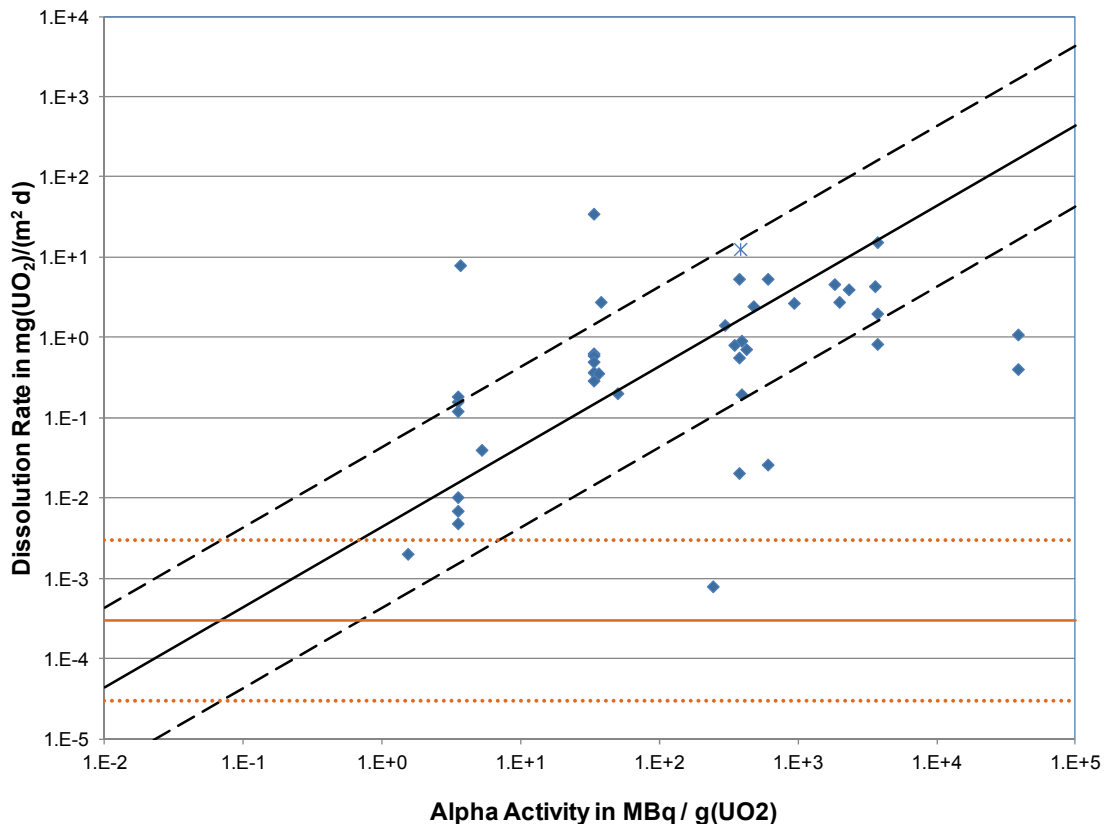


**Figure E.1: Corrosion rates measured as a function of specific alpha activity (data compiled mainly by Poinssot et al. 2005). New data are identified using the \* symbol. The red lines show the selected chemical fuel dissolution rate and its bounds.**

Based on the fit of the data in Figure E.1, it is found that

$$\text{Corrosion Rate (mgUO}_2\text{/m}^2\text{/d)} = 4.35 \times 10^{-3} * \text{Activity (MBq/g(UO}_2\text{))} \quad (\text{E.5})$$

The activity in used fuel (which can be calculated from the radionuclide inventory in Tait et al. (2000)) can be approximately expressed in terms of the alpha dose rate at the fuel surface, i.e.,

$$\text{Alpha Dose Rate (Gy/a)} = 4.2 \times 10^4 \text{ Activity (MBq/g(UO}_2\text{))} \quad (\text{E.6})$$

This relationship can be used to express the corrosion in Equation E.5 in terms of the alpha dose rate at the fuel surface. We find,

$$\begin{aligned} \text{Corrosion Rate (molUO}_2\text{/m}^2\text{/a)} &= (4.35 \times 10^{-3} / 4.2 \times 10^4) \times 365(\text{d/a}) \times 3.7 \times 10^{-6}(\text{mol/mg}) \times D_\alpha \text{ (Gy/a)} \\ &= 1.4 \times 10^{-10} \times D_\alpha \text{ (Gy/a)} \end{aligned} \quad (\text{E.7})$$

Comparing Equations E.7 and E.1 it can be determined that  $G_\alpha = 1.4 \times 10^{-10} \text{ mol/m}^2\text{/Gy}$ .

Based on the variation of the experimental data in Figure E.1, we describe  $G_\alpha$  by a lognormal probability density function (PDF) with geometric mean (GM) equal to  $1.4 \times 10^{-10} \text{ mol/m}^2\text{/Gy}$ , a geometric standard deviation (GSD) of 6.0 and bounds of  $3.5 \times 10^{-12}$  to  $2.1 \times 10^{-9} \text{ mol/m}^2\text{/Gy}$ .

This selected value of  $G_\alpha$  agrees well with the value  $8.3 \times 10^{-11} \text{ mol/m}^2\text{/a}$  for  $G_{\text{eff}}(\alpha)$  used in the Third Case Study even though these two values were obtained using very different sets of experimental data.

As in previous assessments, we assume that  $G_\beta = G_\gamma$  because beta and gamma radiation are both low linear energy (LET) radiation. Low LET radiation produces more radicals (e.g., H,  $\text{O}_2^-$ ) than high LET radiation, such as  $\alpha$ -radiation, which results predominantly in the formation of molecular radiolysis products (e.g.,  $\text{H}_2\text{O}_2$ ).

The values of  $G_\beta$  and  $G_\gamma$  are obtained using the data in the Second Case Study (SCS) (Johnson et al. 1996). For convenience, Figure 5.6 of Johnson et al. (1996) is shown in Figure E.2 below. Based on the data in Table 5.2 of Johnson et al. (1996), for  $100^\circ\text{C}$ ,  $G_\beta = G_\gamma = 10^{-8.543}$  (mol/m<sup>2</sup>/Gy) or  $2.86 \times 10^{-9} \text{ mol/m}^2\text{/Gy}$ . The uncertainty in this value is about  $\pm 0.74$  log units (GSD = 5.5).

For the Fourth Case Study, the temperature in the container is assumed to be  $70^\circ\text{C}$  for a large fraction of the simulation time. Using the activation energy of  $33.5 \text{ kJ/mole}$  (Johnson et al. 1996), we find that  $G_\beta = G_\gamma = 1.11 \times 10^{-9} \text{ mol/m}^2\text{/Gy}$  at  $70^\circ\text{C}$ .

For the Fourth Case Study,  $G_\beta$  and  $G_\gamma$  are described by loguniform PDFs with bounds of  $3.7 \times 10^{-11}$  to  $3.3 \times 10^{-8} \text{ mol/m}^2\text{/Gy}$ , and a best estimate value of  $1.1 \times 10^{-9} \text{ mol/m}^2\text{/Gy}$ .

The selected value of  $G_\beta$  can be compared to the value  $4.6 \times 10^{-10} \text{ mol/m}^2\text{/a}$  for  $G_{\text{eff}}(\beta)$  used in the Third Case Study. Again, the two values are similar.

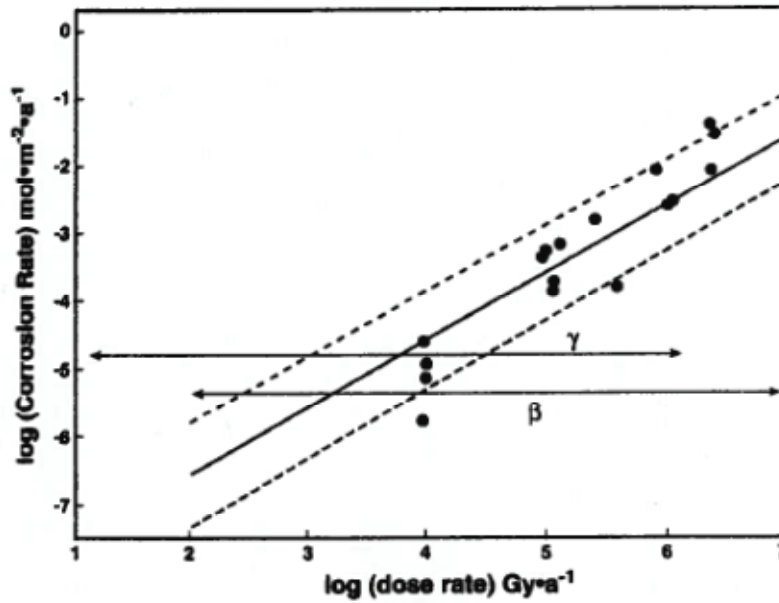


Figure E.2:  $\text{UO}_2$  (fuel) corrosion rates (calculated at  $100^\circ\text{C}$ ) plotted logarithmically as a function of the gamma or beta radiation dose rate (Figure 5.6 from Johnson et al. 1996). The solid line is a fitted line and the dashed lines the  $\pm 1\sigma$  values of this fit. The horizontal lines show the range of dose rates between the fuel ages of 10a and 1000a for beta and gamma radiation.

## E.5 CHEMICAL FUEL DISSOLUTION RATE

When the alpha-radiation field from used fuel becomes sufficiently low, chemical processes will drive fuel dissolution rather than the oxidative dissolution processes resulting from alpha-radiolysis of water. Under the reducing conditions expected in the repository, the chemical dissolution rate is low.

As defined, the chemical dissolution rate,  $R_{\text{ch}}$ , represents the intrinsic rate of  $\text{UO}_2$  dissolution, i.e., the dissolution rate in the absence of solubility constraints and radiolysis. However, as the uranium concentration in solution approaches the solubility of  $\text{UO}_2$ , it is expected that the net fuel dissolution rate would decrease. In this case, the dissolution of the fuel can be described using a solubility limited dissolution model (Lemire and Garisto 1989, Grambow et al. 2010). Since the solubility of  $\text{UO}_2$  is low under reducing conditions, the solubility limited dissolution rate can be substantially lower than the intrinsic chemical dissolution rate, if the rate of transport of uranium away from the container is constrained (e.g., small defect in the container). Thus, use of the intrinsic fuel dissolution rate is conservative.

Data on the chemical dissolution rate have been compiled from the literature. In many cases, these data actually represent the minimum observed fuel corrosion rate, which is taken here to be representative of the chemical dissolution rate. (The data may include radiolysis effects or be at measurement accuracy limits, and thus overestimate the true chemical dissolution rate.)

The compiled chemical dissolution data are shown in Figure E.3. The data are from the following sources:

1. One of the first studies under reducing conditions was performed by Bruno et al. (1991). Using a continuous flow-through reactor, they found dissolution rates of  $(6 \pm 2.5) \times 10^{-5}$  mol/(m<sup>2</sup> a), for neutral to alkaline conditions.
2. Grambow and Giffaut (2006) state that the dissolution rate of spent fuel under reducing conditions is less than 0.01 mg(UO<sub>2</sub>)/(m<sup>2</sup> d), equivalent to  $1.4 \times 10^{-5}$  mol/(m<sup>2</sup> a).
3. The static dissolution tests of Ollila et al. (2003) using U-233 doped UO<sub>2</sub>.
4. The data of Ollila (2007) from the NF-PRO project.
5. The dynamic tests under reducing conditions performed by SCK•CEN for the SFS project with alpha-doped UO<sub>2</sub> in Boom Clay water (Poinssot et al. 2005). Dissolution rates were independent of alpha activity. This is thought to be due to the reducing conditions imposed by the organic reductants in Boom Clay. If this is the case, then chemical dissolution would be expected to prevail.
6. The static dissolution tests of Saleh et al. (2006) using alpha-doped UO<sub>2</sub> in Boom clay suspensions suggest a dissolution rate of  $9.7 \times 10^{-6}$  mol/(m<sup>2</sup> a), independent of alpha activity. In these tests, the chemical dissolution rate may have been increased by sorption onto the suspended clay particles.

As noted above, the data in Figure E.3 are expected to overestimate the chemical dissolution rate. This is taken into account in selecting the value of the chemical dissolution rate to be used in the Fourth Case Study. The UO<sub>2</sub> chemical dissolution rate under reducing conditions (i.e., with no radiolysis effects) is selected to be loguniformly distributed with bounds of  $4.0 \times 10^{-8}$  to  $4.0 \times 10^{-6}$  mol/(m<sup>2</sup> a) and a median value of  $4.0 \times 10^{-7}$  mol/(m<sup>2</sup> a), which is about an order of magnitude higher than the median value used in the Third Case Study. The fuel dissolution rate at long times is expected to be much lower than this median value if the fuel is in equilibrium with the water in the defective container and the chemical dissolution rate is controlled by the diffusion of uranium out of the container.

Given the selected values of  $R_{ch}$  and  $G_{\alpha}$ , and the alpha dose rate at the fuel surface, the dissolution rate due to alpha radiolysis will exceed the chemical dissolution rate for more than 10 million years.

With the selected median value of the chemical dissolution rate and the selected surface area of the fuel (0.2 m<sup>2</sup>/kg), all the fuel in a defective container would dissolve in about 13 million years. In comparison, SKB (2010) selects a (best-estimate) fractional fuel dissolution rate of  $1.0 \times 10^{-7}$ /year, based on the work of Werme et al. (2004); in which case all the fuel dissolves in 10 million years.



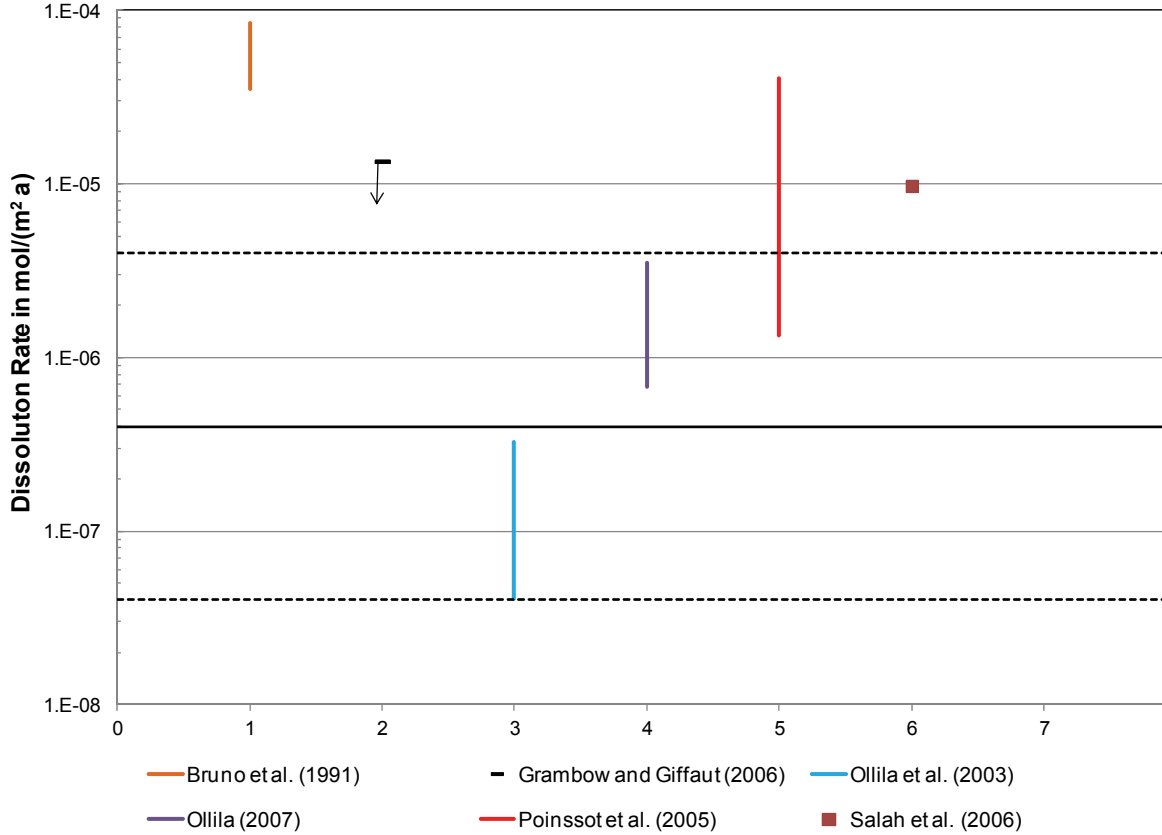


**Figure E.3: UO<sub>2</sub> corrosion rates from various literature sources (see text). The literature data likely overestimate the chemical dissolution rate, as explained in the text. The dashed lines are the selected upper and lower bounds and the solid line is the median chemical dissolution rate.**

## E.6 TOTAL FUEL DISSOLUTION RATE

Table 4.4 summarizes the radiation dose rates at the used fuel surface as a function of time after discharge. Figure E.4 shows the same data in a graphical form. After a few hundred years, the alpha contribution dominates. Figure E.5 shows the total used fuel dissolution rate calculated using Equation E.4 and the data given above. The figure also shows the 5<sup>th</sup> and 95<sup>th</sup> percentile fuel dissolution rate based on the uncertainties in the values of  $G_m$  ( $m = \alpha, \beta$  or  $\gamma$ ) and  $R_{ch}$ .

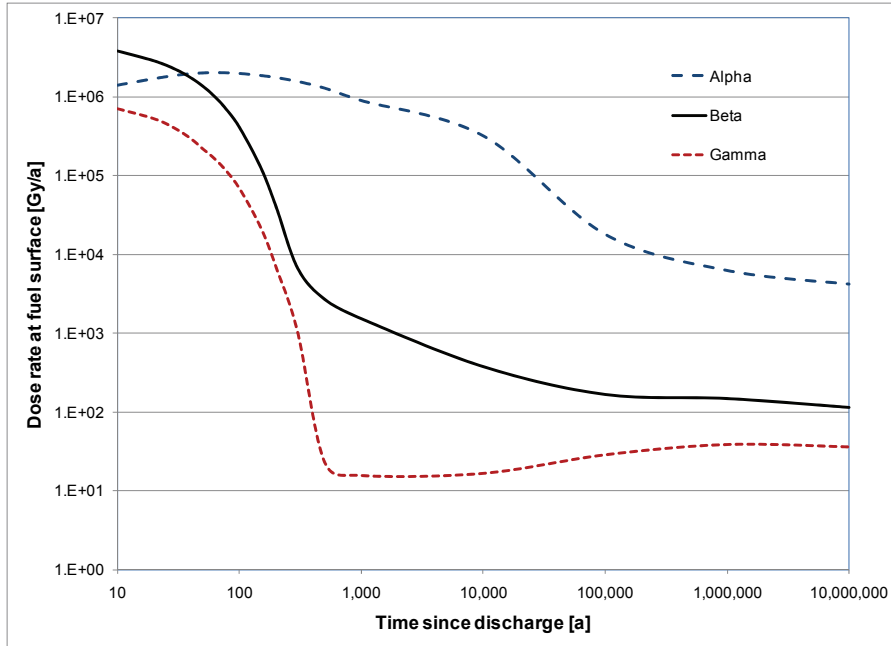


Figure E.4: Radiation dose rate in water at the fuel surface (220 MWh/kgU burnup). Alpha radiolysis dominates after a few hundred years.

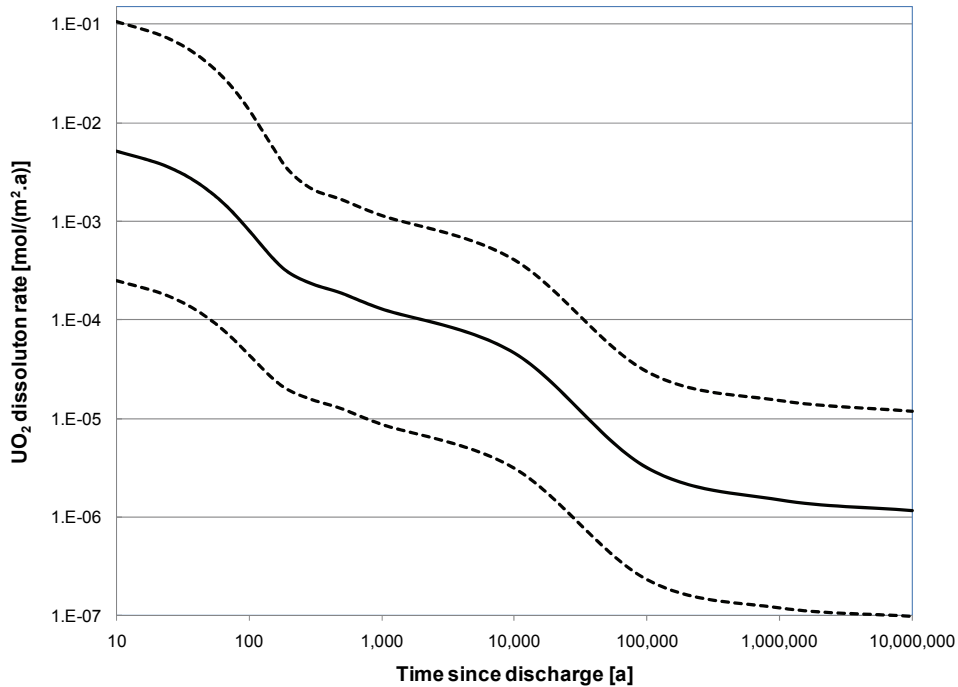


Figure E.5: Calculated total fuel dissolution rate. The solid line gives the best-estimate dissolution rate. The lower and upper dashed lines show the 5<sup>th</sup> and 95<sup>th</sup> percentiles of the fuel dissolution rate.

## E.7 REFERENCES

- Bruno J., I. Casas and I. Puigdomènech. 1991. The kinetics of dissolution of  $UO_2$  under reducing conditions and the influence of an oxidized surface layer ( $UO_{2+x}$ ): Application of a continuous flow-through reactor. *Geochimica et Cosmochimica Acta*, 55, 647-658.
- Forsyth, R. 1997. The SKB spent fuel corrosion programmed. An evaluation of results from the experimental programme performed in the Studsvik Hot Cell Laboratory. SKB Technical Report TR 97-25. Stockholm, Sweden.
- Garisto, F., D.H. Barber, E. Chen, A. Inglot and C.A. Morrison. 2009. Alpha, beta and gamma dose rates in water in contact with used CANDU fuel. Nuclear Waste Management Organization Technical Report NWMO TR-2009-27. Toronto, Canada.
- Grambow, B.G. and E. Giffaut. 2006. Coupling of chemical processes in the near field. *Mat. Res. Soc. Symp. Proc. Vol. 932*, 55-66.
- Grambow, B., A. Loida, A. Martinez-Esparza, P. Diaz-Arocas, J. de Pablo, J.-L. Paul, G. Marx, J.-P. Glatz, K. Lemmens, K. Ollila and H. Christensen. 2000. Source term for performance assessment of spent fuel as a waste form. European Commission Report EUR 19140. Brussels, Belgium.
- Grambow, B., J. Bruno, L. Duro, J. Merino, A. Tamayo, C. Martin, G. Pepin, S. Schumacher, O. Smidt, C. Ferry, C. Jegou, J. Quiñones, E. Iglesias, N. Rodriguez Villagra, J. M. Nieto, A. Martínez-Esparza, A. Loida, V. Metz, B. Kienzler, G. Bracke (GRS), D. Pellegrini, G. Mathieu, V. Wasselin-Trupin, C. Serres, D. Wegen, M. Jonsson, L. Johnson, K. Lemmens, J. Liu, K. Spahiu, E. Ekeröth, I. Casas, J. de Pablo, C. Watson, P. Robinson, and D. Hodgkinson. 2010. MICADO model uncertainty for the mechanism of dissolution of spent fuel in nuclear waste repository. European Commission Report EUR 24597 EN. Brussels, Belgium.
- Johnson, L.H. 1982. The dissolution of irradiated  $UO_2$  fuel in groundwater. Atomic Energy of Canada Limited Report AECL-6837. Pinawa, Canada.
- Johnson, L.H., D.M. LeNeveu, F. King, D.W. Shoesmith, M. Kolar, D.W. Oscarson, S. Sunder, C. Onofrei, and J.L. Crosthwaite. 1996. The disposal of Canada's nuclear fuel waste: A study of postclosure safety of in-room emplacement of used CANDU fuel in copper containers in permeable plutonic rock, Volume 2: Vault model. Atomic Energy of Canada Limited Report AECL-11494-2. Pinawa, Canada.
- Lemire, R.J. and F. Garisto. 1989. The solubility of U, Np, Pu, Th and Tc in a geological disposal vault for used nuclear fuel. Atomic Energy of Canada Limited Report AECL-10009. Pinawa, Canada.
- Muzeau, B., C. Jegou, F. Delaunay, V. Brodic, A. Brevet, H. Catalette, E. Simoni and C. Corbel. Radiolytic oxidation of  $UO_2$  pellets doped with alpha-emitters ( $^{238/239}Pu$ ). *J. Alloys and Comps.* 467, 578-589.
- Ollila, K. 2007. Dissolution of unirradiated  $UO_2$  and  $UO_2$  doped with  $^{233}U$  in low and high ionic strength NaCl under anoxic and reducing conditions. European Commission NF-PRO Report D.1.5.11. Brussels, Belgium.

- Ollila, K. Y. Albinsson, V. Oversby and M. Cowper. 2003. Dissolution rates of unirradiated  $\text{UO}_2$ ,  $\text{UO}_2$  doped with  $^{233}\text{U}$ , and spent fuel under normal atmospheric conditions and under reducing conditions using an isotope dilution method. SKB Technical Report TR 03-13. Stockholm, Sweden.
- Poinsot, C., C. Ferry, M. Kelm, B. Grambow, A. Martinez-Esparza, L. Johnson, Z. Andriambololona, J. Bruno, C. Cachoir, J-M. Cavendon, H. Christensen, C. Corbel, C. Jegou, K. Lemmens, A. Loida, P. Lovera, F. Miserque, J. de Pablo, A. Poulesquen, J. Quinones, V. Rondinella, K. Spahiu and D. Wegen. 2005. Final report of the European project spent fuel stability under repository conditions. European Commission Report CEA-R-6093. Brussels, Belgium.
- Saleh, S., C. Cachoir, K. Lemmens and N. Maes. Static dissolution tests of alpha-doped  $\text{UO}_2$  under repository relevant conditions: Influence of Boom Clay and alpha activity on fuel dissolution rates. Mat. Res. Soc. Symp. Proc. Vol. 932, 481-488.
- Shoesmith, D.W. 2007. Used fuel and uranium dioxide dissolution studies – A review. Nuclear Waste Management Organization Technical Report NWMO TR-2007-03. Toronto, Canada.
- Shoesmith, D.W. and S. Sunder. 1991. An electrochemistry-based model for the dissolution of  $\text{UO}_2$ . Atomic Energy of Canada Limited Report AECL-10488. Pinawa, Canada.
- SKB (Svensk Kärnbränslehantering AB). 2010. Fuel and canister process report for the safety assessment SR-Site. SKB Technical Report SKB TR-10-46. Stockholm, Sweden.
- Tait, J.C., H. Roman and C.A. Morrison. 2000. Characteristics and Radionuclide Inventories of Used Fuel from OPG Nuclear Generating Stations, Volume 2 – Radionuclide Inventory Data. Ontario Power Generation Report 06819-REP-01200-10029-R00. Toronto, Canada.
- Werme, L., L.H. Johnson, V.M. Oversby, F. King, K. Spahiu, B. Grambow and D.W. Shoesmith. 2004. Spent fuel performance under repository conditions: a model for use in SR-Can. SKB Technical Report TR-04-19. Stockholm, Sweden.

## **APPENDIX F: SYVAC3-CC4 GEOSPHERE MODEL DATA**

(Prepared by C. Kitson, T. Chshyolkova and T. Melnyk, Atomic Energy of Canada Limited)

The SYVAC3-CC4 geosphere transport model (also called GEONET) uses a simplified representation of the groundwater flow results from FRAC3DVS-OPG. It uses a network of interconnected 1-D transport path segments to represent the transport of nuclides through the geosphere, from the repository to surface discharge points (see NWMO 2012b and Davison et al. 1994 for a description of the features of this model).

The input data for the network model used to represent the Fourth Case Study is listed in this appendix. The geosphere network model is derived from detailed groundwater flow modelling carried out using the FRAC3DVS-OPG code, and described in NWMO (2012a, Chapter 7). In particular, a detailed FRAC3DVS-OPG groundwater flow model was developed in which the fracture and permeability variation over the entire subregional area was represented. Particles were numerically released across the repository area and tracked to where they intercepted the surface. The particle tracks were then approximated by a network of 1-D segments to form the geosphere transport network described below, taking into account of direct paths for diffusion transport.

The geosphere transport network uses:

- 17 repository sectors;
- 200 segments representing the transport paths;
- 190 nodes at links between segments; and
- 7 surface discharge points.

Figure F.1 and Figure F.2 illustrate the transport network interconnections. The repository is divided conceptually into 17 sectors. In each of these sectors, the movement of contaminants released from any failed container through groundwater to the surface follows a similar path, represented here by the segments. These segment paths have constant properties, characterized by a permeability, temperature (constant 20°C), groundwater flow rate, diffusivity and dispersivity. All transport paths end at the surface, either in the well or at a surface water discharge point. There are four surface discharge points at the Fourth Case Study site - the River, the Lake, the Central and East Wetland. At River and Lake surface discharges, the transport is further divided into a component that enters beneath the water body through sediments (aquatic discharge), and a portion that enters along the edge of the water body (terrestrial discharge). The Central and East Wetland are terrestrial discharges.

Depending on the well pumping rate, contaminants that would otherwise go to the River, the Central or East Wetland may be captured by the well. This pumping-rate dependent branching occurs at several Nodes (i.e., nodes #10, 19, 25, 26, 35, etc) as illustrated in Figure F.1. The well upper and lower reference nodes (190 and 73) are used to locate the well within an aquifer or, in this case, a water-bearing fracture zone.

Table F.1 lists the nodes and the nodal input data. Table F.2 lists the segments and the segment input data. Table F.3 lists slope values only for segments with variable source fractions indicated in Table F.2. The dependence of the flow rate along a pathway on the well demand is approximated with three linear intervals with Break Points A, B, and C (BP<sub>A</sub>, BP<sub>B</sub>, and BP<sub>C</sub>). See Section 7.7 for more information. Table F.4 is a full listing of the geosphere model \*.FXD input file. For further details on the input parameters and format, see the SYVAC3-CC4 User Manual (Kitson et al. 2012).

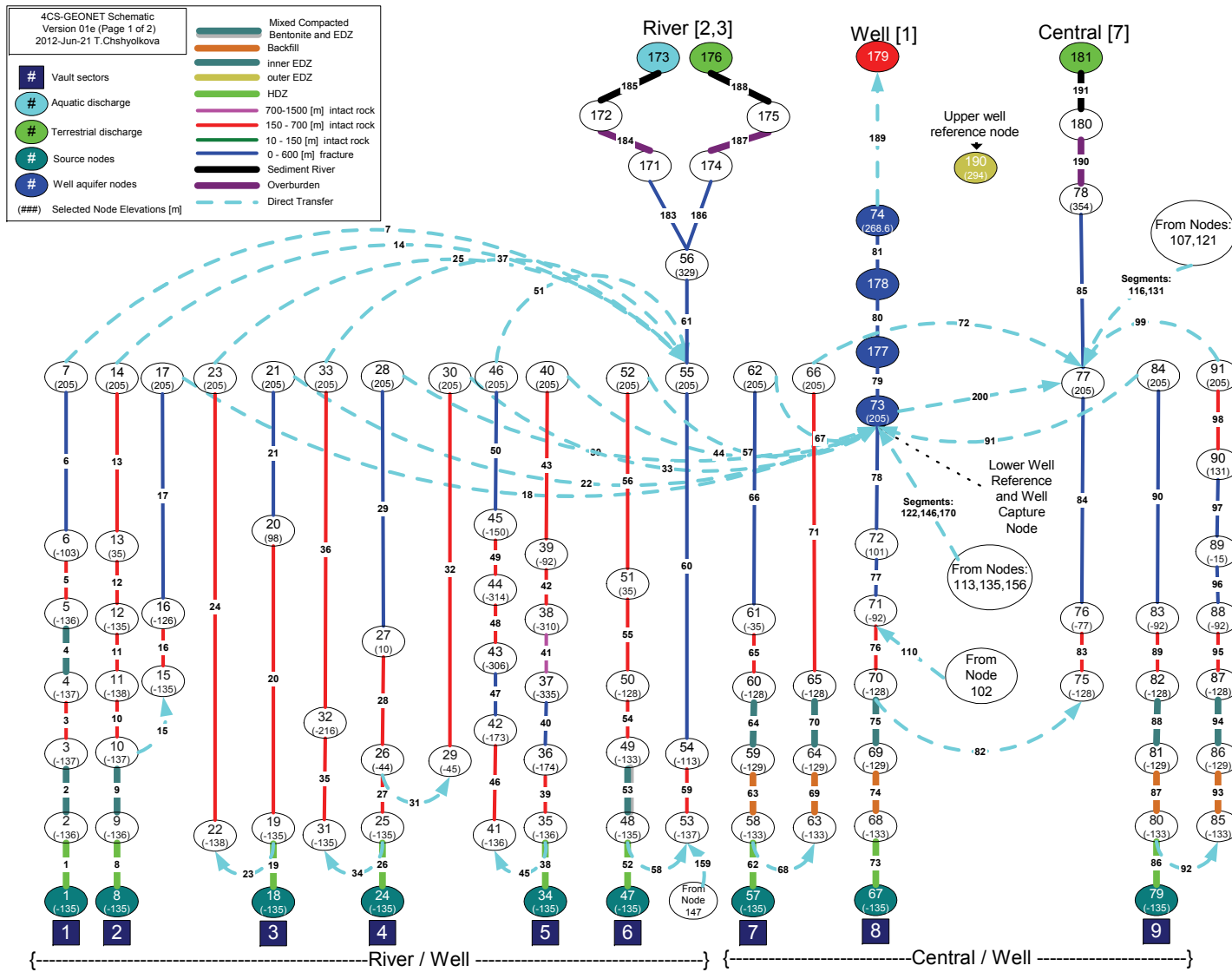


**Figure F.1: SYVAC3-CC4 geosphere transport network schematic showing nodes, segments, material property classes and interconnections from repository sectors to surface discharges.**

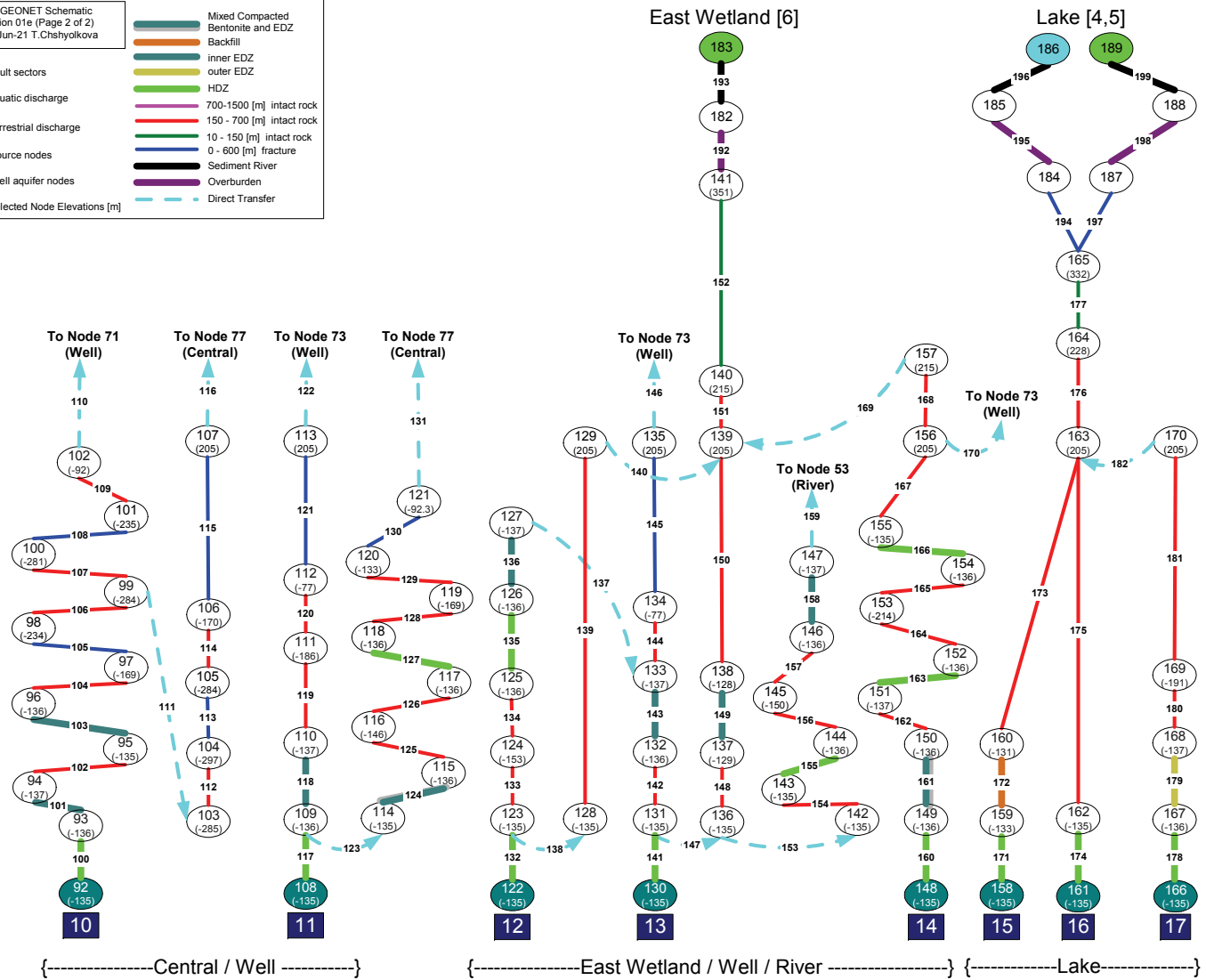
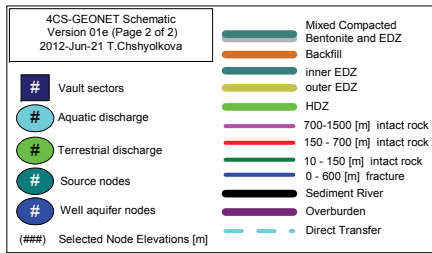


Figure F.2: SYVAC3-CC4 geosphere transport network schematic showing nodes, segments, material property classes and interconnections from repository sectors to surface discharges.

**Table F.1: SCC409 geosphere network - node properties**

<b>Node number</b>	<b>X position NDPOSX [m]</b>	<b>Y position NDPOSY [m]</b>	<b>Z position NDPOSZ [m]</b>	<b>Head NDHEAD<sup>1</sup> [m]</b>	<b>NAQDA1<sup>2</sup> [a/m<sup>2</sup>]</b>
1	9.32300E+02	-8.43250E+02	-1.35350E+02	3.61313E+02	2.08570E-04
2	6.37411E+02	-8.44330E+02	-1.36000E+02	3.61089E+02	2.33110E-04
3	6.33359E+02	-8.44360E+02	-1.37100E+02	3.61039E+02	2.36210E-04
4	6.31571E+02	-8.44210E+02	-1.37000E+02	3.60977E+02	2.40090E-04
5	5.72820E+02	-8.87180E+02	-1.36300E+02	3.60414E+02	2.25380E-04
6	2.53499E+02	-1.05410E+03	-1.02970E+02	3.56092E+02	1.09690E-05
7	6.26481E+01	-1.17430E+03	2.05000E+02	3.54559E+02	4.37810E-06
8	4.38000E+02	-6.43250E+02	-1.35350E+02	3.60687E+02	4.24220E-04
9	6.20000E+01	-6.45750E+02	-1.35800E+02	3.60390E+02	3.57900E-04
10	5.73245E+01	-6.46000E+02	-1.36640E+02	3.60307E+02	3.36750E-04
11	4.16060E+01	-6.97500E+02	-1.37580E+02	3.59813E+02	2.52930E-04
12	1.92089E+01	-7.77870E+02	-1.35000E+02	3.59243E+02	1.87020E-04
13	9.11317E+01	-1.15900E+03	3.50000E+01	3.55544E+02	6.87600E-06
14	6.25142E+01	-1.16820E+03	2.05000E+02	3.54560E+02	4.41200E-06
15	4.50553E+02	-4.83120E+02	-1.35150E+02	3.61637E+02	7.94840E-04
16	4.70424E+02	-4.82850E+02	-1.26100E+02	3.61903E+02	1.01710E-03
17	5.99195E+02	-1.95450E+02	2.05000E+02	3.61159E+02	4.16660E-03
18	4.38000E+02	-1.63250E+02	-1.35350E+02	3.62302E+02	8.34780E-04
19	4.50368E+02	-1.63610E+02	-1.35000E+02	3.62354E+02	9.27830E-04
20	5.66674E+02	-2.57500E+02	9.88230E+01	3.61549E+02	1.85630E-03
21	5.86975E+02	-2.17900E+02	2.04680E+02	3.61175E+02	2.75950E-03
22	1.05820E+02	-1.66000E+02	-1.35290E+02	3.62202E+02	6.76980E-04
23	-2.30156E+02	-9.51150E+02	2.05000E+02	3.54528E+02	5.20680E-06
24	4.38000E+02	6.62500E+01	-1.35350E+02	3.63057E+02	7.43760E-04
25	4.37353E+02	6.35000E+01	-1.35230E+02	3.63057E+02	7.43700E-04
26	4.75323E+02	-1.28900E+02	-4.42230E+01	3.62380E+02	1.22680E-03
27	5.61000E+02	-2.03330E+02	1.00920E+02	3.61747E+02	2.04340E-03
28	5.99421E+02	-1.97620E+02	2.05000E+02	3.61150E+02	4.14680E-03
29	5.54000E+02	-1.17870E+02	-4.50610E+01	3.62408E+02	1.45960E-03
30	6.01928E+02	-1.94410E+02	2.05000E+02	3.61164E+02	4.17440E-03
31	7.51099E+01	6.35000E+01	-1.35340E+02	3.62920E+02	5.87030E-04
32	-2.17571E+02	-4.13140E+02	-2.16340E+02	3.60387E+02	2.11850E-04
33	-7.50829E+02	-5.67690E+02	2.05000E+02	3.54644E+02	1.10900E-06
34	6.44300E+02	5.06250E+02	-1.35350E+02	3.66252E+02	3.49410E-04
35	5.71629E+02	4.83270E+02	-1.36300E+02	3.65424E+02	4.88110E-04
36	4.85231E+02	4.58730E+02	-1.74400E+02	3.64393E+02	6.83260E-04
37	4.65413E+02	2.16060E+02	-3.35000E+02	3.63681E+02	8.61000E-04
38	5.15998E+02	-2.94680E+00	-3.10000E+02	3.63144E+02	1.01100E-03
39	5.50749E+02	-2.38130E+02	-9.22560E+01	3.62244E+02	1.33860E-03
40	6.07515E+02	-2.37930E+02	2.05000E+02	3.60883E+02	3.99640E-03
41	5.71392E+02	4.82480E+02	-1.36300E+02	3.65418E+02	4.89060E-04
42	4.85231E+02	4.58390E+02	-1.73470E+02	3.64393E+02	6.83110E-04



Node number	X position NDPOSX [m]	Y position NDPOSY [m]	Z position NDPOSZ [m]	Head NDHEAD <sup>1</sup> [m]	NAQDA1 <sup>2</sup> [a/m <sup>2</sup> ]
43	4.60456E+02	2.00500E+02	-3.06360E+02	3.63664E+02	8.66730E-04
44	1.20784E+02	1.43500E+02	-3.13950E+02	3.63035E+02	5.19760E-04
45	1.20784E+02	-1.17610E+03	-1.50210E+02	3.56091E+02	7.91910E-06
46	4.69115E+01	-1.18290E+03	2.05000E+02	3.54511E+02	3.85530E-06
47	6.52300E+02	-4.83250E+02	-1.35350E+02	3.62379E+02	5.57070E-04
48	6.34100E+02	-4.83220E+02	-1.35000E+02	3.62370E+02	5.61450E-04
49	6.24629E+02	-4.79860E+02	-1.32500E+02	3.62223E+02	6.33860E-04
50	6.06779E+02	-4.80600E+02	-1.28200E+02	3.62123E+02	6.76540E-04
51	4.95191E+02	-4.97500E+02	3.50700E+01	3.61439E+02	8.52560E-04
52	5.72416E+02	-3.69970E+02	2.05000E+02	3.60670E+02	1.17500E-03
53	6.34379E+02	-6.04560E+02	-1.37100E+02	3.61941E+02	4.32460E-04
54	2.68999E+02	-1.03010E+03	-1.12580E+02	3.56098E+02	1.12560E-05
55	6.28178E+01	-1.17370E+03	2.05000E+02	3.54560E+02	4.38540E-06
56	3.31259E+01	-1.17200E+03	3.29280E+02	3.52754E+02	1.02050E-06
57	8.68300E+02	-3.63250E+02	-1.35350E+02	3.62988E+02	5.97500E-04
58	6.37347E+02	-3.63340E+02	-1.32500E+02	3.62740E+02	7.28510E-04
59	6.36100E+02	-3.63190E+02	-1.29370E+02	3.62674E+02	7.63410E-04
60	6.09420E+02	-3.63440E+02	-1.28200E+02	3.62497E+02	8.63410E-04
61	5.40400E+02	-3.52130E+02	-3.49450E+01	3.61838E+02	1.20550E-03
62	5.89806E+02	-2.70100E+02	2.05000E+02	3.60858E+02	2.47240E-03
63	6.36323E+02	-2.83200E+02	-1.32500E+02	3.62999E+02	8.14160E-04
64	6.36100E+02	-2.83140E+02	-1.29470E+02	3.62926E+02	8.53720E-04
65	6.09481E+02	-2.83920E+02	-1.28200E+02	3.62705E+02	9.69120E-04
66	5.76654E+02	-3.85900E+02	2.05000E+02	3.60649E+02	1.05790E-03
67	6.76300E+02	-2.03250E+02	-1.35350E+02	3.63375E+02	8.10650E-04
68	6.36414E+02	-2.03040E+02	-1.32500E+02	3.63261E+02	8.67520E-04
69	6.36100E+02	-2.02890E+02	-1.29460E+02	3.63173E+02	9.12090E-04
70	6.09298E+02	-2.03180E+02	-1.28200E+02	3.62905E+02	1.03960E-03
71	5.51998E+02	-2.10780E+02	-9.22560E+01	3.62291E+02	1.35190E-03
72	5.78206E+02	-2.40500E+02	1.01220E+02	3.61601E+02	1.99170E-03
73	6.00027E+02	-2.27640E+02	2.05000E+02	3.60988E+02	NA <sup>4</sup>
74	— <sup>3</sup>	— <sup>3</sup>	— <sup>3</sup>	3.60772E+02	NA <sup>4</sup>
75	6.06928E+02	-2.03710E+02	-1.28200E+02	3.62886E+02	1.04870E-03
76	5.51992E+02	-2.29000E+02	-7.68990E+01	3.62209E+02	1.36330E-03
77	5.81743E+02	-3.60080E+02	2.05000E+02	3.60630E+02	1.29330E-03
78	5.98377E+02	-3.97800E+02	3.50000E+02	3.59097E+02	7.50520E-05
79	9.16300E+02	6.62500E+01	-1.35350E+02	3.64858E+02	5.66180E-04
80	6.36213E+02	6.57880E+01	-1.32500E+02	3.64317E+02	7.41310E-04
81	6.36100E+02	6.57360E+01	-1.29480E+02	3.64217E+02	7.73270E-04
82	6.05121E+02	6.35000E+01	-1.28260E+02	3.63880E+02	8.71080E-04
83	5.50856E+02	-5.64760E+01	-9.22560E+01	3.62693E+02	1.29140E-03
84	6.02832E+02	-1.72360E+02	2.05000E+02	3.61265E+02	4.37750E-03
85	6.36139E+02	1.05780E+02	-1.32500E+02	3.64541E+02	6.85460E-04

Node number	X position NDPOSX [m]	Y position NDPOSY [m]	Z position NDPOSZ [m]	Head NDHEAD <sup>1</sup> [m]	NAQDA1 <sup>2</sup> [a/m <sup>2</sup> ]
86	6.36100E+02	1.05770E+02	-1.29490E+02	3.64449E+02	7.12020E-04
87	5.99324E+02	1.03500E+02	-1.28230E+02	3.64072E+02	8.13630E-04
88	5.50953E+02	-3.04740E+01	-9.22560E+01	3.62774E+02	1.26090E-03
89	5.66000E+02	-4.04260E+01	-1.49780E+01	3.62613E+02	1.42750E-03
90	6.01453E+02	-2.06020E+02	1.31000E+02	3.61623E+02	2.54810E-03
91	6.07680E+02	-2.31740E+02	2.05000E+02	3.60922E+02	3.96040E-03
92	9.48300E+02	3.86250E+02	-1.35350E+02	3.66249E+02	3.51110E-04
93	6.36855E+02	3.85660E+02	-1.36000E+02	3.65857E+02	4.18390E-04
94	6.33168E+02	3.85650E+02	-1.37100E+02	3.65773E+02	4.33350E-04
95	6.29597E+02	3.85750E+02	-1.35300E+02	3.65672E+02	4.51020E-04
96	5.78859E+02	3.83500E+02	-1.35950E+02	3.65171E+02	5.39690E-04
97	4.80277E+02	3.46620E+02	-1.69430E+02	3.64170E+02	7.36670E-04
98	4.75323E+02	2.25340E+02	-2.33750E+02	3.63738E+02	8.52700E-04
99	4.98544E+02	1.09000E+02	-2.84060E+02	3.63444E+02	9.34870E-04
100	5.13143E+02	4.62500E+01	-2.80710E+02	3.63233E+02	9.96260E-04
101	5.21000E+02	4.54020E+01	-2.34990E+02	3.63290E+02	9.89520E-04
102	5.50749E+02	-2.38130E+02	-9.22560E+01	3.62244E+02	1.33860E-03
103	4.98442E+02	1.10030E+02	-2.85000E+02	3.63446E+02	9.34180E-04
104	5.14805E+02	1.37500E+01	-2.96660E+02	3.63183E+02	1.00470E-03
105	5.26000E+02	4.22580E+00	-2.84040E+02	3.63164E+02	1.01250E-03
106	5.40400E+02	-2.07210E+02	-1.69940E+02	3.62489E+02	1.19970E-03
107	5.76600E+02	-3.85900E+02	2.04980E+02	3.60650E+02	1.05730E-03
108	1.48725E+03	4.26250E+02	-1.35350E+02	3.68261E+02	1.09310E-04
109	1.13877E+03	4.25530E+02	-1.35700E+02	3.67852E+02	1.40600E-04
110	1.13346E+03	4.25570E+02	-1.37100E+02	3.67838E+02	1.42090E-04
111	1.03637E+03	3.79320E+02	-1.86110E+02	3.66651E+02	2.83690E-04
112	5.53998E+02	-1.01700E+02	-7.70440E+01	3.62515E+02	1.37440E-03
113	6.04913E+02	-1.64040E+02	2.05000E+02	3.61304E+02	4.41650E-03
114	1.13220E+03	1.86110E+02	-1.35050E+02	3.66705E+02	1.94130E-04
115	1.07020E+03	1.36670E+02	-1.36300E+02	3.65914E+02	3.16530E-04
116	1.03637E+03	1.17100E+02	-1.45670E+02	3.65512E+02	4.04350E-04
117	1.01940E+03	1.04650E+02	-1.35700E+02	3.65111E+02	5.16630E-04
118	7.09472E+02	1.03500E+02	-1.35670E+02	3.64710E+02	6.37160E-04
119	5.48352E+02	-1.34500E+02	-1.69250E+02	3.62601E+02	1.24550E-03
120	5.45200E+02	-2.19160E+02	-1.32780E+02	3.62379E+02	1.29090E-03
121	5.46325E+02	-2.60830E+02	-9.22560E+01	3.62191E+02	1.30320E-03
122	1.39125E+03	-2.83250E+02	-1.35350E+02	3.63723E+02	1.81070E-04
123	1.13662E+03	-2.86000E+02	-1.35100E+02	3.63708E+02	2.24860E-04
124	1.03637E+03	-3.52990E+02	-1.53480E+02	3.63220E+02	4.33620E-04
125	1.01748E+03	-3.64710E+02	-1.35700E+02	3.63063E+02	5.48890E-04
126	6.39626E+02	-3.65040E+02	-1.36000E+02	3.62800E+02	6.96820E-04
127	6.34730E+02	-3.65030E+02	-1.37100E+02	3.62787E+02	7.03760E-04
128	1.41424E+03	-5.26000E+02	-1.35160E+02	3.62224E+02	1.43880E-04

Node number	X position NDPOSX [m]	Y position NDPOSY [m]	Z position NDPOSZ [m]	Head NDHEAD <sup>1</sup> [m]	NAQDA1 <sup>2</sup> [a/m <sup>2</sup> ]
129	1.48562E+03	-6.96950E+02	2.05000E+02	3.58409E+02	3.37510E-06
130	1.13525E+03	-1.23250E+02	-1.35350E+02	3.64741E+02	2.34610E-04
131	1.08990E+03	-1.26000E+02	-1.35290E+02	3.64556E+02	3.48690E-04
132	1.01639E+03	-2.03510E+02	-1.36400E+02	3.63721E+02	6.27720E-04
133	6.34712E+02	-2.04420E+02	-1.37100E+02	3.63329E+02	8.32530E-04
134	5.51989E+02	-2.38150E+02	-7.70440E+01	3.62195E+02	1.35860E-03
135	6.07517E+02	-2.37930E+02	2.05000E+02	3.60883E+02	3.99660E-03
136	1.36410E+03	-2.06000E+02	-1.35280E+02	3.64281E+02	1.92420E-04
137	1.36311E+03	-2.40500E+02	-1.29410E+02	3.63989E+02	-1.23190E-04
138	1.36083E+03	-2.43050E+02	-1.28200E+02	3.63986E+02	-1.94100E-04
139	1.46345E+03	-5.97190E+02	2.05000E+02	3.58756E+02	4.25670E-06
140	1.46377E+03	-6.06000E+02	2.15050E+02	3.58582E+02	9.74200E-07
141	1.36972E+03	-7.49230E+02	3.47150E+02	3.56234E+02	7.71680E-09
142	1.21215E+03	-1.26000E+02	-1.35330E+02	3.64766E+02	2.21740E-04
143	1.21025E+03	-1.60500E+02	-1.35370E+02	3.64503E+02	2.21120E-04
144	1.07218E+03	-2.20760E+02	-1.36300E+02	3.63979E+02	3.76900E-04
145	1.03637E+03	-2.75660E+02	-1.50310E+02	3.63575E+02	4.67160E-04
146	1.01190E+03	-3.22290E+02	-1.36400E+02	3.63222E+02	5.76460E-04
147	7.03454E+02	-3.23850E+02	-1.37000E+02	3.62980E+02	7.16210E-04
148	1.80250E+03	4.66250E+02	-1.35350E+02	3.70279E+02	3.22700E-05
149	1.63030E+03	4.66340E+02	-1.35020E+02	3.70054E+02	3.78390E-05
150	1.56867E+03	4.45640E+02	-1.36300E+02	3.69200E+02	6.48090E-05
151	1.51780E+03	4.23750E+02	-1.37000E+02	3.68292E+02	1.07550E-04
152	1.47424E+03	4.23500E+02	-1.35620E+02	3.68250E+02	1.09950E-04
153	1.25966E+03	-1.77500E+02	-2.13590E+02	3.64412E+02	2.32660E-04
154	1.26645E+03	-6.04650E+02	-1.35700E+02	3.61915E+02	1.44533E-04
155	1.44375E+03	-6.06000E+02	-1.35430E+02	3.61818E+02	1.26149E-04
156	1.50222E+03	-7.26280E+02	2.05000E+02	3.58440E+02	3.03993E-06
157	1.47460E+03	-7.24000E+02	2.15420E+02	3.58241E+02	7.42031E-07
158	1.93050E+03	-5.23250E+02	-1.35350E+02	3.62304E+02	4.36648E-05
159	1.78209E+03	-5.25440E+02	-1.32500E+02	3.62208E+02	4.89115E-05
160	1.78192E+03	-5.26000E+02	-1.30730E+02	3.62200E+02	4.87391E-05
161	1.99450E+03	-4.83250E+02	-1.35350E+02	3.62666E+02	4.41131E-05
162	1.77391E+03	-4.86000E+02	-1.35010E+02	3.62544E+02	5.17462E-05
163	1.77327E+03	-6.52920E+02	2.05000E+02	3.56512E+02	1.55761E-06
164	1.78202E+03	-6.46710E+02	2.28000E+02	3.56150E+02	2.93798E-07
165	1.78162E+03	-6.52360E+02	3.31990E+02	3.55016E+02	2.51262E-08
166	2.00250E+03	1.06250E+02	-1.35350E+02	3.68322E+02	4.40529E-05
167	1.65584E+03	1.04460E+02	-1.36000E+02	3.67917E+02	5.89470E-05
168	1.65549E+03	1.04290E+02	-1.37000E+02	3.67911E+02	5.91522E-05
169	1.56043E+03	-8.90000E+01	-1.90960E+02	3.65611E+02	1.15958E-04
170	1.57273E+03	-5.88070E+02	2.05000E+02	3.58261E+02	3.22052E-06
171	— <sup>3</sup>	— <sup>3</sup>	— <sup>3</sup>	3.52176E+02	3.09923E-07

Node number	X position NDPOSX [m]	Y position NDPOSY [m]	Z position NDPOSZ [m]	Head NDHEAD <sup>1</sup> [m]	NAQDA1 <sup>2</sup> [a/m <sup>2</sup> ]
172	— <sup>3</sup>	— <sup>3</sup>	— <sup>3</sup>	3.52176E+02	3.09923E-07
173	3.80214E+01	-1.17000E+03	3.46820E+02	3.52176E+02	3.09923E-07
174	— <sup>3</sup>	— <sup>3</sup>	— <sup>3</sup>	3.52176E+02	3.09923E-07
175	— <sup>3</sup>	— <sup>3</sup>	— <sup>3</sup>	3.52176E+02	3.09923E-07
176	3.80214E+01	-1.17000E+03	3.46820E+02	3.52176E+02	3.09923E-07
177	— <sup>3</sup>	— <sup>3</sup>	— <sup>3</sup>	3.60772E+02	NA <sup>4</sup>
178	— <sup>3</sup>	— <sup>3</sup>	— <sup>3</sup>	3.60772E+02	NA <sup>4</sup>
179	— <sup>3</sup>	— <sup>3</sup>	— <sup>3</sup>	3.59093E+02	1.65280E-04
180	— <sup>3</sup>	— <sup>3</sup>	— <sup>3</sup>	3.59097E+02	7.50525E-05
181	5.98377E+02	-3.97800E+02	3.54000E+02	3.59097E+02	7.50525E-05
182	— <sup>3</sup>	— <sup>3</sup>	— <sup>3</sup>	3.56234E+02	7.91438E-09
183	1.36972E+03	-7.49230E+02	3.51150E+02	3.56234E+02	7.91438E-09
184	— <sup>3</sup>	— <sup>3</sup>	— <sup>3</sup>	3.53728E+02	3.17234E-09
185	— <sup>3</sup>	— <sup>3</sup>	— <sup>3</sup>	3.53728E+02	3.17234E-09
186	1.72852E+03	-6.64940E+02	3.48870E+02	3.53728E+02	3.17234E-09
187	— <sup>3</sup>	— <sup>3</sup>	— <sup>3</sup>	3.53728E+02	3.17234E-09
188	— <sup>3</sup>	— <sup>3</sup>	— <sup>3</sup>	3.53728E+02	3.17234E-09
189	1.72852E+03	-6.64940E+02	3.48870E+02	3.53728E+02	3.17234E-09
190	6.25501E+02	-1.37060E+02	2.93600E+02	3.60667E+02	8.01796E-03

<sup>1</sup> Nodal heads are adjusted for nodal position and for drawdown effects of the well before use.

<sup>2</sup> NAQDA1 is an input parameter used in a semi-empirical equation in CC4 that calculates drawdown of head in nodes outside the well aquifer as a result of the well demand.

<sup>3</sup> Coordinates are calculated based on sediment and overburden thickness, or on well position.

<sup>4</sup> This node is within the well aquifer and the head drawdown due to well demand is calculated within CC4 directly.

**Table F.2: SCC409 geosphere network - segment properties**

Segment number	Segment hydraulic conductivity SGHYCO [m/a]	Segment axial dispersion length factor SGDSPF <sup>1</sup> [-]	Source fraction SGSFRI [-]
1	1.26230E+01	6.81060E-02	1
2	1.26230E-01	4.76350E+00	1
3	1.26230E-03	1.11290E+01	1
4	1.26230E-01	2.74760E-01	1
5	1.26230E-03	5.52710E-02	1
6	3.15570E+01	5.23930E-02	1
7	— <sup>3</sup>	— <sup>3</sup>	1
8	1.26230E+01	5.33650E-02	1
9	1.26230E-01	4.20440E+00	1
10	1.26230E-03	3.71380E-01	Varies <sup>2</sup>
11	1.26230E-03	2.39600E-01	1
12	1.26230E-03	4.72280E-02	1
13	1.26230E-03	1.15850E-01	1
14	— <sup>3</sup>	— <sup>3</sup>	1
15	— <sup>3</sup>	— <sup>3</sup>	Varies <sup>2</sup>
16	1.26230E-03	9.15910E-01	1
17	3.15570E+01	4.37680E-02	1
18	— <sup>3</sup>	— <sup>3</sup>	1
19	1.26230E+01	1.79410E+00	1
20	1.26230E-03	7.20680E-02	Varies <sup>2</sup>
21	3.15570E+01	1.74170E-01	1
22	— <sup>3</sup>	— <sup>3</sup>	1
23	— <sup>3</sup>	— <sup>3</sup>	Varies <sup>2</sup>
24	1.26230E-03	2.17550E-02	1
25	— <sup>3</sup>	— <sup>3</sup>	1
26	1.26230E+01	1.25190E+01	1
27	1.26230E-03	9.25080E-02	Varies <sup>2</sup>
28	1.26230E-03	1.08550E-01	Varies <sup>2</sup>
29	3.15570E+01	1.80030E-01	1
30	— <sup>3</sup>	— <sup>3</sup>	1
31	— <sup>3</sup>	— <sup>3</sup>	Varies <sup>2</sup>
32	1.26230E-03	7.52250E-02	1
33	— <sup>3</sup>	— <sup>3</sup>	1
34	— <sup>3</sup>	— <sup>3</sup>	Varies <sup>2</sup>
35	1.26230E-03	3.53880E-02	1
36	1.26230E-03	2.86950E-02	1
37	— <sup>3</sup>	— <sup>3</sup>	1
38	1.26230E+01	2.66690E-01	1
39	1.26230E-03	2.05000E-01	Varies <sup>2</sup>
40	3.15570E+01	6.85700E-02	1
41	3.15570E-04	8.84330E-02	1
42	1.26230E-03	6.20380E-02	1

Segment number	Segment hydraulic conductivity SGHYCO [m/a]	Segment axial dispersion length factor SGDSPF <sup>1</sup> [-]	Source fraction SGSFRI [-]
43	1.26230E-03	6.60880E-02	1
44	— <sup>3</sup>	— <sup>3</sup>	1
45	— <sup>3</sup>	— <sup>3</sup>	Varies <sup>2</sup>
46	1.26230E-03	2.06440E-01	1
47	3.15570E+01	6.86880E-02	1
48	1.26230E-03	5.80540E-02	1
49	1.26230E-03	1.50410E-02	1
50	3.15570E+01	5.51160E-02	1
51	— <sup>3</sup>	— <sup>3</sup>	1
52	1.26230E+01	1.17830E+00	1
53	1.26230E-01	1.93130E+00	Varies <sup>2</sup>
54	1.26230E-03	1.08840E+00	1
55	1.26230E-03	1.00770E-01	1
56	1.26230E-03	8.84720E-02	1
57	— <sup>3</sup>	— <sup>3</sup>	1
58	— <sup>3</sup>	— <sup>3</sup>	Varies <sup>2</sup>
59	1.26230E-03	3.56240E-02	1
60	3.15570E+01	4.93880E-02	1
61	3.15570E+01	1.56510E-01	1
62	1.26230E+01	8.70550E-02	1
63	2.77700E-03	5.93040E+00	Varies <sup>2</sup>
64	1.26230E-01	7.48880E-01	1
65	1.26230E-03	1.71570E-01	1
66	3.15570E+01	7.74150E-02	1
67	— <sup>3</sup>	— <sup>3</sup>	1
68	— <sup>3</sup>	— <sup>3</sup>	Varies <sup>2</sup>
69	2.77700E-03	6.58160E+00	1
70	1.26230E-01	7.50160E-01	1
71	1.26230E-03	5.71430E-02	1
72	— <sup>3</sup>	— <sup>3</sup>	1
73	1.26230E+01	5.16020E-01	1
74	2.77700E-03	6.53630E+00	1
75	1.26230E-01	7.45330E-01	1
76	1.26230E-03	2.93830E-01	Varies <sup>2</sup>
77	3.15570E+01	1.01270E-01	1
78	3.15570E+01	1.87220E-01	1
79	3.15570E+01	3.21720E-01	1
80	3.15570E+01	1.33330E+00	1
81	3.15570E+01	4.00000E+00	1
82	— <sup>3</sup>	— <sup>3</sup>	Varies <sup>2</sup>
83	1.26230E-03	2.52190E-01	1
84	3.15570E+01	6.40400E-02	1
85	3.15570E+01	1.30180E-01	1

Segment number	Segment hydraulic conductivity SGHYCO [m/a]	Segment axial dispersion length factor SGDSPF <sup>1</sup> [-]	Source fraction SGSFRI [-]
86	1.26230E+01	7.17170E-02	1
87	2.77700E-03	6.61690E+00	Varies <sup>2</sup>
88	1.26230E-01	6.43430E-01	1
89	1.26230E-03	1.46510E-01	1
90	3.15570E+01	6.18710E-02	1
91	— <sup>3</sup>	— <sup>3</sup>	1
92	— <sup>3</sup>	— <sup>3</sup>	Varies <sup>2</sup>
93	2.77700E-03	6.64390E+00	1
94	1.26230E-01	5.42480E-01	1
95	1.26230E-03	1.36140E-01	1
96	3.15570E+01	2.52030E-01	1
97	3.15570E+01	8.94530E-02	1
98	1.26230E-03	2.54490E-01	1
99	— <sup>3</sup>	— <sup>3</sup>	1
100	1.26230E+01	6.44710E-02	1
101	1.26230E-01	5.19770E+00	1
102	1.26230E-03	5.00050E+00	1
103	1.26230E-01	3.93760E-01	1
104	1.26230E-03	1.81070E-01	1
105	3.15570E+01	1.45590E-01	1
106	1.26230E-03	1.55200E-01	1
107	1.26230E-03	3.10020E-01	Varies <sup>2</sup>
108	3.15570E+01	4.31050E-01	1
109	1.26230E-03	6.27310E-02	1
110	— <sup>3</sup>	— <sup>3</sup>	1
111	— <sup>3</sup>	— <sup>3</sup>	Varies <sup>2</sup>
112	1.26230E-03	2.03350E-01	1
113	3.15570E+01	1.03240E+00	1
114	1.26230E-03	8.30950E-02	1
115	3.15570E+01	4.79730E-02	1
116	— <sup>3</sup>	— <sup>3</sup>	1
117	1.26230E+01	5.75940E-02	1
118	1.26230E-01	3.64710E+00	Varies <sup>2</sup>
119	1.26230E-03	1.69220E-01	1
120	1.26230E-03	2.89900E-02	1
121	3.15570E+01	6.81890E-02	1
122	— <sup>3</sup>	— <sup>3</sup>	1
123	— <sup>3</sup>	— <sup>3</sup>	Varies <sup>2</sup>
124	1.26230E-01	2.52180E-01	1
125	1.26230E-03	4.97580E-01	1
126	1.26230E-03	8.58850E-01	1
127	1.26230E+01	6.45310E-02	1
128	1.26230E-03	6.91170E-02	1

Segment number	Segment hydraulic conductivity SGHYCO [m/a]	Segment axial dispersion length factor SGDSPF <sup>1</sup> [-]	Source fraction SGSFRI [-]
129	1.26230E-03	2.16840E-01	1
130	3.15570E+01	3.44020E-01	1
131	— <sup>3</sup>	— <sup>3</sup>	1
132	1.26230E+01	7.89230E-02	1
133	1.26230E-03	1.63970E-01	Varies <sup>2</sup>
134	1.26230E-03	7.02740E-01	1
135	1.26230E+01	5.29300E-02	1
136	1.26230E-01	3.98480E+00	1
137	— <sup>3</sup>	— <sup>3</sup>	1
138	— <sup>3</sup>	— <sup>3</sup>	Varies <sup>2</sup>
139	1.26230E-03	5.16350E-02	1
140	— <sup>3</sup>	— <sup>3</sup>	1
141	1.26230E+01	4.52430E-01	1
142	1.26230E-03	1.87210E-01	Varies <sup>2</sup>
143	1.26230E-01	5.24000E-02	1
144	1.26230E-03	1.85800E-01	1
145	3.15570E+01	6.95750E-02	1
146	— <sup>3</sup>	— <sup>3</sup>	1
147	— <sup>3</sup>	— <sup>3</sup>	Varies <sup>2</sup>
148	1.26230E-03	5.71270E-01	Varies <sup>2</sup>
149	1.26230E-01	5.50960E+00	1
150	1.26230E-03	4.02450E-02	1
151	1.26230E-03	1.49610E+00	1
152	6.31140E-02	9.16590E-02	1
153	— <sup>3</sup>	— <sup>3</sup>	Varies <sup>2</sup>
154	1.26230E-03	5.78830E-01	1
155	1.26230E+01	1.32760E-01	1
156	1.26230E-03	2.98380E-01	1
157	1.26230E-03	3.67200E-01	1
158	1.26230E-01	6.48410E-02	1
159	— <sup>3</sup>	— <sup>3</sup>	1
160	1.26230E+01	1.16980E-01	1
161	1.26230E-01	3.07570E-01	1
162	1.26230E-03	3.61100E-01	1
163	1.26230E+01	4.58920E-01	1
164	1.26230E-03	3.11090E-02	1
165	1.26230E-03	4.60570E-02	1
166	1.26230E+01	1.12800E-01	1
167	1.26230E-03	5.46810E-02	1
168	1.26230E-03	6.75540E-01	Varies <sup>2</sup>
169	— <sup>3</sup>	— <sup>3</sup>	1
170	— <sup>3</sup>	— <sup>3</sup>	Varies <sup>2</sup>
171	1.26230E+01	1.35840E-01	1



Segment number	Segment hydraulic conductivity SGHYCO [m/a]	Segment axial dispersion length factor SGDSPF <sup>1</sup> [-]	Source fraction SGSFRI [-]
172	2.77700E-03	1.07320E+01	1
173	1.26230E-03	5.57070E-02	1
174	1.26230E+01	9.11660E-02	1
175	1.26230E-03	5.28020E-02	1
176	1.26230E-03	7.88040E-01	1
177	6.31140E-02	1.92040E-01	1
178	1.26230E+01	5.78970E-02	1
179	1.26230E-02	1.86840E+01	1
180	1.26230E-03	9.00670E-02	1
181	1.26230E-03	3.13880E-02	1
182	— <sup>3</sup>	— <sup>3</sup>	1
183	3.15570E+01	1.17460E+00	0.34
184	4.10240E-01	1.00000E-01	1
185	3.15650E+02	1.00000E-01	1
186	3.15570E+01	1.15180E+00	0.66
187	4.10240E-01	1.00000E-01	1
188	— <sup>4</sup>	— <sup>4</sup>	1
189	— <sup>3</sup>	— <sup>3</sup>	1
190	4.10240E-01	1.00000E-01	1
191	— <sup>4</sup>	— <sup>4</sup>	1
192	4.10240E-01	1.00000E-01	1
193	— <sup>4</sup>	— <sup>4</sup>	1
194	3.15570E+01	3.52510E-01	0.75
195	4.10240E-01	1.00000E-01	1
196	3.15650E+02	1.00000E-01	1
197	3.15570E+01	3.51900E-01	0.25
198	4.10240E-01	1.00000E-01	1
199	— <sup>4</sup>	— <sup>4</sup>	1
200	— <sup>3</sup>	— <sup>3</sup>	0

<sup>1</sup>Dispersivity factors have values such that the dispersion length is 20 m for all segments, except for sediment where it is 10% of segment length.

<sup>2</sup>Location of divergence in network; values calculated before use.

<sup>3</sup>Segments 7, 14, 25, etc. are not transport segments, but are used for direct transfer of flow rates from one node to another. No segment hydraulic conductivity and dispersivity factors need to be defined.

<sup>4</sup>Sediment layers leading to terrestrial discharges were assigned zero lengths (segment numbers 188, 191, 193, and 199). No segment hydraulic conductivity and dispersivity factors need to be defined.

**Table F.3: SCC409 geosphere network – slope values for segments with variable source fraction**

Segment number	Slope values [ $a/m^3$ ]		
	For well demands lower than BPa	For well demands higher than BPa but lower than BPb	For well demands higher than BPb but lower than BPc
10	1.00000E+38 <sup>1</sup>	1.00000E+38	1.00000E+38
15	0.00000E+00	0.00000E+00	5.30000E-04
20	4.50000E-04	9.67742E-04	2.00000E-05
23	1.00000E+38	1.00000E+38	1.00000E+38
27	1.10000E-04	5.09338E-04	2.30000E-04
28	1.00000E+38	1.00000E+38	1.00000E+38
31	0.00000E+00	0.00000E+00	1.00000E-03
34	1.00000E+38	1.00000E+38	1.00000E+38
39	4.72000E-04	1.69779E-05	1.00000E-05
45	1.00000E+38	1.00000E+38	1.00000E+38
53	3.29000E-05	3.90000E-04	7.20000E-04
58	1.00000E+38	1.00000E+38	1.00000E+38
63	1.09800E-03	0.00000E+00	0.00000E+00
68	1.00000E+38	1.00000E+38	1.00000E+38
76	1.09800E-03	0.00000E+00	0.00000E+00
82	1.00000E+38	1.00000E+38	1.00000E+38
87	1.09800E-03	0.00000E+00	0.00000E+00
92	1.00000E+38	1.00000E+38	1.00000E+38
107	1.03200E-03	3.39559E-05	4.00000E-05
111	1.00000E+38	1.00000E+38	1.00000E+38
118	5.82000E-04	3.39559E-05	5.00000E-05
123	1.00000E+38	1.00000E+38	1.00000E+38
133	0.00000E+00	1.02000E-04	2.00000E-04
138	1.00000E+38	1.00000E+38	1.00000E+38
142	5.71000E-04	6.79000E-04	8.00000E-05
147	1.00000E+38	1.00000E+38	1.00000E+38
148	3.62239E-04	0.00000E+00	0.00000E+00
153	1.00000E+38	1.00000E+38	1.00000E+38
168	1.00000E+38	1.00000E+38	1.00000E+38
170	5.15917E-04	4.41426E-04	2.00000E-05

<sup>1</sup> The value of 1E+38 is used to define a complementary segment for the pairings. Divergent segment pairings are determined in the geosphere model automatically based on the connectivity of the geosphere nodes. The variable source fraction for a group of associated divergent segments is calculated and assigned to the primary segment; the complementary segment is assigned the complementary value (1- calculated fraction).

**Table F.4: Listing of SCC409 geosphere network input data file**

```
! 2012-JUN-22 VERSION 05C L. Wojciechowski C.Kitson
!      new network file for 4CS Flex Geonet
! 2012-JUL-03 VERSION 05E C. Kitson
!      external name of file 4CSBNetFileConnetivity05c.fxd
!      removed node 78 from list of nonaquifer nodes for drawdown calculation
!      Finalized nodes for determination of geosphere consequences for reference case
!      List includes:
!      - Well node 179,
!      - River discharge nodes (Aquatic 173) (Terrestrial 176),
!      - Lake discharge nodes (Aquatic 186) (Terrestrial 189),
!      - East Wetland Terrestrial discharge node 183
!      - Central Wetland Terrestrial discharge node 181
!      - Vault source node (Sector 8) 67
! Generated in 4CSBNetFileConnetivity01a.xlsx in
!
W:\Eba_shr\Projects\SA05_2012\Tasks\02D_4CS_GeosphereNetwork\07_NetworkDev\01_Net
work_FXD
! GEONET - NETWORK FIXED PARAMETER DATA FILE 'NETnn.FXD'
! INPUT FILE FOR SYVAC3-CC409
!      Dimensions of 25 sectors (50 source nodes)
!      200 nodes
!      200 segments
!      10 discharges
!      10 unique glaciation states
! groundwater velocity function indicator []
! 1 = velocity input
! 2 = darcy velocity input
! 3 = hydraulic conductivity and head input and
!   velocity calculated
! 4 = permeability and head input
!   both hydraulic conductivity and
!   velocity calculated from reference water properties
! 5 = permeability and temperature and head input
!   both hydraulic conductivity and
!   velocity calculated from variable water properties
! 6 = permeability and temperature and head input
!   both hydraulic conductivity and
!   velocity calculated from variable water properties
!   with gravitational buoyancy term
3
&! geosphere fixed parameters for segments
&!response function flags []
&!1 =RSMINF, semi-infinite b.c. response function
&!2 =RMSTFR, mass transfer b.c. response function
&!3 =RZROCO, zero concentration b.c. response function
&!4 =pass without change, no response function
&!5 =MULTIC, compartment model mimic a semi-infinite b.c.
&!6 =MULTIC, compartment model mimic a zero concentration b.c.
```

&	1	1	1	1	1	1	4	1	1	1	!10
&	1	1	1	4	4	1	1	4	1	1	!20
&	1	4	4	1	4	1	1	1	1	4	!30
&	4	1	4	4	1	1	4	1	1	1	!40
&	1	1	1	4	4	1	1	1	1	1	!50
&	4	1	1	1	1	1	4	4	1	1	!60
&	1	1	1	1	1	1	4	4	1	1	!70
&	1	1	1	1	1	1	1	1	1	1	!80
&	1	4	1	1	1	1	1	1	1	1	!90
&	4	4	1	1	1	1	1	1	4	1	!100
&	1	1	1	1	1	1	1	1	1	4	!110
&	4	1	1	1	1	4	1	1	1	1	!120
&	1	4	4	1	1	1	1	1	1	1	!130
&	4	1	1	1	1	1	4	4	1	4	!140
&	1	1	1	1	1	4	4	1	1	1	!150
&	1	1	4	1	1	1	1	1	4	1	!160
&	1	1	1	1	1	1	1	1	4	4	!170
&	1	1	1	1	1	1	1	1	1	1	!180
&	1	4	1	1	1	1	1	1	4	1	!190
&	1	1	1	1	1	1	1	1	1	4	!200

&! chemical property class

&	9	10	2	10	2	4	20	9	10	2	!10
&	2	2	2	20	20	2	4	20	9	2	!20
&	4	20	20	2	20	9	2	2	4	20	!30
&	20	2	20	20	2	2	20	9	2	4	!40
&	1	2	2	20	20	2	4	2	2	4	!50
&	20	9	10	2	2	2	20	20	2	4	!60
&	6	9	16	10	2	4	20	20	16	10	!70
&	2	20	9	16	10	2	4	4	5	5	!80
&	5	20	2	4	6	9	16	10	2	4	!90
&	20	20	16	10	2	4	4	2	20	9	!100
&	10	2	10	2	4	2	2	4	2	20	!110
&	20	2	4	2	4	20	9	10	2	2	!120
&	4	20	20	10	2	2	9	2	2	4	!130
&	20	9	2	2	9	10	20	20	2	20	!140
&	9	2	10	2	4	20	20	2	10	2	!150
&	2	3	20	2	9	2	2	10	20	9	!160
&	10	2	9	2	2	9	2	2	20	20	!170
&	9	16	2	9	2	2	3	9	11	2	!180
&	2	20	6	7	8	6	7	8	20	7	!190
&	8	7	8	5	7	8	5	7	8	20	!200

&! physical property class

&	9	10	2	10	2	4	20	9	10	2	!10
&	2	2	2	20	20	2	4	20	9	2	!20
&	4	20	20	2	20	9	2	2	4	20	!30
&	20	2	20	20	2	2	20	9	2	4	!40
&	1	2	2	20	20	2	4	2	2	4	!50
&	20	9	10	2	2	2	20	20	2	4	!60
&	6	9	16	10	2	4	20	20	16	10	!70
&	2	20	9	16	10	2	4	4	5	5	!80
&	5	20	2	4	6	9	16	10	2	4	!90

&	20	20	16	10	2	4	4	2	20	9	!100
&	10	2	10	2	4	2	2	4	2	20	!110
&	20	2	4	2	4	20	9	10	2	2	!120
&	4	20	20	10	2	2	9	2	2	4	!130
&	20	9	2	2	9	10	20	20	2	20	!140
&	9	2	10	2	4	20	20	2	10	2	!150
&	2	3	20	2	9	2	2	10	20	9	!160
&	10	2	9	2	2	9	2	2	20	20	!170
&	9	16	2	9	2	2	3	9	11	2	!180
&	2	20	6	7	8	6	7	8	20	7	!190
&	8	7	8	5	7	8	5	7	8	20	!200

&!node index number for node at inlet of segment

&	1	2	3	4	5	6	7	8	9	10	!10
&	11	12	13	14	10	15	16	17	18	19	!20
&	20	21	19	22	23	24	25	26	27	28	!30
&	26	29	30	25	31	32	33	34	35	36	!40
&	37	38	39	40	35	41	42	43	44	45	!50
&	46	47	48	49	50	51	52	48	53	54	!60
&	55	57	58	59	60	61	62	58	63	64	!70
&	65	66	67	68	69	70	71	72	73	177	!80
&	178	70	75	76	77	79	80	81	82	83	!90
&	84	80	85	86	87	88	89	90	91	92	!100
&	93	94	95	96	97	98	99	100	101	102	!110
&	99	103	104	105	106	107	108	109	110	111	!120
&	112	113	109	114	115	116	117	118	119	120	!130
&	121	122	123	124	125	126	127	123	128	129	!140
&	130	131	132	133	134	135	131	136	137	138	!150
&	139	140	136	142	143	144	145	146	147	148	!160
&	149	150	151	152	153	154	155	156	157	156	!170
&	158	159	160	161	162	163	164	166	167	168	!180
&	169	170	56	171	172	56	174	175	74	78	!190
&	180	141	182	165	184	185	165	187	188	73	!200

&!node index number for node at outlet of segment

&	2	3	4	5	6	7	55	9	10	11	!10
&	12	13	14	55	15	16	17	73	19	20	!20
&	21	73	22	23	55	25	26	27	28	73	!30
&	29	30	73	31	32	33	55	35	36	37	!40
&	38	39	40	73	41	42	43	44	45	46	!50
&	55	48	49	50	51	52	73	53	54	55	!60
&	56	58	59	60	61	62	73	63	64	65	!70
&	66	77	68	69	70	71	72	73	177	178	!80
&	74	75	76	77	78	80	81	82	83	84	!90
&	73	85	86	87	88	89	90	91	77	93	!100
&	94	95	96	97	98	99	100	101	102	71	!110
&	103	104	105	106	107	77	109	110	111	112	!120
&	113	73	114	115	116	117	118	119	120	121	!130
&	77	123	124	125	126	127	133	128	129	139	!140
&	131	132	133	134	135	73	136	137	138	139	!150
&	140	141	142	143	144	145	146	147	53	149	!160
&	150	151	152	153	154	155	156	157	139	73	!170
&	159	160	163	162	163	164	165	167	168	169	!180

```
& 170 163 171 172 173 174 175 176 179 180 !190
& 181 182 183 184 185 186 187 188 189 77 !200
&!unique glaciation states
&! 1 Bora1 !Normal Boreal
&! 2 PrmT1 !Permafrost Talik
&! 3 IceC1 !Icesheet Coldbase
&! 4 PrmT0 !Permafrost No Talik
&! 5 IceW1 !Icesheet Warmbase
&! 6 ProL1 !Proglacial Lake
&! 7 Bora2 !Normal Boreal 2
&! 8 sta08 !state 8
&! 9 sta09 !state 9
&! 10 sta10 !state 10
&!identification of states with impermeable zone and pathway through
&! 0 = no impermeable zone
&! 1 = impermeable zone but no open pathway
&! 2 = impermeable zone with open pathway
& 0 0 0 0 0 0 0 0 0 0 0 !10
&!list of segments in open pathway passing through impermeable zone
& 0 0 0 0 0 0 0 0 0 0 0 !10
& 0 0 0 0 0 0 0 0 0 0 0 !20
& 0 0 0 0 0 0 0 0 0 0 0 !30
& 0 0 0 0 0 0 0 0 0 0 0 !40
& 0 0 0 0 0 0 0 0 0 0 0 !50
& 0 0 0 0 0 0 0 0 0 0 0 !60
& 0 0 0 0 0 0 0 0 0 0 0 !70
& 0 0 0 0 0 0 0 0 0 0 0 !80
& 0 0 0 0 0 0 0 0 0 0 0 !90
& 0 0 0 0 0 0 0 0 0 0 0 !100
& 0 0 0 0 0 0 0 0 0 0 0 !110
& 0 0 0 0 0 0 0 0 0 0 0 !120
& 0 0 0 0 0 0 0 0 0 0 0 !130
& 0 0 0 0 0 0 0 0 0 0 0 !140
& 0 0 0 0 0 0 0 0 0 0 0 !150
& 0 0 0 0 0 0 0 0 0 0 0 !160
& 0 0 0 0 0 0 0 0 0 0 0 !170
& 0 0 0 0 0 0 0 0 0 0 0 !180
& 0 0 0 0 0 0 0 0 0 0 0 !190
& 0 0 0 0 0 0 0 0 0 0 0 !200
&!lists of nodes
&!list of source nodes, last entry zero
& 1 8 18 24 34 47 57 67 79 92 !10
& 108 122 130 148 158 161 166 0 0 0 !20
& 0 0 0 0 0 0 0 0 0 0 !30
& 0 0 0 0 0 0 0 0 0 0 !40
& 0 0 0 0 0 0 0 0 0 0 !50
&!list of vault sector numbers connected to source nodes
& 1 2 3 4 5 6 7 8 9 10 !10
& 11 12 13 14 15 16 17 0 0 0 !20
& 0 0 0 0 0 0 0 0 0 0 !30
& 0 0 0 0 0 0 0 0 0 0 !40
```



&!nodes in well aquifer bounding well position, upper then lower

& 190 73

&!list of biosphere discharge nodes

& 179 173 176 186 189 183 181 0 0 0 !10

&!code number for biosphere discharge

&!1 = AQUA (aquatic discharge)

&!2 = WELL (well discharge)

&!3 = TERR (terrestrial discharge)

&!4 = BOG (swamp or bog discharge)

&!5 = GAS (gaseous discharge)

&!9 = TOTL (a total discharge)

& 2 1 3 1 3 3 3 0 0 0 !10

&!list of nodes for determination of geosphere consequences

& 179 173 176 186 189 183 181 67 0 0 !10

& 0 0 0 0 0 0 0 0 0 0 !20

& 0 0 0 0 0 0 0 0 0 0 !30

& 0 0 0 0 0 0 0 0 0 0 !40

& 0 0 0 0 0 0 0 0 0 0 !50

& 0 0 0 0 0 0 0 0 0 0 !60

& 0 0 0 0 0 0 0 0 0 0 !70

& 0 0 0 0 0 0 0 0 0 0 !80

& 0 0 0 0 0 0 0 0 0 0 !90

& 0 0 0 0 0 0 0 0 0 0 !100

& 0 0 0 0 0 0 0 0 0 0 !110

& 0 0 0 0 0 0 0 0 0 0 !120

& 0 0 0 0 0 0 0 0 0 0 !130

& 0 0 0 0 0 0 0 0 0 0 !140

& 0 0 0 0 0 0 0 0 0 0 !150

& 0 0 0 0 0 0 0 0 0 0 !160

& 0 0 0 0 0 0 0 0 0 0 !170

& 0 0 0 0 0 0 0 0 0 0 !180

& 0 0 0 0 0 0 0 0 0 0 !190

& 0 0 0 0 0 0 0 0 0 0 !200

&!Number of divergent segments affected by well demand

& 0 0 0 0 0 0 0 0 0 2 !10

& 0 0 0 0 0 0 0 0 2 0 !20

& 0 0 0 0 2 2 0 0 0 0 !30

& 0 0 0 0 2 0 0 0 0 0 !40

& 0 0 0 0 0 0 0 2 0 0 !50

& 0 0 0 0 0 0 0 0 0 2 !60

& 0 0 0 0 0 0 0 0 0 2 !70

& 0 0 0 0 0 0 0 0 0 2 !80

& 0 0 0 0 0 0 0 0 0 0 !90

& 0 0 0 0 0 0 0 0 2 0 !100

& 0 0 0 0 0 0 0 0 0 0 !110

& 0 0 2 0 0 0 0 0 0 0 !120

& 2 0 0 0 0 2 0 0 0 0 !130

& 0 0 0 0 0 0 0 0 0 0 !140

& 0 0 0 0 0 2 0 0 0 0 !150

& 0 0 0 0 0 2 0 0 0 0 !160



&	0	0	0	0	0	0	0	0	0	0	!170
&	0	0	0	0	0	0	0	0	0	0	!180
&	0	0	0	0	0	0	0	0	0	0	!190
&	0	0	0	0	0	0	0	0	0	0	!200

**REFERENCES**

Davison, C.C., T. Chan, A. Brown, M. Gascoyne, D. Kamineni, G. Lodha, T. Melnyk, B.W. Nakka, P. O'Connor, D. Ophori, N. Scheier, N. Soonawala, F. Stanchell, D. Stevenson, G. Thorne, T. Vandergraaf, P. Vilks and S. Whitaker. 1994. The disposal of Canada's nuclear fuel waste: The geosphere model for postclosure assessment. Atomic Energy of Canada Limited Report AECL-10719, COG-93-9. Pinawa, Canada.

Kitson, C., T. Melnyk, L. Wojciechowski, and T. Chshyolkova. 2012. SYVAC3-CC4 User Manual. Nuclear Waste Management Organization Technical Report NWMO TR-2012-21. Toronto, Canada.

NWMO (Nuclear Waste Management Organization). 2012a. Used fuel repository conceptual design and postclosure safety assessment in crystalline rock. Nuclear Waste Management Organization Technical Report NWMO TR-2012-16. Toronto, Canada.

NWMO (Nuclear Waste Management Organization). 2012b. SYVAC3-CC4 Theory Manual. Nuclear Waste Management Organization Technical Report NWMO TR-2012-22. Toronto, Canada.



**APPENDIX G: HUMAN INTRUSION MODEL DATA**

Many parameters that are relevant to the human intrusion model have already been discussed earlier in this report. However, for completeness, all parameters values that are included in the human intrusion model are reported in Tables G1 to G-7.

**Table G.1: Parameter values related to used fuel quantities**

<b>Parameter</b>	<b>Value</b>	<b>Comments</b>
Mass of used fuel bundles in a container	8.65×10 <sup>3</sup> kg	Based on data in Table 4.1.
Mass fraction of uranium to used fuel [kgU/kgUF]	0.801	Based on data in Table 4.1.
Mass fraction of Zircaloy to used fuel [kgZr/kgUF]	0.0915	Based on data in Table 4.1.
Fraction of used fuel that is damaged by borehole [-]	0.04	See calculation in Medri (2012)
Fraction of used fuel intercepted brought to surface as core	0.4	Estimated from a typical drill bit of outer and inner diameters of 7.6 cm and 4.8 cm, respectively
Fraction of used fuel intercepted and brought to surface as slurry	0.3	Assumes 30% of intercepted U stays in borehole

**Table G.2: Parameter values related to soil leaching transfer**

<b>Parameter</b>	<b>Value</b>	<b>Comments</b>
Net infiltration rate of water through the soil	0.325 m/a	Average of Canadian Shield locations CSA (2008)
Water content of soil	0.3 m <sup>3</sup> /m <sup>3</sup>	Value for clay from CSA (2008)
Soil bulk density for clay	1400 kg <sub>soil</sub> /m <sup>3</sup>	CSA (2008)
Parameter enabling leaching to begin at time of intrusion	$t \geq t_{leach}$	A Boolean function which returns 1 if true and 0 if false. Default $t_{leach}$ set to 1,000,500 years, such that no leaching occurs until after the last result time in the model. The user may activate leaching by setting an earlier time.

**Table G.3: Parameter values related soil and air concentrations**

Parameter	Value	Comments
Soil area contaminated by slurry for drill crew	30 m <sup>2</sup>	Estimated as a 6m diameter area.
Soil area contaminated by slurry for resident	80 m <sup>2</sup>	Estimated as a 10m diameter area.
Depth of contaminated soil for drill crew	0.2 m	CSA (2008)
Depth of contaminated soil for resident	0.2 m	CSA (2008)
Atmospheric dust loading for drill crew	1×10 <sup>-7</sup> kg <sub>soil</sub> /m <sup>3</sup>	Wuschke (1996)
Atmospheric dust loading for resident	3.2×10 <sup>-8</sup> kg <sub>soil</sub> /m <sup>3</sup>	See Table 8.3

Table G.4 presents the data used in the dose equations for the Human Intrusion Scenario.

**Table G.4: Parameter values related to dose calculations**

Parameter	Value	Reference
Human inhalation rate	8400 m <sup>3</sup> /a	CSA (2008)
Exposure time of drill crew to core sample	1.00 h	Estimated time to retrieve and log core barrel.
Exposure time for drill crew to contaminated site	168 h	12 hours per day for 14 days
Annual exposure time for resident	0.1 a	Gierszewski et al. (2004) (resident spends 10% of year near contaminated soil)
Annual soil ingestion amount (resident)	0.12 kg <sub>soil</sub>	CSA (2008)
Annual plant ingestion amount (resident)	291 kg <sub>plant</sub>	CSA (2008), Table G.9a. Includes all plants ingested by adults with the exception of dulse and honey.
Soil Ingestion amount per intrusion event (drill crew)	4.62×10 <sup>-3</sup> kg <sub>soil</sub>	CSA (2008) (0.33g/d for 14 days)
Contaminated soil fraction	0.1	Based on a total farmland of 1100 m <sup>2</sup> # required to support a family of 3 and on the contaminated soil area (Table G.3.
Contaminated food fraction	0.1	

#Calculated from the annual plant ingestion amount and a plant yield of 0.8 kg/m<sup>2</sup> (see Table 8.7).

The ingestion, inhalation and groundshine dose coefficients used in the safety assessment of the Fourth Case Study Normal Evolution Scenario are shown in Table 9.12. However, not all radionuclides of importance to the Human Intrusion Scenario are present in this table.

Table G.5 lists the dose coefficients used in the human intrusion calculations. The sources of these dose coefficient data are the same as for the data in Table 9.13.

**Table G.5: Human dose coefficients**

Radionuclide	Ingestion Dose Coefficient [Sv/Bq]	Inhalation Dose Coefficient [Sv/Bq]	Groundshine Dose Coefficient [(Sv/a)/(Bq/kg)]	External (Point Source) Dose Coefficient [(Sv/a)/Bq]
<b>Ac-225</b>	$2.43 \times 10^{-8}$	$8.53 \times 10^{-6}$	$3.20 \times 10^{-7}$	$3.05 \times 10^{-10}$
<b>Ac-227</b>	$1.10 \times 10^{-6}$	$5.50 \times 10^{-4}$	$7.97 \times 10^{-10}$	$1.05 \times 10^{-12}$
<b>Ag-108m</b>	$2.30 \times 10^{-9}$	$3.70 \times 10^{-8}$	$2.44 \times 10^{-6}$	$1.98 \times 10^{-9}$
<b>Am-241</b>	$2.00 \times 10^{-7}$	$9.60 \times 10^{-5}$	$1.00 \times 10^{-8}$	$3.40 \times 10^{-11}$
<b>Am-242m</b>	$1.90 \times 10^{-7}$	$9.20 \times 10^{-5}$	$1.24 \times 10^{-8}$	$1.60 \times 10^{-11}$
<b>Am-243</b>	$2.00 \times 10^{-7}$	$9.60 \times 10^{-5}$	$3.36 \times 10^{-8}$	$7.79 \times 10^{-11}$
<b>Ar-39</b>	$0.00 \times 10^0$	$0.00 \times 10^0$	$2.17 \times 10^{-10}$	$1.31 \times 10^{-13*}$
<b>Ba-133</b>	$1.50 \times 10^{-9}$	$1.00 \times 10^{-8}$	$4.92 \times 10^{-7}$	$4.67 \times 10^{-10}$
<b>Bi-208</b>	$1.40 \times 10^{-9}$	$6.20 \times 10^{-9}$	$5.60 \times 10^{-6}$	$3.24 \times 10^{-9}$
<b>C-14</b>	$5.80 \times 10^{-10}$	$5.80 \times 10^{-9}$	$2.97 \times 10^{-12}$	$2.28 \times 10^{-15*}$
<b>Ca-41</b>	$1.90 \times 10^{-10}$	$1.80 \times 10^{-10}$	$0.00 \times 10^0$	$1.33 \times 10^{-14*}$
<b>Cd-113m</b>	$2.30 \times 10^{-8}$	$1.10 \times 10^{-7}$	$1.63 \times 10^{-10}$	$1.87 \times 10^{-13}$
<b>Cl-36</b>	$9.30 \times 10^{-10}$	$7.30 \times 10^{-9}$	$6.72 \times 10^{-10}$	$7.42 \times 10^{-14*}$
<b>Cm-242</b>	$1.20 \times 10^{-8}$	$5.90 \times 10^{-6}$	$3.47 \times 10^{-11}$	$2.22 \times 10^{-14}$
<b>Cm-243</b>	$1.50 \times 10^{-7}$	$6.90 \times 10^{-5}$	$1.44 \times 10^{-7}$	$2.70 \times 10^{-10}$
<b>Cm-244</b>	$1.20 \times 10^{-7}$	$5.70 \times 10^{-5}$	$2.42 \times 10^{-11}$	$3.04 \times 10^{-14}$
<b>Cm-245</b>	$2.10 \times 10^{-7}$	$9.90 \times 10^{-5}$	$8.28 \times 10^{-8}$	$1.83 \times 10^{-10}$
<b>Cm-246</b>	$2.10 \times 10^{-7}$	$9.80 \times 10^{-5}$	$2.24 \times 10^{-11}$	$4.44 \times 10^{-12}$
<b>Co-60</b>	$3.40 \times 10^{-9}$	$3.10 \times 10^{-8}$	$4.17 \times 10^{-6}$	$3.07 \times 10^{-9}$
<b>Cs-134</b>	$1.90 \times 10^{-8}$	$2.00 \times 10^{-8}$	$2.41 \times 10^{-6}$	$1.92 \times 10^{-9}$
<b>Cs-135</b>	$2.00 \times 10^{-9}$	$8.60 \times 10^{-9}$	$8.68 \times 10^{-12}$	$2.00 \times 10^{-9}$
<b>Cs-137</b>	$1.30 \times 10^{-8}$	$3.90 \times 10^{-8}$	$8.65 \times 10^{-7}$	$7.65 \times 10^{-10}$
<b>Eu-152</b>	$1.40 \times 10^{-9}$	$4.20 \times 10^{-8}$	$1.79 \times 10^{-6}$	$1.43 \times 10^{-9}$
<b>Eu-154</b>	$2.00 \times 10^{-9}$	$5.30 \times 10^{-8}$	$1.96 \times 10^{-6}$	$1.56 \times 10^{-9}$
<b>Eu-155</b>	$3.20 \times 10^{-10}$	$6.90 \times 10^{-9}$	$4.37 \times 10^{-8}$	$7.76 \times 10^{-11}$
<b>Fe-55</b>	$3.30 \times 10^{-10}$	$7.70 \times 10^{-10}$	$0.00 \times 10^0$	$3.02 \times 10^{-15*}$
<b>H-3</b>	$1.80 \times 10^{-11}$	$3.60 \times 10^{-11}$	$0.00 \times 10^0$	$0.00 \times 10^0$
<b>Ho-163</b>	$1.20 \times 10^{-6}$	$5.50 \times 10^{-4}$	$6.06 \times 10^{-6}$	$0.00 \times 10^0$
<b>Ho-166m</b>	$2.00 \times 10^{-9}$	$1.20 \times 10^{-7}$	$2.61 \times 10^{-6}$	$2.08 \times 10^{-9}$
<b>I-129</b>	$1.10 \times 10^{-7}$	$3.60 \times 10^{-8}$	$2.58 \times 10^{-9}$	$1.56 \times 10^{-15*}$
<b>Ir-192</b>	$1.40 \times 10^{-9}$	$6.60 \times 10^{-9}$	$1.16 \times 10^{-6}$	$1.05 \times 10^{-9}$
<b>Ir-192m</b>	$3.10 \times 10^{-10}$	$3.90 \times 10^{-8}$	$1.86 \times 10^{-7}$	$1.85 \times 10^{-11}$

Radionuclide	Ingestion Dose Coefficient [Sv/Bq]	Inhalation Dose Coefficient [Sv/Bq]	Groundshine Dose Coefficient [(Sv/a)/(Bq/kg)]	External (Point Source) Dose Coefficient [(Sv/a)/Bq]
Kr- 85	0.00×10 <sup>0</sup>	0.00×10 <sup>0</sup>	3.65×10 <sup>-9</sup>	2.74×10 <sup>-12</sup>
Mo-93	3.10×10 <sup>-9</sup>	2.30×10 <sup>-9</sup>	1.13×10 <sup>-10</sup>	8.11×10 <sup>-15</sup>
Nb-91	1.20×10 <sup>-6</sup>	5.50×10 <sup>-4</sup>	6.06×10 <sup>-6</sup>	8.52×10 <sup>-15</sup>
Nb-93m	1.20×10 <sup>-10</sup>	1.80×10 <sup>-9</sup>	1.99×10 <sup>-11</sup>	0.00×10 <sup>0</sup>
Nb- 94	1.70×10 <sup>-9</sup>	4.90×10 <sup>-8</sup>	2.46×10 <sup>-6</sup>	1.92×10 <sup>-9</sup>
Ni-59	6.30×10 <sup>-11</sup>	4.40×10 <sup>-10</sup>	0.00×10 <sup>0</sup>	1.90×10 <sup>-14</sup>
Ni-63	1.50×10 <sup>-10</sup>	1.30×10 <sup>-9</sup>	0.00×10 <sup>0</sup>	8.84×10 <sup>-18</sup> *
Np-237	1.10×10 <sup>-7</sup>	5.00×10 <sup>-5</sup>	1.88×10 <sup>-8</sup>	5.61×10 <sup>-11</sup>
Np-238	9.10×10 <sup>-10</sup>	3.50×10 <sup>-9</sup>	8.79×10 <sup>-7</sup>	7.19×10 <sup>-10</sup>
Np-239	8.00×10 <sup>-10</sup>	1.00×10 <sup>-9</sup>	1.86×10 <sup>-7</sup>	2.34×10 <sup>-10</sup>
Os-194	3.70×10 <sup>-9</sup>	8.56×10 <sup>-8</sup>	1.42×10 <sup>-7</sup>	1.12×10 <sup>-10</sup>
Pa-231	7.10×10 <sup>-7</sup>	1.40×10 <sup>-4</sup>	4.77×10 <sup>-8</sup>	5.14×10 <sup>-11</sup>
Pa-233	8.70×10 <sup>-10</sup>	3.90×10 <sup>-9</sup>	2.54×10 <sup>-7</sup>	4.16×10 <sup>-10</sup>
Pb-210	6.90×10 <sup>-7</sup>	5.60×10 <sup>-6</sup>	5.35×10 <sup>-10</sup>	1.04×10 <sup>-18</sup> *
Pd-107	3.70×10 <sup>-11</sup>	5.90×10 <sup>-10</sup>	0.00×10 <sup>0</sup>	0.00×10 <sup>0</sup>
Pm-146	9.00×10 <sup>-10</sup>	2.10×10 <sup>-8</sup>	1.12×10 <sup>-6</sup>	9.04×10 <sup>-10</sup>
Pm-145	1.10×10 <sup>-10</sup>	3.60×10 <sup>-9</sup>	6.26×10 <sup>-9</sup>	5.60×10 <sup>-12</sup>
Pm-147	2.60×10 <sup>-10</sup>	5.00×10 <sup>-9</sup>	1.16×10 <sup>-11</sup>	4.23×10 <sup>-15</sup>
Po-210	1.20×10 <sup>-6</sup>	4.30×10 <sup>-6</sup>	1.33×10 <sup>-11</sup>	1.20×10 <sup>-14</sup>
Pt-193	3.10×10 <sup>-11</sup>	2.10×10 <sup>-11</sup>	1.71×10 <sup>-12</sup>	0.00×10 <sup>0</sup>
Pu-236	8.70×10 <sup>-8</sup>	4.00×10 <sup>-5</sup>	4.90×10 <sup>-11</sup>	1.29×10 <sup>-13</sup>
Pu-238	2.30×10 <sup>-7</sup>	1.10×10 <sup>-4</sup>	3.15×10 <sup>-11</sup>	1.03×10 <sup>-13</sup>
Pu-239	2.50×10 <sup>-7</sup>	1.20×10 <sup>-4</sup>	7.12×10 <sup>-11</sup>	4.55×10 <sup>-13</sup>
Pu-240	2.50×10 <sup>-7</sup>	1.20×10 <sup>-4</sup>	3.04×10 <sup>-11</sup>	8.80×10 <sup>-14</sup>
Pu-241	4.80×10 <sup>-9</sup>	2.30×10 <sup>-6</sup>	1.43×10 <sup>-12</sup>	1.86×10 <sup>-15</sup>
Pu-242	2.40×10 <sup>-7</sup>	1.10×10 <sup>-4</sup>	2.68×10 <sup>-11</sup>	1.12×10 <sup>-13</sup>
Ra-223	1.00×10 <sup>-7</sup>	8.71×10 <sup>-6</sup>	3.76×10 <sup>-7</sup>	4.67×10 <sup>-10</sup>
Ra-224	7.13×10 <sup>-8</sup>	3.62×10 <sup>-6</sup>	2.62×10 <sup>-6</sup>	1.89×10 <sup>-9</sup>
Ra-225	9.90×10 <sup>-8</sup>	7.70×10 <sup>-6</sup>	2.33×10 <sup>-9</sup>	8.37×10 <sup>-14</sup> *
Ra-226	2.80×10 <sup>-7</sup>	9.50×10 <sup>-6</sup>	7.88×10 <sup>-9</sup>	1.34×10 <sup>-11</sup>
Ra-228	6.90×10 <sup>-7</sup>	1.60×10 <sup>-5</sup>	1.53×10 <sup>-6</sup>	1.04×10 <sup>-9</sup>
Rh-102	2.60×10 <sup>-9</sup>	1.70×10 <sup>-8</sup>	3.29×10 <sup>-6</sup>	6.08×10 <sup>-10</sup>
Rn-222	2.50×10 <sup>-10</sup>	3.50×10 <sup>-9</sup>	2.86×10 <sup>-6</sup>	2.16×10 <sup>-9</sup>
Ru-106	7.00×10 <sup>-9</sup>	6.60×10 <sup>-8</sup>	3.37×10 <sup>-7</sup>	2.49×10 <sup>-10</sup>
Sb-125	1.10×10 <sup>-9</sup>	1.20×10 <sup>-8</sup>	6.16×10 <sup>-7</sup>	5.22×10 <sup>-10</sup>
Sb-126	2.40×10 <sup>-9</sup>	3.20×10 <sup>-9</sup>	4.34×10 <sup>-6</sup>	3.39×10 <sup>-9</sup>
Se-79	2.90×10 <sup>-9</sup>	6.80×10 <sup>-9</sup>	4.14×10 <sup>-12</sup>	1.09×10 <sup>-13</sup> *
Sm-147	4.90×10 <sup>-8</sup>	9.60×10 <sup>-6</sup>	0.00×10 <sup>0</sup>	0.00×10 <sup>0</sup>

Radionuclide	Ingestion Dose Coefficient [Sv/Bq]	Inhalation Dose Coefficient [Sv/Bq]	Groundshine Dose Coefficient [(Sv/a)/(Bq/kg)]	External (Point Source) Dose Coefficient [(Sv/a)/Bq]
<b>Sm-151</b>	$9.80 \times 10^{-11}$	$4.00 \times 10^{-9}$	$1.83 \times 10^{-13}$	$3.93 \times 10^{-14}$ *
<b>Sn-121</b>	$2.30 \times 10^{-10}$	$2.30 \times 10^{-10}$	$4.63 \times 10^{-11}$	$3.27 \times 10^{-14}$ *
<b>Sn-121m</b>	$3.80 \times 10^{-10}$	$4.50 \times 10^{-9}$	$3.87 \times 10^{-10}$	$3.32 \times 10^{-14}$ *
<b>Sn-126</b>	$4.74 \times 10^{-9}$	$2.80 \times 10^{-8}$	$2.39 \times 10^{-6}$	$1.99 \times 10^{-9}$
<b>Sr-90</b>	$2.80 \times 10^{-8}$	$1.60 \times 10^{-7}$	$1.75 \times 10^{-10}$	$1.09 \times 10^{-13}$ *
<b>Ta-182</b>	$1.50 \times 10^{-9}$	$1.00 \times 10^{-8}$	$2.03 \times 10^{-6}$	$1.65 \times 10^{-9}$
<b>Tc-99</b>	$6.40 \times 10^{-10}$	$1.30 \times 10^{-8}$	$2.93 \times 10^{-11}$	$7.14 \times 10^{-16}$
<b>Te-125m</b>	$8.70 \times 10^{-10}$	$4.20 \times 10^{-9}$	$3.00 \times 10^{-9}$	$1.12 \times 10^{-10}$
<b>Th-227</b>	$8.80 \times 10^{-9}$	$1.00 \times 10^{-5}$	$1.30 \times 10^{-7}$	$1.71 \times 10^{-10}$
<b>Th-228</b>	$7.20 \times 10^{-8}$	$4.00 \times 10^{-5}$	$1.94 \times 10^{-9}$	$2.57 \times 10^{-11}$
<b>Th-229</b>	$4.90 \times 10^{-7}$	$2.40 \times 10^{-4}$	$7.83 \times 10^{-8}$	$1.78 \times 10^{-10}$
<b>Th-230</b>	$2.10 \times 10^{-7}$	$1.00 \times 10^{-4}$	$2.89 \times 10^{-10}$	$1.01 \times 10^{-11}$
<b>Th-231</b>	$3.40 \times 10^{-10}$	$3.30 \times 10^{-10}$	$8.68 \times 10^{-9}$	$5.00 \times 10^{-11}$
<b>Th-232</b>	$2.30 \times 10^{-7}$	$1.10 \times 10^{-4}$	$1.23 \times 10^{-10}$	$4.61 \times 10^{-12}$
<b>Th-234</b>	$3.40 \times 10^{-9}$	$7.70 \times 10^{-9}$	$4.21 \times 10^{-8}$	$4.83 \times 10^{-11}$
<b>Tl-204</b>	$1.20 \times 10^{-9}$	$3.90 \times 10^{-10}$	$1.05 \times 10^{-9}$	$1.44 \times 10^{-12}$
<b>Tm-171</b>	$1.10 \times 10^{-10}$	$1.40 \times 10^{-9}$	$2.54 \times 10^{-10}$	$1.36 \times 10^{-12}$
<b>U -232</b>	$3.30 \times 10^{-7}$	$3.70 \times 10^{-5}$	$2.14 \times 10^{-10}$	$6.30 \times 10^{-12}$
<b>U -233</b>	$5.10 \times 10^{-8}$	$9.60 \times 10^{-6}$	$3.42 \times 10^{-10}$	$8.05 \times 10^{-13}$
<b>U-234</b>	$4.90 \times 10^{-8}$	$9.40 \times 10^{-6}$	$9.29 \times 10^{-11}$	$1.69 \times 10^{-12}$
<b>U-235</b>	$4.70 \times 10^{-8}$	$8.50 \times 10^{-6}$	$1.78 \times 10^{-7}$	$2.17 \times 10^{-10}$
<b>U-236</b>	$4.70 \times 10^{-8}$	$8.70 \times 10^{-6}$	$4.80 \times 10^{-11}$	$1.65 \times 10^{-13}$
<b>U-237</b>	$7.60 \times 10^{-10}$	$1.90 \times 10^{-9}$	$1.30 \times 10^{-7}$	$2.66 \times 10^{-10}$
<b>U-238</b>	$4.50 \times 10^{-8}$	$8.00 \times 10^{-6}$	$2.15 \times 10^{-11}$	$9.60 \times 10^{-14}$
<b>Y -90</b>	$2.70 \times 10^{-9}$	$1.50 \times 10^{-9}$	$1.09 \times 10^{-8}$	$3.76 \times 10^{-17}$
<b>Zr-93</b>	$1.10 \times 10^{-9}$	$2.50 \times 10^{-8}$	$0.00 \times 10^0$	$0.00 \times 10^0$

\*Low intensity Internal Bremsstrahlung emissions from Browne and Firestone (1986)

The external (point source) dose coefficients in Table G.5 were calculated from the mean gamma energies per decay, which are from ICRP 107 (ICRP 2008). Dose coefficients for objects a distance of 1 m away from the point source are obtained by multiplying the mean gamma energy in MeV by the factor  $1.4 \times 10^{13}$  (Sv/h)/(Bq/MeV) (Smith et al. 1988).

Photons with individual energies below 50 keV were not included because the equation used to calculate the dose coefficient for a point source substantially over-estimates doses for energies below this value. Where ICRP 107 does not record having photon energies above 50 keV, low intensity Internal Bremsstrahlung (IB) emissions from Browne and Firestone (1986) were used, as indicated in Table G.5. ICRP does not account for IB emissions.

The used fuel radionuclide inventories 30 years after removal from the reactor shown in Table G.6 were obtained from Tait and Hanna (2001).

The radionuclide half-lives and branching ratios in Table G.7 were taken from the ENDF/B-CII.1 Library (Chadwick et al. 2011). To account for decay branches in AMBER, the parent nuclide is assigned an effective half-life for each branch (Quintessa 2009). The effective half-life of the parent in a decay branch is equal to the actual half-life of the parent nuclide divided by the branching ratio. In this way, the total decay rate of the parent is properly modelled.

**Table G-6: Radionuclide inventories**

<b>Radionuclide</b>	<b>Uranium Inventory [mol/kgU]</b>	<b>Zircaloy Inventory [mol/kgZr]</b>
<b>Ac-225</b>	$1.66 \times 10^{-14}$	-*
<b>Ac-227</b>	$1.57 \times 10^{-11\#}$	-
<b>Ag-108m</b>	$3.06 \times 10^{-8}$	$3.03 \times 10^{-7}$
<b>Am-241</b>	$8.81 \times 10^{-4}$	-
<b>Am-242m</b>	$1.81 \times 10^{-7}$	-
<b>Am-243</b>	$2.34 \times 10^{-5}$	-
<b>Ar-39</b>	$6.28 \times 10^{-8}$	$3.139 \times 10^{-9}$
<b>Ba-133</b>	$1.91 \times 10^{-9}$	$1.90 \times 10^{-12}$
<b>Bi-208</b>	$3.28 \times 10^{-10}$	$1.685 \times 10^{-11}$
<b>C-14</b>	$8.75 \times 10^{-6}$	$2.18 \times 10^{-6}$
<b>Ca-41</b>	$2.35 \times 10^{-6}$	$4.671 \times 10^{-8}$
<b>Cd-113m</b>	$7.09 \times 10^{-8}$	$7.89 \times 10^{-10}$
<b>Cl-36</b>	$9.86 \times 10^{-6}$	$1.34 \times 10^{-6}$
<b>Cm-242</b>	$4.70 \times 10^{-10}$	-
<b>Cm-243</b>	$2.44 \times 10^{-8}$	-
<b>Cm-244</b>	$6.66 \times 10^{-7}$	-
<b>Cm-245</b>	$1.43 \times 10^{-8}$	-
<b>Cm-246</b>	$1.93 \times 10^{-9}$	-
<b>Co-60</b>	$5.33 \times 10^{-7}$	$5.30 \times 10^{-7}$
<b>Cs-134</b>	$4.50 \times 10^{-9}$	$2.20 \times 10^{-11}$
<b>Cs-135</b>	$2.68 \times 10^{-4}$	$9.85 \times 10^{-8}$
<b>Cs-137</b>	$1.29 \times 10^{-03}$	$1.89 \times 10^{-13}$
<b>Eu-152</b>	$8.39 \times 10^{-10}$	$7.63 \times 10^{-14}$
<b>Eu-154</b>	$1.83 \times 10^{-6}$	$5.43 \times 10^{-9}$
<b>Eu-155</b>	$1.20 \times 10^{-7}$	$2.65 \times 10^{-10}$
<b>Fe-55</b>	$5.82 \times 10^{-10}$	$5.54 \times 10^{-9}$
<b>H-3</b>	$2.67 \times 10^{-6}$	$2.46 \times 10^{-7}$
<b>Ho-163</b>	$4.05 \times 10^{-10}$	$1.34 \times 10^{-10}$
<b>Ho-166m</b>	$2.13 \times 10^{-8}$	$7.00 \times 10^{-9}$
<b>I-129</b>	$4.23 \times 10^{-4}$	$2.55 \times 10^{-9}$
<b>Ir-192</b>	$5.93 \times 10^{-13}$	$5.93 \times 10^{-13}$
<b>Ir-192m</b>	$7.06 \times 10^{-10}$	$7.05 \times 10^{-10}$



Radionuclide	Uranium Inventory [mol/kgU]	Zircaloy Inventory [mol/kgZr]
Kr- 85	$1.07 \times 10^{-5}$	$8.06 \times 10^{-15}$
Mo-93	$2.99 \times 10^{-9}$	$1.86 \times 10^{-8}$
Nb-91	$1.56 \times 10^{-13}$	$1.51 \times 10^{-12}$
Nb-93m	$1.28 \times 10^{-8}$	$3.29 \times 10^{-8}$
Nb- 94	$4.85 \times 10^{-7}$	$4.80 \times 10^{-6}$
Ni-59	$6.44 \times 10^{-6}$	$7.46 \times 10^{-6}$
Ni-63	$9.33 \times 10^{-7}$	$1.08 \times 10^{-6}$
Np-237	$1.71 \times 10^{-4}$	-
Np-238	$3.34 \times 10^{-14}$	-
Np-239	$2.05 \times 10^{-11}$	-
Os-194	$5.78 \times 10^{-12}$	$5.69 \times 10^{-12}$
Pa-231	$3.82 \times 10^{-8\#}$	-
Pa-233	$5.90 \times 10^{-12}$	-
Pb-210	$8.60 \times 10^{-15}$	-
Pd-107	$6.90 \times 10^{-4}$	$6.22 \times 10^{-8}$
Pm-145	$5.92 \times 10^{-11}$	$9.10 \times 10^{-12}$
Pm-146	$6.81 \times 10^{-11}$	-
Pm-147	$2.08 \times 10^{-7}$	$1.09 \times 10^{-13}$
Po-210	$1.46 \times 10^{-16}$	-
Pt-193	$2.25 \times 10^{-8}$	$2.23 \times 10^{-8}$
Pu-236	$2.99 \times 10^{-14}$	-
Pu-238	$2.26 \times 10^{-5}$	-
Pu-239	$1.12 \times 10^{-2}$	-
Pu-240	$5.34 \times 10^{-3}$	-
Pu-241	$2.74 \times 10^{-4}$	-
Pu-242	$4.26 \times 10^{-4\#}$	-
Ra-223	$2.24 \times 10^{-14}$	-
Ra-224	$1.10 \times 10^{-12}$	-
Ra-225	$2.46 \times 10^{-14}$	-
Ra-226	$2.35 \times 10^{-12}$	-
Ra-228	$8.37 \times 10^{-13}$	-
Rh-102	$5.17 \times 10^{-14}$	$1.20 \times 10^{-15}$
Rn-222	$1.54 \times 10^{-17}$	-
Ru-106	$9.52 \times 10^{-13}$	$3.00 \times 10^{-23}$
Sb-125	$1.16 \times 10^{-8}$	$4.65 \times 10^{-9}$
Sb-126	$2.46 \times 10^{-12}$	-
Se-79	$1.76 \times 10^{-5}$	$5.16 \times 10^{-9}$
Sm-147	$6.55 \times 10^{-4}$	$8.00 \times 10^{-8}$
Sm-151	$1.46 \times 10^{-5}$	$1.00 \times 10^{-9}$
Sn-121	$3.69 \times 10^{-12}$	$5.73 \times 10^{-12}$

Radionuclide	Uranium Inventory [mol/kgU]	Zircaloy Inventory [mol/kgZr]
<b>Sn-121m</b>	$8.47 \times 10^{-8}$	$1.32 \times 10^{-7}$
<b>Sn-126</b>	$5.18 \times 10^{-5}$	-
<b>Sr-90</b>	$7.56 \times 10^{-4}$	$4.78 \times 10^{-11}$
<b>Ta-182</b>	$3.21 \times 10^{-16}$	$3.16 \times 10^{-15}$
<b>Tc-99</b>	$2.41 \times 10^{-3}$	$2.27 \times 10^{-8}$
<b>Te-125m</b>	$1.64 \times 10^{-10}$	$6.60 \times 10^{-11}$
<b>Th-227</b>	$3.62 \times 10^{-14}$	-
<b>Th-228</b>	$2.10 \times 10^{-10}$	-
<b>Th-229</b>	$4.78 \times 10^{-9}$	-
<b>Th-230</b>	$1.64 \times 10^{-8}$	-
<b>Th-231</b>	$2.94 \times 10^{-14}$	-
<b>Th-232</b>	$2.10 \times 10^{-3}$	-
<b>Th-234</b>	$6.09 \times 10^{-11}$	-
<b>Tl-204</b>	$1.79 \times 10^{-10}$	$1.77 \times 10^{-11}$
<b>Tm-171</b>	$1.45 \times 10^{-12}$	$4.77 \times 10^{-13}$
<b>U -232</b>	$7.43 \times 10^{-9}$	-
<b>U -233</b>	$3.61 \times 10^{-5}$	-
<b>U-234</b>	$1.86 \times 10^{-4}$	-
<b>U-235</b>	$7.24 \times 10^{-3\#}$	-
<b>U-236</b>	$3.50 \times 10^{-3}$	-
<b>U-237</b>	$8.44 \times 10^{-12}$	-
<b>U-238</b>	$4.13 \times 10^0$	-
<b>Y -90</b>	$1.97 \times 10^{-7}$	$1.24 \times 10^{-14}$
<b>Zr-93</b>	$1.37 \times 10^{-3}$	$1.40 \times 10^{-3}$

<sup>#</sup>Median value from Tait et al. (2000) increased to account for "ring sum" correction: Ac-227 (1%), Pa-231 (1.2%), Pu-242 (1.9%) and U-235 (1.7%) (Appendix B, Tait et al. 2000)

\*A dash (-) indicates that the inventory is zero.

**Table G.7: Radionuclide half-lives and branching ratios**

<b>Nuclide</b>	<b>Daughter*</b>	<b>Half-Life [a]</b>	<b>Branching Ratio</b>	<b>Effective Half-Life [a]</b>
<b>Ac-225</b>	<i>Null</i> <sup>#</sup>	2.738×10 <sup>-2</sup>	1	2.738×10 <sup>-2</sup>
<b>Ac-227</b>	Th227	2.177×10 <sup>1</sup>	0.9862	2.208×10 <sup>1</sup>
<b>Ag-108m</b>	<i>Null</i>	4.180×10 <sup>2</sup>	1	4.180×10 <sup>2</sup>
<b>Am-241</b>	Np237	4.380×10 <sup>2</sup>	1	4.380×10 <sup>2</sup>
<b>Am-242m</b>	Cm242	1.410×10 <sup>2</sup>	0.8230	1.713×10 <sup>2</sup>
<b>Am-242m</b>	Pu242	1.410×10 <sup>2</sup>	0.1720	8.198×10 <sup>2</sup>
<b>Am-242m</b>	Np238	1.410×10 <sup>2</sup>	0.0045	3.133×10 <sup>4</sup>
<b>Am-243</b>	Np239	7.370×10 <sup>3</sup>	1	7.370×10 <sup>3</sup>
<b>Ar-93</b>	<i>Null</i>	2.690×10 <sup>2</sup>	1	2.690×10 <sup>2</sup>
<b>Ba-133</b>	<i>Null</i>	1.052×10 <sup>1</sup>	1	1.052×10 <sup>1</sup>
<b>Bi-208</b>	<i>Null</i>	3.680×10 <sup>5</sup>	1	3.680×10 <sup>5</sup>
<b>C-14</b>	<i>Null</i>	5.700×10 <sup>3</sup>	1	5.700×10 <sup>3</sup>
<b>Ca-41</b>	<i>Null</i>	1.020×10 <sup>5</sup>	1	1.020×10 <sup>5</sup>
<b>Cd-133m</b>	<i>Null</i>	1.410×10 <sup>1</sup>	1	1.410×10 <sup>1</sup>
<b>Cl-36</b>	<i>Null</i>	3.010×10 <sup>5</sup>	1	3.010×10 <sup>5</sup>
<b>Cm-242</b>	Pu238	4.461×10 <sup>-1</sup>	1	4.461×10 <sup>-1</sup>
<b>Cm-243</b>	Am243	2.910×10 <sup>1</sup>	0.0024	1.213×10 <sup>4</sup>
<b>Cm-243</b>	Pu239	2.910×10 <sup>1</sup>	0.9976	2.917×10 <sup>1</sup>
<b>Cm-244</b>	Pu240	1.811×10 <sup>1</sup>	1	1.811×10 <sup>1</sup>
<b>Cm-245</b>	Pu241	8.500×10 <sup>3</sup>	1	8.500×10 <sup>3</sup>
<b>Cm-246</b>	Pu-242	4.730×10 <sup>3</sup>	1	4.730×10 <sup>3</sup>
<b>Co-60</b>	<i>Null</i>	5.271×10 <sup>0</sup>	1	5.271×10 <sup>0</sup>
<b>Cs-134</b>	<i>Null</i>	2.065×10 <sup>0</sup>	1	2.065×10 <sup>0</sup>
<b>Cs-135</b>	<i>Null</i>	2.300×10 <sup>6</sup>	1	2.300×10 <sup>6</sup>
<b>Cs-137</b>	<i>Null</i>	3.008×10 <sup>1</sup>	1	3.008×10 <sup>1</sup>
<b>Eu-152</b>	<i>Null</i>	1.354×10 <sup>1</sup>	1	1.354×10 <sup>1</sup>
<b>Eu-154</b>	<i>Null</i>	8.601×10 <sup>0</sup>	1	8.601×10 <sup>0</sup>
<b>Eu-155</b>	<i>Null</i>	4.753×10 <sup>0</sup>	1	4.753×10 <sup>0</sup>
<b>Fe-55</b>	<i>Null</i>	2.700×10 <sup>0</sup>	1	2.700×10 <sup>0</sup>
<b>H-3</b>	<i>Null</i>	1.240×10 <sup>1</sup>	1	1.240×10 <sup>1</sup>
<b>Ho-163</b>	<i>Null</i>	4.570×10 <sup>3</sup>	1	4.570×10 <sup>3</sup>
<b>Ho-166m</b>	<i>Null</i>	1.200×10 <sup>3</sup>	1	1.200×10 <sup>3</sup>
<b>I-129</b>	<i>Null</i>	1.570×10 <sup>7</sup>	1	1.570×10 <sup>7</sup>
<b>Ir-192</b>	<i>Null</i>	2.021×10 <sup>-1</sup>	1	2.021×10 <sup>-1</sup>
<b>Ir-192m</b>	Ir192	2.410×10 <sup>2</sup>	1	2.410×10 <sup>2</sup>
<b>Kr-85</b>	<i>Null</i>	1.076×10 <sup>1</sup>	1	1.076×10 <sup>1</sup>
<b>Mo-93</b>	Nb-93m	3.500×10 <sup>3</sup>	1	3.500×10 <sup>3</sup>
<b>Nb-91</b>	<i>Null</i>	7.000×10 <sup>2</sup>	1	7.000×10 <sup>2</sup>
<b>Nb-93m</b>	<i>Null</i>	1.360×10 <sup>1</sup>	1	1.360×10 <sup>1</sup>
<b>Nb-94</b>	<i>Null</i>	2.030×10 <sup>4</sup>	1	2.030×10 <sup>4</sup>

<b>Nuclide</b>	<b>Daughter*</b>	<b>Half-Life [a]</b>	<b>Branching Ratio</b>	<b>Effective Half-Life [a]</b>
<b>Ni-63</b>	<i>Null</i>	1.012×10 <sup>2</sup>	1	1.012×10 <sup>2</sup>
<b>Ni-59</b>	<i>Null</i>	7.600×10 <sup>4</sup>	1	7.600×10 <sup>4</sup>
<b>Np-237</b>	Pa233	2.144×10 <sup>6</sup>	1	2.144×10 <sup>6</sup>
<b>Np-238</b>	Pu238	5.796×10 <sup>-3</sup>	1	5.796×10 <sup>-3</sup>
<b>Np-239</b>	Pu239	6.450×10 <sup>-3</sup>	1	6.450×10 <sup>-3</sup>
<b>Os-194</b>	<i>Null</i>	6.000×10 <sup>0</sup>	1	6.000×10 <sup>0</sup>
<b>Pa-231</b>	Ac227	3.276×10 <sup>4</sup>	1	3.276×10 <sup>4</sup>
<b>Pa-233</b>	U233	7.385×10 <sup>-2</sup>	1	7.385×10 <sup>-2</sup>
<b>Pb-210</b>	Po210	2.220×10 <sup>1</sup>	1	2.220×10 <sup>1</sup>
<b>Pd-107</b>	<i>Null</i>	6.500×10 <sup>6</sup>	1	6.500×10 <sup>6</sup>
<b>Pm-145</b>	<i>Null</i>	1.770×10 <sup>1</sup>	1	1.770×10 <sup>1</sup>
<b>Pm-146</b>	<i>Null</i>	5.530×10 <sup>0</sup>	1	5.530×10 <sup>0</sup>
<b>Pm-147</b>	<i>Sm-147</i>	2.623×10 <sup>0</sup>	1	2.623×10 <sup>0</sup>
<b>Po-210</b>	<i>Null</i>	3.789×10 <sup>-1</sup>	1	3.789×10 <sup>-1</sup>
<b>Pt-193</b>	<i>Null</i>	5.000×10 <sup>1</sup>	1	5.000×10 <sup>1</sup>
<b>Pu-236</b>	U-236	2.850×10 <sup>0</sup>	1	2.850×10 <sup>0</sup>
<b>Pu-238</b>	U234	8.770×10 <sup>1</sup>	1	8.770×10 <sup>1</sup>
<b>Pu-239</b>	U235	2.411×10 <sup>4</sup>	1	2.411×10 <sup>4</sup>
<b>Pu-240</b>	U236	6.564×10 <sup>3</sup>	1	6.564×10 <sup>3</sup>
<b>Pu-241</b>	Am241	1.429×10 <sup>1</sup>	0.9994	1.430×10 <sup>1</sup>
<b>Pu-241</b>	U237	1.429×10 <sup>1</sup>	0.00002	7.145×10 <sup>5</sup>
<b>Pu-242</b>	U238	3.735×10 <sup>5</sup>	1	3.735×10 <sup>5</sup>
<b>Ra-223</b>	<i>Null</i>	3.129×10 <sup>-2</sup>	1	3.129×10 <sup>-2</sup>
<b>Ra-224</b>	<i>Null</i>	1.002×10 <sup>-2</sup>	1	1.002×10 <sup>-2</sup>
<b>Ra-225</b>	Ac225	4.079×10 <sup>-2</sup>	1	4.079×10 <sup>-2</sup>
<b>Ra-226</b>	Rn222	1.600×10 <sup>3</sup>	1	1.600×10 <sup>3</sup>
<b>Ra-228</b>	Th228	5.750×10 <sup>0</sup>	1	5.750×10 <sup>0</sup>
<b>Rh-102</b>	<i>Null</i>	2.900×10 <sup>0</sup>	1	2.900×10 <sup>0</sup>
<b>Rn-222</b>	Pb210	1.047×10 <sup>-2</sup>	1	1.047×10 <sup>-2</sup>
<b>Ru-106</b>	<i>Null</i>	1.023×10 <sup>0</sup>	1	1.023×10 <sup>0</sup>
<b>Sb-125</b>	Te125m	2.759×10 <sup>0</sup>	0.231	1.194×10 <sup>1</sup>
<b>Sb-126</b>	<i>Null</i>	3.381×10 <sup>-2</sup>	1	3.381×10 <sup>-2</sup>
<b>Se-79</b>	<i>Null</i>	2.950×10 <sup>5</sup>	1	2.950×10 <sup>5</sup>
<b>Sm-147</b>	<i>Null</i>	1.060×10 <sup>11</sup>	1	1.060×10 <sup>11</sup>
<b>Sm-151</b>	<i>Null</i>	9.000×10 <sup>1</sup>	1	9.000×10 <sup>1</sup>
<b>Sn-121</b>	<i>Null</i>	3.090×10 <sup>-3</sup>	1	3.090×10 <sup>-3</sup>
<b>Sn-121m</b>	<i>Sn-121</i>	4.390×10 <sup>1</sup>	0.776	5.657×10 <sup>1</sup>
<b>Sn-121m</b>	<i>Null</i>	4.390×10 <sup>1</sup>	0.224	1.960×10 <sup>2</sup>
<b>Sn-121m</b>	<i>Null</i>	4.390×10 <sup>1</sup>	1	4.390×10 <sup>1</sup>
<b>Sn-126</b>	Sb126	2.300×10 <sup>5</sup>	0.14	1.643×10 <sup>6</sup>
<b>Sr-90</b>	Y90	2.879×10 <sup>1</sup>	1	2.879×10 <sup>1</sup>
<b>Ta-182</b>	<i>Null</i>	3.150×10 <sup>-1</sup>	1	3.150×10 <sup>-1</sup>

<b>Nuclide</b>	<b>Daughter*</b>	<b>Half-Life [a]</b>	<b>Branching Ratio</b>	<b>Effective Half-Life [a]</b>
<b>Tc-99</b>	<i>Null</i>	$2.111 \times 10^5$	1	$2.111 \times 10^5$
<b>Te-125m</b>	<i>Null</i>	$1.572 \times 10^{-1}$	1	$1.572 \times 10^{-1}$
<b>Th-227</b>	Ra223	$5.114 \times 10^{-2}$	1	$5.114 \times 10^{-2}$
<b>Th-228</b>	Ra224	$1.912 \times 10^0$	1	$1.912 \times 10^0$
<b>Th-229</b>	Ra225	$7.340 \times 10^3$	1	$7.340 \times 10^3$
<b>Th-230</b>	Ra226	$7.538 \times 10^4$	1	$7.538 \times 10^4$
<b>Th-231</b>	Pa231	$2.911 \times 10^{-3}$	1	$2.911 \times 10^{-3}$
<b>Th-232</b>	Ra228	$1.405 \times 10^{10}$	1	$1.405 \times 10^{10}$
<b>Th-234</b>	U234	$6.598 \times 10^{-2}$	1	$6.598 \times 10^{-2}$
<b>Tl-204</b>	<i>Null</i>	$3.780 \times 10^0$	1	$3.780 \times 10^0$
<b>Tm-171</b>	<i>Null</i>	$1.920 \times 10^0$	1	$1.920 \times 10^0$
<b>U-232</b>	Th228	$6.890 \times 10^1$	1	$6.890 \times 10^1$
<b>U-233</b>	Th229	$1.592 \times 10^5$	1	$1.592 \times 10^5$
<b>U-234</b>	Th230	$2.455 \times 10^5$	1	$2.455 \times 10^5$
<b>U-235</b>	Th231	$7.038 \times 10^8$	1	$7.038 \times 10^8$
<b>U-236</b>	Th232	$2.342 \times 10^7$	1	$2.342 \times 10^7$
<b>U-237</b>	Np237	$1.848 \times 10^{-2}$	1	$1.848 \times 10^{-2}$
<b>U-238</b>	Th234	$4.468 \times 10^9$	1	$4.468 \times 10^9$
<b>Y-90</b>	<i>Null</i>	$7.301 \times 10^{-3}$	1	$7.301 \times 10^{-3}$
<b>Zr-93</b>	Nb-93m	$1.530 \times 10^6$	0.975	$1.569 \times 10^6$
<b>Zr-93</b>	<i>Null</i>	$1.530 \times 10^6$	0.025	$6.120 \times 10^7$

<sup>1</sup>Daughters with half-lives shorter than 1 day accounted for in dose coefficients.

<sup>#</sup>*Null* indicates that the daughter nuclide is not included in the dose calculations because it is either stable or was screened out.

Table G.8 lists the plant/soil concentration ratios and the soil distribution coefficients and the instant release fractions.

Table G.8: Element-specific parameters

Element	Soil Distribution Coefficient for clay [m <sup>3</sup> /kg]	Ref	Plant/Soil Concentration Ratio [kg <sub>drysoil</sub> /kg <sub>wetplant</sub> ]	Ref	Instant Release Fraction [-] <sup>m</sup>
Ac	2.4	i	0.0012	i*	0
Ag	0.18	a	0.088	a*	0
Am	8.1	a	0.00022	a*	0
Ar	0	k	0	i*	0.04
Ba	0.52	a	0.0098	a*	0.025
Bi	0.6	g	0.0046	g	0.006
C	0.001	a	7.7	a*	0.027
Ca	0.05	h	0.022	h	0
Cd	0.56	i	0.20	i*	0.006
Cl	0.0001	b	3.7	b	0.06
Cm	5.4	a	0.000074	a*	0
Co	0.54	a	0.016	a*	0
Cs	1.8	a	0.018	a*	0.04
Eu	0.65	a	0.0063	a*	0
Fe	0.16	a	0.0018	a*	0
H	0	a	0	a*	0.00001
Ho	1.3	j	0.0035	i*	0
I	0.012	c	0.005	c	0.04
Ir	0.48	j	0.019	i*	0
Kr	0	k	0	i*	0.04
Mo	0.09	a	0.13	a*	0.01
Nb	0.9	a	0.010	a*	0
Ni	0.67	a	0.17	a*	0
Np	0.021	d	0.00060	d	0
Os	1	j	0.0053	i*	0
Pa	2.7	a	0.013	a*	0
Pb	0.55	h	0.00084	h	0.006
Pd	0.27	i	0.053	i*	0.01
Pm	0.65	a	0.0063	a*	0
Po	3	i	0.00088	i*	0.06
Pt	0.36	j	0.033	i*	0
Pu	4.9	a	0.000049	a*	0
Ra	0.047	e	0.0041	e	0.025
Rh	0.226	a	0.053	i*	0.01
Rn	0	k	0	i*	0.04
Ru	0.4	a	0.034	a*	0.01
Sb	0.24	a	0.00053	a*	0.006
Se	0.74	a	0.15	a*	0.006
Sm	1.3	i	0.0035	i*	0
Sn	0.67	a	0.14	a*	0
Sr	0.11	a	0.30	a*	0.025
Ta	1.2	i	0.0035	i*	0
Tc	0.0012	a	1.3	a*	0.01

Element	Soil Distribution Coefficient for clay [m <sup>3</sup> /kg]	Ref	Plant/Soil Concentration Ratio [kg <sub>drysoil</sub> /kg <sub>wetplant</sub> ]	Ref	Instant Release Fraction [-] <sup>m</sup>
Te	0.72	a	0.022	a*	0.006
Th	5.4	a	0.0012	a*	0
Tl	2.1	j	0.0014	j*	0.006
Tm	1.26	j	0.0035	j*	0
U	0.18	f	0.00079	f	0
Y	1	a	0.0077	a*	0
Zr	3.3	a	0.0011	a*	0.025

a. CSA (2008); b. Sheppard et al. (2002); c. Sheppard et al. (2004a); d. Sheppard et al. (2004b); e. Sheppard et al. (2005a); f. Sheppard et al. (2005b); g. Sheppard et al. (2009); h. Sheppard et al. (2010); i. Davis et al. (1993); j. Garisto (2002); k. assumed 0 for noble gases; l. Beak (2002); and m. Gobien and Garisto (2012).

\* Converted to wet weight basis using a dry/wet weight ratio of 0.35, which was calculated assuming a human diet of 2/3 fruits and vegetables and 1/3 grains from CSA (2008).

## REFERENCES

- BEAK International. 2002. Guidance for Calculation of Derived Release Limits for Radionuclides in Airborne and Liquid Effluents from Ontario Power Generation Nuclear Facilities. Ontario Power Generation Report N-REP-03482-10000-R00. Toronto, Canada.
- Browne, E. and R.B. Firestone. 1986. Table of Radioactive Isotopes. J Wiley and Sons. New York, USA.
- Chadwick, M.B., M. Herman, P. Obložinský, M.E. Dunn, Y. Danon, A.C. Kahler, D.L. Smith, B. Pritychenko, G. Arbanas, R. Arcilla, R. Brewer, D.A. Brown, R. Capote, A.D. Carlson, Y.S. Cho, H. Derrien, K. Guber, G.M. Hale, S. Hoblit, S. Holloway, T.D. Johnson, T. Kawano, B.C. Kiedrowski, H. Kim, S. Kunieda, N.M. Larson, L. Leal, J.P. Lestone, R.C. Little, E.A. McCutchan, R.E. MacFarlane, M. MacInnes, C.M. Mattoon, R.D. McKnight, S.F. Mughabghab, G.P.A. Nobre, G. Palmiotti, A. Palumbo, M.T. Pigni, V.G. Pronyaev, R.O. Sayer, A.A. Sonzogni, N.C. Summers, P. Talou, I.J. Thompson, A. Trkov, R.L. Vogt, S.C. van der Marck, A. Wallner, M.C. White, D. Wiarda, P.G. Young. 2011. ENDF/B-VII.1 Nuclear data for science and technology: Cross section, covariances, fission product yields, and decay data. *Nuclear Data Sheets*: 112-12, 2887-2996 (2011).
- CSA. 2008. Guidelines for calculating derived release limits for radioactive material in airborne and liquid effluents for normal operation of nuclear facilities. Canadian Standards Association Report CSA-N288.1-08. Mississauga, Canada.
- Davis, P.A., R. Zach, M.E. Stephens, B.D. Amiro, G.A. Bird, J.A.K. Reid, M.I. Sheppard and M. Stephenson. 1993. The disposal of Canada's nuclear fuel waste: The biosphere model, BIOTRAC, for postclosure assessment. Atomic Energy of Canada Limited Report AECL-10720. Pinawa, Canada.
- Garisto, F. 2002. Radionuclide specific and element specific data for the Radionuclide Screening Model Version 1.1. Ontario Power Generation, Report 06819-REP-01200-10038-R01. Toronto, Canada.
- Gierszewski, P., J. Avis, N. Calder, A. D'Andrea, F. Garisto, C. Kitson, T. Melnyk, K. Wei and L. Wojciechowski. 2004. Third case study - Postclosure safety assessment. Ontario Power Generation Report 06819-REP-01200-10109-R00. Toronto, Canada.
- Gobien, M and F. Garisto. 2012. Data for radionuclide and chemical element screening. Nuclear Waste Management Organization Technical Report NWMO TR-2012-11. Toronto, Canada.
- ICRP (International Commission on Radiological Protection). 2008. Nuclear decay data for dosimetric calculations. ICRP publication 107. *Annals of the ICRP* 38 (3). Pergamon Press, Oxford, UK.
- Medri, C. 2012. Human Intrusion Model for the Fourth and Fifth Case Studies: HIMv2.0. Nuclear Waste Management Organization Technical Report NWMO TR-2012-04. Toronto, Canada.



- Quintessa. 2009. AMBER 5.3 Reference Guide. Quintessa Ltd. report QE-AMBER-1, Version 5.3. Henley-on-Thames, UK.
- Sheppard, M.I., S.C. Sheppard and B. Sanipelli. 2002. Recommended biosphere model values for iodine. Ontario Power Generation Report 06819-REP-01200-10090. Toronto, Canada.
- Sheppard, M.I., S.C. Sheppard and B. Sanipelli. 2004a. Recommended biosphere model values for chlorine. Ontario Power Generation Report 06819-REP-01200-10119. Toronto, Canada.
- Sheppard, M.I., S.C. Sheppard and B. Sanipelli. 2004b. Recommended biosphere model values for neptunium. Ontario Power Generation Report 06819-REP-01200-10120. Toronto, Canada.
- Sheppard, M.I., S.C. Sheppard and B. Sanipelli. 2005a. Recommended biosphere model values for uranium. Ontario Power Generation Report 06819-REP-01200-10088. Toronto, Canada.
- Sheppard, M.I., J.C. Tait, B.L. Sanipelli and S.C. Sheppard. 2005b. Recommended biosphere model values for radium and radon. Ontario Power Generation Report 06819-REP-01200-10144. Toronto, Canada.
- Smith, G.M., H.S. Fearn, K.R. Smith, J.P. Davis and R. Klos. 1988. Assessment of the radiological impact of disposal of solid radioactive waste at Drigg. National Radiological Protection Board Memorandum NRPB-M148. Chilton, UK.
- Sheppard, S.C., J.Long and B. Sanipelli. 2009. Field measurements of the transfer factors for iodine and other trace elements. Nuclear Waste Management Organization NWMO TR-2009-35. Toronto, Canada.
- Sheppard, S.C., J.M.Long, B.Sanipelli. 2010. Plant/soil concentration ratios for paired field and garden crops, with emphasis on iodine and the role of soil adhesion. Journal of Environmental Radioactivity 101; pg 1032-1037.
- Tait, J.C. and S. Hanna. 2001. Characteristics and radionuclide inventories of used fuel from OPG Nuclear Generating Stations, Volume 3 - Radionuclide inventory data. Decay times 10 to 300 years. Ontario Power Generation Report 06819-REP-01200-10029-R00. Toronto, Canada.
- Wuschke, D.M. 1996. Assessment of the long-term risks of inadvertent human intrusion into a proposed Canadian nuclear fuel waste disposal vault in deep plutonic rock - Revision 1. Atomic Energy of Canada Limited Report AECL-10279 Rev. 1, COG-92-151 Rev. 1. Pinawa, Canada.